ISSN 2408-2384 (ONLINE)

Environment and Natural Resources Journal

Volume 22 Number 6 November - December 2024

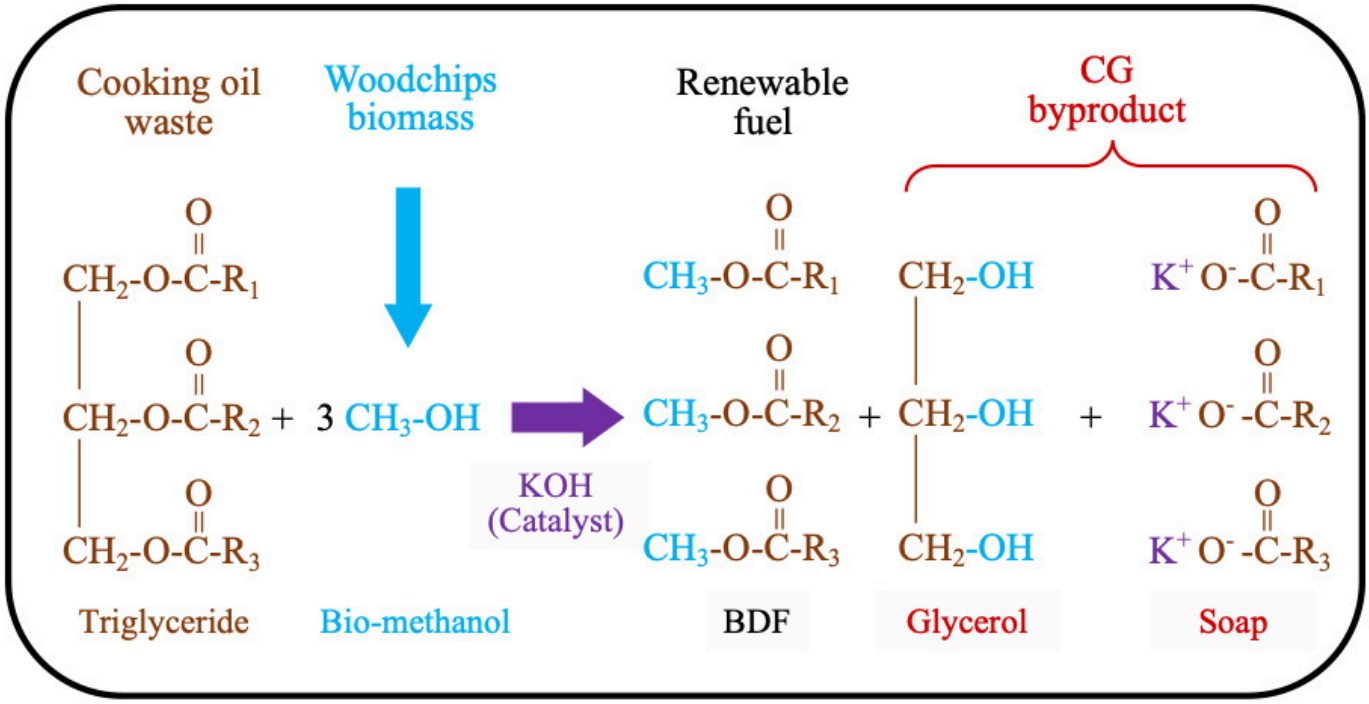

Biodiesel fuel (BDF) production process in a chamber heated by hot spring water at a BDF facility in Unzen City, Nagasaki, Japan.

Source: Zou Z, Kaothien-Nakayama P, Nakayama H. Utilization of high-salinity crude glycerol byproduct from biodiesel production for biosynthesis of γ-aminobutyric acid in engineered *Halomonas elongata*. Page 525-534.

Environment and Natural Resources Journal (EnNRJ)
Volume 22, Number 6, November - December 2024 ISSN: 2408-2384 (Online)

AIMS AND SCOPE

The Environment and Natural Resources Journal is a peer-reviewed journal, which provides insight scientific knowledge into the diverse dimensions of integrated environmental and natural resource management. The journal aims to provide a platform for exchange and distribution of the knowledge and cutting-edge research in the fields of environmental science and natural resource management to academicians, scientists and researchers. The journal accepts a varied array of manuscripts on all aspects of environmental science and natural resource management. The journal scope covers the integration of multidisciplinary sciences for prevention, control, treatment, environmental clean-up and restoration. The study of the existing or emerging problems of environment and natural resources in the region of Southeast Asia and the creation of novel knowledge and/or recommendations of mitigation measures for sustainable development policies are emphasized.

The subject areas are diverse, but specific topics of interest include:

- Biodiversity
- Climate change
- Detection and monitoring of polluted sources e.g., industry, mining
- Disaster e.g., forest fire, flooding, earthquake, tsunami, or tidal wave
- Ecological/Environmental modelling
- Emerging contaminants/hazardous wastes investigation and remediation
- Environmental dynamics e.g., coastal erosion, sea level rise
- Environmental assessment tools, policy and management e.g., GIS, remote sensing, Environmental Management System (EMS)
- Environmental pollution and other novel solutions to pollution
- Remediation technology of contaminated environments
- Transboundary pollution
- Waste and wastewater treatments and disposal technology

Schedule
Environment and Natural Resources Journal (EnNRJ) is published 6 issues per year in January-February, March-April, May-June, July-August, September-October, and November-December.

Publication Fees
There is no cost of the article-processing and publication.

Ethics in publishing
EnNRJ follows closely a set of guidelines and recommendations published by Committee on Publication Ethics (COPE).

Environment and Natural Resources Journal (EnNRJ)
Volume 22, Number 6, November - December 2024 ISSN: 2408-2384 (Online)

Editorial Office Address
Research Management Unit,
Faculty of Environment and Resource Studies, Mahidol University
999, Phutthamonthon Sai 4 Road, Salaya, Phutthamonthon, Nakhon Pathom, Thailand, 73170
Phone +662 441 5000 ext. 2108 Fax. +662 441 9509-10
Website: https://ph02.tci-thaijo.org/index.php/ennrj/index
E-mail: ennrjournal@gmail.com

Environment and Natural Resources Journal (EnNRJ)

Volume 22, Number 6, November - December 2024 ISSN: 2408-2384 (Online)

CONTENT

Environment and Natural Resources Journal

Volume 22
Issue 6
2024

Preliminary Assessment of Morphology and Elemental Composition of Fine Particulates in Selected Urban Areas of Java Island

Feni Fernita Nurhaini[1*], Pascale Ramadhan[2], Muhayatun Santoso[2], Rizal Kurniadi[2], Arbi Dimyati[1], Indah Kusmartini[1], Diah Dwiana Lestiani[1], Syukria Kurniawati[1], Endah Damastuti[1], Djoko Prakoso D. Atmodjo[1], Moch Faizal Ramadhani[1], Woro Yatu N. Syahfitri[1], and Dikdik Sidik Purnama[1]

[1]*Research Organization for Nuclear Energy (ORTN), National Research and Innovation Agency (BRIN), Indonesia*
[2]*Faculty of Mathematics and Natural Science (FMIPA), Institute of Technology Bandung (ITB), Indonesia*

ARTICLE INFO

Received: 30 Apr 2024
Received in revised: 15 Aug 2024
Accepted: 28 Aug 2024
Published online: 6 Nov 2024
DOI: 10.32526/ennrj/22/20240127

Keywords:
$PM_{2.5}$/ Teflon/ SuperSASS/ Morphology/ Elemental

*** Corresponding author:**
E-mail: feni002@brin.go.id

ABSTRACT

Rapid urbanization and high population density in three major cities in Indonesia, Bandung, Jakarta, and Tangerang have led to significant air quality issues. Fine inhalable particles ($PM_{2.5}$) with distinct morphologies and elemental compositions pose considerable health risks. This study evaluates the morphology and chemical composition of $PM_{2.5}$ in these urban areas on Java Island. $PM_{2.5}$ samples were collected for 24-hour periods using a Teflon filter with the Super Speciation-Air Sampling System (SuperSASS) following the EPA sampling schedule, from May to September 2022. The Teflon sample with the highest $PM_{2.5}$ concentration, representative of both weekdays and weekends, was selected for morphological analysis using Scanning Electron Microscopy-Energy Dispersive X-ray (SEM-EDX) and elemental characterization using Energy-Dispersive X-ray Fluorescence (ED-XRF) Epsilon. SEM images revealed distinct morphological characteristics at each site. In Bandung, particles were irregularly shaped, agglomerated, and flaky, with sizes ranging from 1.1-1.6 µm on weekdays and 0.9-1.3 µm on weekends. Jakarta has particles with semi-crystalline, tabular, elongated, and puff-like morphology, with sizes predominantly from 0.5-0.8 µm on weekdays and 0.9-1.3 µm weekends. In Tangerang, particles were irregularly faceted and agglomerated, with sizes between 0.5-1.3 µm on weekdays and 0.9-1.4 µm on weekends. Teflon-derived minerals (C,F) were present across all sites. EDX spectra revealed Ca-rich particles in Bandung, while S-rich particles were observed in Jakarta and Tangerang. XRF analysis further proved the major and minor elements, reflecting local pollution sources. The combined use of SEM-EDX and XRF offers a comprehensive profile of $PM_{2.5}$, highlighting specific pollution sources in each city.

1. INTRODUCTION

Air pollution is a global issue and is recognized as the second-largest contributor to the global disease burden (IHME, 2019). As of 2023, Indonesia ranked as the 14th most polluted country in the World (IQair, 2023a). Among various air pollutants, fine inhalable particulates ($PM_{2.5}$) with aerodynamic dimensions of 2.5 micrometers or smaller, with a size 30 times smaller than human hair diameter (EPA, 2023) poses significant health risks due to their ability to penetrate deeply into the lungs and irritate the alveolar wall (Yang et al., 2020). In Indonesia, rapid urbanization and industrialization have exacerbated $PM_{2.5}$ levels, particularly in densely populated areas like Java Island, where population densities range from 500-1,000 people per square kilometer (Statistics Indonesia, 2023). Data indicate that $PM_{2.5}$ concentrations in major cities on Java Island, such as Bandung, Jakarta, and Tangerang, exceed World Health Organization (WHO) guidelines by 7 to 10 times (IQair, 2023b). This increase can be attributed to various factors, including industrial activities, traffic congestion, agricultural burning, and rapid urbanization (Hopke et al., 2008; Lestari et al., 2020; Santoso et al., 2020; Santoso et al., 2008a). As of 2023, Bandung, the fourth-biggest city, has a

Citation: Nurhaini FF, Ramadhan P, Santoso M, Kurniadi R, Dimyati A, Kusmartini I, Lestiani DD, Kurniawati S, Damastuti E, Atmodjo DPD, Ramadhani MF, Syahfitri WYN, Purnama DS. Preliminary assessment of morphology and elemental composition of fine particulates in selected urban areas of Java Island. Environ. Nat. Resour. J. 2024;22(6):483-499. (https://doi.org/10.32526/ennrj/22/20240127)

population of 2,714,215 (World Population Review, 2024b) and 2.2 million vehicles (Syahrial, 2023), Jakarta is categorized as a megacity with a population of 11,436,004 (World Population Review, 2024a) and approximately 24 million vehicles as of 2024 (Adji, 2024), Tangerang, the third-biggest city, has an estimated population of 2,570,980 (World Population Review, 2024c) with around 934,720 vehicles as of 2022 (Statistics Indonesia, 2022). Therefore, monitoring of $PM_{2.5}$ levels in these three cities-Bandung, Jakarta, and Tangerang is a significant concern in understanding the sources and composition for effective air quality management.

Extensive research on $PM_{2.5}$ has been conducted globally (Hopke et al., 2020; Manisalidis et al., 2020). In Indonesia, research on air pollution began in the early 2000s, focusing on various aspects such as the elemental analysis of industrial emissions in major cities (Santoso et al., 2019), health impacts of air pollution (Ramdhan et al., 2021), the effects of biomass burning and forest fires (Permadi and Kim Oanh, 2013; Santoso et al., 2022), and integration of satellite data with real-time monitoring (Sinaga et al., 2020; Siregar et al., 2022). Despite the growing research on $PM_{2.5}$, studies focusing on the surface morphology of $PM_{2.5}$ in Indonesia are still limited, particularly in Urban Areas on Java Island. Existing research primarily relies on data from other regions, which may not fully capture the unique characteristics of Indonesian urban areas. The morphology of $PM_{2.5}$, including its size, shape, and surface characteristics, plays a crucial role in understanding its sources, transport, and potential health impacts. The shape of particulate matter (PM) significantly influences its deposition efficiency and interactions with biological fluids in the lungs (Mokbel, 2024; Pallarés et al., 2020; Stearns et al., 2001). The irregular and sharp-edged particles, in particular, can cause injury to lung tissues upon inhalation (Fatima et al., 2022). Previous research has documented various common shapes of $PM_{2.5}$, such as spherical particles associated with anthropogenic and combustion sources (González et al., 2016; Khobragade and Ahirwar, 2023), aggregated and irregular particles linked to carbonaceous material and road dust (Khobragade and Vikram Ahirwar, 2023), the lamellar appearance of silicates (Khobragade and Ahirwar, 2023), rectangular particle (EPA, 2002), and prismatic regular shapes associated with Si-rich particles from natural sources (González et al., 2016; Paoletti et al., 2003). Despite the importance of this information, research on the surface morphology of $PM_{2.5}$ in Indonesia remains scarce. Therefore, investigating the morphology and elemental composition of fine particulates in selected urban areas is essential for gaining comprehensive understanding of $PM_{2.5}$ in the region. Currently, urbanization in Indonesia is accelerating, with 56% of the population residing in urban areas (Statistics Indonesia, 2023). Compared to other Asian countries, Indonesia's urbanization rate is growing rapidly at 4.1% per year (The World Bank, 2016). This urbanization trend is likely contributing to rising $PM_{2.5}$ levels. The cities of Jakarta, Bandung, and Tangerang were selected for this study to represent urban areas on Java Island.

The research involves the collection of $PM_{2.5}$ samples using Super Speciation Air Sampling System (SuperSASS), determination of $PM_{2.5}$ concentration through the gravimetric method, analysis of $PM_{2.5}$ surface morphology using Scanning electron microscopy-energy dispersive X-ray (SEM-EDX), and characterization of elemental composition using Energy Dispersive XRF(ED-XRF) Epsilon 5. Accordingly, this study aims to bridge the existing gap by conducting a preliminary assessment of $PM_{2.5}$ morphology and elemental composition to obtain a more comprehensive profile of $PM_{2.5}$ in selected urban areas of Java Island.

2. METHODOLOGY

2.1 Collection of fine particulate ($PM_{2.5}$) sample using SuperSASS

The $PM_{2.5}$ was collected from May to September 2022 in three selected cities in Indonesia (Bandung, Jakarta, and Tangerang) following the Environmental Protection Agency (EPA) sampling schedule in 2022. The sampling sites of the selected three urban areas on Java Island are shown in Figure 1. Bandung site (1), the largest city on the southern tip of Java Island is 630 meters above sea level, Bandung sampling site is located at Kawasan Kerja Bersama (KKB)-BRIN JL. Tamansari number 71 (-6.8885 407208374305, 107.60795837023203). The Bandung site has a distinctive geographical landscape, characterized by a mountainous landscape with basin topography which affects air circulation and may trap pollutants within the basin (Kurniawati et al., 2024). As depicted in Figure 1, KKB Tamansari is located in a densely populated region. Within a 1-kilometer radius, there is a public sports area (SABUGA) to the north, Bandung Zoo (Kebun Binatang Bandung) to the

south, the Bandung Institute of Technology (ITB) to the east, and department stores and hotels to the west.

The Jakarta site (2) is located at the Laboratorium Lingkungan Hidup Daerah (LLHD), Jl. Casablanca Kav. 1 Kuningan, Jakarta Selatan (-6.2243 38159194404, 106.83546398262821). The Jakarta site at LLHD is positioned on the main road of south Jakarta and surrounded by the offices area, hotels, and train station. Within a 1-kilometer radius, there are hotels and a plaza mall to the north and west, public residences to the east, and an LRT station to the south.

Tangerang Site (3) is located at the Science and Technopark/Kawasan Sains dan Teknologi (KST) B.J. Habibie, Serpong, Jl. Raya Puspitek Serpong, Kecamatan Setu, Kota Tangerang Selatan (-6.353488465685582, 106.67229646758928). The sampling site in Tangerang is situated close to the main road of Serpong. About 1 km to the north,are public school, several offices, and a bus station. To the east, there are public sports areas and residential housing, while the west and south are occupied by offices and residential areas.

Figure 1. Sampling site of $PM_{2.5}$ of three urban Areas (Bandung, Jakarta, and Tangerang) on Java Island in Indonesia

$PM_{2.5}$ was collected over 24-hour using the Super Speciation Air Sampling System (SuperSASS) instrument, developed and field-tested by the United States Environmental Protection Agency (US EPA). The samples were collected on a 47 mm PTFE (Polytetrafluoroethylene) $(C_2F_4)_n$/Teflon filter with pore size of 0.2 um, maintained at a constant flow rate of 6.7 L/min. The SuperSASS consists of two canister sets: Set 1, containing canisters 1, 2, 3, and 4, and Set 2, containing canisters 5, 6, 7, and 8, as illustrated in Figure 2. The canister sets were used alternately on a weekly basis, following the EPA schedule. The PTFE filter was placed inside the 1st, 2nd, 3rd, and 4th canisters, designed for elemental and inorganic analysis of $PM_{2.5}$ samples (Met One Instruments, 2001). Each canister in the SuperSASS is equipped with a sharp cut cyclone (SCC), which efficiently separates solid and liquid coarse particles without grease or oil. The sampling data , including duration, filter volume, flow rate, temperature, and pressure were extracted via an RS-232 port and transferred to a PC using SASSCommAQ software (Met One

Instruments, 2001). The recorded pressure during the sampling period remained relatively stable at each site, with pressure ranging from 693 to 694 mmHg in Bandung, 755 to 756 mmHg in Jakarta, and 752 to 753 mmHg in Tangerang.

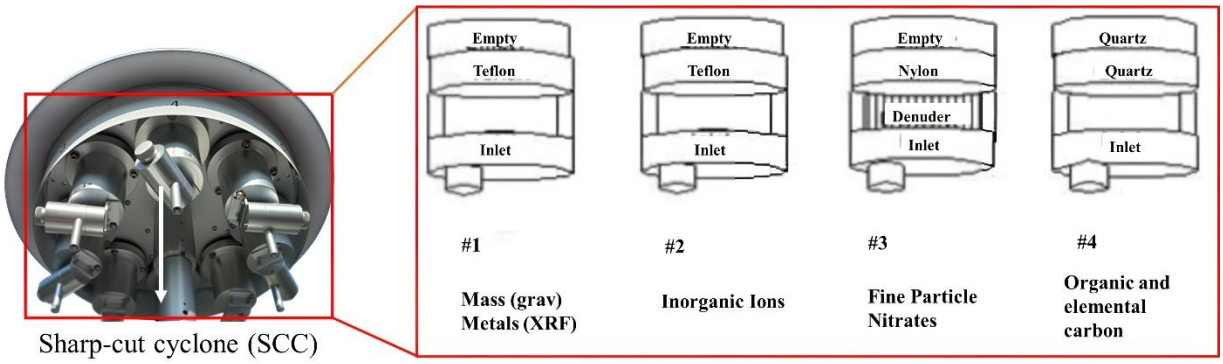

Figure 2. Canister sets of Super Speciation Air Sampling System (SuperSASS)

2.2 Gravimetric analysis of $PM_{2.5}$

The concentration of $PM_{2.5}$ was determined by gravimetric analysis, which involved weighing the initial and final mass of the Teflon filter using the microbalance (model MX5 Mettler Toledo) at room humidity of around 45% and air temperature at 20±2°C. The $PM_{2.5}$ concentration was calculated based on Equation 1 (Research Triangle Institute, 2008), where the difference mass of the filter after sampling (Mf) and before sampling (Mi) was divided by filter volume (Va). During the sampling period, the Teflon filter containing the highest $PM_{2.5}$ levels on both weekdays and weekends was chosen for morphology and elemental analysis.

$$PM_{2.5}\left(\frac{\mu g}{m^3}\right) = \frac{Mf\,(mg) - Mi(mg)}{Va\,(m^3)} \times 1{,}000 \qquad (1)$$

2.3 Morphology analysis using SEM-EDX

The morphology, including the shape and size of $PM_{2.5}$ was characterized using Scanning electron microscopy (SEM) coupled with energy dispersive X-ray analysis (EDX) (JEOL JSM 6510LA) in the Research Center for Nuclear Beam Analysis Technology, National Research and Innovation Agency (BRIN). The SEM analysis was conducted in three cycles throughout 2022: July 28-29, September 23, and October 29. For the SEM-EDX analysis, the non-conductive Teflon filter with the highest $PM_{2.5}$ concentration from both weekends and weekdays was cut into 5 mm^2 size, and coated with a thin layer of gold (Au) to render it electrically conductive. This coating was applied using a vacuum plasma coating device. The coated Teflon sample was measured at an accelerating voltage of 10 kV, with a working distance (WD) of 10 mm, and a magnification ranging from 1,000-10,000x. Particle sizes observed in SEM images were estimated using ImageJ software.

2.3 Elemental analysis using ED-XRF

2.3.1 EDXRF Epsilon 5 set up

The elemental characterization of the Teflon filter with the highest $PM_{2.5}$ levels on both weekdays and weekends was carried out using a non-destructive three-dimensional EDXRF Epsilon 5 spectrometer (PANalytical) in the Research Center for Nuclear Beam Analysis Technology, National Research and Innovation Agency. The elemental analysis was conducted using ED-XRF Epsilon 5 with the following specifications: 100 kV, Gd anode element, polarizing optical path, and secondary target (i.e., Al_2O_3, Fe, CaF_2, Ge, Zr, CeO_2, Mo, Ag, and Al), providing low detection limit of ng/cm^2. The instrument's calibration was set up using standard micromatter®, and a blank standard for multielement. The Teflon filters were loaded into the StainlessSteel sample holders. The sample holder containing 8 filters was positioned in the fixed tray inside the instrument. The system has a fully integrated X-Y sample changer, and the suction device integrated with the handling arm will automatically move each sample to the sample holding (airlock) position (PANalytical, 2005). Each sample was irradiated by a secondary X-ray resulting from the polarizing target, for 1 h. The spectrum of the excitation energy of the sample is recorded by the PAN-32 Ge X-ray detector, placed along the third axis, with an energy resolution of <140 eV (PANalytical, 2009, PANalytical, 2005).

2.3.2 Elemental concentration quantification

To determine the elemental concentration, a calibration and sensitivity curve was made by measuring the thin-film micrometer standards from Micromatter Technologies Inc, with a concentration range of 17-64 µg/cm^2. The standard was measured and the Epsilon software automatically plotted the calibration curve, with the elemental concentration on the X axis and the corresponding intensities on the Y-axis. The detailed calibration steps have been described by (Royani et al., 2016). To assess elemental sensitivity, the atomic number (Z) of the element was plotted on the X-axis against its sensitivity on the Y axis (Royani et al., 2016).

Prior to quantifying the elemental concentration, method validation was conducted using Standard Reference Material (SRM) NIST 2783, Air Particulate on Filter Media, which contains known elemental concentrations. This validation was necessary to ensure that the method's recovery and standard deviation were within acceptable limits. The Teflon filter samples were then analyzed using the same experimental procedure. The elemental concentration (Ci) in Teflon filter was calculated using Equation (2) and (3) (Arana et al., 2014).

$$N_i = aCi + b \quad (2)$$

$$Ci\ (ng/cm^2) = \frac{(Ni \times Fi)}{(Time \times Current \times Sen_i)} \quad (3)$$

Where; a is the slope of calibration curve, b is the intercept, Ni is the net peak area of particular element (i) characteristic X-ray (counts), Fi is the absorption factor of element i (≈1), Sen_i is sensitivity of element I in the sample (counts/ng/cm^2/s/mA), Time is measurement time (sec), Current is the current of X-Ray tube (mA), and Ci is the concentration (ng/cm^2). The concentration obtained from EDXRF Epsilon was then converted to ng/m^3 using Equation (4).

$$Ci\ (ng/m^3) = \frac{Ci\ (\frac{ng}{cm^2})}{V\ (m^3)} \times \text{area of dust on filter } (cm^2) \quad (4)$$

Where; Ci is the elemental concentration of $PM_{2.5}$ (ng/m^3), V is the sampling volume using SuperSASS (±9.7 m^3), and the area of dust on the filter (circular area) is 12.56 cm^2.

3. RESULTS AND DISCUSSION

3.1 Gravimetric analysis of $PM_{2.5}$

The $PM_{2.5}$ concentration at each sampling site is depicted in Figure 3. During the sampling period, fluctuation in $PM_{2.5}$ levels was observed. Bandung recorded the most data points compared to Jakarta and Tangerang, as the SuperSASS instrument was initially installed in Bandung, resulting in an extended sampling period. Following the completion of sampling in Bandung, the SuperSASS was to Jakarta and Tangerang. As illustrated in Figure 3(b), Jakarta has only two data points on weekends, due to some samplings not adhering to the EPA sampling schedule, thus excluded in this work.

The $PM_{2.5}$ concentrations determined through gravimetric analysis are presented in Figure 3. In Bandung, the $PM_{2.5}$ concentrations on weekends were found to be relatively higher than on weekdays. The average $PM_{2.5}$ concentration in Bandung was 41 µg/m³ on weekdays and 42 µg/m³ on weekends. The slight difference between weekday and weekend concentrations is likely attributable to increased transportation activity and a higher number of visitors during the holiday season, particularly around public areas such as the Bandung Zoo. The highest $PM_{2.5}$ concentrations recorded were 86.5 µg/m³ on weekdays and 63.2 µg/m³ on weekends, both of which exceed the Indonesian daily standard of 55 µg/m^3 (The Ministry of State Secretariat of Republic Indonesia, 2021).

In Jakarta and Tangerang, as shown in Figures 3(b) and 3(c), $PM_{2.5}$ levels were higher during weekdays compared to weekends. In Jakarta, the average $PM_{2.5}$ concentration was 36.5 µg/m^3 on weekdays and 36.3 µg/m^3 on weekends. The highest concentrations were 51.6 µg/m^3 on weekdays and 37.4 µg/m^3 on weekends, both below the daily standard of 55 µg/m^3 (The Ministry of State Secretariat of Republic Indonesia, 2021). The sampling site in Jakarta (LLHD-Jakarta) is situated along a main road and is surrounded by office buildings, contributing to elevated traffic and $PM_{2.5}$ levels during weekdays.

In Tangerang, the average concentration of $PM_{2.5}$ was 48.3 µg/m^3 on weekdays and 38.5 µg/m^3 on weekends. The highest concentration recorded was 69.0 µg/m^3 on weekdays, exceeding the daily standard of Indonesian regulation, while the highest weekend concentration was 52.3 µg/m^3, falling below the standard. The SuperSASS instrument in Tangerang is located within the Science and Technopark, approximately 500 meters from the main road, which likely accounts for the higher $PM_{2.5}$ levels during weekdays due to local office and transport activities.

A t-test was conducted to compare the $PM_{2.5}$ concentration between weekdays and weekends at each site (Bandung, Jakarta, Tangerang). The p-values

obtained were 0.74 for Bandung, 0.94 for Jakarta, and 0.13 for Tangerang, indicating no statistically significant difference between weekday and weekend concentration at any of the sites ($p>0.05$).

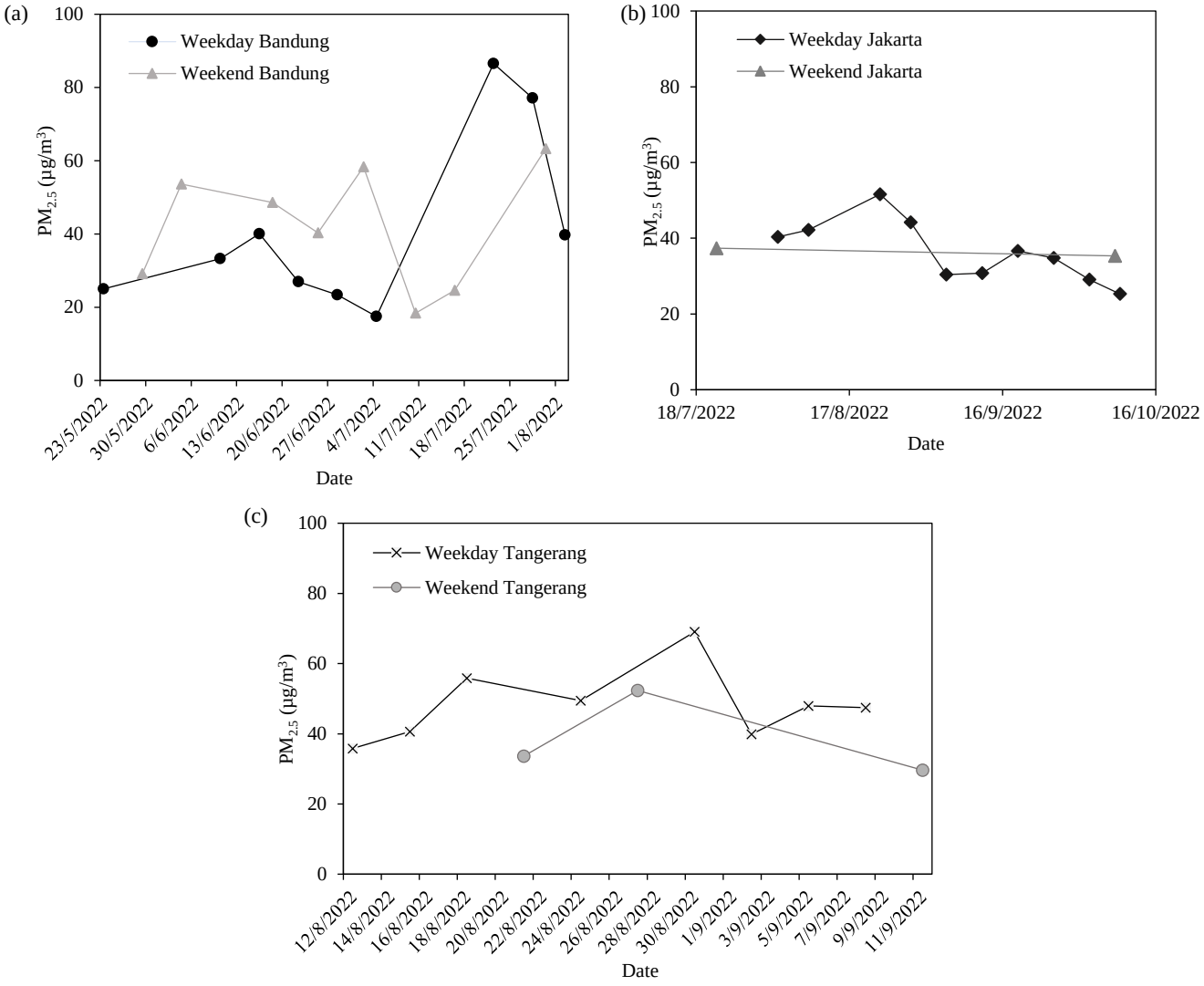

Figure 3. $PM_{2.5}$ of Bandung (a), Jakarta (b), and Tangerang (c) on weekdays and weekends during the sampling period for each site.

3.2 Morphology analysis of $PM_{2.5}$

The morphology of $PM_{2.5}$ was assessed using a blank Teflon filter, which was cut into small parts for SEM analysis. To ensure adequate conductivity during SEM analysis, a thin layer of gold (Au) was sputter-coated onto the Teflon filter. A high magnification of 10,000x was utilized to observe the filter matrix profile in detail. The resulting morphology of the Teflon $(C_2F_4)_n$ filter is depicted in Figure 4. The surface profile of the blank Teflon filter closely resembles that reported in previous studies (Casuccio et al., 2004). It consists of fibrous material made of carbonaceous particles (C) and fluorine (F), interwoven to form a web-like structure. As shown in the Energy Dispersive X-ray (EDX) profile, the Teflon material is primarily composed of carbon (C) and fluorine (F). The Teflon filter is classified as the "depth" filter, effectively capturing fine particles throughout its depth rather than merely on the surface (EPA, 2002), which leads to a lower probability of particle overlap. During the collection of $PM_{2.5}$, fine particles were trapped below the surface or within the filter's web-like structure. As a result, the 24-hour sampling period is unlikely to significantly affect SEM analysis. However, particle agglomeration remains a possibility (Fatima et al., 2022; Liu et al., 2018; Wu et al., 2015), despite the Teflon medium's higher sampling capacity (EPA, 2002).

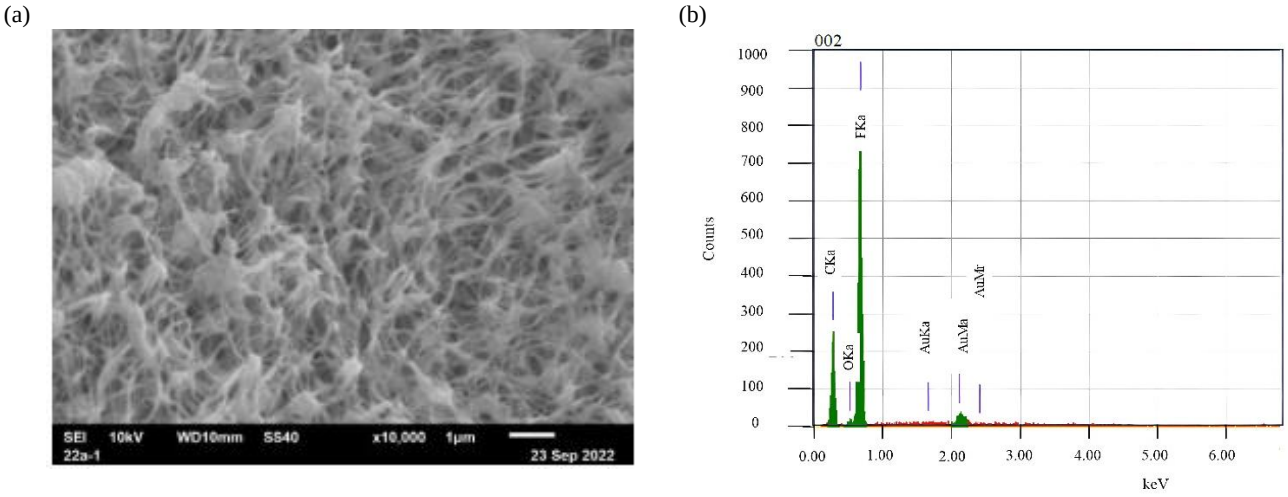

Figure 4. Morphology of Blank Teflon filter with 10,000x magnification (a) EDX profile of Teflon filter (b)

3.2.1 Morphology of $PM_{2.5}$ in Bandung

The Teflon filters exhibiting the highest $PM_{2.5}$ concentrations were selected for detailed morphological and energy-dispersive X-ray (EDX) analysis. The analysis was conducted across multiple magnifications (1200x, 2000x, 3000x, 4000x, 4500x, 5000x), with representative images presented in Figure 5. Additional images are available in the supplementary materials.

The morphological analysis revealed that $PM_{2.5}$ particles on both weekdays and weekends displayed irregular shapes. The particle size distribution, detailed in Figure 6, was assessed by measuring 78 particles on weekdays and 80 particles on weekends at various magnifications. On weekdays, 47 particles had diameters less than 2.5 µm, whereas 70 particles exhibited diameters less than 2.5 µm on weekends. The particle size distribution was comparable between the two periods, with weekdays primarily showing particles in the range of 1.1-1.6 µm, and weekends showing particles in the range of 0.9-1.3 µm. However, particle agglomeration still observed on both weekdays and weekend, having diameter greater than 2.5 µm.

The EDX spectra revealed that both periods were predominantly composed of carbon (C), fluorine (F), and calcium (Ca), as depicted in Figure 5. The high levels of C and F are attributed to the Teflon filter material and carbonaceous components within $PM_{2.5}$. Calcium, likely originating from dust, was present at approximately 21.7% (Figure 5(a)) and 20.3% (Figure 5(b)) by mass on weekdays. However, Ca mass% was notably higher on weekends, with values of 33.1% (Figure 5(c)) and 12.9% (Figure 5(d)). Weekday EDX analysis identified amorphous, agglomerated Ca-rich particles, consistent with prior research (González et al., 2016) and detected soot aggregates indicative of gasoline emissions and biomass combustion (Khobragade and Vikram Ahirwar, 2023). On weekends, Ca-rich particles exhibited an irregular flaky morphology, potentially sourced from windblown dust and road dust (Yue et al., 2013).

The EDX spectra indicated that Ca-rich particles contained significant amounts of carbon and oxygen, suggesting the presence of $CaCO_3$ and limestone/$CaCO_3$ deposits in proximity to the sampling site. Figure 5(a) shows the detection of carbonate minerals along with trace levels of sodium (Na), magnesium (Mg), sulfur (S), and silicon (Si). Elevated sulfur content, indicative of secondary sulfate formation from biomass burning and vehicular emissions, was also observed. Additionally, the presence of secondary Ca-rich particles containing S and O points to the formation of $CaSO_4$ through reactions between $CaCO_3$ and SO_2 during fuel combustion. On weekends, the EDX spectra predominantly featured carbonate minerals (C, O, Ca) with minimal Mg. However, due to the limitation of EDX, other elements contained in $PM_{2.5}$ of Bandung were not observed. Thus, the remaining elements are shown in Figure 11(a).

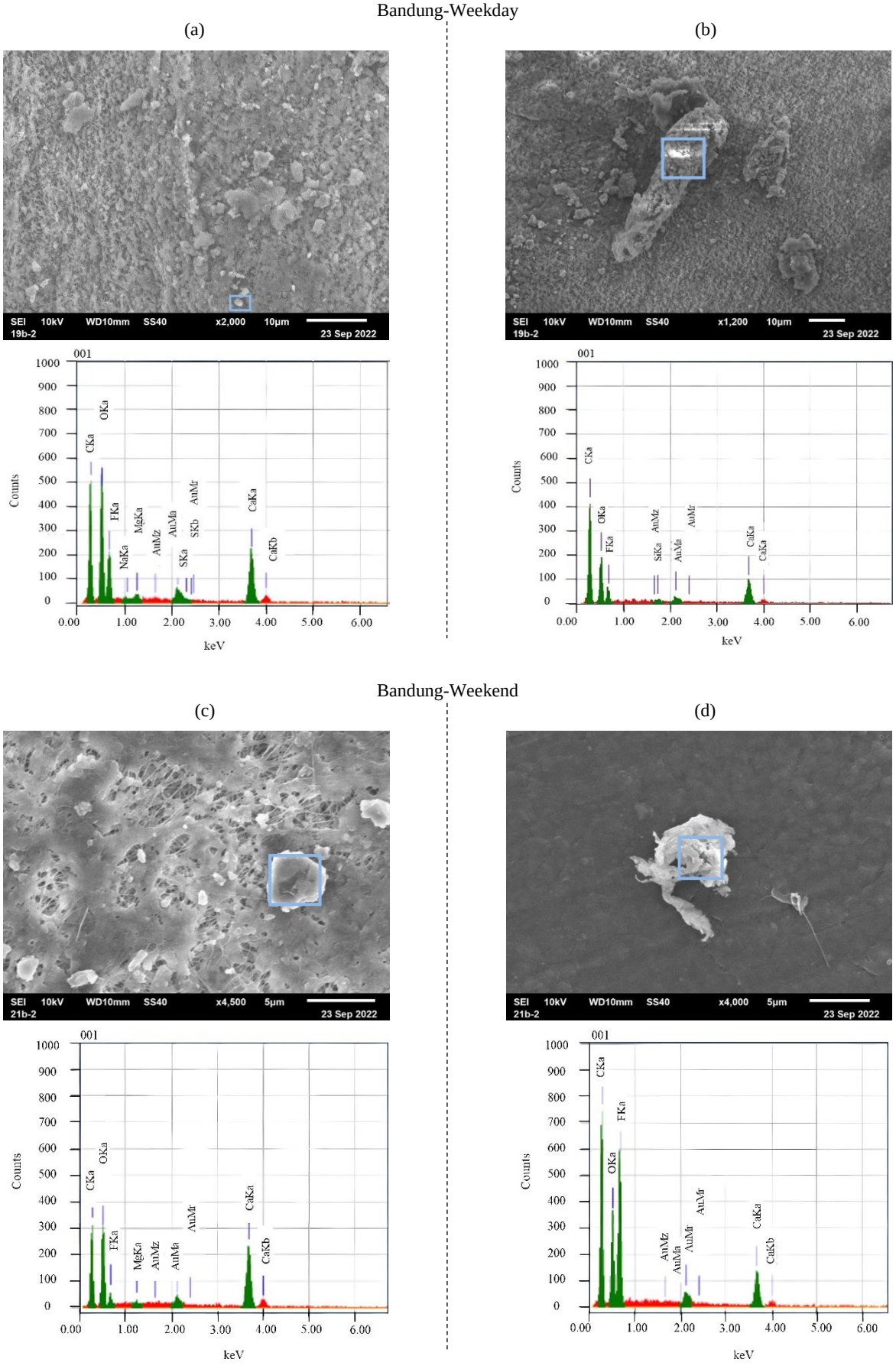

Figure 5. Morphology and EDX spectrum of $PM_{2.5}$ in Bandung on weekdays at 2000x (a) and 1200x (b) magnification, on weekends (b) at 4500x (c) and 4000x (d) magnification.

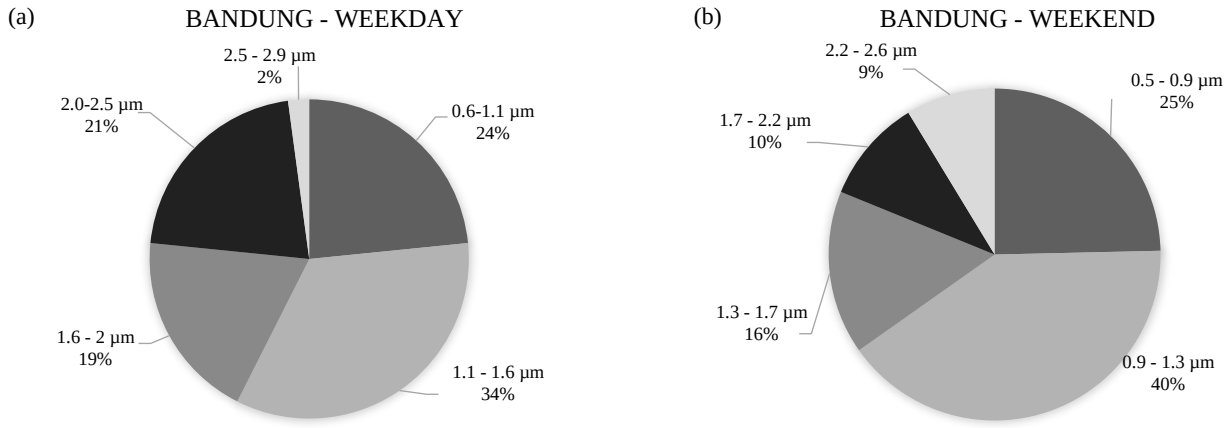

Figure 6. Size distribution of $PM_{2.5}$ collected on weekdays with total selected particle (n=78) (a) and weekends (n=80) (b) in the Bandung site

3.2.2 Morphology of $PM_{2.5}$ in Jakarta

Figure 7 presents the surface characterization of $PM_{2.5}$ in Jakarta. On weekdays, $PM_{2.5}$ particles were predominantly semi-crystalline tabular and elongated forms, while on weekends, they exhibited irregular, puff-like morphologies. In Jakarta sites, the particle size distribution for both weekdays and weekends is shown in Figure 8. The analysis involved measuring 127 particles on weekdays and 115 particles on weekends across various magnifications (2000x, 3000x, 4000x, 5000x, 8000x, 10000x). Results showed that on weekdays, 117 particles had diameters less than 2.5 µm, whereas 109 particles on weekends fell below this size threshold. Weekday $PM_{2.5}$ primarily comprised particles in the size range of 0.5-0.8 µm, whereas weekend particles were mostly in the 0.9-1.3 µm range. However, particle agglomeration was still observed on both weekdays and weekends, with diameters exceeding 2.5 µm.

The EDX spectra presented in Figures 7(a) and 7(b) for weekdays reveal that the tabular particles are mainly composed of carbonaceous material (C) and aluminosilicate minerals (Al, O, Si), along with trace amounts of sodium (Na), potassium (K), sulfur (S), and nitrogen (N), indicating contributions from urban/soil dust (Li et al., 2016), and vehicular emissions. Specifically, Figure 7(b) shows a sulfur-rich elongated particle, suggesting the presence of sulfate (SO_4) (Li et al., 2016). Additionally, both weekdays and weekends showed Teflon-related elements (C and F) and carbon species from $PM_{2.5}$. On weekdays, the EDX spectrum revealed sulfur mass percentages of 6.6% (Figure 7(a)) and 0.3% (Figure 7(b)).

During weekends, as shown in Figures 7(c) and 7(d), the EDX spectra also identified aluminosilicates (Al, O, Si), salt (Na, Cl), magnesium (Mg), sulfur (S), and potassium (K). Figure 7(c) illustrates aggregates containing Na, S, and O, indicative of sodium sulfate (Na_2SO_4) (Li et al., 2016). Notably, the EDX spectrum for a specific SEM image area on weekends showed elevated aluminum (Al) and silicon (Si) levels, with mass percentages of 8.2% for Al and 9.4% for Si (Figure 7(d)).

A more comprehensive elemental profile of Jakarta's $PM_{2.5}$, obtained through EDXRF analysis, is depicted in Figure 11(b). The presence of sulfur (S) and potassium (K) in $PM_{2.5}$ indicates contributions from both biomass burning (K) and gasoline-powered vehicles (S) (Santoso et al., 2014). Compared to Bandung and Tangerang, Jakarta's $PM_{2.5}$ uniquely features NaCl minerals in tabular and irregular forms, likely originating from sea salt due to its proximity to local rivers and its location approximately 11 km north of Ancol Beach (Li et al., 2016).

3.2.3 Morphology of $PM_{2.5}$ in Tangerang

The morphology of $PM_{2.5}$ particles collected in Tangerang is illustrated in Figure 9. Analysis revealed that during weekdays, the $PM_{2.5}$ particle in Tangerang tends to have facetted morphology with relatively small particle size. The particle size distribution for Tangerang is shown in Figure 10, based on measurements of 142 particles on weekdays and 91 particles on weekends. On weekdays, all 120 particles had diameters below 2.5 µm, while on weekends, 65 out of 91 particles were under this size threshold. Weekday $PM_{2.5}$ was predominantly composed of particles in the size range of 0.5-1.3 µm, while weekend particles were mostly in the 0.9-1.4 µm range. However, particle agglomeration still occured on both weekdays and weekends, with diameters exceeding 2.5 µm.

On weekends, the particles were observed to have irregular, agglomerated shapes. Both weekday and weekend samples contained carbonaceous particles (C), including carbonates (Ca, O, C), and sulfur (S)-rich particles.

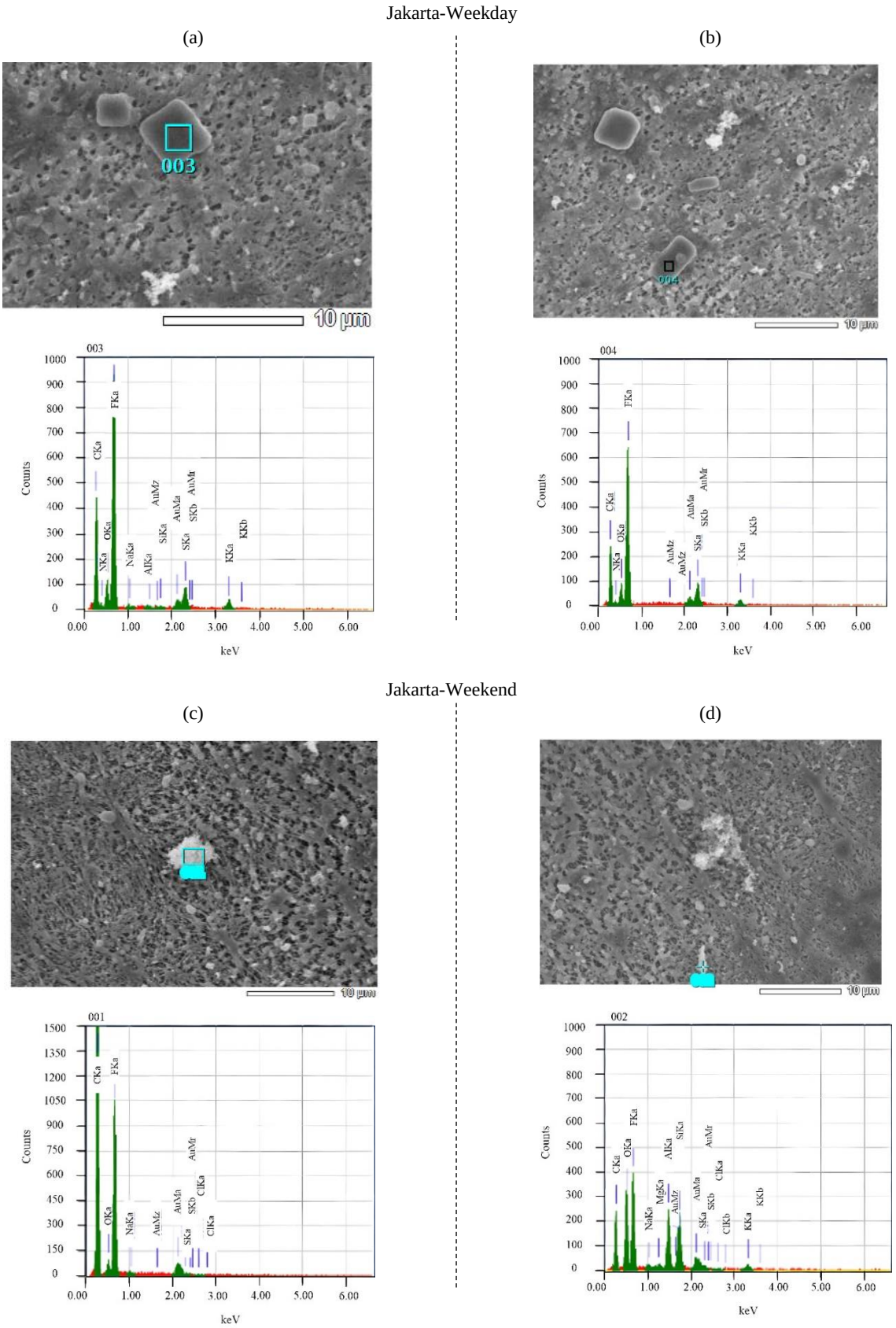

Figure 7. Morphology and EDX spectrum of $PM_{2.5}$ in Jakarta on weekdays at 3000x on area 3 (a) and area 4 (b) and weekends at 3000x magnification on area 1 (c) and area 2 (d).

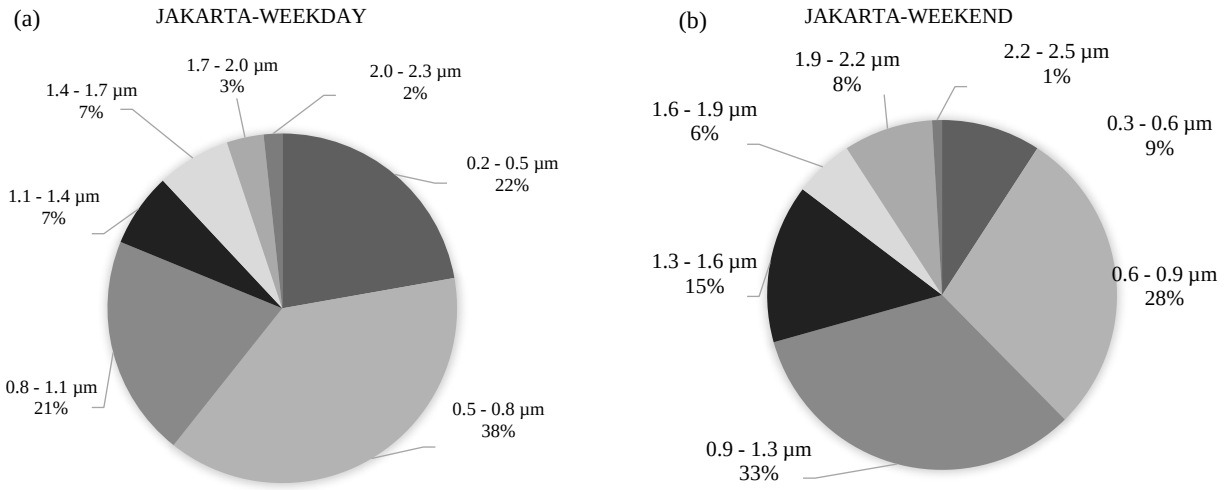

Figure 8. Size distribution of $PM_{2.5}$ collected on weekdays with total selected particles (n=127) (a) and weekends (n=115) (b) in Jakarta site

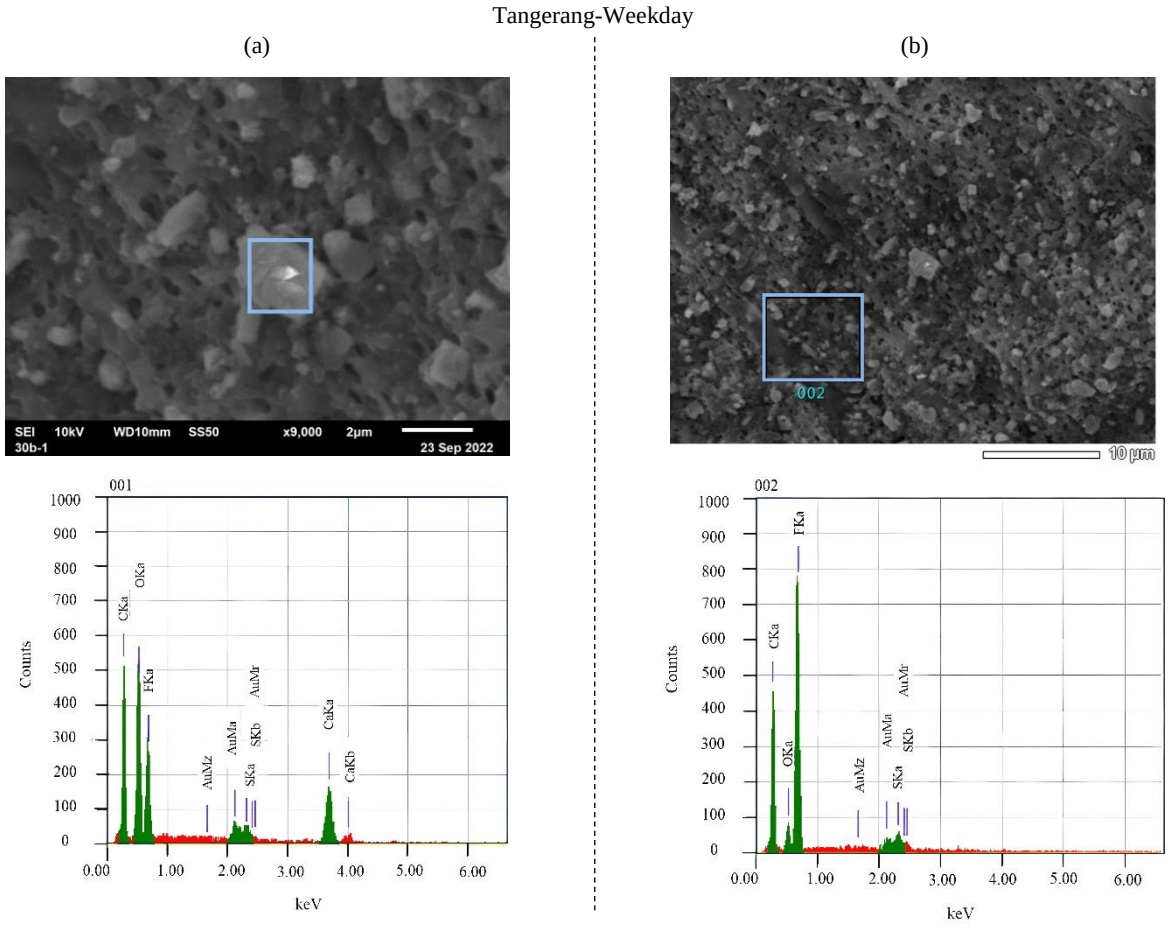

Figure 9. Morphology and EDX spectrum of $PM_{2.5}$ in Tangerang on weekdays at 9000x (a) and 3000x (b), on weekends on 9000x (c) and 8000x (d) magnification

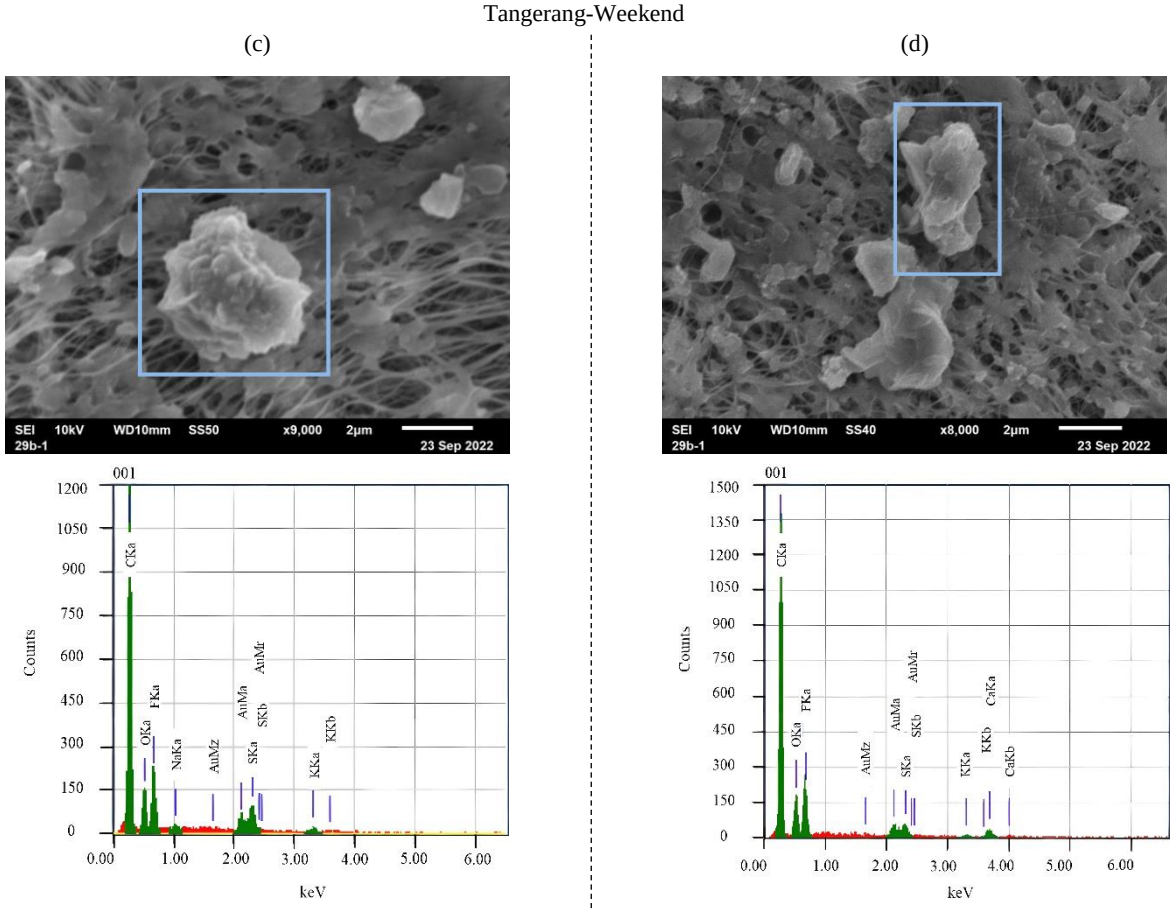

Figure 9. Morphology and EDX spectrum of $PM_{2.5}$ in Tangerang on weekdays at 9000x (a) and 3000x (b), on weekends on 9000x (c) and 8000x (d) magnification (cont.)

The EDX spectra for Tangerang provide detailed elemental composition data for specific areas, as shown in Figures 9(a), 9(b), and 9(d). Both weekday and weekend samples exhibited the presence of Teflon-related elements (C and F) and carbon species. On weekdays, significant levels of calcium (Ca) and sulfur (S) were observed, with Ca content measuring 16.2% (Figure 9(a)) and S content at 3% (Figure 9(b)). On weekends, Ca content increased to 33% (Figure 9(d)), while S content was 4% (Figure 9(d)).

The predominance of sulfur (S), calcium (Ca), and oxygen (O) on weekdays, and sulfur (S), sodium (Na), potassium (K), and oxygen (O) on weekends, suggests that the faceted morphology of the particles is influenced by emissions from coal power plants (Li et al., 2016). During weekends, the presence of soil dust particles, characterized by S-rich components along with K and Na from soot, indicates contributions from heavy-duty vehicles (Santoso et al., 2014) and biomass burning (Fatima et al., 2022). These particles exhibited near-spherical, amorphous, and aggregate forms. The elemental composition of $PM_{2.5}$ in Tangerang, including additional details, is further depicted in Figure 11(c).

3.3 Elemental characterization of $PM_{2.5}$ by ED-XRF

3.3.1 Elemental composition of $PM_{2.5}$ in Bandung

The elemental concentration of $PM_{2.5}$ at the Bandung site was calculated following the methodology explained in section 2.3.2. The elemental composition of $PM_{2.5}$ is illustrated in Figure 11(a) and is consistent with the results obtained from EDX analysis. The data reveals that both weekdays and weekends show significant concentrations of various elements on the Teflon filters, with sulfur (S), potassium (K), iron (Fe), sodium (Na), aluminum (Al), and silicon (Si) being the predominant elements. Additionally, heavy metals such as lead (Pb), zinc (Zn), titanium (Ti), and copper (Cu) were detected in the $PM_{2.5}$ samples. The major concentrations of Al, Si, and Ca were regarded as soil dust sources (Santoso et al., 2008b).

In Bandung, the elevated levels of sulfur (S) and potassium (K) are linked to open burning and biomass combustion, as local residents frequently burn trash and wood for cooking and heating. Notably, the sulfur content is higher on weekends (3,256 ng/m^3) than on weekdays (1,798 ng/m^3), which is likely due to increased local vehicle emissions around the sampling site, as detailed in the gravimetric analysis of Bandung. Additionally, natural sources such as the Tangkuban Perahu volcano, located approximately 30 km north of Bandung in the Lembang area, may also contribute to the elevated sulfur levels (Santoso et al., 2008b). Interestingly, despite the local government's prohibition of leaded gasoline since July 2006, which led to a significant reduction in Pb concentrations over the years (from 12.69 ng/m^3 in 2012) (Santoso et al., 2014). The $PM_{2.5}$ in Bandung still shows a relatively high lead content of 100 ng/m^3. This anomaly suggests that further investigation into the sources and persistence of high Pb levels in Bandung is warranted.

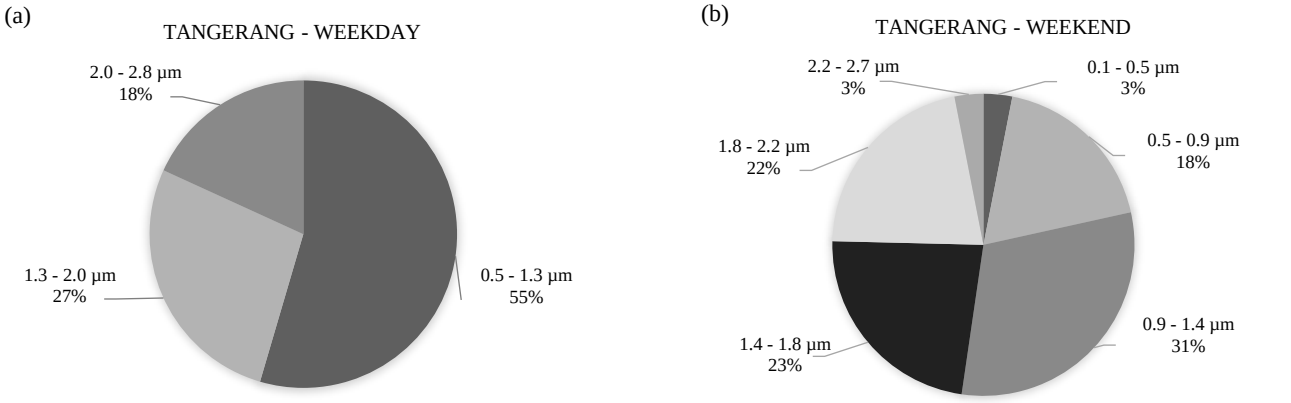

Figure 10. Size distribution of $PM_{2.5}$ collected on weekdays with total selected particles (n=142) (a) and weekends (n=91) (b) in Tangerang site

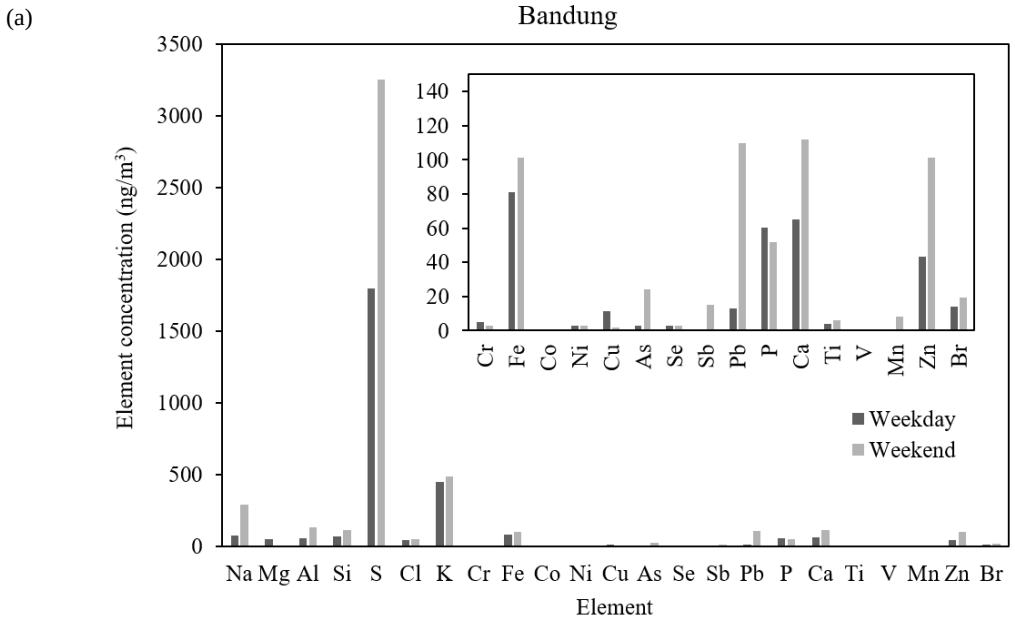

Figure 11. The elemental concentration of $PM_{2.5}$ in Bandung (a), Jakarta (b), and Tangerang (c) on weekdays and weekends with the highest $PM_{2.5}$ concentration during the sampling period.

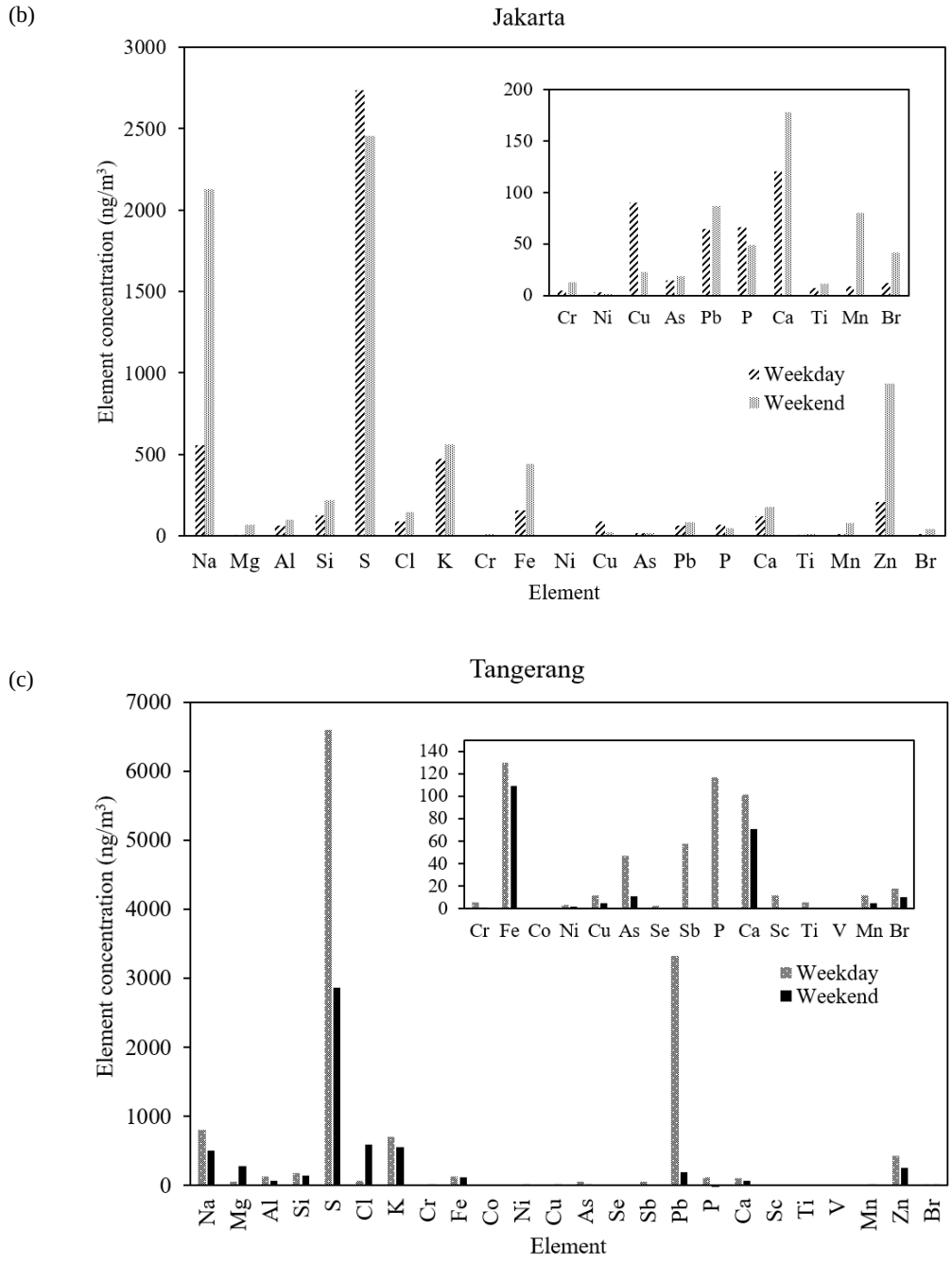

Figure 11. The elemental concentration of $PM_{2.5}$ in Bandung (a), Jakarta (b), and Tangerang (c) on weekdays and weekends with the highest $PM_{2.5}$ concentration during the sampling period (cont.).

3.3.2 Elemental composition of $PM_{2.5}$ in Jakarta

The elemental concentration of $PM_{2.5}$ at the Jakarta site was calculated following the methodology explained in section 2.3.2. The elemental composition is detailed in Figure 11(b). The analysis indicates that sulfur (S), sodium (Na), potassium (K), zinc (Zn), and iron (Fe) are the most concentrated elements. Other elements, including aluminum (Al), magnesium (Mg), silicon (Si), copper (Cu), arsenic (As), lead (Pb), phosphorus (P), calcium (Ca), manganese (Mn), and bromine (Br), were detected but in lower concentrations (below 300 ng/m³). The high levels of Al, Si, Ca, and Fe are attributed to soil dust sources (Santoso et al., 2013). Sulfur concentration is notably elevated at 2,734 ng/m³ on weekdays, likely due to the high density of motor and diesel vehicles in the area (Santoso et al., 2013), as discussed in the gravimetric section. The reduced sulfur levels on weekends are associated with decreased vehicle activity due to the closure of offices. Arsenic (As) is present, possibly originating from coal-burning power plants located approximately 11 km from the sampling site. The medium levels of sodium

(Na) and chlorine (Cl) are attributed to sea salt, as evidenced by the presence of NaCl minerals in Jakarta's $PM_{2.5}$ morphology (Hopke et al., 2020), as evidenced by the presence of NaCl mineral in Jakarta's morphology in Figure 7. Although lead (Pb) is detected, its concentration in Jakarta is lower compared to Tangerang, suggesting that Pb may be transported from Tangerang by wind (Santoso et al., 2011). The presence of lead (Pb) and copper (Cu) on weekdays is likely due to brake wear in urban environments (Khobragade and Ahirwar, 2023), while manganese (Mn) and zinc (Zn) are typically associated with crustal sources (Liu et al., 2018).

3.3.2 Elemental composition of $PM_{2.5}$ in Tangerang

The elemental concentration of $PM_{2.5}$ at Tangerang site was analyzed according to the methodology explained in section 2.3.2. Figure 11(c) reveals that the highest concentrations of elements include sulfur (S), lead (Pb), sodium (Na), potassium (K), and zinc (Zn), with variations observed when compared to Jakarta and Bandung. The high Sulfur concentrations observed on weekdays are primarily attributed to emissions from heavy-duty vehicles, given that the sampling site is situated along a busy inter-provincial route. On weekends, the reduction in vehicular traffic leads to a notable decrease in Sulfur levels, approximately 50% lower than on weekdays. Additionally, the high Sulfur content in Tangerang is further linked to emissions from coal-burning power plants located around 40 km north of Tangerang, as evidenced by the presence of arsenic (As) from these combustion sources (Wang et al., 2018). The exceptionally high lead (Pb) concentration in Tangerang is attributed to non-formal lead smelting industries in the vicinity (Santoso et al., 2011). This source of Pb contributes significantly to the elevated levels observed at the site.

4. CONCLUSION

CONCLUSIONThe morphological analysis reveals distinct characteristics in $PM_{2.5}$ particles across different sites. At Bandung, $PM_{2.5}$ particles exhibit amorphous surfaces with irregularly agglomerated and flaky shapes. Jakarta's $PM_{2.5}$ particles are noted for their semi-crystalline, tabular, and elongated forms, along with puff-like structures. In Tangerang, the particles are primarily irregularly faceted and agglomerated. EDX spectra from all sites indicate the presence of carbonate minerals (C, O, Ca) in $PM_{2.5}$. Calcium-rich particles are specifically observed in Bandung, while Sulfur-rich particles are detected in Jakarta and Tangerang. Additionally, fingerprint elements corresponding to specific pollution sources have been successfully identified through ED-XRF analysis. The integration of SEM-EDX and ED-XRF methodologies provides a comprehensive understanding of the $PM_{2.5}$ composition, offering valuable insights into the particle characteristics. However, further analysis could be conducted to deeply analyze each pollution source at each site.

ACKNOWLEDGEMENTS

This research is supported through RIIM Kompetisi funding from Indonesia Endowment Fund for Education Agency, Ministry of Finance of the Republic Indonesia and National Research and Innovation Agency of Indonesia (BRIN) program in 2022-2024 with contract number No:B-811/II.7.5/FR/6/2022 and No: B-2103/III.2/HK.04.03/7/2022 and Dr. Muhayatun as the person in charge. We also thanks to the Research Center for Nuclear Beam Analysis Technology, Research Organization for Nuclear Energy (ORTN). Feni Fernita Nurhaini, Pascale Ramadhan, and Muhayatun Santoso are the main contributors to this article.

REFERENCES

Adji EW. Number of Motorized Vehicles in Jakarta This Month: 24 Million Units [Internet]. 2024. [cited 2024 Aug 14]. Available from: https://otodriver.com/berita/2024/jumlah-kendaraan-bermotor-di-jakarta-bulan-ini-24-jutaan-unit-jumdedgcnit (in Indonesian).

Arana A, Loureiro AL, Barbosa HMJ, Grieken R Van, Artaxo P. Optimized energy dispersive X-ray fluorescence analysis of atmospheric aerosols collected at pristine and perturbed Amazon Basin sites. X-Ray Spectrometry 2014;43:228-37.

Statistics Indonesia. Number of Motorized Vehicles by Regency [Internet]. 2022 [cited 2024 Aug 14]. Available from: https://banten.bps.go.id/ indicator/17/308/1//City and Type of Vehicle in Banten Province (Unit), 2020-2022 jumlah-kendaraan-bermotor-menurut-kabupaten-kota-danjenis-kendaraan-di-provinsi-banten.html (in Indonesian).

Statistics Indonesia. Statistical Yearbook of Indonesia 2023, [Internet]. 2023 [cited 2024 Aug 14]. Available from: https://www.bps.go.id/en/publication/2023/02/28/18018f9896f09f03580a614b/statistik indonesia-2023.html (in Indonesian).

Casuccio GS, Schlaegle SF, Lersch TL, Huffman GP, Chen Y, Shah N. Measurement of fine particulate matter using electron microscopy techniques. Fuel Processing Technology 2004;85(6-7):763-79.

Environmental Protection Agency (EPA). Particulate matter (PM) basics [Internet]. 2023 [cited 2023 Apr 29]. Available from: https://www.epa.gov/pm-pollution/particulate-matter-pm-basics#:~:text=PM2.5%3.

Environmental Protection Agency (EPA). Guidelines for the Application of SEM/EDX Analytical Techniques to Particulate Matter Samples. US Environmental Protection Agency; 2002. p. 1-102.

Fatima S, Mishra SK, Ahlawat A, Dimri AP. Physico-chemical properties and deposition potential of $PM_{2.5}$ during severe smog event in Delhi, India. International Journal of Environmental Research and Public Health 2022;19(22): Article No. 15387.

González LT, Rodríguez FEL, Sánchez-Domínguez M, Leyva-Porras C, Silva-Vidaurri LG, Acuna-Askar K, et al. Chemical and morphological characterization of TSP and $PM_{2.5}$ by SEM-EDS, XPS and XRD collected in the metropolitan area of Monterrey, Mexico. Atmospheric Environment 2016; 143:249-60.

Hopke PK, Cohen DD, Begum BA, Biswas SK, Ni B, Pandit GG, et al. Urban air quality in the Asian region. Science of the Total Environment 2008;404(1):103-12.

Hopke PK, Dai Q, Li L, Feng Y. Global review of recent source apportionments for airborne particulate matter. Science of the Total Environment 2020;740:Article No. 140091.

Institute for Health Metrics and Evaluation (IHME). Global Burden of Disease Study [Internet]. 2019 [cited 2024 Apr 29]. Available from: https://ourworldindata.org/grapher/disease-burden-by-risk-factor.

IQair. World's most polluted countries and regions [Internet]. 2023a [cited 2024 Apr 29]. Available from: https://www.iqair.com/world-most-polluted-countries.

IQair. World's most polluted cities [Internet]. 2023b [cited 2024 Apr 29]. Available from: https://www.iqair.com/world-most-pollutedcities?continent=59af92b13e70001c1bd78e53&country=Rqrg4reHqi8taY4re&state=&sort=-rank&page=1&perPage=50&cities=.

The Ministry of State Secretariat of Republic Indonesia. Annex VII. Protection and Management of Air Quality. Environmental quality standards. Goverment Regulation No. 22 of 2021 on Environmental Protection and Management 2021;(1):1-5 (in Indonesian).

Khobragade PP, Ahirwar AV. Chemical and morphological characterization of $PM_{2.5}$ samples collected over an urban industrial region Raipur, Chhattisgarh. Acta Geophysica 2023;71(6):3057-76.

Kurniawati S, Santoso M, Nurhaini FF, Atmodjo DPD, Lestiani DD, Ramadhani MF, et al. Assessing low-cost sensor for characterizing temporal variation of $PM_{2.5}$ in Bandung, Indonesia. Kuwait Journal of Science 2024;52(1):Article No. 100297.

Lestari P, Damayanti S, Arrohman MK. Emission Inventory of Pollutants (CO, SO_2, $PM_{2.5}$, and NO_X) in Jakarta Indonesia. IOP Conference Series: Earth and Environmental Science 2020;489(1):Artocle No. 012014.

Li CY, Ding M, Yang Y, Zhang P, Li Y, Wang Y, et al. Portrait and classification of individual haze particulates. Journal of Environmental Protection 2016;7(10):1355-79.

Liu Z, Gao W, Yu Y, Hu B, Xin J, Sun Y, et al. Characteristics of $PM_{2.5}$ mass concentrations and chemical species in urban and background areas of China: Emerging results from the CARE-China network. Atmospheric Chemistry and Physics 2018; 18(12):8849-71.

Manisalidis I, Stavropoulou E, Stavropoulos A, Bezirtzoglou E. Environmental and health impacts of air pollution: A review. Frontiers in Public Health 2020;8:1-13.

Met One Instruments I. Model SASS TM and SuperSASS TM $PM_{2.5}$ Ambient Chemical Speciation Samplers Field Operation Manual. Washington: Met One Instruments, Inc; 2001.

Mokbel K. Breath of danger: Unveiling $PM_{2.5}$'s stealthy impact on cancer risks. Anticancer Research 2024;44(4):1365-8.

Pallarés S, Gómez ET, Martínez Á, Jordán MM. Morphological characterization of indoor airborne particles in seven primary schools. International Journal of Environmental Research and Public Health 2020;17(9):1-13.

PANalytical B.V. Analysis of Solid Alternative Fuel Materials. The Netrherlands: Bruker; 2009.

PANalytical B.V. The Epsilon 5 Spectrometer. The Netherlands: Bruker; 2005.

Paoletti L, De Berardis B, Arrizza L, Passacantando M, Inglessis M, Mosca M. Seasonal effects on the physico-chemical characteristics of $PM_{2.1}$ in Rome: A study by SEM and XPS. Atmospheric Environment 2003;37(35):4869-79.

Permadi DA, Kim Oanh NT. Assessment of biomass open burning emissions in Indonesia and potential climate forcing impact. Atmospheric Environment 2013;78:250-8.

Ramdhan DH, Kurniasari F, Tejamaya M, Fitri A, Indriani A, Kusumawardhani A, et al. Increase of cardiometabolic biomarkers among vehicle inspectors exposed to $PM_{0.25}$ and compositions. Safety and Health at Work 2021;12(1):114-8.

Royani S, Santoso M, Lestiani DD, Sari DK, Anggraeni A. Optimization for method in determination of chlor concentration in $PM_{2.5}$ using Edxrf Epsilon 5 Sri. Indonesian Journal of Nuclear Science and Technology 2016;20(1):81-90.

Research Triangle Institute (RTI). Standard Operating Procedure for Particulate Matter (PM) Gravimetric Analysis. North Carolina: RTI International; 2008. p. 1-22.

Santoso M, Hopke PK, Damastuti E, Lestiani DD, Kurniawati S, Kusmartini I, et al. The air quality of Palangka Raya, Central Kalimantan, Indonesia: The impacts of forest fires on visibility. Journal of the Air and Waste Management Association 2022;72(11):1191-200.

Santoso M, Hopke PK, Hidayat A, Diah Dwiana L. Sources identification of the atmospheric aerosol at urban and suburban sites in Indonesia by positive matrix factorization. Science of the Total Environment 2008a;397(1):229-37.

Santoso M, Hopke PK, Hidayat A, Diah Dwiana L. Sources identification of the atmospheric aerosol at urban and suburban sites in Indonesia by positive matrix factorization. Science of the Total Environment 2008b;397(1-3):229-37.

Santoso M, Lestiani DD, Kurniawati S, Damastuti E, Kusmartini I, Atmodjo DPD, et al. Assessment of urban air quality in Indonesia. Aerosol and Air Quality Research 2020;20(10): 2142-58.

Santoso M, Lestiani DD, Kurniawati S, Damastuti E, Kusmartini I, Prakoso D, et al. Elemental composition of particulate matter air pollution collected around industrial area in East Java. IOP Conference Series: Earth and Environmental Science 2019;303:Article No. 012036.

Santoso M, Lestiani DD, Kurniawati S, Markwitz A, Trompetter WJ, Barry B, et al. Long term airborne lead pollution monitoring in Bandung, Indonesia. International Journal of PIXE 2014;24:151-9.

Santoso M, Lestiani DD, Markwitz A. Characterization of airborne particulate matter collected at Jakarta roadside of an arterial road. Journal of Radioanalytical and Nuclear Chemistry 2013;297(2):165-9

Santoso M, Lestiani DD, Mukhtar R, Hamonangan E, Syafrul H, Markwitz A, et al. Preliminary study of the sources of ambient air pollution in Serpong, Indonesia. Atmospheric Pollution Research 2011;2(2):190-6.

Sinaga D, Setyawati W, Cheng FY, Lung SCC. Investigation on daily exposure to $PM_{2.5}$ in Bandung City, Indonesia using low-cost sensor. Journal of Exposure Science and Environmental Epidemiology 2020;30(6):1001-12.

Siregar S, Idiawati N, Pan WC, Yu KP. Association between satellite-based estimates of long-term $PM_{2.5}$ exposure and cardiovascular disease: Evidence from the Indonesian Family Life Survey. Environmental Science and Pollution Research 2022;29(14):21156-65.

Stearns RC, Paulauskis JD, Godleski JJ. Endocytosis of ultrafine particles by A549 cells. American Journal of Respiratory Cell and Molecular Biology 2001;24(2):108-15.

Syahrial M. The Number of Vehicles in Bandung is Almost Equal to the Population, Transportation Experts Say Odd-Even Is Not a Solution [Internet]. 2023 [cited 2024 Aug 14]. Available from: https://bandung.kompas.com/read/2023/ 02/11/ 155004078/jumlah-kendaraan-di-kota-bandung-hampir-setara-populasi-penduduknya-pakar (in Indonesian).

The World Bank. Indonesia's Urban Story [Internet]. 2016 [cited 2024 Apr 29]. Available from: https://www.worldbank.org/en/ news/feature/2016/06/14/indonesia-urban-story#.

Wang C, Liu H, Zhang Y, Zou C, Anthony EJ. Review of arsenic behavior during coal combustion: Volatilization, transformation, emission and removal technologies. Progress in Energy and Combustion Science 2018;68:1-28.

World Population Review. Jakarta Population 2024 [Internet]. 2024a [cited 2024 Aug 14]. Available from: https://world populationreview.com/world-cities/jakarta-population.

World Population Review. Bandung Population 2024 [Internet]. 2024b [cited 2024 Aug 14]. Available from: https://world populationreview.com/world-cities/bandung-population.

World Population Review. Tangerang Population 2024, [Internet]. 2024c [cited 2024 Aug 14]. Available from: https://world populationreview.com/world-cities/tangerang-population.

Wu Z, Liu F, Fan W. Characteristics of PM_{10} and $PM_{2.5}$ at Mount Wutai Buddhism scenic spot, Shanxi, China. Atmosphere 2015;6(8):1195-210.

Yang L, Li C, Tang X. The impact of $PM_{2.5}$ on the host defense of respiratory system. Frontiers in Cell and Developmental Biology 2020;8:1-9.

Yue DL, Hu M, Wang ZB, Wen MT, Guo S, Zhong LJ, et al. Comparison of particle number size distributions and new particle formation between the urban and rural sites in the PRD region, China. Atmospheric Environment 2013;76:181-8.

Environment and Natural Resources Journal

Volume 22
Issue 6
2024

A Two-Stage Feature Selection Method to Enhance Prediction of Daily $PM_{2.5}$ Concentration Air Pollution

Siti Khadijah Arafin[1], Ahmad Zia Ul-Saufie[1], Nor Azura Md Ghani[1], and Nurain Ibrahim[1,2*]

[1]School of Mathematical Sciences, College of Computing, Informatics and Mathematics, Universiti Teknologi MARA, Shah Alam, Selangor, Malaysia
[2]Institute for Big Data Analytics and Artificial Intelligence (IBDAAI), Kompleks Al-Khawarizmi, Universiti Teknologi MARA, Shah Alam, Selangor, Malaysia

ARTICLE INFO

Received: 28 Feb 2024
Received in revised: 9 Sep 2024
Accepted: 11 Sep 2024
Published online: 4 Nov 2024
DOI: 10.32526/ennrj/22/20240049

Keywords:
Adjusted correlation sharing t-test/ Air pollution/ Particulate matter $PM_{2.5}$/ Radial basis function neural network

*** Corresponding author:**
E-mail:
nurain@tmsk.uitm.edu.my

ABSTRACT

In recent decades, air pollution has negatively affected human health and the environment. One of the important features contributing to air pollution is called $PM_{2.5}$. However, daily prediction of $PM_{2.5}$ is still lacking, especially using feature selection infused into the model. Hence, the main objective of this research is to utilize the feature selection procedures by proposing two stages feature selection methods namely adjusted correlation sharing t-test (adjcorT) and radial basis function neural network (RBFNN) in identifying the important features. This consequently also helps enhance the prediction of daily $PM_{2.5}$ concentrations. Secondary data were obtained from the Department of Environment Malaysia (DOE) from 2018 until 2022 that consists of 5 years of air pollutant daily data. The results found that adjcorT-RBFNN identified the NO_2, $PM_{2.5}$, PM_{10}, CO, O_3, wind speed and SO_2 as important features. The finding revealed that the accuracy, sensitivity, specificity, precision, F1 score and AUROC value, for a day-ahead prediction in Shah Alam are 0.756, 0.801, 0.717, 0.717, 0.757, and 0.758 respectively. Additionally, the predicted model may serve as an instrument for an early warning system, providing local authorities with information on air quality for formulation of strategies of air quality improvement.

1. INTRODUCTION

Air is the mixture of gases that surrounds the Earth and extends into its atmosphere. About 78% of it is nitrogen, 21% is oxygen, and the remaining other gases such as argon, carbon dioxide, and water vapor. Since air contains the oxygen that people, animals, and most other species require to breathe, it is essential for sustaining life on Earth. Air quality is important, where a low concentration of pollutants that endangers both human health and the environment is indicative of good air quality. Conversely, low air quality denotes high pollution concentrations. The air quality is typically assessed based on the concentration of various pollutants such as particulate matter ($PM_{2.5}$ and PM_{10}), nitrogen dioxide (NO_2), sulfur dioxide (SO_2), carbon monoxide (CO), ozone (O_3), and others.

The air quality is a growing concern worldwide. Air pollution has been shown to increase the risk and mortality of various pulmonary diseases, including lung cancer, chronic obstructive pulmonary disease (COPD), asthma, and infectious diseases such as pneumonia and tuberculosis, as evidenced by Ko and Kyung's (2022) research on its adverse effects on pulmonary diseases. There are serious risks to the environment and public health associated with air pollution, especially when fine particulate matter ($PM_{2.5}$) is present. $PM_{2.5}$ refers to particulate matter with a diameter of 2.5 micrometers or less, which is a major air pollutant and a significant component of air quality (Wang and Tian, 2018). Even at low concentrations, long-term exposure to PM2.5 has been shown to cause lung cancer (Ko and Kyung, 2022).

Citation: Arafin SK, Ul-Saufie AZ, Md Ghani NA, Ibrahim N. A two-stage feature selection method to enhance prediction of daily $PM_{2.5}$ concentration air pollution. Environ. Nat. Resour. J. 2024;22(6):500-509. (https://doi.org/10.32526/ennrj/22/20240049)

Accurate air quality prediction can channel strategically valuable information to the government for air pollution control and management. However, it is a challenging task to predict air quality movements as it is subject to big data elements, including many internal and external factors, and poses a big challenge to researchers who try to predict it (Sokhi et al., 2021; Zhao et al., 2022). Artificial Neural Network (ANN) has gained popularity in various fields due to its ability to solve non-linear problems and its potential for accurate predictions (Larasati et al., 2018). In the context of predicting air quality, ANN has been widely used due to its capability to build air quality models with comparable or better accuracy than other methods (Suleiman et al., 2019). Moreover, the Radial Basis Function Neural Network (RBFNN) has been utilized to predict air quality. The research conducted by Yadav and Nath (2018) comparing the predictive performance of RBFNN and Generalized Regression Neural Network (GRNN) models for the prediction of PM_{10} levels in Ardali Bazar, Varanasi, India, found that RBFNN performed better in measured and predicted PM_{10} values compared to GRNN. A study from Algeria claimed that RBFNN outperformed other models being compared in their study for electric consumption forecast (Kahoui and Chekouri, 2024). Another study also employed RBFNN with an optimization technique for classification purposes, and it obtained good classification performances (Ali et al., 2024).

Feature selection is crucial for predicting air quality due to the complex nature of the factors influencing air pollution. As there are numerous environmental factors involved in building a model, variable selection is used to effectively filter out the important variables that affect air quality. However, air quality data can indeed face multicollinearity issues due to the interrelationship of environmental variables. Several studies have highlighted the presence of multicollinearity in air quality data and its implications for statistical modelling. For instance, Farrell et al. (2019) highlighted the challenges posed by multicollinearity among covariates in statistical models for analyzing the effects of environmental factors on the spatial distribution of species. Hence, this study aims to predict the next day's air quality based on $PM_{2.5}$ concentrations while considering the multicollinearity issues between the features. Consequently, the important features will be identified, and these features can be used for the next day's air quality based on $PM_{2.5}$ prediction in the future, reducing the air pollution that exists in the air.

2. METHODOLOGY

2.1 Research framework

This section discusses the research framework as shown in Figure 1, the data, feature selection methods, classification modelling and model evaluation used in this research. Specifically, air quality data is extracted from the Department of Environment, Malaysia and data management was done on the respective dataset including data conversion, normalization and SMOTE. This research also aim to explore the collinearity among the features in air quality data followed by the feature selection procedures. Then, the proposed two stages adjcorT-RBFNN were compared to the adjcorT and RBFNN in the model evaluation. Finally, the best model are identified in this research.

Our research data consist of variables or pollutant factors involve in air quality data which is Particulate Matter (PM_{10} and $PM_{2.5}$), Carbon Monoxide (CO), Nitrogen Dioxide (NO_2), Ground-Level Ozone (O_3) and Sulphur Dioxide (SO_2) that due to the burning of natural gas, coal and wood, industries and vehicles. Besides pollutant factors, the meteorological parameters are wind direction, wind speed, relative humidity and ambient temperature taken as variables that might have an impact on the air quality. 43824 sample sizes of a dataset from air quality monitoring stations at Shah Alam, Selangor in hourly data format is obtained from the collaborators, which is the Department of Environmental (DOE) for duration of five-year period from 2018 to 2022. Table 1 shows the description of air quality data consisting of 10 variables obtained from the DOE.

2.2 Adjusted correlation sharing t-test

Adjusted correlation sharing t-test (adjcorT) is an extended variable selection method which is correlation sharing t-test (corT). The variable selection method, corT only considers positive relationships between the variables which might produce less accurate results (Ibrahim, 2020). However, the adjcorT method allows both positive and negative correlations between the variables from -1 to 1. The equation of adjcorT is displayed in (1):

$$r_i = \text{sign}\left(\frac{\bar{x}_{i1} - \bar{x}_{i0}}{s_i}\right) \times \left[\max_{(0 \le \rho \le 1)} \frac{1}{w} \sum_{j \in C_\rho(i)} |T_j|\right] \quad (1)$$

Where; max is the maximum. In addition, each variable is assigned a score r_i, which equals to the average of all t-statistics for variables having correlation (absolute) at least ρ with variable i, choosing the best value of ρ to maximize the average. AdjcorT is a filter feature selection method, and it is easy to use. This method is only applicable for continuous variables as it calculates the t-score of each variable and assesses the correlation with the other independent variables.

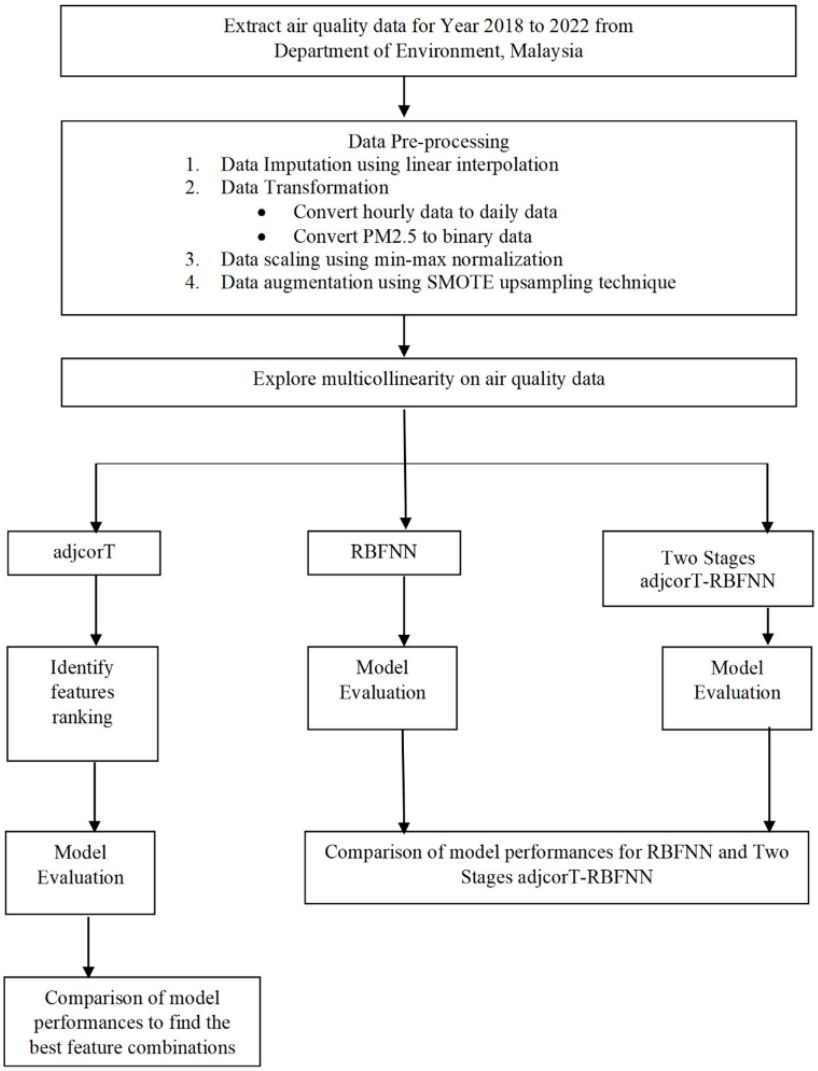

Figure 1. Research flowchart

Table 1. Air quality data description

Variable	Unit	Description
$PM_{2.5}$	($\mu g/m^3$)	Particulate matter 2.5 micrometres or less in diameters
PM_{10}	($\mu g/m^3$)	Particulate matter 10 micrometres or less in diameters
SO_2	(ppm)	Sulphur dioxide
NO_2	(ppm)	Nitrogen dioxide
O_3	(ppm)	Ground-level ozone
CO	(ppm)	Carbon monoxide
WD	(°)	Wind direction
WS	(m/s)	Wind speed
Humidity	(%)	Relative humidity
Temperature	(°C)	Ambient temperature

2.3 Radial basis function neural network

Radial Basis Function Neural Network (RBFNN) is a type of artificial neural network that uses radial basis functions as activation functions in its hidden layer. The input layer, hidden layer, and output layer are the three main layers of an RBFNN, and they are typically connected by weights. First, a source node, also known as the independent variable, connects the network to its surroundings in the input layer. Meanwhile, a nonlinear transformation from input space to a high-dimension hidden space takes place in the hidden layer. The RBF neurons in the hidden layer use Gaussian or other radial basis functions to compute their activations based on the distance between their centres and the input data. The final layer is called the output layer, which is the result of the network applied to the input layer, also known as the predicted output. The network's output is then created by combining and weighting these activations. RBFNNs can approximate complex functions with comparatively few parameters which are very helpful for tasks involving function approximation and pattern recognition. This method can effectively handle high-dimensional input spaces and is particularly useful when handling nonlinear relationships in data such as air quality data. Figure 2 shows the theoretical framework for RBFNN.

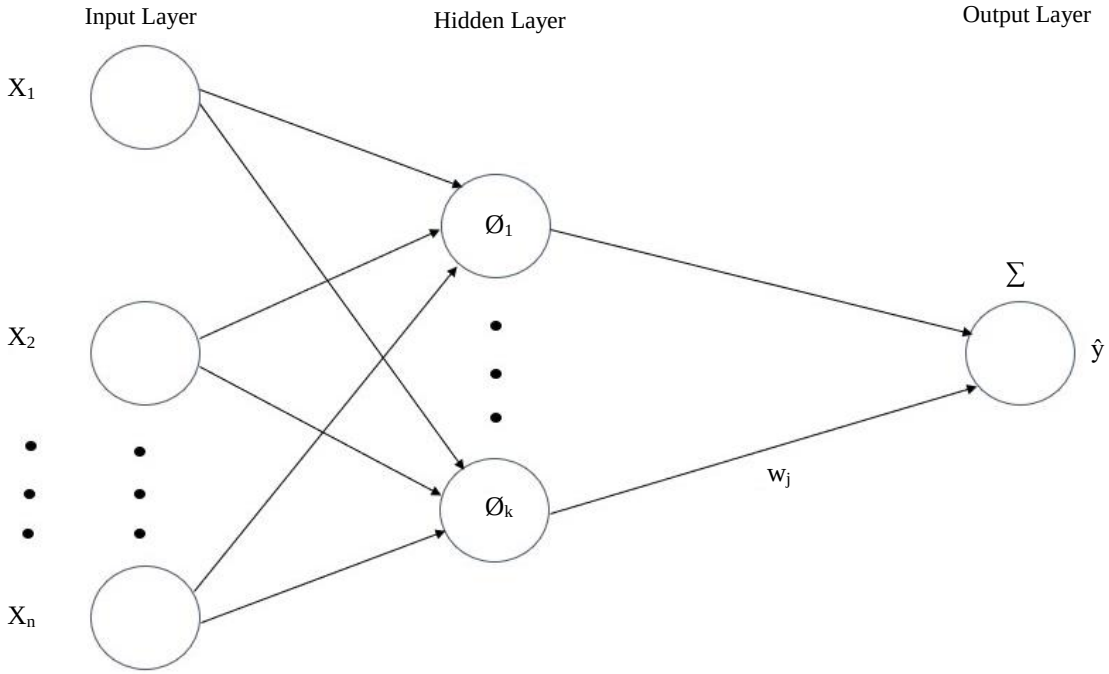

Figure 2. Theoretical framework for RBFNN (Wu, 1998)

2.4 Artificial neural network

An artificial neural network, or ANN, is a type of computational model that's design and operations are modelled after biological neural networks. It consists of networked nodes, sometimes known as "neurons," which work together to process and generate complex information. ANNs learn through by continuously modifying the connections among neurons, utilizing feedback to enhance predictions in comparison to intended results. This iterative learning process allows ANNs to gradually improve their capacity for prediction, also known as backpropagation.

2.5 Model evaluation

This research uses accuracy, sensitivity, specificity, precision, F1 score and Area Under the Receiver Operating Characteristic (AUROC) to evaluate the ANN classification model. Accuracy represents the proportion of correct predictions among the total predictions made by the model. To determine the accuracy of the model, the number of correct predictions is divided by the total number of predictions (Atif et al., 2023; Md Noh et al., 2023). Sensitivity, also known as the true positive rate, measures the proportion of actual positive cases that are correctly identified by the model (Zhang-James et

al., 2023). While specificity, or the true negative rate, quantifies the proportion of actual negative cases that are correctly identified by the model (Oboya et al., 2023). Precision measures the proportion of true positive predictions among all positive predictions made by the model (Holakoei and Sajedi, 2023). The F1 score is the harmonic mean of precision and sensitivity, providing a balance between the two metrics (Peng et al., 2023). Lastly, the AUROC measures a classifier's ability to discriminate between groups (Weng et al., 2023).

3. RESULTS AND DISCUSSION

3.1 Results

This section presents and analyses the results obtained from our study, delving into the implications and significance of our findings. Table 2 shows missing values of variables in Shah Alam from the period 2018 to 2022. All variables have missing values below 8% except NO_2 with 12.65% of missing values. In this research, we use linear interpolation method to impute the missing values in the hourly dataset.

Table 2. Percentage of missing values

Variable	N	Missing value
$PM_{2.5}$	43,257	567 (1.29%)
PM_{10}	43,151	673 (1.54%)
SO_2	41,242	2582 (5.89%)
NO_2	38,280	5544 (12.65%)
O_3	41,198	2626 (5.99%)
CO	40,629	3195 (7.29%)
WD	42,925	899 (2.05%)
WS	42,868	956 (2.18%)
Humidity	42,907	917 (2.09%)
Temperature	42,926	898 (2.05%)

3.2 Data pre-processing

Data transformation and data cleaning are parts of the data pre-processing to improve the quality of the dataset. To facilitate the process of predicting $PM_{2.5}$ category for the following day ($PM_{2.5Dt1}$), the hourly dataset is converted to daily dataset. The $PM_{2.5}$ breakpoints (24-hour average) in the Table 3 below are based on the U.S. Environmental Protection Agency (EPA) that aims to protect public health from the harmful effects of fine particle pollution. Since our goal is to forecast the $PM_{2.5Dt1}$ category, we adopted a binary classification framework for air pollution prediction, where Air Quality Index (AQI) categories "good" and "moderate" were combined to represent the "not polluted" class, while the others AQI categories were grouped into the "polluted" class, following Kalajdjieski et al. (2020).

According to the descriptive statistics of independent variables in Table 4, the standard deviations range from 0 to 11.712. Data normalization was applied since it is clear that different scales were observed across variables in this study by using min-max normalization similar to a study by Du et al. (2019) on hybrid deep learning framework for air quality prediction. Besides, the histogram of the $PM_{2.5Dt1}$ category shows that the distribution of the category is not balanced as shown in Figure 3. Thus, this research also applied Synthetic Minority Over-sampling Technique (SMOTE) to balance the datasets.

Table 3. Binary labels for the respective $PM_{2.5}$ breakpoint and AQI categories

AQI category	$PM_{2.5}$ breakpoints	Binary labels
Good	0.0-12.0	Not polluted
Moderate	12.1-35.4	Not polluted
Unhealthy for sensitive groups	35.5-55.4	Polluted
Unhealthy	55.5-150.4	Polluted
Very unhealthy	150.5-250.4	Polluted
Hazardous	250.5 and above	Polluted

Table 4. Descriptive statistics before data pre-processing

Variable	N	Mean	Median	Std. Dev.	Skewness	Min	Max
$PM_{2.5}$	1,825	23.321	21.187	11.712	4.142	5.466	144.917
PM_{10}	1,825	32.554	30.244	13.739	3.086	7.184	156.553
SO_2	1,825	0.001	0.001	0.000	1.330	0.000	0.001
NO_2	1,825	0.015	0.015	0.005	0.308	0.002	0.037
O_3	1,825	0.020	0.019	0.007	0.800	0.002	0.060
CO	1,825	0.770	0.754	0.266	0.447	0.148	1.967
WD	1,825	206.597	205.583	48.507	0.106	86.023	317.928
WS	1,825	0.820	0.783	0.240	1.468	0.386	2.504
Humidity	1,825	80.138	80.109	6.603	-0.151	56.347	99.155
Temperature	1,825	27.552	27.573	1.247	-0.155	22.310	31.939

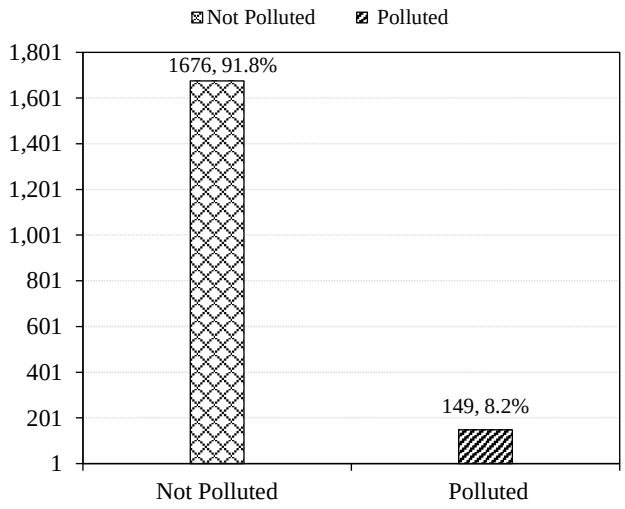

Figure 3. $PM_{2.5Dt1}$ distribution (Before SMOTE)

Descriptive statistics in Table 5 shows significant changes following the application of SMOTE and data normalization. Now, all mean, median values are within the range of 0 and 1 indicates that scaling to a standard range has been achieved. Following normalization, standard deviations have dropped, suggesting less variability among variables. In general, the values of skewness are closer to value 0, indicating a more balanced distribution. Figure 4 displayed the $PM_{2.5Dt1}$ distribution after SMOTE up sampling was applied to the dataset. It shows that both categories have a consistent number of sample sizes in which 1,676 (50.6%) are not polluted and 1,639 (49.4%) are polluted. Meanwhile, Figure 5 shows other features' distribution after the data pre-processing applied to the dataset. There are bell-shaped distributions for all features except for $PM_{2.5}$, PM_{10}, SO_2 and wind speed. By addressing issues of class imbalance and ensuring fair comparison across features, these transformations improve the dataset's suitability for developing precise predictive models.

Table 5. Descriptive statistics after data pre-processing

Variable	N	Mean	Median	Std. Dev.	Skewness	Min	Max
$PM_{2.5}$	3,315	0.176	0.144	0.142	3.239	0	1
PM_{10}	3,315	0.219	0.190	0.146	2.820	0	1
SO_2	3,315	0.227	0.215	0.100	1.332	0	1
NO_2	3,315	0.426	0.423	0.165	0.279	0	1
O_3	3,315	0.333	0.315	0.130	1.301	0	1
CO	3,315	0.395	0.388	0.165	0.512	0	1
WD	3,315	0.522	0.510	0.183	0.078	0	1
WS	3,315	0.214	0.201	0.100	1.174	0	1
Humidity	3,315	0.520	0.517	0.146	0.025	0	1
Temperature	3,315	0.559	0.565	0.118	-0.253	0	1

3.3 Correlation between features

The correlation between the features were examined in order to explore the correlation between features in the air quality data. The spearman correlation matrix provides insight into the relationships between the features. Values closer to 1 denote a strong positive correlation, while values closer to -1 denote a strong negative correlation, and

values around 0 suggest no linear correlation between the independent variables. Based on the spearman correlation matrix output, there is a strong positive correlation between $PM_{2.5}$ and PM_{10} which is 0.97, indicating a significant association between these two pollutants. Similarly, NO_2 and O_3 have a fairly positive correlation (0.66), which illustrates moderate positive relationship between these two variables. Conversely, humidity shows a significant negative correlation (-0.8) with temperature, indicating a strong negative relationship between these meteorological variables. Other correlation values are not showing any multicollinearity issue exists seriously in the air quality data.

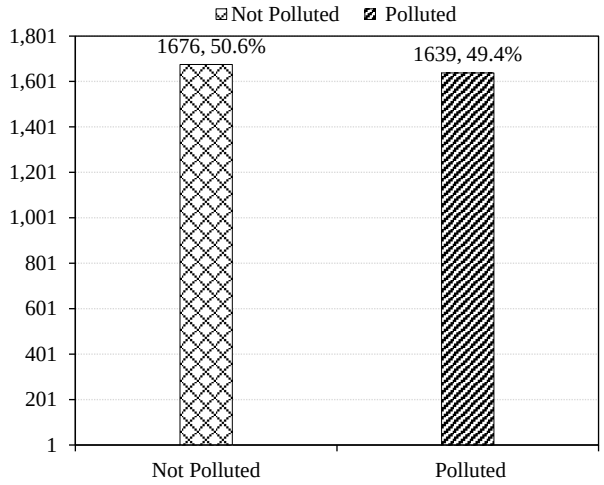

Figure 4. $PM2.5_{Dt1}$ distribution (After SMOTE)

3.4 Optimizing feature selection

The adjcorT values were ranked, the higher the value indicates the more significant the variable for developing a new model to predict the category of $PM_{2.5D+1}$ in Shah Alam, Selangor. As shown in Figure 5, the most important variable to predict $PM_{2.5D+1}$ is NO_2 while the least important variable is temperature with adjcorT value 23.81 and 14.99 respectively. By adding features one by one to the ANN model based on features ranking, we can determine the number of optimized features to predict $PM_{2.5D+1}$. The number of hidden nodes used for the ANN are followed as suggestion by Ul-Saufie et al. (2022), number of hidden nodes=(number of attributes + number of classes) / 2+1, while the learning rate values are set to 0.01. Based on the performance of ANN model in Table 6, the accuracy, sensitivity, specificity, precision and F1 score shows that the optimize features to predict $PM_{2.5D+1}$ is top 8 variables ranked by adjcorT method which is NO_2, $PM_{2.5}$, PM_{10}, CO, O_3, WS and SO_2. Figure 6 displays the various performances in a line charts for a clearer comparison view.

3.5 Model comparison

This research used RBFNN to verify the number of optimized features to predict $PM_{2.5D+1}$. The number of hidden nodes used for RBFNN and adjcorT-RBFNN model are 7 and 6 respectively as suggested by Ul-Saufie et al. (2022), number of hidden nodes = (number of attributes + number of classes) / 2 + 1, while the learning rate values are set to 0.01. Table 7 and Bar graph in Figure 7 shows the performance of the RBFNN model when using all 10 variables and using top 8 variables provided by adjcorT values ranking. We can conclude that the model using the top 8 variables in adjcorT-RBFNN outperformed the traditional RBFNN with higher accuracy, specificity, precision, F1 Score and AUROC which are 0.756, 0.801, 0.701, 0.757, and 0.758 respectively.

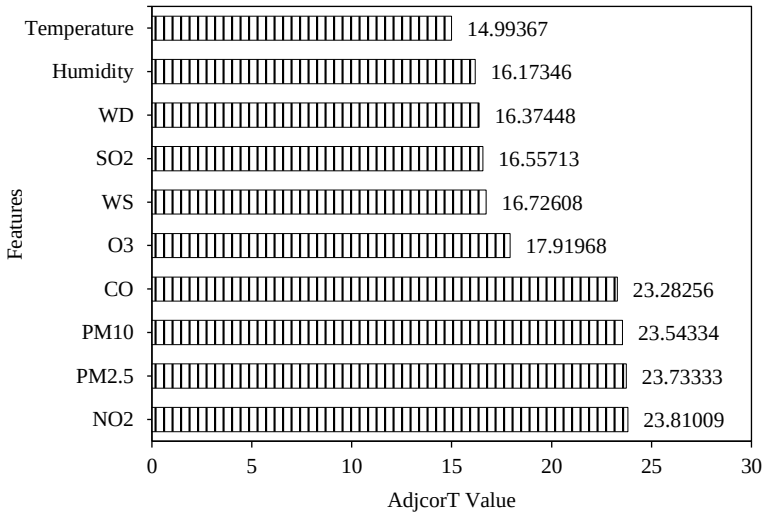

Figure 5. adjcorT values for each features

Table 6. Model performances for different numbers of features combination

No of features	1	2	3	4	5	6	7	8	9	10
Accuracy	0.67	0.75	0.76	0.76	0.75	0.80	0.78	0.81	0.80	0.80
Sensitivity	0.72	0.77	0.79	0.79	0.79	0.85	0.84	0.87	0.86	0.86
Specificity	0.63	0.73	0.73	0.74	0.71	0.75	0.73	0.76	0.75	0.76
Precision	0.63	0.73	0.73	0.74	0.71	0.75	0.73	0.76	0.75	0.76
F1 score	0.67	0.75	0.76	0.76	0.75	0.80	0.78	0.81	0.80	0.81
AUROC	0.67	0.75	0.76	0.76	0.75	0.80	0.78	0.81	0.80	0.81

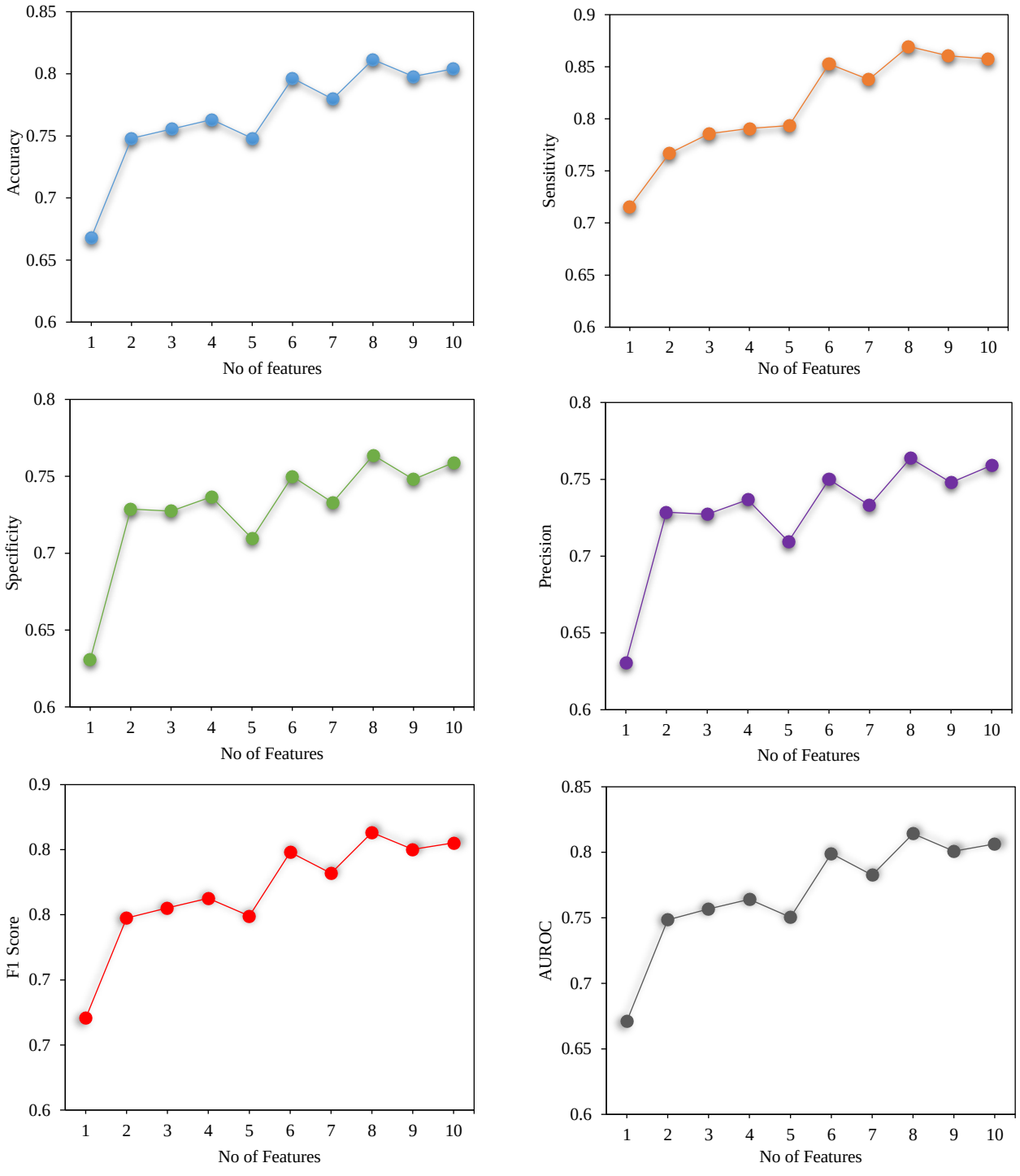

Figure 6. The model performances in different features combination included into the model

According to a study by Shaziayani et al. (2020), they found that combining SVM and BRT with feature selection techniques effectively reduced the prediction error and identified city-specific important variables for PM_{10} prediction. They found that the most important variables are PM_{10} followed by NO_2, CO, SO_2, relative humidity, temperature, and the least important is O_3 while wind speed is excluded from the model. Their findings have similarities with our research, in which all the important variables are the same with ours except the relative humidity and temperature. However, their research did not consider the multicollinearity issues in the air quality data since the researcher used other variable selection methods that did not consider the high correlation between the independent variables. Additionally, according to research by Afrin et al. (2021) has discovered wind speed and wind direction are the significant variables to predict $PM_{2.5}$ concentrations with 94% of total $PM_{2.5}$ variability explained by the model. Artificial neural networks have been used widely for prediction and classification including in air quality areas. A study by Hamami and Fithriyah (2020) focused on the classification of air pollution levels using artificial neural networks. They highlight the application of neural networks for air pollution classification into their model giving high accuracy, sensitivity and also specificity which is above 90%.

Table 7. RBFNN and adjcorT-RBFNN model performances

Model	RBFNN	adjcorT-RBFNN
Accuracy	0.753	0.756
Sensitivity	0.801	0.801
Specificity	0.712	0.717
Precision	0.712	0.717
F1 score	0.754	0.757
AUROC	0.755	0.758

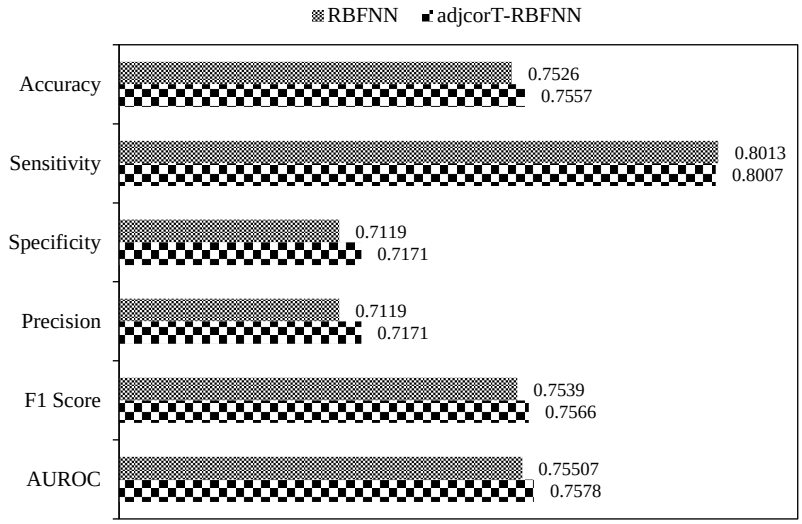

Figure 7. Horizontal Barchart of RBFNN and adjcorT-RBFNN model performances

4. CONCLUSION

This research utilizes the feature selection procedures especially on air quality data in enhancing prediction of $PM_{2.5}$. The result revealed that the model with two stages feature selection technique, adjcorT-RBFNN has proven to have better performance with higher accuracy, specificity, precision, F1 score and AUROC compared to RBFNN model. Ultimately, the daily $PM_{2.5}$ concentrations in Shah Alam may be anticipated using the proposed models. Additionally, the predicted model may serve as an instrument for an early warning system, providing local authorities with information on air quality for formulation of strategies of air quality improvement. In terms of the limitation, this study explored a comprehensive feature selection method applied on air quality data in Shah Alam, Selangor. However, further and in-depth studies may

be needed to confirm its effectiveness in different monitoring stations in Klang Valley. Future study may study other feature selection methods and other machine learning classification techniques to apply on the air quality data. In addition, these methods also can be applied to other data in different fields.

ACKNOWLEDGEMENTS

The authors would like to specially acknowledge the Ministry of Higher Education (MOHE) for funding under the Fundamental Research Grant Scheme (FRGS) (FRGS/1/2023/STG06/ UITM/02/8). We are also thankful to the Institute for Big Data Analytics and Artificial Intelligence (IBDAAI), Research Nexus UiTM (ReNeU) and College of Computing, Informatics and Mathematics, UiTM.

REFERENCES

Afrin S, Islam MM, Ahmed T. A meteorology based particulate matter prediction model for megacity Dhaka. Aerosol and Air Quality Research 2021;21(4):1-14.

Ali M, Khan F, Atta MN, Khan A, Khan A. Hybrid crow search and RBFNN: A novel approach to medical data classification. Journal of Informatics and Web Engineering 2024;3(1):252-64.

Atif M, Anwer F, Talib F, Alam R, Masood F. Analysis of machine learning classifiers for predicting diabetes mellitus in the preliminary stage. International Journal of Artificial Intelligence 2023;12(3):1302-11.

Du S, Li T, Yang Y, Horng SJ. Deep air quality forecasting using hybrid deep learning framework. IEEE Transactions on Knowledge and Data Engineering 2019;33(6):2412-24.

Farrell A, Wang G, Rush SA, Martin JA, Belant JL, Butler AB, et al. Machine learning of large-scale spatial distributions of wild turkeys with high-dimensional environmental data. Ecology and Evolution 2019;9(10):5938-49.

Hamami F, Fithriyah I. Classification of air pollution levels using artificial neural network. Proceedings of the International Conference on Information Technology Systems and Innovation; 2020 Oct 19-23; Bandung-Padang: Indonesia; 2020.

Holakoei HR, Sajedi F. Compressive strength prediction of SLWC using RBFNN and LSSVM approaches. Neural Computing and Applications 2023;35(9):6685-97.

Ibrahim N. Variable Selection Methods for Classification: Application to Metabolomics Data [dissertation]. University of Liverpool; 2020.

Kahoui H, Chekouri SM, Sahed A. A comparative study of ARIMA, RBFNN, and Hybrid RBFNN-ARIMA models for electricity net consumption forecasting in Algeria. Review of Socio-Economic Perspectives 2024;9(1):189-98.

Kalajdjieski J, Zdravevski E, Corizzo R, Lameski P, Kalajdziski S, Pires IM, et al. Air pollution prediction with multi-modal data and deep neural networks. Remote Sensing 2020; 12(24):1-9.

Ko UW, Kyung SY. Adverse effects of air pollution on pulmonary diseases. Tuberculosis and Respiratory Diseases 2022; 85(4):313-9.

Larasati A, Dwiastutik A, Ramadhanti D, Mahardika A. The effect of Kurtosis on the accuracy of artificial neural network predictive model. Proceedings of the MATEC Web of Conferences; 2018 Aug 30-31; Malang: Indonesia; 2018.

Noh SS, Ibrahim N, Mansor MM, Yusoff M. Hybrid filtering methods for feature selection in high-dimensional cancer data. International Journal of Electrical and Computer Engineering 2023;13(6):6862-71.

Oboya WM, Gichuhi AW, Wanjoya A. A Hybrid DNN-RBFNN model for intrusion detection system. Journal of Data Analysis and Information Processing 2023;11(04):371-87.

Peng HY, Duan SJ, Pan L, Wang MY, Chen JL, Wang YC, et al. Development and validation of machine learning models for nonalcoholic fatty liver disease. Hepatobiliary and Pancreatic Diseases International 2023;22(6):615-21.

Shaziayani WN, Ahmat H, Razak TR, Zainan Abidin AW, Warris SN, Asmat A, et al. A novel hybrid model combining the support vector machine (SVM) and boosted regression trees (BRT) technique in predicting PM_{10} concentration. Atmosphere 2022;13(12):1-17.

Sokhi RS, Moussiopoulos N, Baklanov A, Bartzis J, Coll I, Finardi S, et al. Advances in air quality research-current and emerging challenges. Atmospheric Chemistry and Physics Discussions 2021;22(7):4615-703.

Suleiman A, Tight MR, Quinn AD. Applying machine learning methods in managing urban concentrations of traffic-related particulate matter (PM_{10} and $PM_{2.5}$). Atmospheric Pollution Research 2019;10(1):134-44.

Ul-Saufie AZ, Hamzan NH, Zahari Z, Shaziayani WN, Noor NM, Zainol MR, et al. Improving air pollution prediction modelling using wrapper feature selection. Sustainability 2022;14(18):Article No. 11403.

Wang Z, Tian Z. Analysis of correlation between $PM_{2.5}$ and major pollutants by the method of path analysis. Proceedings of the International Symposium on Communication Engineering and Computer Science; 2018 Jul 28-29; Hohhot: China; 2018.

Weng S, Chen J, Ding C, Hu D, Liu W, Yang Y, et al. Utilizing machine learning algorithms for the prediction of carotid artery plaques in a Chinese population. Frontiers in Physiology 2023;14:1-12.

Yadav V, Nath S. Daily prediction of PM_{10} using radial basis function and generalized regression neural network. Proceedings of the Recent Advances on Engineering, Technology and Computational Sciences; 2018 Feb 6-8; Allahabad: India; 2018.

Zhang-James Y, Hoogman M, Franke B, Faraone SV. Machine learning and MRI-based diagnostic models for ADHD: Are we there yet? Journal of Attention Disorders 2023;27(4),335-53.

Zhao Z, Wu J, Cai F, Zhang S, Wang YG. A statistical learning framework for spatial-temporal feature selection and application to air quality index forecasting. Ecological Indicators 2022;144:1-16.

Environment and Natural Resources Journal

Volume 22
Issue 6
2024

Antioxidant Activity and Suppression of Intracellular Radical Generation of *Streptomyces* Strains and Genome Analysis of Strain ET3-23

Khaing Zar Wai[1], Nantiya Bunbamrung[2], Pattama Pittayakhajonwut[2], Nisachon Tedsree[3], Somboon Tanasupawat[4], and Rataya Luechapudiporn[5,6*]

[1]*Pharmaceutical Sciences and Technology Program, Faculty of Pharmaceutical Sciences, Chulalongkorn University, Bangkok 10330, Thailand*
[2]*National Center for Genetic Engineering and Biotechnology (BIOTEC), Thailand Science Park, Pathum Thani 12120, Thailand*
[3]*Faculty of Science and Arts, Burapha University, Chanthaburi Campus, Chanthaburi 22170, Thailand*
[4]*Department of Biochemistry and Microbiology, Faculty of Pharmaceutical Sciences, Chulalongkorn University, Bangkok 10330, Thailand*
[5]*Department of Pharmacology and Physiology, Faculty of Pharmaceutical Sciences, Chulalongkorn University, Bangkok 10330, Thailand*
[6]*Center of Excellence for Ageing and Chronic Diseases, Chulalongkorn University, Bangkok 10330, Thailand*

ARTICLE INFO

Received: 26 Feb 2024
Received in revised: 30 Aug 2024
Accepted: 17 Sep 2024
Published online: 5 Nov 2024
DOI: 10.32526/ennrj/22/20240047

Keywords:
Antioxidant activity/ Genome analysis/ RAW264.7 macrophage cells/ *Streptomyces*/ Soil

*** Corresponding author:**
E-mail:
rataya.L@pharm.chula.ac.th

ABSTRACT

Actinomycetes, predominantly found in soil, represent a remarkable source of natural products. The natural antioxidants obtained from them have been employed for human infectious diseases. In particular, *Streptomyces* strains serve as significant sources of natural antioxidants with demonstrated health benefits. The *in vitro* antioxidant activity and the inhibition of intracellular radical generation by crude extracts from various *Streptomyces* strains were evaluated and the genome sequence of selected strains was analyzed. Strains CT2-10, NE1-12, and ET3-23 showed 16S rRNA gene sequence similarity to *Streptomyces capoamus* JCM 4734^T (98.94%), *Streptomyces nigra* 452^T (99.78%), and *Streptomyces morookaense* LMG 20074^T (99.49%), respectively . The genome analysis of strain ET3-23 had 106 contigs, with a total length of 8121874 bp and an average G+C content of 71.46%. Ethyl acetate extracts of strains CT2-10, ET3-23, and NE1-12 exhibited, 1,1-diphenyl-2-picrylhydrazyl (DPPH) radical scavenging activity with IC_{50} 555.9 µg/mL, 66.5 µg/mL, and 463.3 µg/mL and showed NO scavenging activity, except for CT2-10. Strain NE1-12 significantly inhibited ROS production induced by hydrogen peroxide on macrophage cells, while strains NE1-12 and CT2-10 inhibited NO production induced by lipopolysaccharides with IC_{50} 82.4 µg/mL and 2.3 µg/mL, respectively. These findings suggest their ability to modulate NO production which is crucial in inflammatory responses and tissue injury. The antioxidant activities of *Streptomyces* strains indicate their potential as valuable sources of bioactive natural products and effective antioxidant agents, warranting further investigation for therapeutic applications.

1. INTRODUCTION

Soil is a complex habitat with a diverse range of organisms (EL-Kamali et al., 2017). Among these, microbes have been extensively explored as sources of bioactive natural products, essential for defense and survival in harsh environments. More than 95% of Actinomycetes strains have been isolated from soil, with *Streptomyces* being the dominant genus (Rammali et al., 2022).

Citation: Wai KZ, Bunbamrung N, Pittayakhajonwut P, Tedsree N, Tanasupawat S, Luechapudiporn R. Antioxidant activity and suppression of intracellular radical generation of *Streptomyces* strains and genome analysis of strain ET3-23. Environ. Nat. Resour. J. 2024;22(6):510-524. (https://doi.org/10.32526/ennrj/22/20240047)

Actinobacteria are Gram-positive bacteria with high G+C content, and the largest genus of actinobacteria is *Streptomyces*, belonging to the family *Streptomycetaceae* (Kämpfer, 2006). *Streptomyces* strains are renowned for producing numerous bioactive secondary metabolites such as antibiotic and antitumor agents (Hasani et al., 2014). Over 23,000 bioactive secondary metabolites have been isolated from microorganisms, and more than 10,000 of these compounds are from Actinomycetes, with nearly 7,600 produced by *Streptomyces* strains (Bérdy 2005).

In recent years, there has been increasing interest in the potential of *Streptomyces* strains as a source of natural antioxidants, which may have potential health benefits by preventing or reducing oxidative stress, a factor implicated in various diseases. Several studies have reported that extracts of the *Streptomyces* strain MUM292 from mangrove soil exhibited DPPH radical scavenging activities, highlighting its potential as an antioxidant agent (Tan et al., 2018). Actinomycin C2, benthocyanins, and carquinostatin isolated from *Streptomyces lavendulae* SCA5, *Streptomyces prunicolor*, and *Streptomyces exfoliates*, respectively have shown antioxidant activities (Karthik et al., 2013). Neocarazostatin A, B, and C from the culture of *Streptomyces* strain GP38 demonstrated inhibitory effects on lipid peroxidation induced by free radicals in rat brain homogenates (Kato et al., 1991) while pyrrolopyrazine-1,4-dione, hexahydro- from the extract of the novel *Streptomyces* strain MUSC149^{T} isolated from mangrove soil exhibited strong antioxidant activity by scavenging or reducing free radicals using the reducing power assay (Ser et al., 2015).

Nowadays, natural products from microorganisms have become a focus of modern research for safe therapeutics (Kim et al., 2014). Screening of natural products has concentrated on discovering and identifying bioactive metabolites based on genetic information to evaluate their biosynthetic potential (Ayuso-Sacido and Genilloud, 2005). This study investigated the antioxidant activity and intracellular radical suppression of various *Streptomyces* strains, with particular focus on the genome analysis of ET3-23. This research contributes to the identification of novel natural antioxidants and the development of therapeutic agents for oxidative stress-related diseases. The outcomes provide insights into the antioxidant potential of *Streptomyces* strains, their phenotypic characteristics, chemotaxonomic features for *Streptomycetes* classification, and their genetic features. The sequencing of specific genes also provides a deeper understanding of the phylogenetic relationships of these prokaryotes at the genus, species and subspecies level.

2. METHODOLOGY

2.1 Sample collection and isolation of actinomycetes

Soil samples were obtained from Nong Khai, Phichit, and Chachoengsao Provinces for actinomycete isolation. The collection involved sampling soil from a 5-10 cm depth beneath the surface. To facilitate the isolation process, the soil samples were air-dried, heated to 100°C, and treated with 1.5% phenol (Vargas Gil et al., 2009). Subsequently, serial dilutions (10^{-1}-10^{-4}) of these soil samples were prepared and spread plated onto a medium supplemented with humic acid and vitamins. Nalidixic acid and cycloheximide were included in the medium to prevent the growth of Gram- negative bacteria and fungi, respectively. The plates were then incubated at 30°C for 14 days to facilitate the growth and isolation of actinomycetes.

2.2 Identification methods of actinomycetes

Phenotypic characteristics were studied according to Shirling and Gottlieb (1966). Morphological characteristics were examined after cultivation on ISP 2 medium at 30°C for 7-14 days (Shirling and Gottlieb, 1966). The cell morphology of the selected isolate was observed using a scanning electron microscope (model JEOL JSM-IT500HR) after cultivation on ISP 3 medium at 30°C for 14 days. The colors of aerial and substrate mycelia and soluble pigments were determined using the NBS/ISCC color system (Kelly et al., 1965). Physiological characteristics were evaluated for the growth response of actinobacteria on ISP 2 medium at temperatures (28°C and 45°C), pH values (5, 7, and 10) and tolerance of NaCl concentration (2-6%) (Shirling and Gottlieb, 1966). Biochemical characteristics included starch hydrolysis, milk peptonization, milk coagulation, nitrate reduction, and gelatin liquefaction (Gordon, et al., 1974). The ability to produce acid from various carbon sources (L-arabinose, D-cellobiose, D-galactose, lactose, inositol, D-mannitol, D-maltose, D-raffinose, D-sorbitol, and D-xylose) were determined using standard methods (Shirling and Gottlieb, 1966).

Chemotaxonomic features were based on the diamino acid components in cell wall peptidoglycan. Cell wall type is the primary chemotaxonomic for identifying a strain to the genus level (Wai et al., 2022).

The diamino acid components as diaminopimelic acid (DAP) isomers in cell wall peptidoglycan were determined using the standard thin layer chromatography (TLC) method as described by Staneck and Roberts (1974). Dried cells were obtained from cultures grown in ISP 2 broth on an orbital shaker (180 rpm) at 30°C for 3-5 days. The cultured mycelium was washed with distilled water and then air-dried.

The genomic DNA was extracted from a pure culture inoculated in fresh ISP 2 broth at 30°C, 200 rpm for 2 days, and evaluated using physical and chemical combination methods (Tamaoka and Komagata 1984). The 16S ribosomal DNA was amplified from the extracted genomic DNA by sequencing with the universal primers 1492R (5´ACGGCTACC TTGTTACGACTT 3´) and 27F (5´AGTTTGATCCTGGCTCAG 3´) directions. The amplified PCR product was visualized by gel electrophoresis and purified and the obtained sequences were analyzed (Macrogen, Seoul, Korea) using EzTaxon-e server BLASTn searching program (http://www.ezbiocloud.net/eztaxon) and aligned against the selected type strain sequences received from GenBank using Bioedit software (Yoon et al., 2017).

2.3 Genome analysis

Genomic DNA was extracted using a PureLink™ Genomic DNA mini kit (Invitrogen; USA) and sequenced using the MiSeq sequencing system (Illumina; USA). The bioinformatics data of the genome were analyzed using the bacterial bioinformatics database and analysis resource (Seemann, 2014). The biosynthetic gene cluster in the genome was determined using the antiSMASH database (Bankevich et al., 2012). A phylogenetic tree based on genome data was constructed using the TYGS web server (Meier-Kolthoff and Göker, 2019).

2.4 Fermentation and preparation of ethyl acetate extracts

The spore suspensions of actinomycetes were inoculated into seed culture broth (100 mL) for 3 days and cultivated into ISP 2 broth (1,000 mL) at 37°C for 14 days. These fermentation broths were extracted with two volumes of ethyl acetate and cell suspension (2:1 v/v). The ethyl acetate extracts were evaporated to dryness before testing various biological activities (Janardhan et al., 2014).

2.5 Determination of total phenolic content

The total phenolic content (TPC) was determined through a reaction in which a phenol molecule released an H^+ ion, forming a phenolate ion capable of reducing the Folin-Ciocalteu (FC) reagent. In the assay, ethyl acetate extract, FC reagent, sodium bicarbonate, and DI water were sequentially added to a 96-well plate, incubated for 30 min at room temperature and measured with a microplate reader at 765 nm (Govindan and Muthukrishnan, 2013). Gallic acid was used as a positive control to establish a standard curve. The TPC was calculated and expressed as µg/gallic acid equivalent (GAE)/mg of extract.

2.6 Determination of ferric reducing antioxidant potency

The Fe^{3+}-reducing potential was determined by the reduction of ferric iron (Fe^{3+}) and 2,3,5-triphenyl-1,3,4-triaza-2-azoniacyclopenta-1,4-diene chloride (TPTZ) to the ferrous form (Fe^{2+}) at low pH 3.6, following the method described by Benzie and Strain (Sarma et al., 2010). Ethyl acetate extracts were incubated with the FRAP reagent at room temperature for 15 min and then measured at 593 nm. Ascorbic acid was used as a positive control. FRAP values were expressed as µg of ascorbic acid equivalent (AAE)/mg of extract (Bajpai et al., 2017).

2.7 DPPH radical scavenging activity assay

The scavenging activity against the 1,1-diphenyl-2-picryl hydrazyl (DPPH) radical was assessed following the method outlined by Brand-Williams et al. (1995) with slight modifications (Kawahara et al., 2012). Briefly, various concentrations (50- 1,000 µg/mL) of ethyl acetate extracts (100 µL) were mixed with 100 µL ethanolic DPPH solution (50 µM) and incubated at room temperature in the dark for 20 min. The absorbance was measured at 550 nm to calculate the DPPH radical scavenging ability.

2.8 Determination of nitric oxide (NO) scavenging

Nitric oxide generated from sodium nitroprusside (SNP) reacts with oxygen to produce nitrite ions, forming a purple chromophore through the Griess reaction (Hazra et al., 2009). Different concentrations (50- 1,000 µg/mL) of ethyl acetate extracts were incubated with sodium nitroprusside (10 mM) in phosphate buffer saline (pH 7.4) at 30°C for 2 h. Griess reagent was added and incubated for 15 min. The absorbance of the resulting purple azo chromophore was measured at 542 nm and then the NO

scavenging activity was calculated. Ascorbic acid was used as a positive control.

2.9 Cell cytotoxicity assay

RAW264.7 macrophage cells (ATCC TIB71) were seeded at a density of 2×10^5 cells per well and incubated for 24 h to allow cell attachment and growth. Ethyl acetate extracts at concentrations ranging from 50 to 1,000 µg/mL were added to the cells and further incubated for 24 h. The MTT reagent was then added and incubated for 3 h, followed by solubilization of the purple formazan crystals with DMSO (Chen et al., 2011). Absorbance was measured at 540 nm. All experiments were conducted in triplicate.

To induce intracellular radical generation, 100 µM hydrogen peroxide (H_2O_2) was utilized (Jung et al., 2006). Cells were treated with non-toxic concentrations (10-200 µg/mL) and (1-20 µg/mL) of ethyl acetate extracts and incubated for 24 h. Subsequently, the cells were incubated with 100 µM H_2O_2 for 30 min. After incubation, the MTT assay was performed as described earlier.

2.10 Determination of intracellular ROS generation in RAW264.7 macrophage cells

Intracellular reactive oxygen species (ROS) levels were assessed by monitoring the fluorescent signal generated from the oxidation of non-fluorescent 2′,7′-dichlorofluorescein diacetate (DCFH-DA) inside the cells. DCFH-DA is cleaved by esterase to form DCFH, which is then oxidized by ROS to produce the fluorescent compound DCF (Aranda et al., 2013). RAW264.7 macrophage cells were seeded at a density of 2×10^5 cells/mL in a black 96-well plate and incubated at 37°C for 24 h. Different concentrations (0.1-200 µg/mL) and (0.1-10 µg/mL) of ethyl acetate extracts in serum-free medium were added to the cells and incubated for 24 h. Then, 10 µM DCFH-DA in serum-free medium was added and incubated for 30 min. The cells were washed with PBS before intracellular ROS induction by adding 100 µM H_2O_2 for 30 min. Fluorescence intensities were measured using a fluorescence microplate reader at excitation and emission wavelengths of 485 nm and 530 nm, respectively (Chansriniyom et al., 2018).

2.11 Determination of nitric oxide production in RAW264.7 macrophage cells

Nitric oxide (NO) production was assessed by measuring nitrite levels using the Griess reagent reaction. RAW264.7 macrophage cells were treated with different concentrations (0.1-200 µg/mL) and (0.1-10 µg/mL) of ethyl acetate extracts in serum-free medium, along with lipopolysaccharide (LPS) at 100 ng/mL for 24 h. After incubation, the cell culture supernatant was mixed with Griess reagent and incubated for 15 min at room temperature. The absorbance was then measured at 540 nm (Jung et al., 2014). A standard curve using sodium nitrite was used to quantify NO production.

2.12 Chemical profile analysis of the crude extracts

The chemical profile of the crude extract was analyzed using High-Performance Liquid Chromatography (HPLC) equipped with a C-18 column and a UV/UVVIS detector. A linear gradient system was employed during the analysis. The HPLC chromatograms were compared with an in-house database to identify the components present in the extract.

The LC-MS/MS system, equipped with an Inertsil ODS-4 column, was utilized to measure the LC-ESI-MS spectra. This allowed for a more detailed analysis of the chemical composition. The chemical profile including retention time, UV absorbance, and pseudomolecular ion was compared with the reported chemical profiles in the in-house database and the Dictionary of Natural Products database. This comparison helped to identify and characterize the compounds present in the crude extract.

3. RESULTS AND DISCUSSION

3.1 Identification of actinomycetes

Based on the phenotypic and chemotaxonomic characteristics, these three strains belonged to the *Streptomyces* genus. Through analysis of the 16S rRNA gene sequence similarity, strain CT2-10 (accession number LC635735) exhibited a close relationship to *Streptomyces capoamus* JCM 4734^T (98.94%), strain ET3-23 (accession number LC635739) showed similarity to *Streptomyces morookaense* LMG 20074^T (99.49%), and strain NE1-12 (accession number LC635728) displayed high similarity to *Streptomyces nigra* 452^T (99.78%). The morphological characteristics of strain ET3-23 are shown in Figure 1(a) and 1(b). These three isolates contained LL-DAP in the cell wall peptidoglycan. Detailed information regarding the cultural, genotypic, and phenotypic characteristics of the strains is shown in Table 1.

(a) (b)

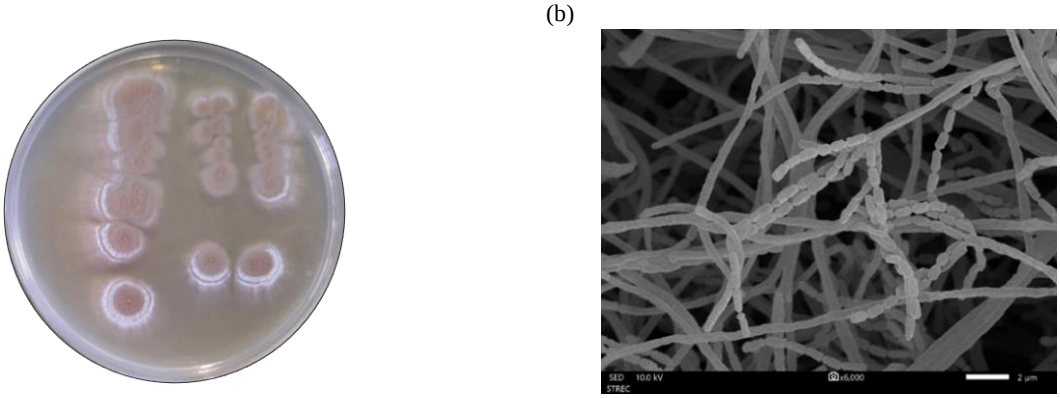

Figure 1. Colonial appearance (a) and scanning electron micrograph (b) of *Streptomyces* strain ET3-23 grown on ISP 3 agar at 30°C for 14 days.

Table 1. Characteristics of *Streptomyces* strains

Characteristics	Isolate No.		
	CT2-10	ET3-23	NE1-12
Cultural characteristics			
Upper surface color	Greyish white	Light yellowish brown	Grey greenish yellow
Reverse surface color	Moderate yellow	Pale yellow	Moderate greenish yellow
Genotypic characteristics			
Similarity (%)	98.94	99.49	99.78
Accession No.	LC635735	LC635739	LC635728
Nearest type strain	*Streptomyces capoamus* JCM 4734^T	*Streptomyces morookaense* LMG 20074^T	*Streptomyces nigra* 452^T
Phenotypic characteristics			
Growth on 2-6% NaCl	+	+	+
Growth at 28 °C	+	+	+
Growth at 45 °C	-	-	+
Growth at pH 5, 7, 10	+	+	+
Nitrate reduction	+	+	+
Hydrolysis of starch	-	+	-
Gelatinization	-	+	-
Milk coagulation	+	-	+
Milk peptonization	+	-	-
Acid production from:			
L-Arabinose	+	w	+
D-Cellobiose	+	w	+
D-Galactose	+	+	+
Lactose	+	w	+
Inositol	+	+	+
D-Mannitol	+	+	w
D-Maltose	+	+	+
D-Raffinose	+	-	w
D-Sorbitol	+	-	-
D-Xylose	+	+	+

Note: +, positive reaction; w, weak positive reaction; -, negative reaction.

3.2 Genome analysis

The draft genome of strain ET3-23 was submitted to GenBank. The accession number was JAJEJY000000000, and the assembled genome consisted of 106 contigs, with a total length of 8,121,874 base pairs, and an average G+C content of

71.46%. It contained 7,718 protein-coding sequences (CDS), along with 79 transfer RNA (tRNA) and 3 ribosomal RNA (rRNA) genes, as detailed in Supplementary Table S1.

The analysis of the biosynthesis gene clusters of secondary metabolites using antiSMASH revealed that strain ET3-23 harbored genes associated with the production of terpene, lanthipeptide, and thiopeptide, as indicated in Table 2. Notably, geosmin and neocarazostatin A exhibited a 100% similarity value. Neocarazostatin A1, derived from *Streptomyces* sp. MA37, demonstrated potent free radical scavenging properties, effectively protecting cells against damage (Liu et al., 2019). Neocarazostatins A, B, and C from *Streptomyces* sp. GP38 also exhibited strong inhibitory effects on free radical-induced lipid peroxidation in rat brain homogenate (Kato et al., 1991). Furthermore, carquinostatins A and B, lavanduquinocin, neocarazostatins A-C, carbazoquinocins A-F, and carbazomycins A-H showed promising antioxidant potential in protecting neuronal cells against oxidative damage caused by free radicals. This study reported the biological activities and provided insights into the genome sequence of the type strain of *Streptomyces morookaense* LMG 20074^T.

Table 2. Distribution of biosynthetic gene clusters in strain ET3-23 with similarity values greater than 20%

Cluster	Type	Most similar known cluster (class)	Similarity (%)
1	T2PKS	Spore pigment (Polyketide)	66
2	NRPS, T1PKS	Divergolide (Polyketide)	100
3	Terpene	Geosmin (Terpene)	100
4	Amglyccycl	B-D galactosylvalidoxylamine (Saccharide)	22
7	Lanthipeptide	SBI-06990 A1, SBI-06989 A2 (Lanthipeptide)	75
11	Siderophore	Desferrioxamine (Other)	83
13	NRPS	Coelichelin (NRP)	100
16	Terpene	Isorenieratene (Terpene)	75
19	NRPS, Nucleoside	Nogalamycin (Polyketide)	40
22	T3PKS	Germicidin (Other)	100
25	T1PKS, T3PKS, NRPS, Oligosaccharide	Lobophorin A (Polyketide)	73
26	Terpene, NRPS	Hopene (Terpene)	92
27	Ecotine	Ecotine (Other)	50
37	T1PKS	X 14547 (Polyketide)	21
38	T1PKS, Other	Lobophorin A (Polyketide)	26
43	T1PKS	Sceliphrolactam (Polyketide)	24

3.3 Total phenolic content

Strain NE1-12 exhibited the highest phenolic content (21.2±1.13 µg GAE/mg), followed by CT2-10 (16.8±0.66µg GAE/mg), while ET3-23 showed a lower phenolic content (9.1±0.54 µg GAE/mg). Notably, strain NE1-12 demonstrated significant levels of phenolic compounds, particularly those containing phenolic hydroxyl groups, indicating its strong antioxidant potential in relation to scavenging activities against DPPH radicals and NO.

Studies have reported the potential benefits of phenolic compounds in the prevention of inflammation, neurodegenerative, cardiovascular diseases and even cancer (Aleixandre-Tudo and Du Toit, 2019). Lee et al. (2014) found that the ethyl acetate extract of *Streptomyces* sp. strain MJM10778 had a total phenolic content of 8.8±0.2 µg GAE/g dry weight (Lee et al., 2014). In the case of *Streptomyces cavouresis* KUV39, the ethyl acetate extract exhibited a total phenolic content of 20.24 µg GAE/mg of the extract (Narendhran et al., 2014).

3.4 Ferric reducing antioxidant potential (FRAP)

Among the tested strains, ET3-23 exhibited the highest antioxidant capacity in terms of FRAP, with a value of 95.0±3.14 µgAAE/mg while strains CT2-10 and NE1-12 showed a moderate antioxidant capacity of 31.4±3.84 µgAAE/mg and 33.9±0.55 µgAAE/mg, respectively.

The significant antioxidant capacity displayed by strain ET3-23 suggested its potential as a strong antioxidant, with ferric reducing capacity indicating its ability to donate electrons, an important characteristic of antioxidants. This property enabled the strain to act

as a free radical inhibitor or scavenger, effectively neutralizing harmful radicals and serving as a primary antioxidant. The proton-donating ability of ET3-23 further contributed to its overall antioxidant activity.

These findings highlighted the potential of strain ET3-23 as a valuable source of natural antioxidants with significant free radical scavenging capabilities and the ability to protect against oxidative stress.

3.5 DPPH radical scavenging activity

Vitamin C demonstrated potent DPPH radical scavenging activity with a concentration-dependent response and an IC_{50} value of 5.7 µg/mL (Figure 2(a)). Strain ET3-23 exhibited DPPH radical scavenging with an IC_{50} value of 66.5 µg/mL. At 200 µg/mL concentration, it achieved a maximum activity of 77.7±0.98% (Figure 2(c)). The strains CT2-10 and NE1-12 also exhibited DPPH radical scavenging with IC_{50} values of 555.9 µg/mL and 463.3 µg/mL, respectively (Figure 2(b) and (d)). Among the strains tested, ET3-23 displayed more effective DPPH radical scavenging activity, with a lower IC_{50} value than NE1-12 and CT2-10. The observed DPPH radical scavenging activity of ET3-23 was attributed to its high phenol content and FRAP value. The strain reduced stable DPPH free radicals and exhibited characteristics of a hydroxyl radical scavenger by donating hydrogen atoms to free radicals and neutralizing their reactivity by removing odd electrons.

Similar studies have reported the DPPH radical scavenging activity of ethyl acetate extracts from other *Streptomyces* strains. For instance, ethyl acetate crude extracts from *Streptomyces olivaceus* (MSU3) demonstrated increasing inhibition at higher concentrations, with an IC_{50} value of 75.21 µg/mL (Sanjivkumar et al., 2016). *Streptomyces* sp. R56-07 strains JBIR-94 and JBIR-125 exhibited DPPH radical scavenging activity with IC_{50} values 11.4 µM and 35.1 µM, respectively (Taechowisan et al., 2017). An ethyl acetate extract of *Streptomyces* sp. AM-S1 culture demonstrated strong DPPH radical scavenging activity with an IC_{50} value of 68.4 µg/mL. Its mechanism of antioxidant action involves acting as a hydrogen donor, terminating the oxidation process by converting free radicals into stable forms (Sowndhararajan and Kang, 2013).

3.6 Nitric oxide radical scavenging activity

Vitamin C demonstrated potent activity, with NO scavenging activity of 85% and IC50 value 405.6 µg/mL in a concentration-dependent manner (Figure 3A). Strains NE1-12 and ET3-23 showed NO scavenging of 44.1±3.69% and 45.0±0.56%, respectively at 400 µg/mL. As the concentration increased, the NO scavenging activity decreased, indicating a relatively low capacity for NO scavenging (Figure 3(b) and 3(c)). These strains exhibited concentration-dependent scavenging of the nitrite radical, reaching a plateau where further increases in concentration did not result in increased quenching of the nitrite radical.

Lee et al. (2014) reported that the extract of *Streptomyces* strain MJM10778 displayed NO scavenging activities at increasing concentration, with highest scavenging rates of 95.4±0.1% and IC50 value 0.02 µg/mL. The soil-borne actinobacteria exhibited potential antioxidant activity against NO radicals (Lee et al., 2014).

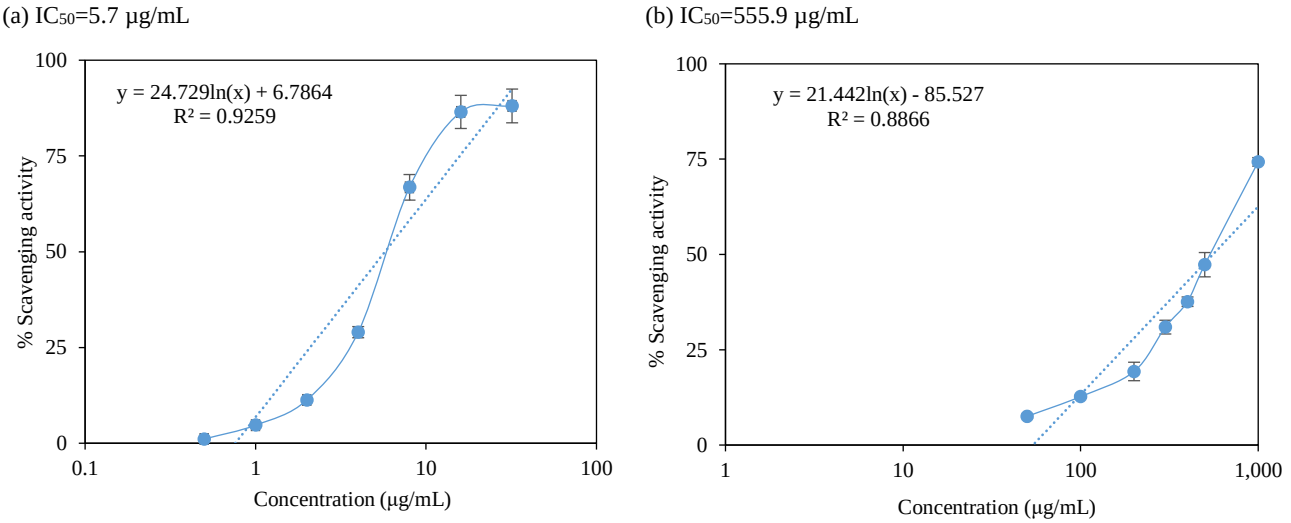

Figure 2. IC_{50} values of vitamin C (a) and ethyl acetate extracts of CT2-10 (b), ET3-23 (c) and NE1-12 (d) for DPPH radical scavenging activity. Data are expressed as mean±SEM (n=3).

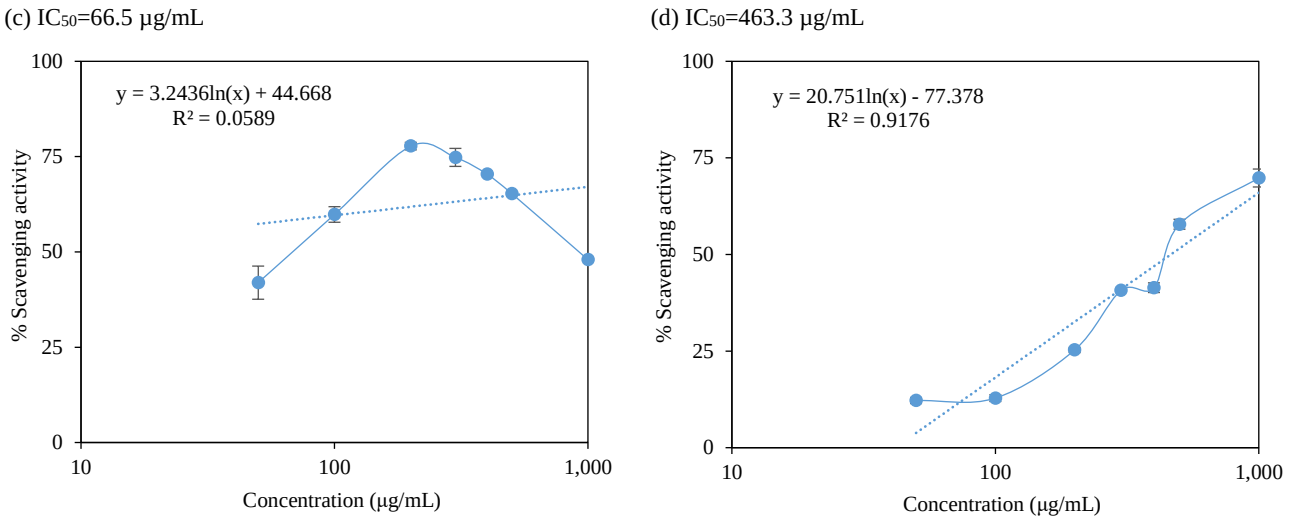

Figure 2. IC_{50} values of vitamin C (a) and ethyl acetate extracts of CT2-10 (b), ET3-23 (c) and NE1-12 (d) for DPPH radical scavenging activity. Data are expressed as mean±SEM (n=3) (cont.).

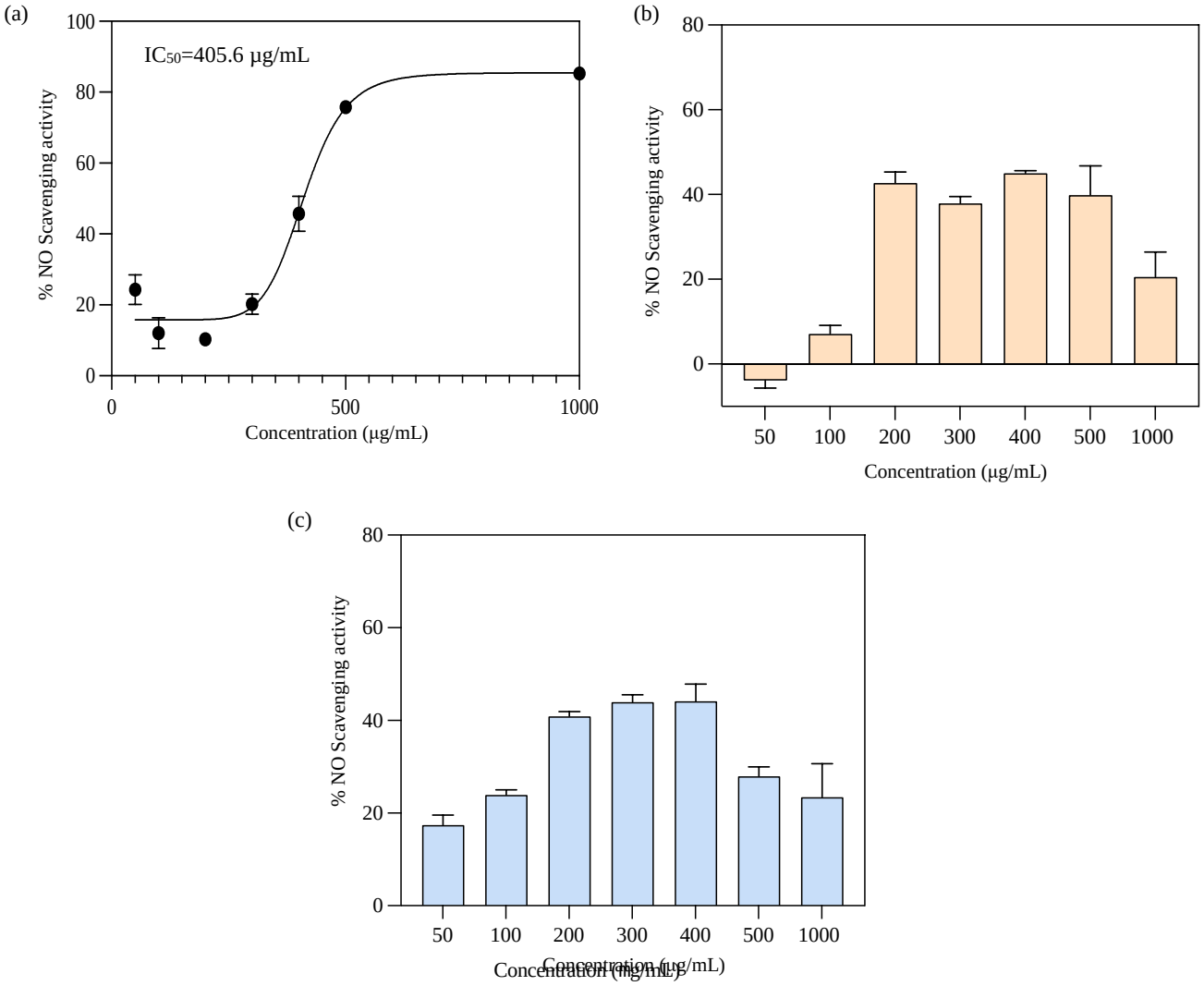

Figure 3. IC_{50} values of vitamin C (a) and NO scavenging activities of ethyl acetate extracts of ET3-23 (b) and NE1-12 (c). Data are expressed as mean±SEM (n=3).

3.7 Cytotoxic effects of Streptomyces strains

The cytotoxic effects of *Streptomyces* strains ET3-23, NE1-12, and CT2-10 were evaluated using the MTT assay on RAW264.7 macrophage cells. The ethyl acetate extracts of ET3-23 and NE1-12 showed no cytotoxicity, with high cell viability across concentrations of 10-200 µg/mL and 10-1,000 µg/mL, respectively (Figure 4(b) and (c)).

The cell viability of CT2-10 was 90% at 10 µg/mL. However, at a higher concentration of 50 µg/mL, the viability dropped to 46%. Further increasing the concentration from 100 µg/mL to 1,000 µg/mL resulted in consistently low cell viability, with values of 0-2%. (Figure 4(a)). These findings suggested that CT2-10 exhibited a concentration-dependent cytotoxic effect on the tested cells. Notably, the cytotoxicity of CT2-10 on macrophage cells suggested its potential as a chemotherapeutic drug, with the ability to selectively target and impact the viability of cancer cells.

Based on these results, non-toxic concentrations of the crude extracts were selected for further investigation of intracellular ROS and NO production in macrophage cells stimulated by hydrogen peroxide and lipopolysaccharide. ET3-23 and NE1-12 were studied in the 10-200 µg/mL range, while CT2-10 was studied in the 1-20 µg/mL range. The low cytotoxicity of the extracts suggested their potential as therapeutic agents for use in clinical settings for oxygen radical diseases.

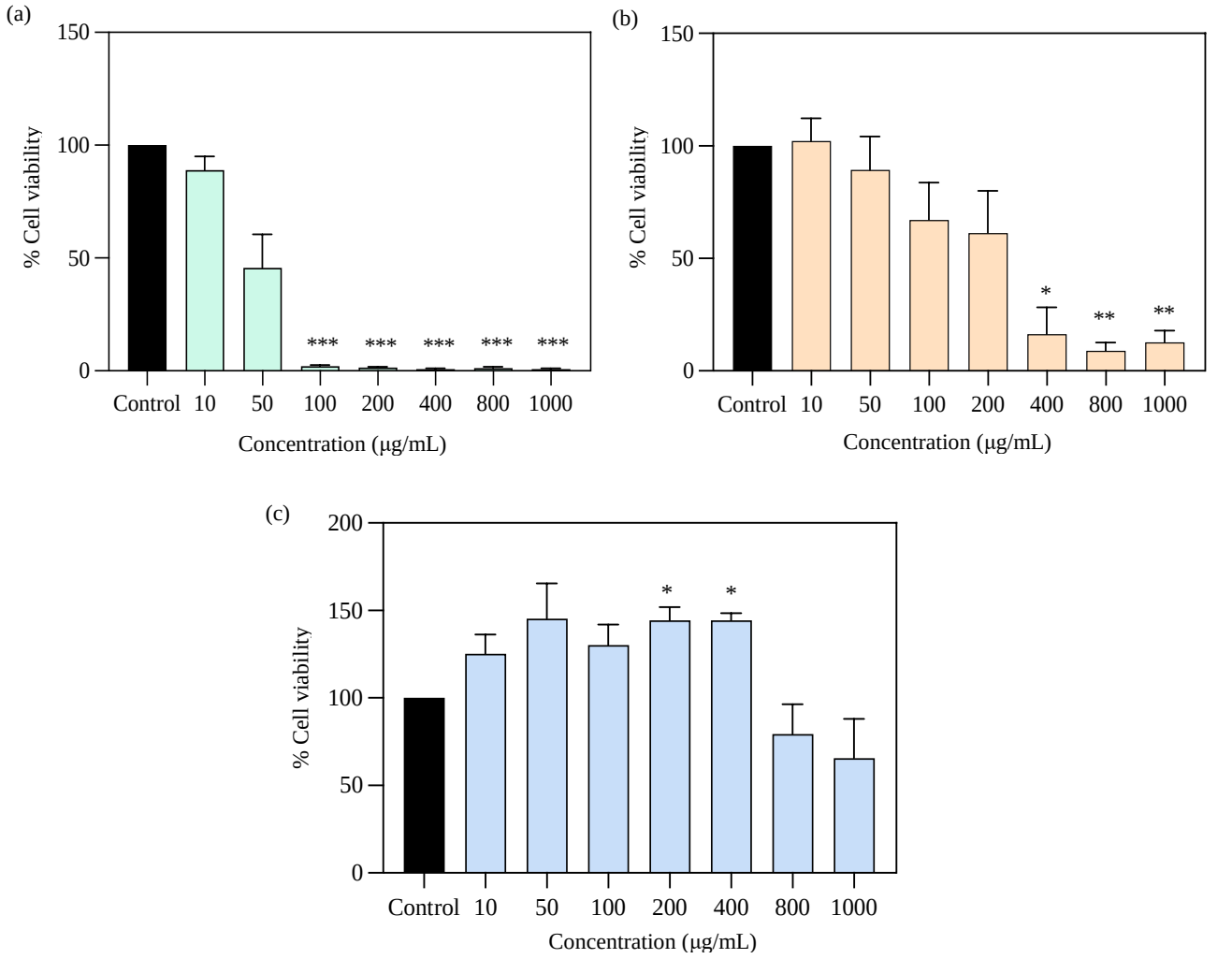

Figure 4. Cell viability of ethyl acetate extracts of CT2-10 (a), ET3-23 (b) and NE1-12 (c) on RAW264.7 macrophage cells. Data are presented as mean ± SEM (n=3). *p<0.05, **p<0.01, ***p<0.001 compared to the control (DMSO).

3.8 Inhibition of intracellular ROS generation

CT2-10 displayed ROS production ranging from 99% to 88% at concentrations of 0.1 µg/mL to 10 µg/mL (Figure 5(a)). Strain NE1-12 demonstrated a significant reduction in ROS production, ranging from 91% to 38% across a concentration range of 0.1 µg/mL

to 200 µg/mL (Figure 5(a)). Strain NE1-12 showed 74% inhibition of ROS production induced by hydrogen peroxide, with an IC_{50} value of 1.64 µg/mL (Figure 5(b)). Similarly, ET3-23 exhibited 67% inhibition of ROS production, with IC_{50} value 1.41 µg/mL (Figure 5(b)). ET3-23 efficiently suppressed H_2O_2-induced ROS production, as indicated by lower DCF fluorescence intensity. The reduction in ROS production observed in ET3-23 suggested its antioxidant potential in inhibiting radical release, possibly attributed to phenolic compounds isolated by ethyl acetate solvent.

When exposed to H_2O_2, elevated ROS levels reached 119±2.7% compared to the control cells. Leirós et al. (2014) found that compounds B and E from a *Streptomyces* strain exhibited significant reductions in ROS levels at a concentration of 1 µM in the presence of H_2O_2. Furthermore, compounds A, B, and C at a concentration of 0.1 µM noticeably decreased H_2O_2-induced ROS production while compound F, at a concentration of 0.01 µM, exhibited inhibition of H_2O_2-induced ROS production. These findings highlighted the potential of these compounds derived from *Streptomyces* to attenuate ROS generation under oxidative stress conditions (Leirós et al., 2014).

(a) Intracellular ROS production

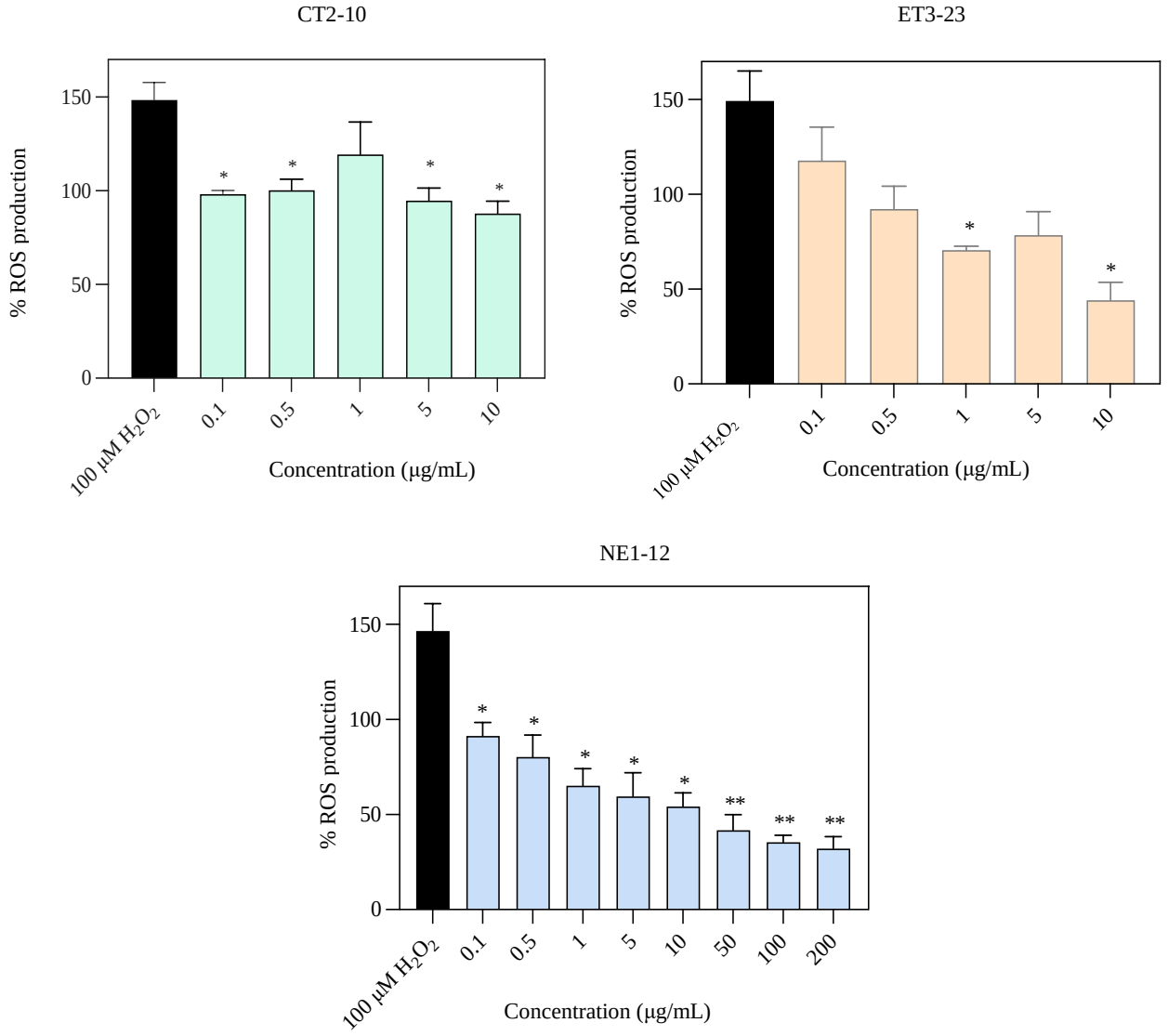

Figure 5. Effect of strains CT2-10, ET3-23 and NE1-12 on intracellular ROS production (a) and percentage inhibition (b) in H_2O_2 induced macrophage cells. Data are presented as mean±SEM (n=3). *p<0.05, **p<0.01 compared to the control (H_2O_2).

(b) Percentage inhibition of ROS production

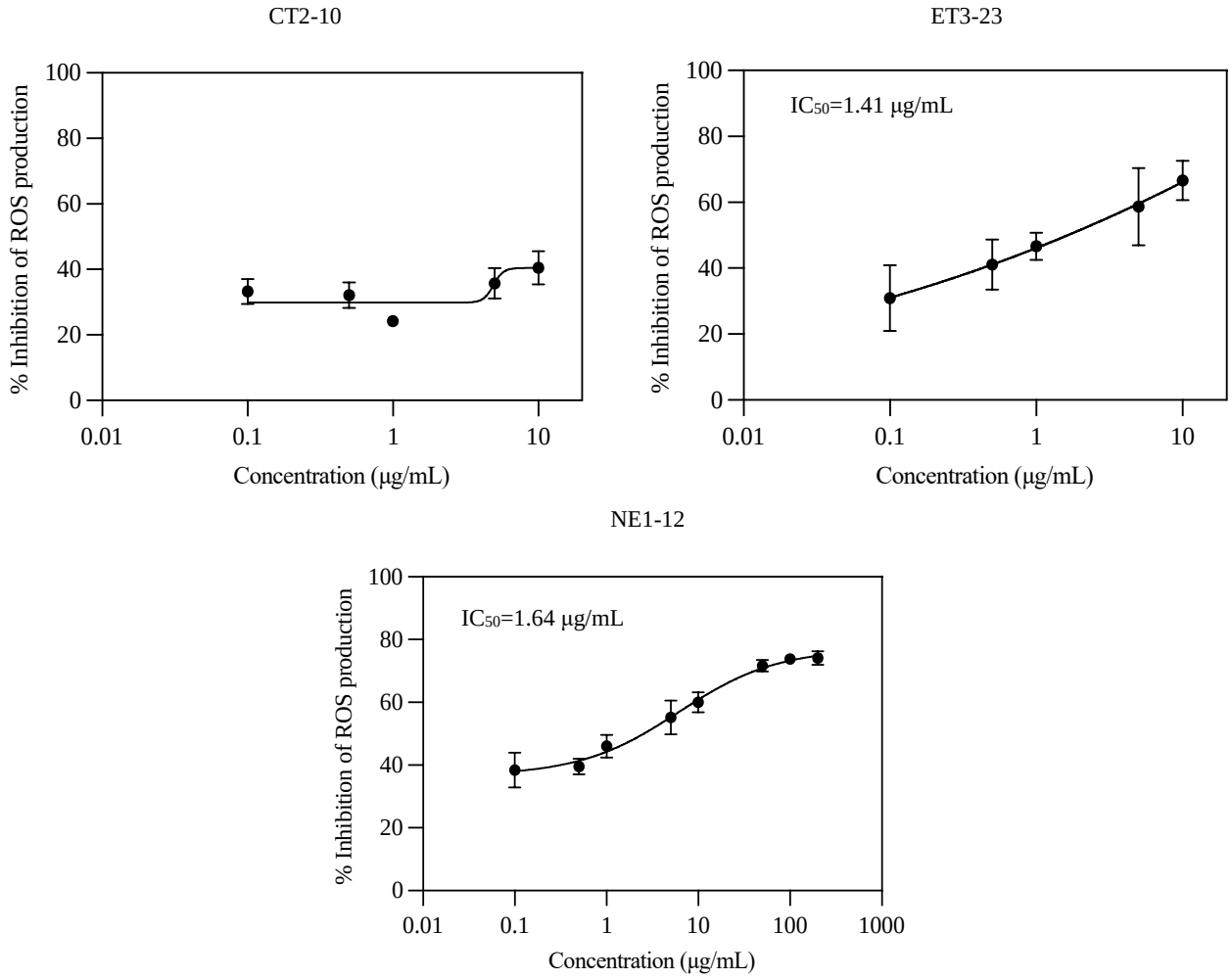

Figure 5. Effect of strains CT2-10, ET3-23 and NE1-12 on intracellular ROS production (a) and percentage inhibition (b) in H_2O_2 induced macrophage cells. Data are presented as mean±SEM (n=3). *p<0.05, **p<0.01 compared to the control (H_2O_2).

3.9 Inhibition of NO generation

Strains CT2-10 and NE1-12 reduced NO production across a range of concentrations (Figure 6A) and demonstrated IC50 values of 2.3 µg/mL and 82.4 µg/mL, respectively (Figure 6B). ET3-23 also showed 70% inhibition of NO production at 0.01 µg/mL. This reduction in NO generation was attributed to the antioxidant properties of these extracts which contributed to the decrease in nitrite levels. Notably, the low IC50 value of CT2-10 and ET3-23 suggested that some compounds within these extracts played a significant role in inhibiting oxygen radicals, indicating the potential of *Streptomyces*-derived compounds to treat diseases associated with excessive free radicals.

Nitric oxide is an important chemical mediator generated by various cell types including endothelial cells, macrophages, and neurons while NO plays a significant role in physiological processes such as vasodilation, neurotransmission, and immune response. However, excessive production of NO is associated with inflammatory reactions and can lead to cellular and tissue injury. In another study, geldanamycin from *Streptomyces* sp. W14 isolated from the rhizome tissue of *Zingiber zerumbet* (L.) Smith, inhibited the production of NO in LPS-induced RAW264.7 cells in a dose-dependent manner at concentrations of 1-5 µg/mL (Taechowisan et al., 2019). Similarly, Park et al. (2012) observed that dechlorothienodolin and thienodolin, isolated from *Streptomyces* sp. CNY325, inhibited NO production in LPS-stimulated RAW264.7 cells, suggesting their potential as anti-inflammatory and cancer chemoprevention agents (Park et al., 2012). These findings highlighted the ability of *Streptomyces*-derived compounds to modulate NO production which is crucial in inflammatory responses and tissue injury.

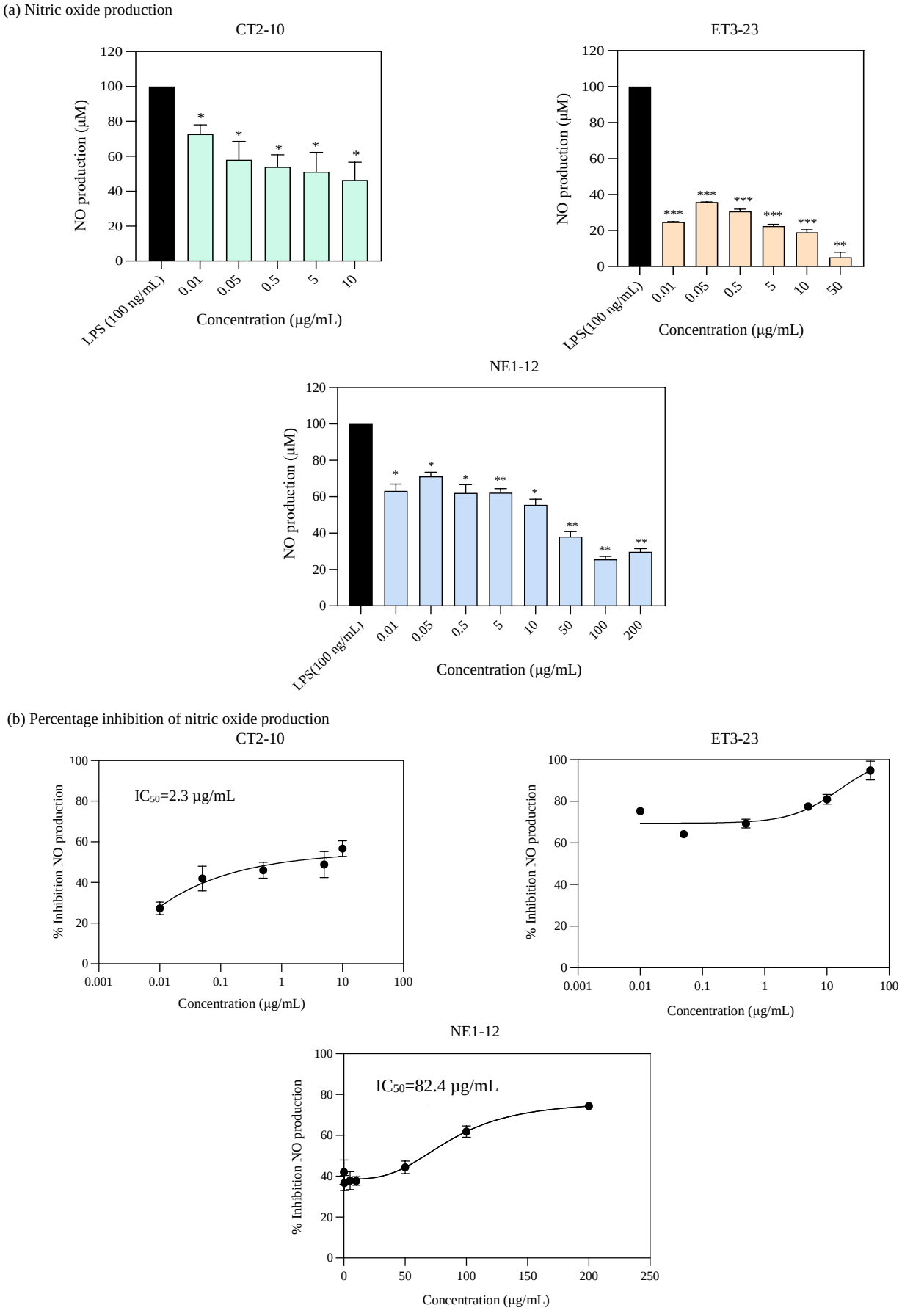

Figure 6. Effect of strains CT2-10, ET3-23 and NE1-12 on nitric oxide (NO) production (a) and percentage inhibition (b) in lipopolysaccharide induced RAW264.7 macrophage cells. Data are presented as mean±SEM (n=3). *p<0.05, **p<0.01 ***p<0.001 compared to the positive control (LPS).

3.10 Chemical profile analysis of secondary metabolites of *Streptomyces* strains

Chemical profile analysis of secondary metabolites from *Streptomyces* strains provides valuable information about the presence and quantity of various compounds, including phenolic compounds. UV-visible spectroscopy is a reliable method for quantifying phenolic compounds, renowned for their antioxidant properties. Different sub-families of phenolics are identified by their absorption maxima at specific wavelengths based on their ability to absorb UV light (Supplementary, Table S2). The absorbance at 280 nm is a key indicator for flavanol monomers, polymers, and some phenolic acids due to the phenolic ring's ability to absorb UV light, while hydroxycinnamic acids are quantified at 320 nm, flavonols at 360 nm, and anthocyanins at 520 nm (Aleixandre-Tudo and Du Toit 2019).

The chemical profiles of the secondary metabolites from *Streptomyces* strains were analyzed using UV-visible spectroscopy, with results presented in Figures S1, S2, and S3. These profiles provided insights into the presence and abundance of various compounds, particularly phenolic compounds. The presence of these compounds suggested that the crude extracts from *Streptomyces* strains contained potential antioxidant compounds. However, the compounds could not be identified using the in-house database. Thus, isolation and purification are necessary to identify the bioactive ingredient(s).

The effective antioxidant activity exhibited by *Streptomyces* strains highlights their potential as a valuable microbial source for drug discovery, particularly for developing effective antioxidant agents. Our findings provide insight into developing suitable candidates for pharmaceutical and bioactive natural products. Nevertheless, further investigation is needed to purify and determine the structures of the active components in the extracts.

4. CONCLUSION

This study evaluated the potential of soil-dwelling *Streptomyces* strains as natural sources of antioxidants. The strains CT2-10, NE1-12, and ET3-23 were identified and showed similarity to *Streptomyces capoamus* JCM 4734^T, *Streptomyces nigra* 452^T, and *Streptomyces morookaense* LMG 20074^T, respectively. For in vitro antioxidant activity, ET3-23 exhibited notable radical scavenging activity with an IC50 value of 66.5 µg/mL. ET3-23 and NE1-12 significantly reduced the generation of ROS in macrophage cells induced by hydrogen peroxide, while CT2-10, with an IC50 value of 2.3 µg/mL, effectively reduced lipopolysaccharide-induced NO generation. These findings suggested that *Streptomyces* strains possessed promising antioxidant properties, making them potential sources for bioactive natural products and the development of powerful antioxidants.

ACKNOWLEDGEMENTS

This study was supported by the 90th Anniversary of Chulalongkorn University Fund, Graduate School, Chulalongkorn University. The authors would like to thank the Pharmaceutical Research Instrument Center, Faculty of Pharmaceutical Sciences, Chulalongkorn University for providing research facilities.

REFERENCES

Aleixandre-Tudo JL, du Toit W. The Role of UV-Visible Spectroscopy for Phenolic Compounds Quantification in Winemaking [Internet]. 2019 [cited 2024 April 28]. Available from: http://dx.doi.org/10.5772/intechopen.79550.

Aranda A, Sequedo L, Tolosa L, Quintas G, Burello E, Castell JV, et al. Dichloro-dihydro-fluorescein diacetate (DCFH-DA) assay: A quantitative method for oxidative stress assessment of nanoparticle-treated cells. Toxicology In Vitro 2013; 27(2):954-63.

Ayuso-Sacido A, Genilloud O. New PCR primers for the screening of NRPS and PKS-I systems in Actinomycetes: Detection and distribution of these biosynthetic gene sequences in major taxonomic groups. Microbial Ecology 2005;49(1):10-24.

Bajpai VK, Baek KH, Kang SC. Antioxidant and free radical scavenging activities of taxoquinone, a diterpenoid isolated from *Metasequoia glyptostroboides*. South African Journal of Botany 2017;111:93-8.

Bankevich A, Nurk S, Antipov D, Gurevich AA, Dvorkin M, Kulikov AS, et al. SPAdes: A new genome assembly algorithm and its applications to single-cell sequencing. Journal of Computational Biology 2012;19(5):455-77.

Bérdy J. Bioactive microbial metabolites. Journal of Antibiotics 2005;58(1):1-26.

Brand-Williams W, Cuvelier ME, Berset C. Use of a free radical method to evaluate antioxidant activity. LWT-Food Science and Technology 1995;28(1):25-30.

Chansriniyom C, Bunwatcharaphansakun P, Eaknai W, Nalinratana N, Ratanawong A, Khongkow M, et al. A synergistic combination of *Phyllanthus emblica* and *Alpinia galanga* against H_2O_2-induced oxidative stress and lipid peroxidation in human ECV304 cells. Journal of Functional Foods 2018;43:44-54.

Chen B, Liu Y, Song WM, Hayashi Y, Ding XC, Li WH. In vitro evaluation of cytotoxicity and oxidative stress induced by multiwalled carbon nanotubes in murine RAW 264.7 macrophages and human A549 lung cells. Biomedical and Environmental Sciences 2011;24(6):593-601.

EL-Kamali HH, Hassan HI, EL-Kheir MSM. Effect of soil physico-chemical properties and plant species on bacterial

diversity in semi-arid parts in Central Sudan. Part III: AL-Gaeli Region, Khartoun North. Open Access Library Journal.2017;4(3):1-11.

Gordon RE, Barnett DA, Handerhan JE, Pang CH-N. Nocardia coeliaca, Nocardia autotrophica, and the Nocardin strain. International Journal of Systematic Bacteriology 1974; 24(1):54-63.

Govindan P, Muthukrishnan S. Evaluation of total phenolic content and free radical scavenging activity of *Boerhavia erecta*. Journal of Acute Medicine 2013;3(3):103-9.

Hasani A, Kariminik A, Issazadeh K. *Streptomycetes*: Characteristics and their antimicrobial activities. International Journal of Advanced Biological and Biomedical Research 2014;2(1):63-75.

Hazra B, Sarkar R, Mandal S, Biswas S, Mandal N. Studies on antioxidant and antiradical activities of Dolichos biflorus seed extract. African Journal of Biotechnology 2009;8:3927-33.

Janardhan A, Kumar AP, Viswanath B, Saigopal DVR, Narasimha G. Production of bioactive compounds by Actinomycetes and their antioxidant properties. Biotechnology Research International 2014;2014:Article No. 217030.

Jung CH, Jun CY, Lee S, Park CH, Cho K, Ko SG. *Rhus verniciflua* stokes extract: Radical scavenging activities and protective effects on H_2O_2-induced cytotoxicity in macrophage RAW 264.7 cell lines. Biological and Pharmaceutical Bulletin 2006;29(8):1603-7.

Jung H, Kwak H-K, Hwang KT. Antioxidant and antiinflammatory activities of cyanidin-3-glucoside and cyanidin-3-rutinoside in hydrogen peroxide and lipopolysaccharide-treated RAW264.7 cells. Food Science and Biotechnology 2014;23(6):2053-62.

Kämpfer P. The family Streptomycetaceae, part I: Taxonomy. In: Dworkin M, Falkow S, Rosenberg E, Schleifer K-L, Stackebrandt E, editors. The Prokaryotes. Volume 3: Archaea Bacteria: Firmicutes, Actinomycetes. New York: Springer; 2006. p. 538-604.

Karthik L, Kumar G, Rao KVB. Antioxidant activity of newly discovered lineage of marine actinobacteria. Asian Pacific Journal of Tropical Medicine 2013;6(4):325-32.

Kato S, Shindo K, Kataoka Y, Yamagishi Y, Mochizuki J. Studies on free radical scavenging substances from microorganisms. II. Neocarazostatins A, B and C, novel free radical scavengers. Journal of Antibiotics 1991;44(8):903-7.

Kawahara T, Izumikawa M, Otoguro M, Yamamura H, Hayakawa M, Takagi M, et al. JBIR-94 and JBIR-125, Antioxidative phenolic compounds from *Streptomyces* sp. R56-07. Journal of Natural Products 2012;75(1):107-10.

Kelly KL, Judd DB. Inter-society color council. ISCC-NBS Color-name Charts Illustrated with Centroid Colors. Washington, DC: U.S. National Bureau of Standards; 1965.

Kim MC, Lee J, Kim DH, Son HJ, Heo MS. Isolation and identification of antioxidant producing marine-source actinomycetes and optimal medium conditions. Food Science and Biotechnology 2014;23(5):1629-35.

Lee DR, Lee SK, Choi BK, Cheng J, Lee YS, Yang SH, et al. Antioxidant activity and free radical scavenging activities of *Streptomyces* sp. strain MJM 10778. Asian Pacific Journal of Tropical Medicine 2014;7(12):962-7.

Leirós M, Alonso E, Sanchez JA, Rateb ME, Ebel R, Houssen WE, et al. Mitigation of ROS insults by *Streptomyces* secondary metabolites in primary cortical neurons. ACS Chemical Neuroscience 2014;5(1):71-80.

Liu Y, Su L, Fang Q, Tabudravu J, Yang X, Rickaby K, et al. Enzymatic reconstitution and biosynthetic investigation of the bacterial carbazole Neocarazostatin A. Journal of Organic Chemistry 2019;84(24):16323-8.

Meier-Kolthoff JP, Göker M. TYGS is an automated high-throughput platform for state-of-the-art genome-based taxonomy. Nature Communications 2019;10(1):Article No. 2182.

Narendhran S, Rajiv P, Vanathi P, Sivaraj R. Spectroscopic analysis of bioactive compounds from *Streptomyces cavouresis* KUV39: Evaluation of antioxidant and cytotoxicity activity. International Journal of Pharmacy and Pharmaceutical Sciences 2014;6(7):319-22.

Park EJ, Pezzuto JM, Jang KH, Nam SJ, Bucarey SA, Fenical W. Suppression of nitric oxide synthase by thienodolin in lipopolysaccharide-stimulated RAW 264.7 murine macrophage cells. Natural Product Communications 2012;7(6):789-94.

Rammali S, Hilali L, Dari K, Bencharki B, Rahim A, Timinouni M, et al. Antimicrobial and antioxidant activities of *Streptomyces* species from soils of three different cold sites in the Fez-Meknes region Morocco. Scientific Reports 2022;12(1):Article No. 17233.

Sanjivkumar M, Babu DR, Suganya AM, Silambarasan T, Balagurunathan R, Immanuel G. Investigation on pharmacological activities of secondary metabolite extracted from a mangrove associated actinobacterium *Streptomyces olivaceus* (MSU3). Biocatalysis and Agricultural Biotechnology 2016;6:82-90.

Sarma AD, Mallick AR, Ghosh AK. Free radicals and their role in different clinical conditions: An overview. International Journal of Pharma Sciences and Research 2010;1(3):185-92.

Seemann T. Prokka: Rapid prokaryotic genome annotation. Bioinformatics 2014;30(14):2068-9.

Ser HL, Palanisamy UD, Yin WF, Abd Malek SN, Chan KG, Goh BH, et al. Presence of antioxidative agent, Pyrrolo[1,2-a]pyrazine-1,4-dione, hexahydro- in newly isolated *Streptomyces mangrovisoli* sp. nov. Frontiers in Microbiology 2015;6:Article No. 854.

Shirling EB, Gottlieb D. Methods for characterization of *Streptomyces* species. International Journal of Systematic Bacteriology 1966;16:313-40.

Sowndhararajan K, Kang SC. Evaluation of in vitro free radical scavenging potential of *Streptomyces* sp. AM-S1 culture filtrate. Saudi Journal of Biological Sciences 2013;20(3):227-33.

Staneck JL, Roberts GD. Simplified approach to identification of aerobic actinomycetes by thin-layer chromatography. Applied Microbiology 1974;28(2):226-31.

Taechowisan T, Chaisaeng S, Phutdhawong WS. Antibacterial, antioxidant and anticancer activities of biphenyls from *Streptomyces* sp. BO-07: An endophyte in *Boesenbergia rotunda* (L.) Mansf A. Food and Agricultural Immunology 2017;28(6):1330-46.

Taechowisan T, Puckdee W, Phutdhawong W. Streptomyces zerumbet, a novel species from *Zingiber zerumbet* (L.) Smith and isolation of its bioactive compounds. Advances in Microbiology 2019;09:194-219.

Tamaoka J, Komagata K. Determination of DNA base composition by reversed-phase high-performance liquid chromatography. FEMS Microbiology Letters 1984;25(1):125-8.

Tan LT, Chan KG, Chan CK, Khan TM, Lee LH, Goh BH. Antioxidative potential of a *Streptomyces* sp. MUM292

isolated from mangrove soil. Biomed Research International 2018;2018:Article No. 4823126.

Vargas Gil S, Pastor S, March GJ. Quantitative isolation of biocontrol agents *Trichoderma* spp., *Gliocladium* spp. and actinomycetes from soil with culture media. Microbiological Research 2009;164(2):196-205.

Wai KZ, Luechapudiporn R, Tedsree N, Phongsopitanun W, Malisorn K, Tanasupawat S. *Streptomyces barringtoniae* sp. nov., isolated from rhizosphere of plant with antioxidative potential. International Journal of Systematic and Evolutionary Microbiology 2022;72(5):Article No. 005364.

Yoon SH, Ha SM, Kwon S, Lim J, Kim Y, Seo H, et al. Introducing EzBioCloud: A taxonomically united database of 16S rRNA gene sequences and whole-genome assemblies. International Journal of Systematic and Evolutionary Microbiology 2017;67(5):1613-7.

Environment and Natural Resources Journal

Volume 22
Issue 6
2024

Utilization of High-Salinity Crude Glycerol Byproduct from Biodiesel Production for Biosynthesis of γ-Aminobutyric Acid in Engineered *Halomonas elongata*

Ziyan Zou[1], Pulla Kaothien-Nakayama[1], and Hideki Nakayama[1,2,3*]

[1]*Graduate School of Fisheries and Environmental Sciences, Nagasaki University, Japan*
[2]*Institute of Integrated Science and Technology, Nagasaki University, Japan*
[3]*Organization for Marine Science and Technology, Nagasaki University, Japan*

ARTICLE INFO

Received: 6 Feb 2024
Received in revised: 15 Sep 2024
Accepted: 19 Sep 2024
Published online: 5 Nov 2024
DOI: 10.32526/ennrj/22/20240033

Keywords:
Halomonas elongata/ Crude glycerol/ Biodiesel byproduct/ Salting out/ γ-aminobutyric acid/ *H. elongata* cell factory

*** Corresponding author:**
E-mail:
nakayamah@nagasaki-u.ac.jp

ABSTRACT

As the development of renewable energy has become imperative, biodiesel fuel (BDF) has been used as renewable biofuel with the advantage of having lower levels of greenhouse gas emissions. However, the transesterification reaction that produces BDF generates a high-salinity crude glycerol (CG) byproduct, which is difficult to recycle. *Halomonas elongata* is a moderately halophilic bacterium being used as a cell factory due to its ability to assimilate varieties of substrates for growth in high-salinity conditions. Previously, we engineered a recombinant *H. elongata* GOP-Gad to biosynthesize and accumulate γ-aminobutyric acid (GABA) as a high-value product. Here, we tested the ability of *H. elongata* GOP-Gad to use CG as a substrate for cell growth and GABA production. The CG byproduct was obtained from a BDF facility in Unzen City, Nagasaki, Japan, where geothermal energy catalyzed BDF production from waste cooking oil and biomethanol. Prior to use as the sole carbon (C) source in culture media, the CG byproduct was partially purified to remove soap substances and other impurities. Finally, we showed that *H. elongata* GOP-Gad could grow and accumulate GABA up to 28 µmol/g cell fresh weight in a minimal M63 medium containing 7% w/v NaCl with 4% w/v glycerol from the partially purified CG as a C source and 15 mM $(NH_4)_2SO_4$ as a nitrogen (N) source. This result demonstrates a new circulatory bioprocess of C and N, in which *H. elongata* GOP-Gad can use partially purified CG and $(NH_4)_2SO_4$ as the sole C and N sources for growth and GABA production.

1. INTRODUCTION

Global energy demand sharply increases as the human population grows. However, fossil fuel resources are limited. Adding to the problem are environmental and climate issues caused by the usage of fossil fuels. Therefore, the development of renewable energy has become imperative. Biodiesel fuel (BDF) is a renewable biofuel alternative to diesel fuel, offering the additional advantage of lower greenhouse gas emissions (Kosamia et al., 2020). BDF is formed as a methyl or ethyl ester of fatty acid and is usually produced by the transesterification reaction between vegetable oils or animal fats with short-chain alcohols under high-temperature conditions (Gerpen, 2005). During transesterification, 1 mole of triglyceride produces 3 moles of biodiesel and 1 mole of glycerol byproduct, which contains high concentrations of salt (Figure 1). Every batch of biodiesel production generates approximately 10% w/v glycerol and other impurities, which are harvested together as crude glycerol (CG) byproducts. The main impurities in CG are methanol, soap, free fatty acids, salt (inorganic salts residues from catalysts), unreacted mono-, di- and tri-glycerides, and water (Pagliaro and Rossi, 2010).

Citation: Zou Z, Kaothien-Nakayama P, Nakayama H. Utilization of high-salinity crude glycerol byproduct from biodiesel production for biosynthesis of γ-aminobutyric acid in engineered *Halomonas elongata*. Environ. Nat. Resour. J. 2024;22(6):525-534. (https://doi.org/10.32526/ennrj/22/20240033)

Although the public and government of Unzen City, Nagasaki, Japan, aim to be more environmentally friendly by producing BDF with biomass-derived methanol, waste cooking oil, and hot spring geothermal energy (Nakagawa et al., 2007; Tominaga et al., 2014; Tominaga et al., 2015), the CG byproduct has not been used effectively. Due to its high salinity, CG byproducts generated in Nagasaki are generally only used as an additive to compost to promote fermentation (Tominaga et al., 2014; Tominaga et al., 2015).

Biotechnology for synthesizing high-value products, such as medicine, chemicals, and food additives, has been developed for decades, aiming to gradually replace the traditional petroleum-based industry. *H. elongata* strains are among the bacteria being used as microbial cell factories due to their ability to use different substrates to grow under high-salinity conditions (Schwibbert et al., 2011; Tanimura et al., 2013; Nakayama et al., 2020; Ye and Chen, 2021; Chen et al., 2022). For example, many *H. elongata* strains can utilize glucose, glycerol, or lignocellulosic biomass-derived sugars such as cellobiose, xylose, and arabinose as C sources and ammonium and amino acids as N sources (Vreeland et al., 1980; Ono et al., 1998; Tanimura et al., 2013). Unlike the *H. elongata* type-strain DSM 2581^T, the *H. elongata* OUT30018 (Ono et al., 1998; Ono et al., 1999) exhibits a unique ability to utilize putrefactive non-volatile amines, such as histamine and tyramine, derived from biomass waste as sources of carbon and nitrogen for cell growth. (Nakayama et al., 2020). *H. elongata* OUT30018 was also found to assimilate amino acids derived from biomass waste, such as CG byproducts of biodiesel industries (Bozbas, 2008; Ayoub and Abdullah, 2012). Therefore, *H. elongata* OUT30018 is one of the most promising bacterial strains for developing cell factories for producing fine chemicals from biomass waste.

Previously, we engineered a recombinant *H. elongata* GOP-Gad to biosynthesize and accumulate γ-aminobutyric acid (GABA) as a major osmolyte under high-salinity growth conditions (Zou et al., 2024). As *H. elongata* GOP-Gad has *H. elongata* OUT30018 genetic background, we explored the possibility of using KOH-neutralized high-salinity CG as a C source in the culture medium of *H. elongata* GOP-Gad for GABA production. As a result, we found that *H. elongata* GOP-Gad can use CG as the sole C source to produce GABA, which was accumulated in the cells up to 28 μmol/g cell fresh weight (CFW). In the future, we will continue to develop *H. elongata* strain, growth condition, and medium formula to increase GABA yield. The work presented here represents the initial phase in the development of *H. elongata* cell factory into single-cell feed additive. The cells will be used directly without further purification steps, creating a low-cost circulatory bioprocess of C and N to support a more recycling-oriented feed industry.

2. METHODOLOGY

2.1 Partial purification process of CG byproduct

KOH-neutralized CG byproduct of BDF production was obtained from a BDF production facility operated by the Social Welfare Corporation COSMOS association in Unzen City, Nagasaki, Japan, with the assistance of the Nagasaki Environmental Health Research Center, Omura City, Nagasaki, Japan. To remove soap substance and other impurities, 200 g of CG byproducts was mixed with 500 mL of 25% w/v NaCl solution in a salting-out process. The soap substance was separated from CG by centrifugation at 7,500×g for 10 min; then the CG solution was filtered through Qualitative filter paper (Advantec) to remove the remaining soap substance and other impurities. The resulting CG solution was filter-sterilized through a 0.22 μm pore size bottle top filter (Sartorius) and stored at room temperature until use. CG was diluted 100 times in pure water for High-performance liquid chromatography (HPLC) analysis or diluted 1,000 times in pure water and digested with nitric acid for analysis of Na and K ions content by Inductively Coupled Plasma Atomic Emission Spectroscopy (ICP-AES; ICPS-7500, SHIMADZU) analysis. Because purified CG contains high Na concentration, the concentration of Na added to M63 minimal medium was adjusted accordingly.

2.2 Bacterial strain

In this study, *H. elongata* GOP-Gad (Zou et al., 2024) is used in all growth tests. The *H. elongata* GOP-Gad was generated from the glutamic acid overproducing mutant *H. elongata* GOP by introducing an artificial bicistronic *mCherry-HopGadmut* operon, which confers salt-inducible expression of 2 genes: The *mCherry* gene, which encodes a red fluorescent reporter mCherry protein that was used as a visual selection marker to facilitate transformant screening and as a marker to confirm transgene expression, and the *HopGadmut* gene, which encodes a mutant L-glutamic acid decarboxylase B (GadBmut) enzyme, which is active at a wide pH range to convert glutamate (Glu) to GABA (Figure 2).

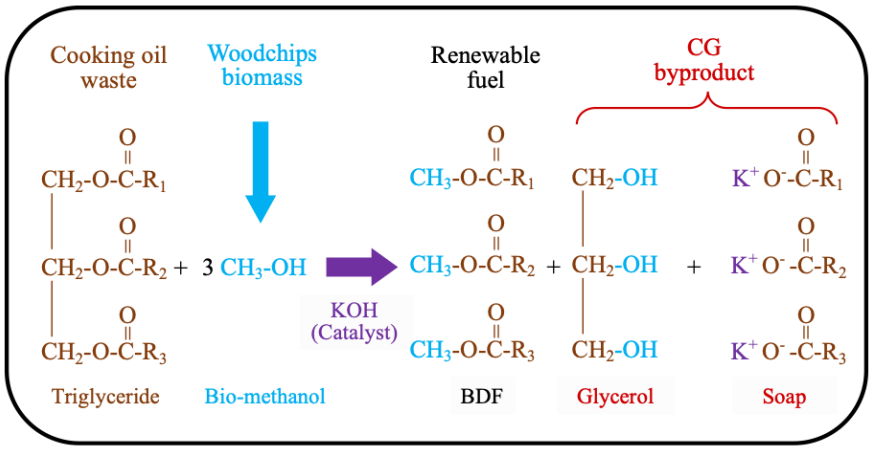

Figure 1. Biodiesel fuel (BDF) production process in a chamber heated by hot spring water at a BDF facility in Unzen City, Nagasaki, Japan.

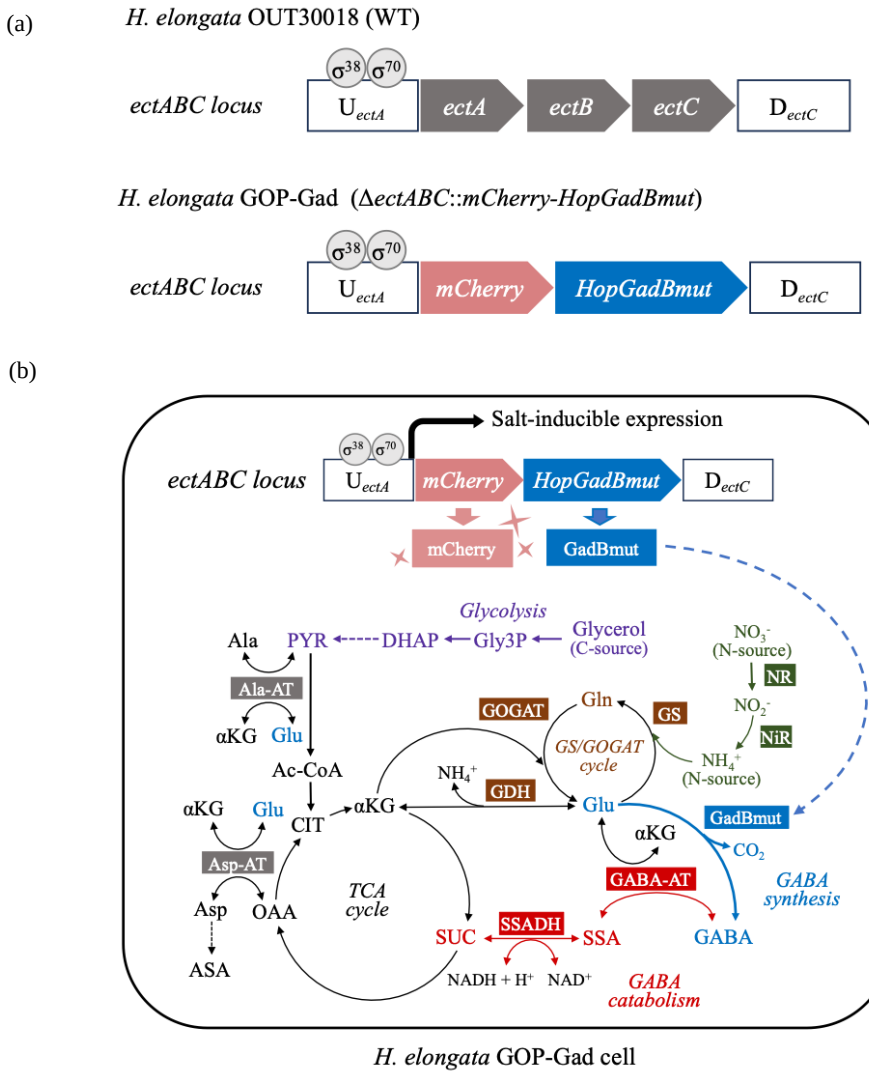

Figure 2. Engineered GABA metabolic pathway in *H. elongata* GOP-Gad. (a) Comparison of the genomic structures at the ectABC locus on the genome of the wild-type *H. elongata* OUT30018 and the engineered *H. elongata* GOP-Gad. UectA, A 1-kb upstream region of the ectA gene that contains an ectA promoter with putative binding sites for the osmotically induced sigma factor σ38 and the vegetative sigma factor σ70. This region was used as a target for homologous recombination at the ectABC locus; DectC, A 1-kb downstream region of the ectC gene that contains an ectC terminator. This region was used as a target for homologous recombination at the ectABC locus; ectA, a gene that encodes an L-2,4-diaminobutyric acid acetyltransferase; ectB, a gene that encodes a DABA transaminase; ectC, a gene that encodes an ectoine synthase; mCherry, a gene that encodes a red fluorescent reporter protein mCherry; HopGadBmut, a synthetic *H.*

elongata's codon-usage optimized (Hop) GadB mutant gene (HopGadBmut), which encodes a mutant L-glutamic acid decarboxylase B (GadBmut) with activity across broader pH ranges than the wild-type GAD. (b) GABA metabolic pathway in *H. elongata* GOP-Gad cell cultured in a medium containing glycerol as a C source and NH_4^+ or NO_3^- as an N source. Ac-CoA, acetyl coenzyme A; Ala, L-alanine; Ala-AT, L-alanine aminotransferase; α-KG, α-ketoglutaric acid; ASA, L-aspartate-β-semialdehyde; Asp, L-aspartic acid; Asp-AT, L-aspartic acid aminotransferase; CoA, coenzyme A; DHAP, dihydroxyacetone phosphate; GABA, γ- aminobutyric acid; GABA-AT, γ-aminobutyric acid aminotransferase; GadBmut, a mutant L-glutamic acid decarboxylase; Glu, L-glutamic acid/glutamate; GDH, L-glutamic acid dehydrogenase; GOGAT, L-glutamic acid synthetase; Gln, L-glutamine; GS: L-glutamine synthetase; Gly3P, glycerol 3-phosphate; NR, nitrate reductase; NiR; nitrite reductase OAA, oxaloacetate; PYR, pyruvate; SSA, succinate semialdehyde; SSADH, succinate semialdehyde dehydrogenase; and SUC, succinate.

2.3 Culture media

2.3.1 High-salinity LB media

As a complex medium for routine culture of *H. elongata* GOP-Gad, LB medium (Sambrook and Russel, 2001) was modified to contain high NaCl concentration (high-salinity LB medium), which contains 10 g/L Bacto-tryptone, 5 g/L Bacto-yeast extract, and 3% or 6% w/v NaCl. For solid medium, 15 g/L agarose was added before autoclave sterilization. A high-salinity LB medium containing 6% w/v NaCl was used for culturing the inoculum for the main culture in the M63 medium containing 7% w/v NaCl.

2.3.2 High-salinity M63 media containing pure glycerol (PG) or CG as the sole C source

The high-salinity M63 media was modified from the M63 minimal medium (Perroud and Le Rudulier, 1985) for culturing *H. elongata* GOP-Gad as described previously (Zou et al., 2024). High-salinity M63 media contain 100 mM KH_2PO_4, 1 mM $MgSO_4$, 3.9 µM $FeSO_4$, 3% or 7% w/v NaCl, 15 mM $(NH_4)_2SO_4$ or 30 mM $NaNO_3$ as the sole N source, and 4% w/v glycerol from PG, which contains 100% w/v glycerol, or CG, which contains 64% or 66% glycerol (Table 1), as the sole C source. A higher amount of CG was supplemented so that the final glycerol concentration of the medium was 4% w/v. The pH of the medium was adjusted to 7.2 with KOH solution before filter sterilization.

The C, N-free high-salinity M63 medium was prepared as described above without adding C and N sources.

2.4 Culture condition

H. elongata GOP-Gad was cultured in glass test tubes incubated in a 37°C water bath with 120 rpm agitation.

2.5 Extraction of major osmolytes accumulated in *H. elongata* GOP-Gad cells

Major osmolytes were extracted from *H. elongata* cells as previously described (Zou et al., 2024). In brief, *H. elongata* GOP-Gad was cultured in high-salinity LB medium until OD_{600} reached more than 1, when the cells were harvested by centrifugation at 10,000 × g for 3 min, and the weight of the cell pellets was recorded as cell fresh weight (CFW). Mimicking the bacterial milking process (Sauer and Galinski, 1998; Cánovas et al., 1997), the cell pellets were resuspended in pure water (20 µL/mg CFW) for hypo-osmotic extraction of major osmolytes from the cells. After centrifugation at 10,000 × g for 3 min, the supernatant containing the free amino acids and major osmolytes was collected as a major osmolytes sample.

2.6 Amino acids dabsylation

As previously described (Zou et al., 2024), 10 µL aliquot of free amino acids samples or standard amino acids was mixed with 2 µL of 2.5 mM internal standard norvaline and 8 µL of 1 M $NaHCO_3$ pH adjustment solution. Then, the sample was mixed with 40 µL of dabsylation reagents containing 2 mg/mL dabsyl chloride dissolved in acetonitrile and incubated at 70°C for 15 min. After the incubation, 440 µL of 250 mM $NaHCO_3$ solution was added, and the samples were centrifuged at 10,000 × g for 3 min. The supernatant of each sample was collected and filtered through a filter vial with 0.2-µm pore size polytetrafluoroethylene (PTFE) membrane (SEPARA Syringeless filter, GVS Japan K.K., Tokyo, Japan) prior to HPLC analysis.

2.7 HPLC analysis

Determination of dabsyl amino acids derived from *H. elongata* cells was carried out as previously described (Zou et al., 2024) using a high-performance liquid chromatography system (Shimazdu, Kyoto, Japan) equipped with an UV/VIS detector (SPD-10 A VP), an autosampler (SIL-10 AD VP), two pumps (LC-10 AD VP), degasser (DGU-14A), system controller (SCL-10A Vp), and column oven (CTO-10AC VP). LabSolutions LC software (Shimadzu, Kyoto, Japan) was used for system control and data acquisition. Chromatographic separation of dabsyl amino acids was achieved through an analytical C18 column (Poroshell 120 2.7 µm, EC-C18, 4.6×75 mm, Agilent Technologies Inc.) with C18 guard column

(Poroshell 120 2.7 µm Fast Guard, EC-C18, 4.6×5 mm, Agilent Technologies Inc.) using a mobile-phase gradient system consisting of 15% acetonitrile in 20 mM sodium acetate (pH 6.0) (mobile phase A) and 100% acetonitrile (mobile phase B). Dabsyl amino acids were determined by UV/VIS detector at 468 nm. The injection volume was 10 µL, the flow rate was 0.5 mL/min, and the column temperature was maintained at 27°C.

2.8 ICP-AES analysis

The concentrations of Na and K ions in the partially purified CG were determined by ICP-AES analysis. The PG and partially purified CG were diluted 1,000 times with distilled water, and 2.5 µL aliquot of each sample was transferred to a 50 mL polypropylene tubes. After mixing with 25 mL of Milli-Q water and 5 mL of 70% v/v HNO_3 (Nacalai Tesque Inc., Kyoto, Japan), the samples were incubated in a 65°C digestion block (DigiPREP jr., SCP Science, Quebec, Canada) for 15 min, followed by the incubation at 105°C for 120 min. After the samples cooled down to room temperature, 0.5 mL of 30% v/v H_2O_2 (Fujifilm Wako Pure Chemical, Ltd., Osaka, Japan) was added to each mixture, and the samples were further incubated at 105°C for 60 min. After the samples cooled down to room temperature, they were filtered through a 0.45 µm-pore-size Teflon membrane filter (DigiFILTER, SCP Science, Quebec, Canada). After rinsing the filter with Milli-Q water, the volume of each filtered sample was adjusted to 50 mL with Milli-Q water. Quantification of ions concentrations was performed on an ICP-AES (ICPS-7500, Shimadzu Corporation, Kyoto, Japan) following the manufacturer's instructions (Nakayama et al., 2019).

3. RESULTS AND DISCUSSION

3.1 Partial purification of CG by the salting-out process

As shown in Figure 1, at a BDF production facility in Unzen City, Nagasaki, Japan, heat generated by hot spring water facilitates a transesterification reaction between triglyceride in used cooking oil collected from households and restaurants in Nagasaki prefecture and biomethanol derived from wood chip biomass to produce BDF. KOH was used as an alkaline catalyst at this facility instead of NaOH because the resulting CG byproduct will be used as an additive to compost for agricultural fields that are sensitive to sodium salt. During the BDF production process, a saponification reaction partially occurs between triglyceride and KOH to form soap in the CG byproduct. As this study aims to use the CG in the BDF byproduct as the sole C source of *H. elongata* GOP-Gad's culture medium, soap must be removed due to its cytotoxic effect.

The first step in removing soap and other impurities was a salting-out step (Figure 3), in which the CG byproduct was mixed with 25% w/v NaCl solution. After mixing, the solution is centrifuged to separate the solution into two phases: the liquid phase, which contains the partially purified CG, and the solid phase, which contains soap and other impurities. After the solid phase, which floated on top of the liquid phase, was spooned out, the liquid phase was collected and further purified by filtration through a standard quantitative filter paper. The resulting partially purified CG contains 40% w/v CG. The concentrations of Na and K ions in the partially purified CG were analyzed by ICP-AES, and the glycerol concentration was analyzed by HPLC. The analysis results for different partially purified CG batches are shown in Table 1. Based on the results, NaCl concentrations of the partially purified 40% w/v CG batches were determined to be 17% w/v. With this information, the amount of NaCl added to the M63 minimal media used in the following growth tests was adjusted accordingly.

Table 1. Concentrations of Na^+, K^+, and glycerol in the partially purified crude glycerol (CG).

Chemical (unit)	Pure glycerol (PG)	CG-1	CG-2	CG-3
Na^+ (M)	ND	2.93	3.00	2.82
K^+ (M)	ND	0.41	0.42	0.39
Glycerol (% w/v)	100	66	64	66

The concentrations of Na and K ions in CG were analyzed by ICP-AES and the concentrations of glycerol in CG samples in different batches of partially purified CG (CG-1, CG-2, and CG-3) were analyzed by HPLC. CG samples were diluted 100 times in pure water for HPLC analysis or diluted 1,000 times in pure water and digested with nitric acid for ICP-AES analysis. ND, not detected.

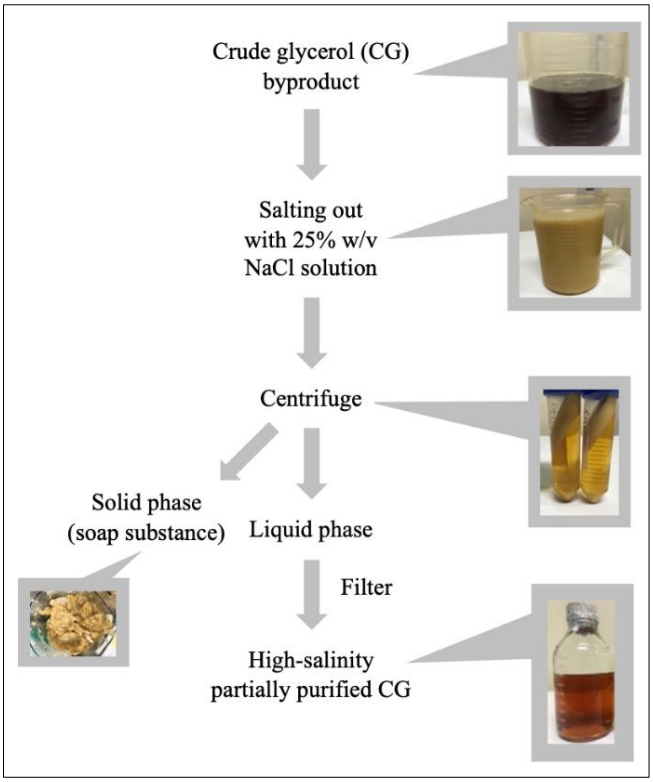

Figure 3. Partial purification of the crude glycerol (CG) byproduct. After salting-out treatment with a 25% w/v NaCl solution, the partially purified CG contains 40% w/v CG and high Na and K ions concentrations.

3.2 *H. elongata* GOP-Gad can utilize CG as the sole C source and ammonia or nitrate as the sole N source

To test whether the partially purified CG can work as the sole C source in a culture medium to sustain the growth and production of valuable compounds by bacterial cell factory, we tested the ability of the GABA-producing cell factory, *H. elongata* GOP-Gad (Zou et al., 2024), to produce GABA in a minimal M63 medium, which contains partially purified CG as its sole C source. As PG is known to be a good C source for bacterial growth, *H. elongata* GOP-Gad was precultured in the M63 minimal medium containing 3% w/v NaCl, 4% w/v PG as a C source, and 15 mM $(NH_4)_2SO_4$ as an N source. When the optical density at 600 nm (OD_{600}) of the culture reached the value of 1.00, the cells were collected and washed 3 times in the C, N-free M63 minimal medium containing 3% w/v NaCl before being used as a 5% v/v inoculum for the main cultures in the M63 minimal medium containing 3% w/v NaCl, 15 mM $(NH_4)_2SO_4$ or 30 mM $NaNO_3$, and 4% w/v glycerol derived from PG (100 w/v glycerol) or partially purified CG (64% or 66% w/v glycerol; Table 1). When the OD_{600} of the main cultures reached 0.90 to 1.20, major osmolytes in the *H. elongata* GOP-Gad cells were extracted and analyzed by HPLC. The expressions of transgenes were verified by the red fluorescent of the reporter mCherry protein (Figure 4(a)), and the profiles of major osmolytes accumulated in *H. elongata* GOP-Gad cells cultured in different media are shown in Figures 4(b) and 4(d). From these profiles, we found no significant difference in the amount of GABA accumulated in *H. elongata* GOP-Gad cells cultured in different media. However, when the total osmolytes inside the cells were compared (Figures 4(c) and 4(e)), it became more evident that *H. elongata* GOP-Gad cells cultured in the medium containing $(NH_4)_2SO_4$ as an N source accumulated more osmolytes than the cells cultured in the medium containing $NaNO_3$ as an N source. Interestingly, we also found that *H. elongata* GOP-Gad cannot survive in a medium containing 6% w/v NaCl when $NaNO_3$ was used as an N source (data not shown). Therefore, $(NH_4)_2SO_4$ was selected as an N source for our medium formula.

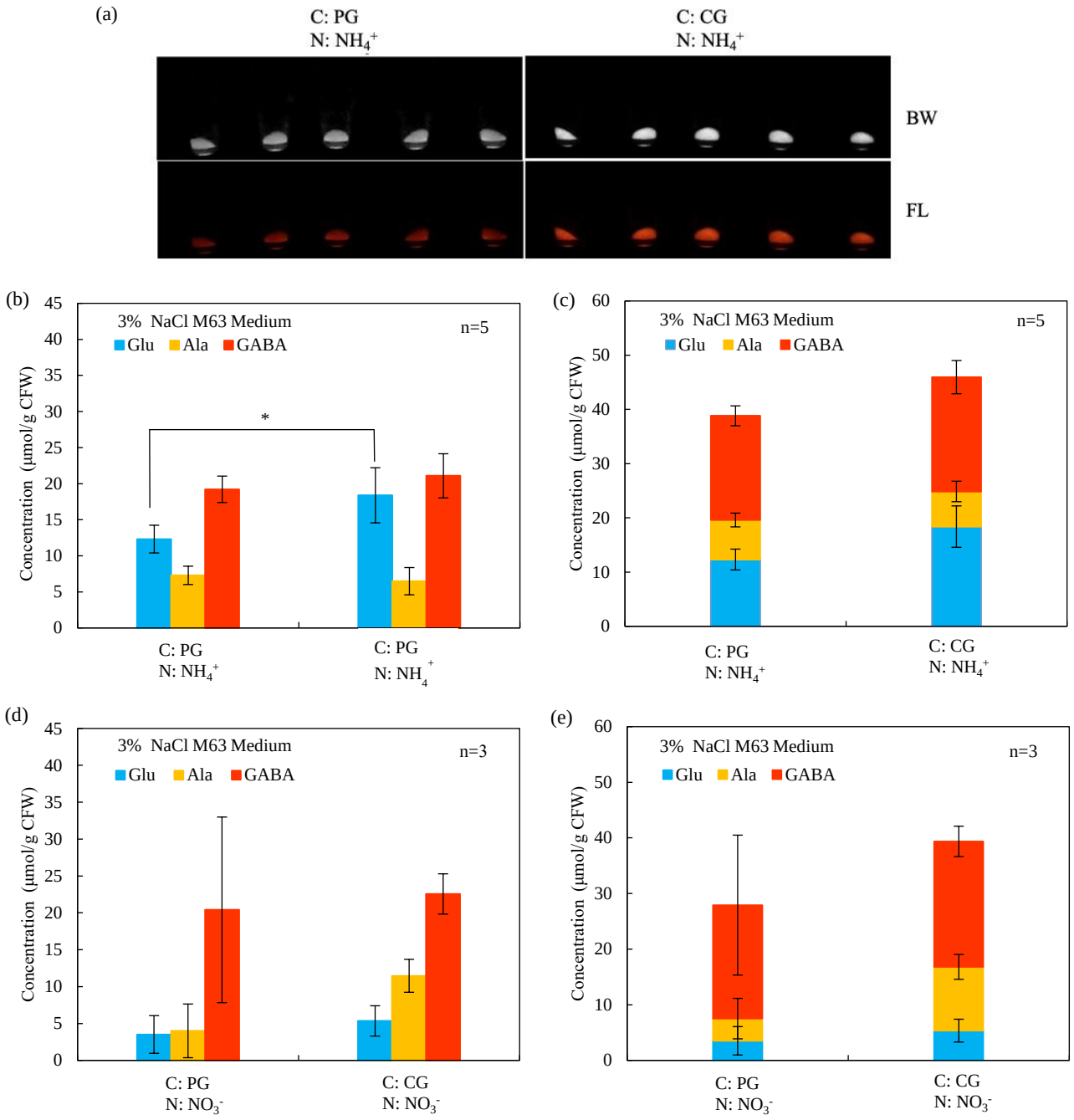

Figure 4. Profiles of major osmolytes in the cells of *H. elongata* GOP-Gad cultured in M63 media containing 3% w/v NaCl, 4% w/v glycerol derived from PG or CG as a C source, and 15 mM $(NH_4)_2SO_4$ or 30 mM $NaNO_3$ as an N source. Major osmolytes were extracted when OD_{600} of the main culture reached 0.9-1.2 and analyzed by HPLC. Data was normalized with internal standard norvaline. Values are mean±standard deviation (n=5). Glu, blue columns; Ala, yellow columns; GABA, red columns. *H. elongata* GOP-Gad was precultured in an M63 medium containing 3% w/v NaCl and 4% w/v PG. When the culture's OD_{600} reached 1.0, the cells were washed with a C, N-free M63 medium containing 3% w/v NaCl and used as 5% v/v inoculum for the main cultures. (a) Images of the pellets of *H. elongata* GOP-Gad cells. The cells were harvested when OD_{600} reached 1.0, and photos of the pellet were taken to visualize the red fluorescent of the reporter mCherry protein accumulated in *H. elongata* GOP-Gad as a marker to show correct expression from the salt-inducible *mCherry-HopGadBmut* operon. FL, fluorescent images of the cell pellets taken under blue light using an orange filter; BW, black and white images modified from FL images to show cell pellets. (b) Profiles of major osmolytes accumulated in *H. elongata* GOP-Gad cultured in M63 medium containing 4% w/v glycerol derived from PG or CG as a C source and 15 mM $(NH_4)_2SO_4$ as an N source. (c) Profiles of total osmolytes accumulated in *H. elongata* GOP-Gad cultured in M63 medium containing 4% w/v glycerol derived from PG or CG as a C source and 15 mM $(NH_4)_2SO_4$ as an N source. (d) Profiles of major osmolytes accumulated in *H. elongata* GOP-Gad cultured in M63 medium containing 4% w/v glycerol derived from PG or CG as a C source and 30 mM $NaNO_3$ as an N source. (e) Profiles of total osmolytes accumulated in *H. elongata* GOP-Gad cultured in M63 medium containing 4% w/v glycerol derived from PG or CG as a C source and 30 mM $NaNO_3$ as an N source.

3.3 Production of GABA by *H. elongata* GOP-Gad cultured in high-salinity medium containing CG and ammonia as the sole C and N sources

H. elongata GOP-Gad was precultured in LB medium containing 6% w/v NaCl to OD_{600} of more than 1.00, then the cells were washed 3 times in LB medium containing 6% w/v NaCl without C source and used as 10% v/v inoculum for the main culture in M63 minimal medium containing 7% w/v NaCl, 15 mM $(NH_4)_2SO_4$, and 4% w/v glycerol derived from PG or the partially purified CG. Major osmolytes in the cells were harvested when OD_{600} of the cultures reached 0.80 to 1.00. The expressions of transgenes were verified by the red fluorescent of the reporter mCherry protein (Figure 5a), and as shown in Figure 5b, the cells grown in high-salinity medium containing PG as C source accumulate GABA at the concentration of 26 µmol/g CFW, while those grown in high-salinity medium containing CG as C source accumulate GABA at the concentration of 28 µmol/g CFW. As expected, the concentration of GABA accumulated in *H. elongata* GOP-Gad cells cultured in higher salinity media (containing 7% w/v NaCl) is higher than those cultured in lower salinity (3% w/v NaCl) media (Figure 4). Based on data shown in Figures 4 and 5, *H. elongata* GOP-Gad can effectively use CG and ammonia as the sole C and N sources for GABA production.

Although an engineered *Escherichia coli* could produce 19.8 g of GABA per 1 L medium (Yu et al., 2019) and a recombinant *Corynebacterium glutamicum* expressing *E. coli*' GAD mutant could produce 38.6 g of GABA per 1 L medium (Choi et al., 2015), these strains cannot grow in a medium with high-salinity. Besides, these strains do not accumulate GABA in their cells. GABA produced by these strains is exported into the medium. Therefore, comparing our yield to those obtained by these strains is difficult. Further development of GABA-producing *H. elongata* strains, the medium formula, and the growth conditions are underway in our laboratory to improve GABA yield from *H. elongata* cell factory.

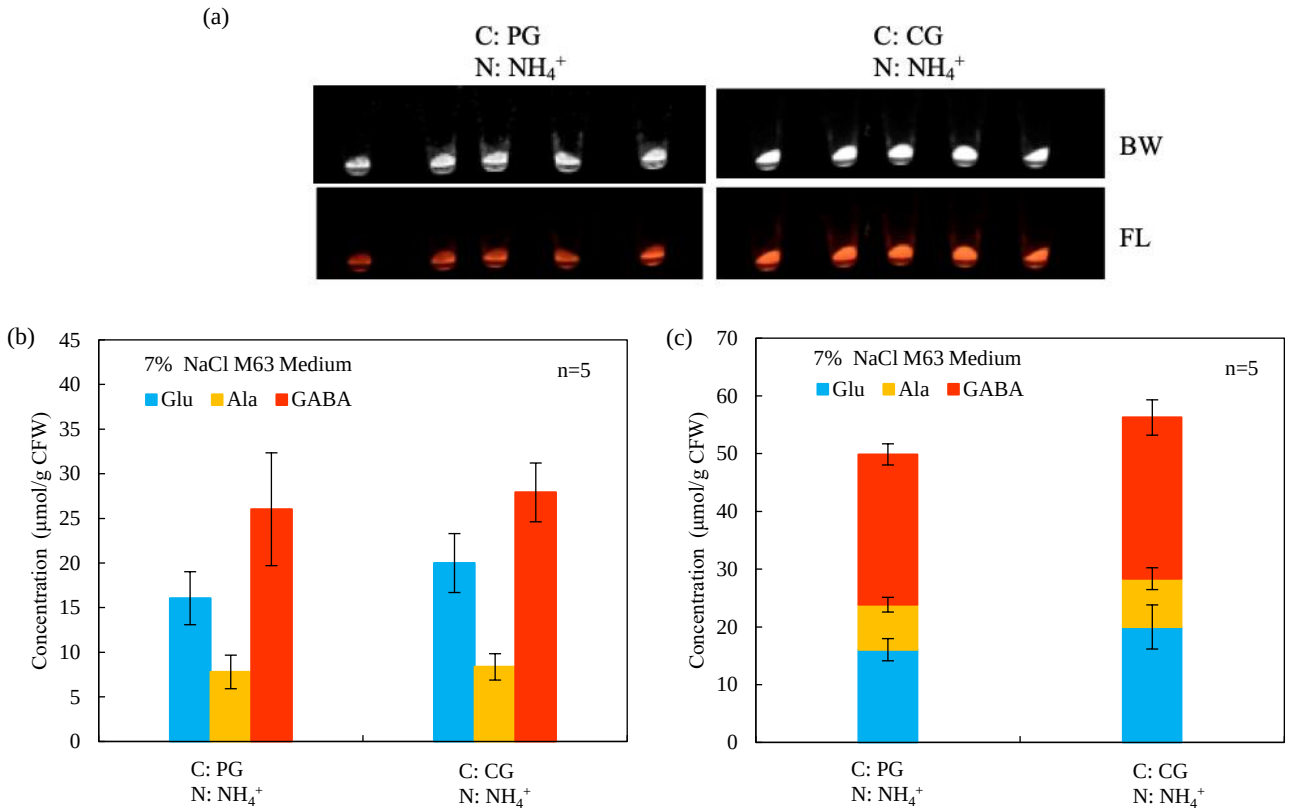

Figure 5. Profiles of major osmolytes in the cells of *H. elongata* GOP-Gad cultured in high-salinity M63 medium containing 6% w/v NaCl, 4% w/v glycerol from PG or CG as a C source, and 15 mM $(NH_4)_2SO_4$ as an N source. *H. elongata* GOP-Gad was precultured in high-salinity LB medium containing 6% w/v NaCl until the OD_{600} reached 1.0 when the cells were washed with C, N-free M63 medium containing 6% NaCl before being used as a 5% v/v inoculum for the main cultures in M63 medium containing 7% w/v NaCl, 4% w/v glycerol derived from PG or CG as a C source, and 15 mM $(NH_4)_2SO_4$ as an N source. Major osmolytes were extracted when OD_{600} of the main culture reached 0.8 to 1.0 and analyzed by HPLC. Data was normalized with internal standard norvaline. Values are mean±standard deviation (n=3 or 5 as indicated). Glu, blue columns; Ala, yellow columns; GABA, red columns. (a) Images of the pellets

of *H. elongata* GOP-Gad cells. The cells were harvested when OD_{600} reached 1.0, and photos were taken to visualize the red fluorescent of mCherry protein accumulated in *H. elongata* GOP-Gad as a marker to show correct expression from the salt-inducible *mCherry-HopGadBmut* operon. FL, fluorescent images of the cell pellets taken under blue light using an orange filter; BW, black and white images modified from FL images to show cell pellets. (b) Profiles of major osmolytes accumulated in *H. elongata* cells cultured in M63 medium containing 7% w/v NaCl, 4% w/v glycerol derived from PG or CG as a C source, and 15 mM $(NH_4)_2SO_4$ as an N source. (c) Profiles of total osmolytes accumulated in *H. elongata* cells cultured in M63 medium containing 7% w/v NaCl, 4% w/v glycerol derived from PG or CG as a C source, and 15 mM $(NH_4)_2SO_4$ as an N source.

4. CONCLUSION

BDF is currently in demand as a renewable energy source. For every gallon of BDF produced, approximately 0.3 kg of CG is generated (Ayoub and Abdullah, 2012; Bozbas, 2008). However, CG derived from the biodiesel production process contains high concentrations of salt and other impurities, which interfere with the downstream purification process, increasing the cost of CG application (Thompson and He, 2006). Here, we successfully used CG, partially purified by a simple and low-cost method, as a C source in the medium for culturing the GABA-producing *H. elongata* GOP-Gad. We confirmed that *H. elongata* GOP-Gad cultured in the high-salinity medium (7% w/v NaCl) containing CG as the sole C source could produce and accumulate GABA up to 28 µmol/g CFW. This concentration is comparable to that obtained from the *H. elongata* GOP-Gad cells cultured in the same medium supplemented with PG.

Industrial wastewater contains much higher N concentration than groundwater, and the most problematic N compounds in industrial wastewater are ammonia and nitrate (Islam and Suidan, 1998; Feleke and Sakakibara, 2002; Terada et al., 2003; Sumino et al., 2006). Our result shows that *H. elongata* GOP-Gad can use ammonia and nitrate as N sources for cell growth and GABA production. Therefore, N in industrial wastewater can be used directly in the production of GABA by *H. elongata* GOP-Gad without additional nitrification and denitrification processes, which would decrease the cost of wastewater treatment.

GABA is a natural feed supplement that benefits egg production (Zhang et al., 2012; Park and Kim, 2015). Therefore, GABA-producing *H. elongata* GOP-Gad cells have the potential to be further developed into an eco-friendly functional feed supplement for the poultry farming industry.

ACKNOWLEDGEMENTS

We thank the Nagasaki Prefectural Institute of Environment and Public Health, Omura City, Nagasaki, Japan, and the Social Welfare Corporation COSMOS association, Minami Shimabara City, Nagasaki, Japan, for providing the CG byproduct of BDF. We also thank Dr. Yasuyuki Ikegami and Dr. Kazuya Urata of the Institute of Ocean Energy, Saga University, Japan, for technical assistance with ICP-AES analysis, and Dr. Masaya Nishiyama and Dr. Mitsuhiko Koyama of Nagasaki University, Japan for insightful discussions. This work was partially supported by JSPS KAKENHI Grant Numbers 19K12400 and 22K12446, JST Grant Number JPMJPF2117, IFO Grant Number LA-2022-035, the Nagasaki University WISE Program, and the Nagasaki University Priority Research Subject Project.

REFERENCES

Ayoub M, Abdullah AZ. Critical review on the current scenario and significance of crude glycerol resulting from biodiesel industry towards more sustainable renewable energy industry. Renewable and Sustainable Energy Reviews 2012;16(5): 2671-86.

Bozbas K. Biodiesel as an alternative motor fuel: Production and policies in the European Union. Renewable and Sustainable Energy Reviews 2008;12(2):542-52.

Cánovas D, Vargas C, Iglesias-Guerra F, Csonka LN, Rhodes D, Ventosa A, et al. Isolation and characterization of salt-sensitive mutants of the moderate halophile *Halomonas elongata* and cloning of the ectoine synthesis genes. Journal of Biological Chemistry 1997;272(41):25794-801.

Chen GQ, Zhang X, Liu X, Huang W, Xie Z, Han J, et al. *Halomonas* spp., as chassis for low-cost production of chemicals. Applied Microbiology and Biotechnology 2022;106(21):6977-92.

Choi JW, Yim SS, Lee SH, Kang TJ, Park SJ, Jeong KJ. Enhanced production of gamma-aminobutyrat (GABA) in recombinant *Corynebacterium glutamicum* by expressing glutamate decarboxylase active in expanded pH range. Microbial Cell Factory 2015;14:Article No. 21.

Feleke Z, Sakakibara Y. A bio-electrochemical reactor coupled with adsorber for the removal of nitrate and inhibitory pesticide. Water Research 2002;36(12):3092-102.

Gerpen JV. Biodiesel processing and production. Fuel Processing Technology 2005;86(10):1097-107.

Islam S, Suidan MT. Electrolytic denitrification: Long term performance and effect of current intensity. Water Research 1998;32(2):528-36.

Kosamia NM, Samavi M, Uprety BK, Rakshit SK. Valorization of biodiesel byproduct crude glycerol for the production of bioenergy and biochemicals. Catalysts 2020;10(6):Article No. 609.

Nakagawa H, Harada T, Ichinose T, Takeno K, Matsumoto S, Kobayashi M, et al. Biomethanol production and CO_2 emission reduction from forage grasses, trees, and crop

residues. Japan Agricultural Research Quarterly 2007;41(2): 173-80.

Nakayama H, Shin Y, Sumita T, Urata K, Ikegami Y. Characterization of manganese oxide-biomineralization by the psychrophilic marine bacterium, *Arthrobacter* sp. Strain NI-2 and its spontaneous mutant strain NI-2´. Environment and Natural Resources Journal 2019;17(4):68-77.

Nakayama H, Kawamoto R, Miyoshi K. Ectoine production from putrefactive non-volatile amines in the moderate halophile *Halomonas elongata*. IOP Conference Series: Earth and Environmental Science 2020;439:Article No. 012001.

Ono H, Okuda M, Tongpim S, Imai K, Shinmyo A, Sakuda S, et al. Accumulation of compatible solutes, ectoine and hydroxyectoine, in a moderate halophile, *Halomonas elongata* KS3 isolated from dry salty land in Thailand. Journal of Fermentation and Bioengineering 1998;85(4):362-8.

Ono H, Sawada K, Khunajakr N, Tao T, Yamamoto M, Hiramoto M, et al. Characterization of biosynthetic enzymes for ectoine as a compatible solute in a moderately halophilic eubacterium, *Halomonas elongata*. Journal of Bacteriology 1999; 181(1):91-9.

Pagliaro M, Rossi M. The future of glycerol. RSC Green Chemistry Series. 2nd ed. Cambridge: RSC Publishing; 2010.

Park J, Kim I-S. Effects of dietary gamma-aminobutyric acid on egg production, egg quality, and blood profiles in layer hens. Veterinární Medicína 2015;60(11):629-34.

Perroud B, Le Rudulier D. Glycine betaine transport in *Escherichia coli*: Osmotic modulation. Journal of Bacteriology 1985;161(1):393-401.

Sambrook J, Russel DW. Molecular Cloning: A Laboratory Manual. 3rd ed. New York: Cold Spring Harbor Laboratory Press; 2001.

Sauer T, Galinski EA. Bacterial milking: A novel bioprocess for production of compatible solutes. Biotechnology and Bioengineering 1998;57(3):306-13.

Schwibbert K, Marin-Sanguino A, Bagyan I, Heidrich G, Lentzen G, Seitz H, et al. A blueprint of ectoine metabolism from the genome of the industrial producer *Halomonas elongata* DSM 2581T. Environmental Microbiology 2011;13(8):1973-94.

Sumino T, Isaka K, Ikuta H, Saiki Y, Yokota T. Nitrogen removal from wastewater using simultaneous nitrate reduction and anaerobic ammonium oxidation in single reactor. Journal of Bioscience and Bioengineering 2006;102(4):346-51.

Tanimura K, Nakayama H, Tanaka T, Kondo A. Ectoine production from lignocellulosic biomass-derived sugars by engineered *Halomonas elongata*. Bioresource Technology 2013;142:523-9.

Terada A, Hibiya K, Nagai J, Tsuneda S, Hirata. Nitrogen removal characteristics and biofilm analysis of a membrane-aerated biofilm reactor applicable to high-strength nitrogenous wastewater treatment. Journal of Bioscience and Bioengineering 2003;95(2):170-8.

Thompson JC, He BB. Characterization of crude glycerol from biodiesel production from multiple feedstocks. Applied Engineering in Agriculture 2006;22(2):261-5.

Tominaga Y, Funagoshi A, Koga Y, Yamaguchi Y. Examination of promotion the BDF using biomethanol. Annual Report of Nagasaki Prefectural Institute of Environment and Public Health 2014;60:105-8 (in Japanese).

Tominaga Y, Funagoshi A, Koga Y, Yamaguchi Y. Examination of promotion the biodiesel fuel using biomethanol (2). Annual Report of Nagasaki Prefectural Institute of Environment and Public Health 2015;61:93-6 (in Japanese).

Vreeland RH, Litchfield CD, Martin EL, Elliot E. *Halomonas elongata*, a new genus and species of extremely salt-tolerant bacteria. International Journal of Systematic and Evolutionary Microbiology 1980;30(2):485-95.

Ye JW, Chen GQ. *Halomonas* as a chassis. Essays in Biochemistry 2021;65(2):393-403.

Yu P, Ren Q, Wang X, Huang X. Enhanced biosynthesis of γ-aminobutyric acid (GABA) in *Escherichia coli* by pathway engineering. Biochemical Engineering Journal 2019;141:252-8.

Zhang M, Zou XT, Li H, Dong XY, Zhao W. Effect of dietary γ-aminobutyric acid on laying performance, egg quality, immune activity and endocrine hormone in heat-stressed Roman hens. Animal Science Journal 2012;83(2):141-7.

Zou Z, Kaothien-Nakayama P, Ogawa-Iwamura J, Nakayama H. Metabolic engineering of high-salinity-induced biosynthesis of γ-aminobutyric acid improves salt-stress tolerance in a glutamic acid-overproducing mutant of an ectoine-deficient *Halomonas elongata*. Applied and Environmental Microbiology 2024;90(1):e01905-23.

Environment and Natural Resources Journal

Volume 22
Issue 6
2024

Perceived Impacts of Climate Change on Coastal Aquaculture in the Cyclone Prone Southwest Region of Bangladesh

Al Amin, Zahid Hasan, Syed Rubaiyat Ferdous, Mariom, and Md Samsul Alam*

Department of Fisheries Biology and Genetics, Bangladesh Agricultural University, Mymensingh 2202, Bangladesh

ARTICLE INFO

Received: 27 Apr 2024
Received in revised: 17 Sep 2024
Accepted: 19 Sep 2024
Published online: 31 Oct 2024
DOI: 10.32526/ennrj/22/20240117

Keywords:
Climate change/ Coastal aquaculture/ Socio-economic impacts/ Aquatic ecosystems/ Vulnerability/ Human migration

*** Corresponding author:**
E-mail: samsul.alam@bau.edu.bd

ABSTRACT

The southwest region of Bangladesh is particularly vulnerable to a range of climatic threats, including cyclones, prolonged flooding, sea level rise, saltwater intrusion, drought, and riverbank erosion. The study investigates how these different drivers affect aquaculture systems and aims to provide critical insights for sustainable management. The survey work focused on the problems, vulnerabilities, migration, and adaptive strategies of communities of the southwest region of Bangladesh, that rely heavily on shrimp, fish, and crab production for their livelihoods. Data were collected from the 80 respondents across four unions (Atulia, Burigoalini, Gabura, and Bhurulia) in Shyannagar Upazila, Satkhira District, using a structured questionnaire survey and focus group discussions. Findings reveal that climate change events have significantly changed shrimp farming in enclosures, pond aquaculture, and crab point management, and negatively impacted livelihoods. Pond aquaculture appeared to be the most vulnerable to climate change conditions, followed by shrimp farming in enclosures and crab points. Furthermore, the adverse effects of climate change compelled human migration within the study area, primarily driven by the search for employment. This study provides evidence of the effects of various climate change stressors on shrimp, fish, and crab production systems and the adaptive difficulties of the communities dependent on aquatic ecosystems. As the natural calamity like cyclone cannot be prevented, understanding the impact of previous events may help people of the affected area as well as the policy makers to plan for better survival.

1. INTRODUCTION

Over the past two decades, discussions of the effects of climate change and related impacts have become common in national and international forums. Scientists, environmentalists, and even politicians have stated various opinions and findings regarding the changing climate and its current and anticipated impacts. The impact of global climate change is being researched by the Intergovernmental Panel on Climate Change (IPCC) and the United Nations Framework Convention on Climate Change (UNFCCC). Climate impacts could be confined to a single location or affect the entire planet and could happen in terms of average weather conditions or the distribution of weather events around an average (Yazdi and Shakouri, 2010). Humans have been recognized as the major contributors to climate change through the use of fossil fuels such as coal, oil, and gas (Doubleday et al., 2013; Gao et al., 2016; Palmer and Stevens, 2019) as well as deforestation and forest degradation (Khaine and Woo, 2015) that emit greenhouse gases (GHGs) into the atmosphere.

Bangladesh is highly exposed to natural disasters and vulnerable to the effects of climate change (Kabir et al., 2016; Alam et al., 2020; Sarker et al., 2020; Rahaman et al., 2021). Bangladesh was ranked sixth among the nations most adversely affected by climate change between 1997 and 2016 by the Global Climate Risk Index 2018 (Naser et al., 2019). Global climate change-related problems, such

Citation: Amin A, Hasan Z, Ferdous SR, Mariom, Alam MS. Perceived impacts of climate change on coastal aquaculture in the cyclone prone Southwest Region of Bangladesh. Environ. Nat. Resour. J. 2024;22(6):535-546. (https://doi.org/10.32526/ennrj/22/20240117)

as saltwater intrusion, sea level rise, drought, and riverbank erosion, significantly impact Bangladesh's southern region (Alam et al., 2010; Khan et al., 2011; Rana et al., 2011). Around the Indian subcontinent, the IPCC expects sea levels to rise between 15 and 38 cm by 2050 and 46 and 59 cm by 2100. By noting the percentage of inundation for the Sundarbans, the World Bank Report 2000 estimated the sea level rise for those areas step by step (Das, 2022).

Human activity and climate change have directly impacted coastal aquaculture. This human intervention directly forces human migration (Naser et al., 2019). Islam et al. (2022) showed that people in southwest areas of Bangladesh were particularly exposed to climate stressors such as riverbank erosion, salinity intrusion, temperature increase, salinity increase, and drought.

Shyamnagar Upazila (sub-district) of Satkhia District covers an area of 1,968 km^2, located between 21°36' and 22°24' north latitudes and in between 89°00' and 89°19' east longitudes. A total of 19,997 ha of land of Shyamnagar Upazila is currently used for fish, shrimp, and crab farming, which is 10.5% of the total area of the Upazila. The Bay of Bengal is on the south of Shyamnagar Upazila. So, it is prone to almost all the cyclones originating in the Bay of Bengal that traverse to the Bangladesh Coast. The major cyclones since 2007, namely Sidr, Aila, and Amphan, caused widespread damage in Shyamnagar Upazila (Tajrin and Hossain, 2017).

Due to Shyamnagar's significance as a fish, shrimp, and crab farming area and the threat posed by climate change on Bangladesh's Southwest Coast, we investigated how residents of Shyamnagar Upazila perceive the effects of climate change on fish, shrimp, and crab farming. This study also provides new information on the geographical human movement and vulnerability of Bangladesh's southwest shore.

2. METHODOLOGY

2.1 Study areas

The study was conducted in Shyamnagar Upazila in the Satkhira District of Bangladesh. As of the 2011 census, Shyamnagar Upazila had 72,279 households and a population of 318,254. Shyamnagar Upazila has 12 Unions. We collected data from four Unions (the smallest rural administrative and local government unit in Bangladesh comprising several villages): Atulia, Burigoalini, Gabura, and Bhurulia (Figure 1). The GPS coordinates of all four locations were recorded. Atulia union is located between 22°20'59" and 22°21'19" N latitude, and 89°12'14" and 89°11'47" E longitude; Burigoalini union is located between 22°28'27" and 22°26'17" N latitude and 89°20'27" and 89°19'07" E longitude; Gabura union is located between 22°24'07" and 22°22'17" N latitude and 89°27'15" and 89°25'05" E longitude; Bhurulia union is located between 22°09'29" and 22°08'19" N latitude, and 89°13'11" and 89°12'01" E longitude.

2.2 Secondary data review

We collected secondary data from the Department of Fisheries (Bangladesh), Bangladesh Bureau of Statistics, and existing literature. We also collected secondary data on annual sea level rises and occurrences of floods in Shyamnagar Upazila from the Bangladesh Meteorological Department (BMD) in Dhaka.

2.3 Collection and analysis of primary data

We developed a questionnaire that included the socio-economic information of the respondents, fish farmer types, names of fish/shellfish/mollusk species used for farming, trend in the production and profitability of fish, shrimp, and crab, and the driving forces behind the changes, threats to these production systems, livelihood opportunities, and trends in human migration. We obtained a list of people involved in fish/shrimp/crab farming from the Shyamnagar Upazila office of the Department of Fisheries of the Government of Bangladesh. We then randomly selected and interviewed 20 respondents from the four selected unions. 59% of participants were between 20 and 40 years old, with 30% above 40 years old and 11% under 20 years old. We performed four Focus Group Discussions (FGD), one in each of the four study unions with randomly selected group members. FGD participants included fish farmers, shrimp farmers, crab point owners, and community members. Based on the gathered information, we categorized the farms in the study area into three types: small (less than 0.8 ha), Medium (0.8 to 1.6 ha), and large (greater than 1.6 ha).

2.4 Vulnerability assessment

We measured the vulnerability of location based on Exposure (E), sensitivity (S), and adaptive capacity (AC) by the following equation (Yohe et al., 2002):

$$\text{Vulnerability} = E + S - AC$$

Where Exposure = Likelihood of threats × Magnitude of the impacts

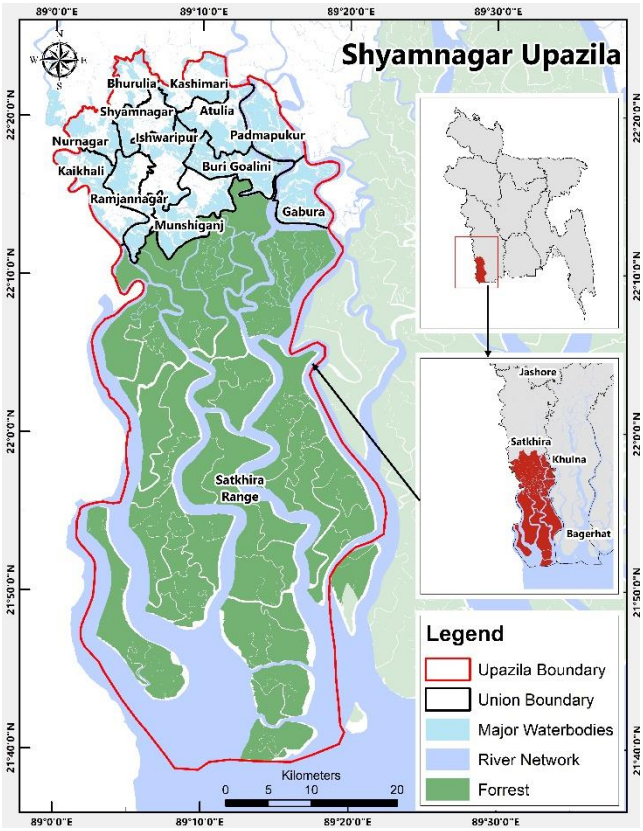

Figure 1. Map of Bangladesh showing the study area. The names of the Unions are shown in the map.

Threats and impacts are floods, erratic rain, salinity, sea level rise, temperature, and storm surge.

2.5 Quantifying the vulnerability assessment factors

1) Likelihood of flood (number of times): 5=very high (more than three times in a year), 4=high (3 times in a year), 3=moderately high (2 times in a year), 2=medium (1 time in a year, and 1=Low (flood with no impact)

2) Magnitude of the impacts of the flood (Duration of flood): 5=very high (more than 15 days), 4=high (10-14 days), 3=moderately high (7-9 days), 2=medium (4-6 days), and 1=low (2-3 days)

3) Likelihood and magnitude of the impacts of erratic rain, sea level rise, salinity intrusion, temperature rise, and storm surge: 5=very high, 4=high, 3=moderately high, 2=medium, and 1=low

4) Sensitivity (S): Sensitivity means the degree to which fish/shrimp/crab farmers depend on aquatic resources as a primary livelihood strategy, and are therefore susceptible to any change in the sector. 25=very high (80% or above people impacted), 20= high (70-79% of people impacted), 15=medium (50-69% of people impacted), and 10=low (50% or less of people impacted).

5) Adaptive Capacity (AC): Adaptive capacity is determined based on poverty status, literacy, access infrastructure in the form of community support, roads, educational institutes, medical facilities, government and NGO assistance during emergencies, electricity coverage, drinking water facilities and presence of other amenities. 50=excellent, 30=very good, 20=good, 10=moderate, 5=poor, 2=very poor, 1=extremely poor.

6) Migration: Community perceptions of permanent, temporary migration, and non-migrants were analyzed based on a questionnaire survey and FGDs. The values indicate the percentages of the respondents who agreed with the statement that natural hazards forced people to migrate.

All collected data were processed and analyzed by using MS Excel 2021, version 2107 (Microsoft Corporation, NY, USA).

3. RESULTS AND DISCUSSION

Bangladesh, due to its geographical location, receives about 40% of the total impacts of global climate change (Dasgupta et al., 2010). We analyzed the perceived impacts of climate change on the production systems of fish, shrimp, and crab farms and the livelihoods, vulnerability, and coping strategies of

the fish, shrimp, and crab farmers of Bangladesh's natural calamity-prone southwest region. The education level of respondents in the study area appears to be very poor: 24% were illiterate, 40% could sign only, 20% had primary level education, and only 6% had above secondary level education. Most respondents (56%) had small-sized farms (less than 0.8 ha), 18% had medium-sized farms (between 0.8 and 1.6 ha), and 16% had large-sized farms (greater than 1.6 ha). We analyzed the perceived impacts of climate change on the production systems of fish, shrimp, and crab farms and the livelihoods, vulnerability, and coping strategies of the fish, shrimp, and crab farmers of Bangladesh's natural calamity-prone southwest region.

3.1 Perceptions of the respondents on the aquaculture systems

Cultured species varied in the three systems (Shrimp farming enclosure, Crab point, and fish ponds). The most preferred cultivable species for livelihoods ranked according to the focus group discussions of the respondents are listed in Table 1. In shrimp farming enclosures, the black tiger prawn (*Penaeus monodon*) was the most cultured species. *P. monodon* is a marine species and can grow well in normal seawater. The growth and production rate of *P. monodon* is higher than other shrimp species farmed in Bangladesh. As the salinity in the shrimp farming enclosures is high, no freshwater species can grow well in these enclosures. From July 2021 to June 2022, 24,802 metric tonnes of *P. monodon* were produced in Satkhira District, whereas the total production of all finfish species was 38,474 metric tonnes (FRSS, 2022). The high price of *P. monodon* in the local and international markets also inspires farmers to culture this species. Brown shrimp (*Metapenaeus monoceros*), Giant freshwater prawn (*Macrobrachium rosenbergii*), and Indian white prawn (*Metapenaeus affinis*) were also cultured with the black tiger shrimp. Mud crab (*Scylla serrata*) was the only cultured species in crab points. Several species were cultured in fish ponds, including Nile tilapia (*Oreochromis niloticus*), barramundi (*Lates calcarifer*), rohu *(Labeo rohita*), catla (*Catla catla*), mrigal (*Cirrhinus cirrhosus*), and pangasius (*Pangasianodon hypophthalmus*).

Post larvae (PL) of *P. monodon* are readily available in hatcheries and local rivers and estuaries. Brown shrimp (*Metapenaeus monoceros*), mud crab (*Scylla serrata*), and barramundi (*Lates calcarifer*) were the second, third, and fourth-ranked cultured species, respectively, because these species were sold rather than consumed for subsistence, due to their high market value. Nile tilapia ranked fifth because of its low demand and lower market price. Pangasius, rohu, catla, Indian white prawn andsilver barb (*Barbodes gonionotus*) were the sixth, seventh, eighth, ninth, and tenth-ranked cultured species, respectively (Table 1). All these species are cultured due to availability, high demand, and reasonable price.

Table 1. Important cultured fish, shrimp, and crab species, ranks and reasons of importance

Mean rank	Local name	Common English name	Scientific name	Reasons	Production trend
1	Bagda	Black tiger shrimp	*Penaeus monodon*	High price and market demand, cash crop	Increasing
2	Horina chingri	Brown shrimp	*Metapenaeus monoceros*	High market demand, easily cultivable with Bagda, medium price, available	Stable
3	Kankra	Mud crab	*Scylla serrata*	High market demand, high price, available, cash crop.	Increasing
4	Bhetki	Barramundi	*Lates calcarifer*	High market demand, less available	Decreasing
5	Tilapia	Nile Tilapia	*Oreochromis niloticus*	Market demand, available, cheap	Increasing
6	Thai Pangas	Thai Pangas	*Pangasianodon hypophthalmus*	Available, high growth rate, sold	Increasing
7	Rohu	Indian Major carp	*Labeo rohita*	Available, high demand, eaten	Stable
8	Catla	Indian Major carp	*Catla catla*	Available, high demand, eaten, sold	Stable
9	Chaka Chingri	Indian white prawn	*Metapenaeus affinis*	Available, good price, sold	Decreasing
10	Sarpunti	Thai barbs	*Barbodes gonionotus*	Good price, eaten, sold	Decreasing

The first four species (*P. monodon, M. monoceros, S. serrata*, and *L. calcarifer*) are marine or brackishwater species and are the most preferred species for culture in this region. *P. hypophthalmus* has become one of the cheapest protein sources in Bangladesh because of its wide range of environmental tolerance, excellent growth, and survival rate. Pangasius can be cultured at four ppt salinity with a desirable growth rate similar to freshwater (Mandal et al., 2020). Hasan et al. (2023) reported that the pangasius fingerlings can be cultured in salinities up to 10 ppt without negatively affecting growth and survival rate. Nile tilapia is another important aquaculture species in Bangladesh. *O. niloticus* can tolerate brackish water conditions and can be grown in intensive farming systems. De Alvarenga et al. (2018) recommended salinity between 4 and 8 ppt (6 ppt) salinity to improve the growth performance of tilapia in the initial culture phase of biofloc. The final weight and specific growth rate of tilapia fingerlings were reported to be higher in shrimp farming enclosure at salinities of 4 and 8 ppt compared to 0 ppt under biofloc systems (Khanjani and Alizadeh, 2024) and recirculating aquaculture systems (RAS) (Dawood et al., 2023). Mirera and Okemwa (2023) state that *O. niloticus* could fully acclimate to seawater.

The present study indicates that the farmers of Shyamnagar upazila also culture the Indian major carp to some extent, and efforts have been made to assess the potentiality of these species in inland saline-affected areas. The Indian major carp rohu can tolerate salinity up to 10 ppt, but it is expected to perform well in less than six ppt salinity (Kumar et al., 2018). However, with an increase in salinity, the survival rate, growth, and tissue ascorbic acid level in *L. rohita* decreases, which indicates that it is vulnerable when exposed to salinity for a long durations (Sarma et al., 2020). An increase in salinity level significantly impacted the growth and physiology of the Indian major carp. This species can be reared in low-saline areas for some time, which will not only help in the utilization of salt-affected areas but also help generate employment and income (Ahirwal et al., 2021). The salinity of inland ponds in the coastal region varies over time, even having 0 ppt salinity during periods of extreme rainfall. Diversification of cultured species may help farmers cope with the impact of calamities linked to climate change.

3.2 The productivity of different systems

The respondents identified the key factors affecting productivity in each aquaculture system in the study area, and the main impacts and responses.

In shrimp farming enclosures, collected data included i) the size of the farming enclosure, ii) species composition (number of species and abundance of each species), iii) input costs (seed, fertilizer, and other chemicals), and iv) profitability as the critical factors affecting changes in productivity (Table 2). Profitability has changed due to increased production costs, unavailability of good quality seed (shrimp post-larvae and juveniles), and the incidence of bacterial and viral diseases.

According to the respondents, the siltation of shrimp farming enclosures due to cyclones including Sidr in 2007, Aila in 2009, Amphan in 2020, and many other climate change adversities are the critical factors in the negative changes in shrimp farming enclosures.

The key factors reported for the crab points included productivity (kg/unit area), the average size of the crab point, species composition, input costs (seed, feed), and profitability (Table 2). The significant changes in the crab culture system were- a) Sidr, Aila, and Amphan destroyed a substantial number of crab points; b) natural catch of crab used for stocking the crab points decreased substantially; and c) over the last 2-3 years (post-Amphan), hundreds of people became involved in crab fattening; d) crab consumption by villagers of all religions and castes followed an increasing trend.

The significant changes reported for freshwater fish ponds were; a) Sidr, Aila, and Amphan destroyed all the valuable freshwater wild fish species people used to catch for their household consumption; b) tilapia increased slightly during the pre-Amphan period, and a considerable increase was observed in the culture ponds afterwards; and c) stocked culture fish (Indian major carps) not growing well (Table 2).

3.3 Major changes in coastal aquaculture systems

The respondents in the FGDs identified the major events over the last 20 years that shaped their aquaculture systems regarding farm design and practice, species selection, and use of inputs (Table 3). The participants reported that cyclones Sidr (2007) and Aila (2009) caused the devastation of cereal crops, vegetables, fruits, and timbers, salinized the land and water, and lowered soil and water fertility. Several years after Sidr and Aila, the villagers had difficulty

growing plants in the soil and farming freshwater fish in the ponds. Therefore, among others, Sidr (2007), Aila (2009), and Amphan (2020) cyclone were considered in almost every response by the villagers concerning the changes in the culture practices and species over the selected period.

Table 2. Changes in productivity and profitability in different systems (shrimp farming enclosure, crab point, and fish pond) compared to 5/10 years back

System	Changes in productivity	Changes in profitability	Realized impacts		Livelihood responses
			From climate change action	From management	
Shrimp farming enclosure	Size (+) Species richness (+) Input costs (+) Water depth (−)	Profitability increasing or sometimes the same or decreasing	- Silt increase - Unviability of Post-larvae/juvenile - Salinity levels are increasing extremely	- Decrease in farming enclosure size - Increasing stocking density - Do not follow - Good Aquaculture Practice (GAP) - Shrimp disease	Diversification of species
Crab point	Size (+) Input costs (+) Water depth (−)	Profitability increasing	- Reducing natural catch - Devastation of crab points by cyclone	- Feeding crabs small pieces of tilapia	- Newcomers to crab fattening - Increased intake of crab
Fish pond	Water depth (−) Species composition (−) Input costs (+)	Profitability decreasing	- Salinity intrusion in pond water - Decreasing wild stock	- Tilapia increase - Stocked culture fish decrease	- Re-excavate ponds - Regular change of pond water

Table 3. Major events over the last 20 years affecting aquatic systems productivity

Factors	2002	2012	2022
Farm design and practice	- Large farm area - Proper water depth in shrimp farming enclosure, crab point, and fish pond	- Large farm area - Due to siltation, the depth of the water in shrimp farming enclosures and ponds dropped - Due to siltation and Sidr, the depth of the water in shrimp farming enclosures and ponds further dropped	- Smaller and divided farm area - Due to siltation, Aila, Amphan, and other factors, the water depth in shrimp farming enclosures and ponds further dropped.
Species abundance	- Rich in species diversity of freshwater wild fishes in ponds - No aquaculture done in fish in ponds	- River species diversity decreased - Exotic craps stocked in ponds - Introduction of tilapia (*Oreochromis niloticus*) in ponds and shrimp farming enclosures	- Wild fish decreased extensively from ponds - Ponds stocked with native and exotic carps, poor production
Input used	- No feed in the farm area - No fertilizer in the farm area	- No feed and fertilizer in fish ponds - Feeding shrimp with snail meat, using a yeast-molasses mixture, lime, and other fertilizers in shrimp shrimp farming enclosure - Chopped tilapia and eel fish for crab	- No feed and fertilizer in fish ponds - Many shrimp farming enclosure owners attempt to prepare the enclosure by removing bottom mud, liming, and feeding shrimp with feed pellets. - Chopped tilapia and other low-value fish for crab

3.4 Driving forces behind the changes

Many actors in the study area have changed productivity and livelihood. Shyamnagar Upazila is very vulnerable and influenced by climate change effects. The major threats related to climate change, as reported by respondents in the study areas, include increased salinity, sea level rise, drought, storm surge, long-term floods, riverbank erosion, and lack of finance (Table 4).

Drought (due to increased temperature or reduced rainfall) was found to be the most hazardous environmental factor for the three aquaculture systems (shrimp farming enclosure, crab point, and fishpond). Kabir et al. (2016) studied Baliatali and Ghopkhali villages of Amtali Upazila of Barguna District and found similar results.

Table 4. Driving forces behind the changes

Effects	The Magnitude of effects on different systems			Impact on coastal aquaculture
	Shrimp farming enclosure	Crab point	Fish pond	
Increased salinity	H	M	VH	- Disease outbreaks in different systems - Production is gradually decreasing.
Drought	VH	H	VH	- Loss of wild and cultured stock. - Increased production costs - Loss of opportunity as production is limited.
Storm surge	H	VH	VH	- Loss of aquaculture stock and damage to or loss of aquaculture facilities and fishing gear. - Additional cost for designing new facilities. Increased insurance cost.
Long time flood	VH	VH	VH	- Disease outbreak - Cultured area is flooded.
Riverbank erosion	VH	VH	VH	- Reduced area available for culture - Increased system management costs
Sea level rise	H	M	VH	- Reduced area available for freshwater aquaculture. - Shifts in species abundance, distribution and composition of fish stocks and aquaculture seed. - Reduced freshwater availability for aquaculture and a shift to brackish water species. - Reduced seed for aquaculture. Worsenede Exposure to waves and storm surges and risk that inland aquaculture becomes inundated.
Finance	VH	VH	VH	- Problem in management

VH=Very High, H=High, M=Medium

In shrimp farming enclosures, long floods and riverbank erosion cause very high adverse effects, and drought and salinity intrusion cause high and medium adverse effects on production, respectively. Anzum et al. (2023) also reported that increased temperature, reduction in rainfall, long summers, floods, and cyclones affected the farmers. People in the study area expressed interest in traditional methods rather than modern aquaculture practices. Howlader and Akanda (2016) reported the same outcomes in Galachipa and Patuakhali Sadar upazila under the Patuakhali District of Bangladesh. In crab points, drought, riverbank erosion, and longtime floods affected the study area highly, and salinity intrusion and storm surges affected moderately and highly, respectively. Hossain et al. (2018) also reported similar findings in their Atulia Union of Shyamnagar Upazila study. In fishponds, salinity intrusion, sea level rise, long duration flood, riverbank erosion, and drought affected the study area very highly. Shaibur et al. (2017) also observed the same facts for Shyamnagar, Satkhira. Chowdhury et al. (2012) reported that, on average, there are five storms per year or once every 9.5 weeks, and if the increasing trend continues, the cyclonic frequency may reach eight storms per year or once every 6.5 weeks by 2050 in Shyamnagar upazila.

3.5 Vulnerability and human migration in the study area

Natural hazards such as cyclones, long-duration floods, and droughts force humans to migrate from one place to another, temporarily or permanently, to take up employment or establish residence. We identified both temporary and permanent migration in the study area. The present study showed that the highest level of permanent (not returning to the place of origin) human migration (40%) occurred in the Bhurulia Union, where only 5% of people did not practice any form of migration. On the contrary, 40% of respondents were nonimmigrants in Atulia Union. The rates of permanent migration of Atulia, Burigoalini, Gabura, and Bhurulia Union were 10%, 25%, 35%, and 40%, respectively.

On the contrary, the rates of temporary migration (migration to avoid calamities but returning to the place of origin) in Atulia, Burigoalini, Gabura, and Bhurulia Union were 50%, 60%, 55%, and 55%, respectively. Searching for new jobs was found to be the most common cause of human migration (60%), followed by avoiding climate disasters (26%). In the last several years, people in the study area have lost wage-earning and livelihood opportunities due to climate-induced disasters and have become poor. They migrated to nearby and faraway districts for

laborious jobs like rickshaw pulling, brick field labour, and seasonal labour. This study revealed that migrations were mainly limited to the male population. Most of the people who migrated (seasonal or permanent) were unskilled. Climatic disasters were cited as the reason for migration in 26% of cases. Besides, 14% migrated for various other reasons (for a better lifestyle, opportunities, and study).

The present study's findings also aid in our understanding of the adaptive strategies available to achieve ecological and livelihood sustainability. Recent studies assessed the adaptive capacity of coastal aquaculture to cope with climate change (Melnychuk et al., 2014; Leith et al., 2014). Based on the findings of the present study and the body of current literature (Das, 2010; Chowdhury et al., 2012; Didar-Ul Islam et al., 2015; Akhter et al., 2016; Hossain and Hasan, 2017; Anzum et al., 2023) and South Asian countries (SA) contexts', primary adaptive reactions identified to the vulnerability of various coastal aquaculture systems are rising human migration, and diversifying livelihoods.

Due to its unique geographical features, Bangladesh suffers from regular natural hazards, including floods, tropical cyclones, storm surges, and droughts. These hazards lead to loss of life, damage to infrastructure, adverse impacts on livelihoods, and often displace individuals and communities from their places of residence. Khatun et al. (2021) reported that the people of the alluvial lands of the three major rivers of Bangladesh, namely -the Padma, the Jamuna, and the Meghna, remain under threat of erosion. They migrate seasonally or even permanently to neighbouring areas as an adaptation strategy to reduce risks and uncertainties. According to Mallick et al. (2022) and Black et al. (2013), climate-induced migration has somewhat stagnated in theorizing the concept of "migration as adaptation" and investigating the causes, drivers, factors, and dynamics of decision-making concerning migration or displacements. Migration to the cities not only creates an opportunity for temporary/alternative solutions for resettlement and livelihoods but also creates tremendous challenges for urban policies to adapt (Vinke, 2020).

Notably, the government of Bangladesh has initiated short-term, mid-term, and long-term development planning strategies, which include Five-Year Plans, Vision 2041, Second Perspective Plan, and Bangladesh Delta Plan 2100, along with the UN Agenda 2030 for achieving the sustainable development goals (SDGs). These plans mainly focus on thematic/sectoral and hotspot-specific strategies, policies, and programs, ignoring the regional imbalance and disparities in development and resource distribution, population size (Nahar et al., 2019), the occurrence of natural disasters, and production of climate/environmental migrants (Jones et al., 2016).

Shyamnagar Upazila is area in the Khulna division that produces the most migrants, and the study showed that the level of migration in the four Unions of Shyamnagar Upazila is similar to that reported in previous reports (Wiig et al., 2023; Akhter et al., 2016; Didar-Ul Islam et al., 2015). Since 2008, the number of disasters and internally displaced persons has increased enormously. The number of disasters recorded between 2008 and 2021 strongly correlates with the number of displaced persons in Bangladesh (Sakapaji, 2023).

3.6 Livelihood opportunities in the study area

There are limited livelihood opportunities in the study area (Figure 2). Most of the respondents were agriculture farmers/labourers (67), migrant workers (72), or brick kiln labourers (53). Other livelihoods are government service, rickshaw puller, NGO worker (trainers and micro credit providers), auto-rickshaw driver, wood collector, shopkeeper, motorcyclist, pseudomedicine practitioner, street vendor, cooking fuel collector, and palm-leaf collector/seller.

People of this locality have very few options for livelihood diversification. Most people are attached to farming or labouring (Hossain and Hasan, 2017). Climate change makes life miserable for this locality's people and forces them to abandon their family occupations (shrimp farming, crab fattening, and fish culture). Moreover, the scope of their work opportunities could be bigger. Most farmers opt for day labour, van or rickshaw pulling, and working in brick kilns for their livelihood diversification (Rahaman et al., 2021).

Fishers are firmly attached to their work, and diversifying has associated costs (Shaffril et al., 2017). So, the appropriate agencies should establish programs to intensify the promotion of non-fishing, non-natural resource dependent income-producing activities among small-scale fishers, which in turn should reduce their dependency on fishing and diversify their income (Shaffril et al., 2017). Examples of such mechanisms include diversification of livelihoods, such as switching between farming and fishing in response to seasonal and inter-annual

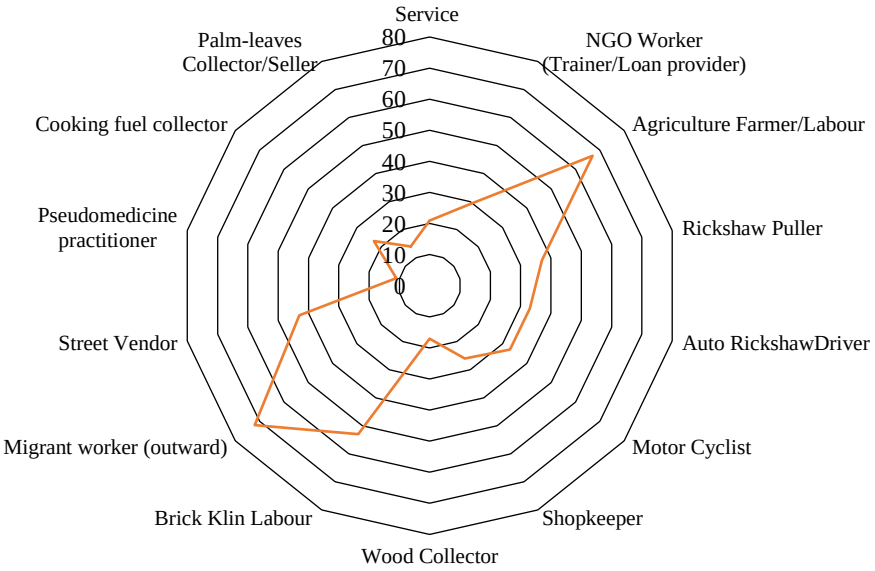

Figure 2. Livelihood opportunities other than aquaculture in the study area. The values indicate the number of respondents who opted for the opportunities. Each respondent opted for multiple livelihood opportunities.

variation in fish availability, providing opportunities with training, and taking up alternative income-generating activities.

One example of a growing activity in the study area is crab fattening. As indicated by participants in the focus groups, crab fattening is potentially profitable and a feasible fishery venture in and around the Satkhira Coast. The mud crab, *Scylla serrata* is widely distributed in the Pacific and Indian Oceans, including the Bangladesh Coast. The crabs produced in the crab fattening farms are quite healthy (nearly half of the total harvest), and the production is scaling up rapidly in the coastal areas. Several factors hinder the crab sector's sustainable development, including the supply of crablets. The collection of crablets from wild sources like rivers and estuaries is becoming risky for the environment, and the natural stock has already suffered overexploitation. In order to support the crab fattening industry, it is essential to establish crab hatcheries in the southwest region of Bangladesh.

3.7 Vulnerability of production systems in the study area

The respondents said fish ponds were the most vulnerable among those three systems. Freshwater species like pangasius, rohu, catla and tilapia are cultured in fishponds and cannot tolerate high salinity. Vulnerability levels of crab points, shrimp farming enclosures, and fishponds were 15.01, 23.05, and 30.99, respectively (Figure 3).

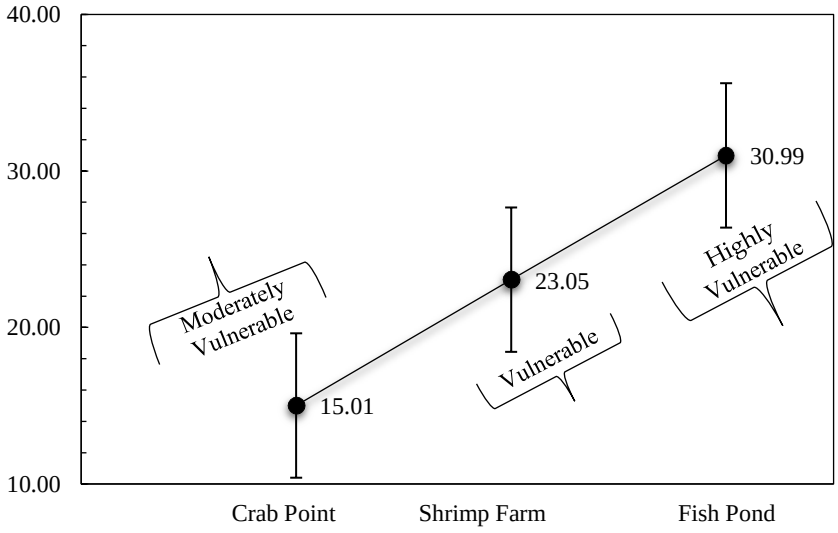

Figure 3. System-wise vulnerability of the study area

Salinity intrusion, sea level rise, long duration floods, riverbank erosion, and storm surges are the major problems contributing to coastal vulnerability. The participants of the FGD raised these issues and considered significant barriers to sustainable livelihoods and adaptation in the area. Hossain and Hasan (2017) stated that the Shyamnagar Upazila is highly vulnerable. Several natural calamities affect this study area every year. Climate change directly or indirectly affects people in this locality (Anzum et al., 2023). With the increased salinization of groundwater, fish, shrimp, and crab production faced many difficulties in this area (Rahaman et al., 2021). Kabir et al. (2016) studied the impact of cyclone Sidr on the Amtali Upazila of Barguna District, and cyclone Aila affected the Koyra Upazila of Khulna District and reported that they had severe consequences for the livelihood patterns of the affected population and their overall health status. Broadly, there is difficulty in gaining sufficient drinking water, which makes households very vulnerable to impacts in aquatic systems and exacerbates poverty (Hossain et al., 2018). The present study's findings suggest that bridging the different approaches to adapt vulnerable livelihoods to the more severe impacts seen in the aquatic system is crucial.

4. CONCLUSION

The southwest coast of Bangladesh is highly prone to cyclones and other natural calamities, the frequency of which has increased significantly due to climate change. Climate change impacts have challenged the sustainability of the pond fish culture, shrimp culture, and crab fattening. We assessed the perceptions of the fish, shrimp, and crab farmers on the impacts of climate change on the production systems, livelihoods, and vulnerability of the region's households. The southwest coast of Bangladesh experienced the significant economic losses in the aquaculture sector due to storm surges, long duration floods, salinity increases, sea level rise, droughts, and river bank erosion. Building the capacity of fish farming communities is necessary to apply the suggested adaptation measures. The government should implement a pragmatic program to support the region’s inhabitants during natural calamities and reduce temporary or permanent human migration.

ACKNOWLEDGEMENTS

We acknowledge the generous support of the FGD participants and the questionnaire survey respondents. We also acknowledge the Fisheries Division of the Space Research and Remote Sensing Organization (Bangladesh) for creating the study area map. The study involving human subjects was approved by the Institutional Review Board (IRB) committees of the Faculty of Fisheries, Bangladesh Agricultural University, with approval No. FOF-2021/07. We are also thankful to Dr. Benjamin Belton for reading the manuscript and editing the language.

REFERENCES

Ahirwal SK, Das PC, Sarma K, Kumar T, Singh J, Kamble SP. Effect of salinity changes on growth, survival, and biochemical parameters of freshwater fish *Gibelion catla* (Hamilton, 1822). Journal of Environmental Biology 2021; 42:1519-25.

Akhter MN, Chakraborty TK, Ghosh GC, Ghosh P, Jahan S. Migration due to climate change from the southwest coastal region of Bangladesh: A case study on Shymnagor Upazilla, Satkhira District. American Journal of Environmental Protection 2016;5(6):145-51.

Alam GMM, Alam K, Mushtaq S, Sarker MNI, Hossain M. Hazards, food insecurity and human displacement in rural riverine Bangladesh: Implications for policy. International Journal of Disaster Risk Reduction 2020;43(1):Article No. 101364.

Alam M, Hassan A, Khan AS, Major DC, Rosenzweig C, Ruane AC, et al. Bangladesh-Climate change risks and food security in Bangladesh. Washington, D.C.: World Bank Group [Internet]. 2010 [cited 2024 Jun 26]. Available from: http://documents.worldbank.org/curated/en/419531467998254867/.

Anzum HMN, Chakraborty TK, Bosu H. Farmer’s perception and factors influencing adoption of adaptation measures to cope with climate change: An evidence from coastal Bangladesh. Environment and Natural Resources Journal 2023;21(2): 113-26.

Black R, Arnell NW, Adger WN, Thomas D, Geddes A. Migration, immobility and displacement outcomes following extreme events. Environmental Science Policy 2013;27: S32-43.

Chowdhury SR, Hossain MS, Shamsuddoha M, Khan SMMH. Coastal fishers’ livelihood in peril: Sea surface temperature and tropical cyclones in Bangladesh [Internet]. 2012 [cited 2024 Jun 26]. Available from: https://www.academia.edu/61526530/

Das GK. Climate change and coastal hazards in Sunderbans. In: Das GK, editor. Coastal Environments of India. Springer Cham; 2022. p. 175-98.

Dasgupta S, Huq M, Khan ZH, Ahmed MMZ, Mukherjee N, Khan ME, et al. Vulnerability of Bangladesh to cyclones in a changing climate potential damages and adaptation cost. In; World Bank Policy Research Working Paper 5280. World Bank; 2010.

Dawood M, Madkour K, Mugwanya M, Kimera F, Sewilam H. Growth performances, body composition, and blood variables of Nile tilapia (*Oreochromis niloticus*) juveniles grown in a recirculatory aquaculture system under different water salinity levels. Journal of Applied Aquaculture 2023;36(2):1-15.

De Alvarenga ER, Alves GFdO, Fernandes AFA, Costa GR, Da Silva MA, Teixeira EdA, et al. Moderate salinity enhances growth performance of Nile tilapia (*Oreochromis niloticus*) fingerlings in the biofloc system. Aquaculture Research 2018; 49:2919-26.

Didar-Ul Islam SM, Bhuiyan MAH, Ramanathan A. Climate change impacts and vulnerability assessment in coastal region of Bangladesh: A case study on Shyamnagar Upazila of Satkhira District. Journal of Climate Change 2015;1(1-2):37-45.

Doubleday ZA, Clarke SM, Li X, Pecl GT, Ward TM, Battaglene S, et al. Assessing the risk of climate change to aquaculture: A case study from south-east Australia. Aquaculture Environment Interaction 2013;3(2):163-75.

Fisheries Resources Survey System (FRSS). Yearbook of Fisheries Statistics of Bangladesh (July 2021-June 2022): Volume 39. Bangladesh: Department of Fisheries, Ministry of Fisheries and Livestock; 2022.

Gao Y, Yu G, Yang T, Jia Y, He N, Zhuang J. New insight into global blue carbon estimation under human activity in land-sea interaction area: A case study of China. Earth-Science Review 2016;159:36-46.

Hasan A, Ulla A, Bibi R, Ullah U, Younas B, Raza M, et al. Effects of different salinity levels and temperature on growth performance of pangas catfish, *Pangasius hypophthalmus*. Central Asian Journal of Medical and Natural Sciences 2023;4(6):771-800.

Hossain MAR, Hasan MR. An Assessment of Impacts from Shrimp Aquaculture in Bangladesh and Prospects for Improvement. FAO Fisheries and Aquaculture Technical Paper, 618. Italy: Food and Agriculture Organization of the United Nations; 2017.

Hossain MAR, Ahmed M, Ojea E, Fernandes JA. Impacts and responses to environmental change in coastal livelihoods of southwest Bangladesh. Science of the Total Environment 2018;637:954-70.

Howlader MS, Akanda MGR. Problems in adaptation to climate change effects on coastal agriculture by the farmers of Patuakhali District of Bangladesh. American Journal of Rural Development 2016;4(1):10-4.

Islam MS, Samreth S, Islam AHMS, Sato M. Climate change, climatic extremes, and households' food consumption in Bangladesh: A longitudinal data analysis. Environmental Challenge 2022;**7**:Article No. 100495.

Kabir R, Khan HT, Ball E, Caldwell K. Climate change impact: The experience of the coastal areas of Bangladesh affected by cyclones Sidr and Aila. Journal of Environment and Public Health 2016;2016:1-9.

Khaine I, Woo SY. An overview of interrelationship between climate change and forests. Forest Science and Technology 2015;11(1):11-8.

Jones G, Mahbub AQM, Haq MI. Urbanization and Migration in Bangladesh. United Nations Population Fund (UNFPA) Bangladesh Office, Dhaka [Internet]. 2016 [cited 2024 Jun 26]. Available from: https://bangladesh.unfpa.org/en/publications/urbanization-and-migration-bangladesh.

Khan AE, Xun WW, Ahsan H, Vineis P. Climate change, sea-level rise, and health impacts in Bangladesh. Environment: Science and Policy Sustainable Development 2011;53(5):18-33.

Khanjani MH, Alizadeh M. Effects of different salinity levels on performance of Nile tilapia fingerlings in a biofloc culture system. Annals of Animal Science 2024;24(1):235-45.

Khatun H, Kabir, MH, Nahar L. Out migration as a survival strategy for char dwellers. In: Zaman M, Alam M, editors. Living on the Edge: Char Dwellers in Bangladesh. Springer Nature; 2021 p. 307-22.

Kumar MU, Ansal MD, Kaur VI. Salinity tolerance and survival of freshwater carp, *Labeo rohita* Ham. (rohu) in inland saline water. Indian Journal of Ecology 2018;45(4):872-5.

Leith P, Ogier E, Pecl G, Hoshino E, Davidson J, Haward M. Towards a diagnostic approach to climate adaptation for fisheries. Climate Change 2014;122:55-66.

Mallick B, Rogers KG, Sultana Z. In harm's way: Non-migration decisions of people at risk of slow-onset coastal hazards in Bangladesh. Ambio 2022;51(1):114-34.

Mandal SC, Kadir S, Hossain A. Effect of salinity on the growth, survival and proximate composition of pangas *Pangasius hypophthalmus*. Bangladesh Journal of Zoology 2020; 48(1):141-9.

Melnychuk MC, Banobi JA, Hilborn R. The adaptive capacity of fishery management systems for confronting climate change impacts on marine populations. Reviews in Fish Biology and Fisheries 2014;24:561-75.

Mirera DO, Okemwa D. Salinity tolerance of Nile tilapia (*Oreochromis niloticus*) to seawater and growth responses to different feed and culture systems. Western Indian Ocean Journal of Marine Science 2023;22(2):75-85.

Nahar A, Kashem S, Das A. Regionalization of Bangladesh: A key to identify regional disparities of the pattern of population distribution. Lands Architecture Regional Plan 2019;4(1):5-9.

Naser MM, Swapan MSH, Ahsan R, Afroz T, Ahmed S. Climate change, migration and human rights in Bangladesh: Perspectives on governance. Asia Pacific Viewpoint 2019; 60(2):175-90.

Palmer T, Stevens B. The scientific challenge of understanding and estimating climate change. Proceedings of the National Academy of Sciences USA 2019;116(49):24390-5.

Rahaman MA, Hossain MI, Kamal A, Sharif MN, Mursheduzzaman, Chowdhury AM. Climate-induced displacement and human migration landscape in Bangladesh. In: Filho WL , Luetz, Ayal DJ, editors. Handbook of Climate Change Management. Springer International Publishing; 2021. p. 1865-82.

Rana SM, Kamruzzaman M, Rajib MA, Rahman MM. Changes in cyclone pattern with climate change perspective in the coastal regions of Bangladesh. Environmental Research Engineering and Management 2011;56(2):20-7.

Sakapaji SC. Climate induced migration a new normal? A systematic research analysis of the climate-induced migration crisis in Bangladesh. European Journal of Theoretical and Applied Sciences 2023;1(4):463-89.

Sarker MNI, Wu M, Alam GM, Shouse RC. Retracted: Life in riverine islands in Bangladesh: Local adaptation strategies of climate vulnerable riverine island dwellers for livelihood resilience. Land Use Policy 2020;94:Article No.104574.

Sarma K, Dey A, Kumar S, Chaudhary BK, Mohanty S, Kumar T, et al. Effect of salinity on growth, survival and biochemical alterations in the freshwater fish *Labeo rohita* (Hamilton 1822). Indian Journal of Fisheries 2020;67(2):41-7.

Shaffril HAM, Samah AA, D'Silva JL. Adapting towards climate change impacts: Strategies for small-scale fishermen in Malaysia. Marine Policy 2017;81:196-201.

Shaibur MR, Khan MH, Rashid MS. Climate change may cause natural disasters in Shyamnagar, Satkhira: The southwestern

parts of Bangladesh. Bangladesh Journal of Environmental Science 2017;32:101-10.

Tajrin MS, Hossain B. The socio-economic impact due to cyclone Aila in the coastal zone of Bangladesh. International Journal of Law, Humanities and Social Science 2017;1(6):60-7.

Vinke K. Unsettling Settlements-Cities, Migrants, Climate Change: Rural-Urban Climate Migration as Effective Adaptation? Vol. 18. Germany: LIT Verlag Münster; 2020.

Wiig A, Mahmud M, Kolstad I, Lujala P, Bezu S. Digging in? Migration preferences in communities afected by climate change-evidence from Bangladesh. Regional Environmental Change 2023;23:96:1-15.

Yazdi SK, Shakouri B. The effects of climate change on aquaculture. International Journal of Environmental Science and Development 2010;1(5):Article No. 378.

Yohe G, Richard S, Tol J. Indicators for social and economic coping capacity-moving toward a working definition of adaptive capacity. Global Environtal Change 2002;12:25-40.

Environment and Natural Resources Journal

Volume 22
Issue 6
2024

Waste Analysis and Characterization Study in a Philippine Science and Technology Research and Development Institution

Joven Barcelo*, Maria Theresa Artuz, Myra Tansengco, David Herrera, Johnemma Mae Chuayana, and Reynaldo Esguerra

Environment and Biotechnology Division, Industrial Technology Development Institute, Department of Science and Technology, Bicutan, Taguig City, Metro Manila, Philippines

ARTICLE INFO

Received: 28 Apr 2024
Received in revised: 17 Sep 2024
Accepted: 19 Sep 2024
Published online: 5 Nov 2024
DOI: 10.32526/ennrj/22/20240119

Keywords:
Waste analysis and characterization/ Solid waste management/ Institutional sources/ Waste segregation/ Bulk density

*** Corresponding author:**
E-mail:
jrbarcelo@itdi.dost.gov.ph

ABSTRACT

This paper presents the conduct of Waste Analysis and Characterization Study (WACS) in the Industrial Technology Development Institute of the Department of Science and Technology (DOST-ITDI) in Taguig City, Philippines. The study was produced following the introduction of 2020 guidelines developed by the Japan International Cooperation Agency for the Philippines to determine waste generation and generation rate per source, as well as waste composition, per capita generation, and bulk densities of the generated wastes. This then provided fundamental data in the formulation of initial plans and programs for the proper management of solid wastes in the institution. From the gathered results, DOST-ITDI generates 91.56 kg/day of solid waste during the dry season, and 77.54 kg/day during the wet season. The generated waste is composed of residuals for disposal (35.93% and 37.75%, dry and wet season), biodegradables (27.80% and 21.46%), and recyclables (22.54% and 28.95%). Per capita generation rates of 0.21 kg/capita/day (dry season) and 0.18 kg/capita/day (wet season) were also recorded. The research and development cluster of divisions was determined as a major contributor of waste at 42.37 to 57.62 kg/day. Bulk density values varied between waste fractions, with the main residuals for disposal components being the bulkiest at 29.27 to 32.90 kg/m^3. The data collected from the study provided significant information useful in efforts to initiate programs for diversion of biodegradables, recyclables, and residuals-with further potential for recycling wastes, reducing residuals for disposal through proper segregation and recovery, and determining gaps and opportunities in plans, policies, and programs to improve solid waste management of the institution.

1. INTRODUCTION

According to the status report published by the National Solid Waste Management Commission (NSWMC) for 2008-2018, institutional sources such as government offices, medical, and educational institutions contribute about 12.10% of waste generated in a year (EMB, 2018), or about 2.75 million out of the total estimated 23 million tons of municipal waste generated for 2023 (NSWMCa, 2023). Although this is dwarfed by other waste sources like households and commercial establishments, the amount of waste contributed by institutions still requires attention for management and diversion from sanitary landfills. This need for proper waste management is also highlighted by the considerable expectations placed on government offices to adhere to the environmental laws of the land, specifically Republic Act 9003 or the Ecological Solid Waste Management Act of 2000 (DENR, 2001). The Industrial Technology Development Institute or DOST-ITDI is an attached agency of the Department of Science and Technology (DOST) located in Bicutan, Taguig City, Philippines, and is one of DOST's research and development (R&D) institutes that undertakes multidisciplinary

Citation: Barcelo J, Artuz MT, Tansengco M, Herrera D, Chuayana JM, Esguerra R. Waste analysis and characterization study in a Philippine Science and Technology Research and Development Institution. Environ. Nat. Resour. J. 2024;22(6):547-564. (https://doi.org/10.32526/ennrj/22/20240119)

industry R&D, technical services, and knowledge translation or technology transfer and commercialization. DOST-ITDI's R&D activities are focused on five major areas, namely: food processing, materials science, chemicals and energy, environment and biotechnology, and packaging technology (DOST-ITDI, 2023).

Determining the actual amount of waste generated in institutions as well as its components and source generation to verify the effectiveness of the current practices of the sector in waste diversion and management requires the conduct of waste analysis and characterization study or WACS. The conduct of WACS is an important activity for local government units and other waste generators for managing their solid waste. Data gathered from the study can be used as basis for preparation of solid waste management program, for designing waste storage system, collection system, processing facilities, for developing diversion strategies, and for identifying markets for recovered materials (ADB, 2003). Last September 2020, the National Solid Waste Management Commission approved and released new guidelines for the conduct of WACS (NSWMCb, 2020). The said guidelines provided updated procedures from the preparatory stages, the actual conduct of WACS using international standard procedures described in American Society for Testing and Materials or ASTM for waste characterization, and the needed data processing and report preparation (JICA, 2020). WACS is done through two methods, at-source or generator-based, and end-of-pipe. Generator-based WACS gathers information from the generation stage or from the waste sources, while end-of-pipe WACS collects information before final treatment or disposal such as in transfer stations, waste processing and conversion facilities, and in landfill sites. Generator-based WACS is particularly recommended since these better captures the total waste generation prior to waste diversion, as well as the generation rate of each waste sources (JICA, 2020).

Published articles regarding the conduct of WACS in institutional sources in the Philippines mostly focus on educational institutions. The end-of-pipe WACS of the University of the Philippines Los Baños determined an average daily waste generation of 593.670 kg/day and focused only on the overall generation of non-biodegradable wastes in the university, with plastic and paper wastes determined as the main waste components (Palomar et al., 2019). On the other hand, the pre-COVID-19 conduct of generator-based WACS in the Caraga State University estimates 85.527 kg/day of waste generation. The study was also able to determine the College of Arts and Sciences as its major waste source, and recyclable wastes as the major waste component at 46% (Ciudad et al., 2022). Finally, an average waste generation of 126.010 kg/day was recorded in the 12-day WACS of the University of Southern Philippines-Cagayan de Oro campus, with paper wastes as the major component at 28.42% (Elayan et al., 2019). These studies on academes yielded comparable per capita generation rates, particularly, 0.0132 kg/capita/day for the University of the Philippines Los Baños, 0.018 kg/capita/day for the Caraga State University, and 0.0126 kg/capita/day for the University of Southern Philippines-Cagayan de Oro campus. However, for other institutional sources such as national government agencies, published and accessible WACS data is often sparse. Although previous WACS data in the Department of Science and Technology (DOST) is available and determined that the agency generates 65.630 kg/day of waste and was largely composed of biodegradable wastes at 73%, the end-of-pipe study was not able to determine the waste generation rate of each of DOST's attached agencies, which includes DOST-ITDI, as well as to estimate the per capita generation for the whole of the agency (Tansengco et al., 2016).

The conduct of WACS in DOST-ITDI would determine and update the characteristics and waste generation rate of the institution. The data collected from the study is crucial for developing initial strategies to properly manage and divert waste in compliance with the mandates of RA 9003 and in setting an example for other government institutions to analyze their waste, contributing to a more comprehensive database of waste generation from institutional sources, which can aid in estimating and projecting both local and national waste generation.

2. METHODOLOGY

2.1 Waste characterization study period

The conduct of WACS covered selected dates to represent dry and wet season, specifically, March 13-17, and July 10-14, 2023, respectively. These selected dates were in close concurrence with the dates prescribed by Philippine Atmospheric, Geophysical, and Astronomical Services Administration or DOST-PAGASA regarding the beginning of dry (DOST-PAGASA, 2023a) and wet seasons (DOST-PAGASA, 2023b) for 2023. The study only considered the 4-day

waste generation of DOST-ITDI (Monday to Thursday), to cover the actual operations of the Institution as provided in the adopted flexible work arrangements. The selected WACS period is within the 3-7 days sampling prescribed in the new guidelines (JICA, 2020).

2.2 Identification of waste sources

The waste sources selected for DOST-ITDI includes all the divisions of the institute and are clustered per strategic function, namely, research and development, technical services, and support services. In total, DOST-ITDI is composed of a total of 13 divisions, a testing laboratory under the Materials Science Division, and one cooperative office considered under "other sources". Table 1 shows the selected waste sources as well as their total staff population (regular and contract of service (COS)/job order (JO)/casual staff) during dry and wet season. Staff population was gathered through data collected from the human resources office of DOST-ITDI, as well as field interviews with the divisional focal persons.

Table 1. Waste sources and corresponding staff population

	Waste sampling source	Number of staff	
		Dry season	Wet season
Research and development (R&D)	Chemicals and Energy Division (CED)	50	50
	Environment and Biotechnology Division (EBD)	54	54
	Food Processing Division (FPD)	39	39
	Materials Science Division (MSD)	27	27
	Advanced Device and Materials Testing Laboratory (ADMATEL)	22	22
	Packaging Technology Division (PTD)	34	34
Technical services	National Metrology Division (NMD)	33	33
	Standards and Testing Division (STD)	53	53
	Technological Services Division (TSD)	38	43
Support services	Administrative Division (ADM)	28	28
	Financial Management Division (FMD)	23	23
	Planning and Management Information Systems Division (PMISD)	12	12
	Office of the Director (OD)	4	4
	Office of the Deputy Director (ODD)	6	6
Other sources	Science Savings and Loan Association, Inc. (SSLAI)	6	6
Total		437	442

2.3 Collection of wastes

Full day waste generation from each waste source were collected by their designated utility personnel. A set of labeled garbage bags were distributed to the utility personnel prior to daily waste collection between 3:00-4:00 pm. Collectors were reminded to avoid mixing waste with previously collected waste or wastes coming from other divisions or sources, to consider only the waste generated during the work day, and to not include chemical, infectious, and other hazardous wastes generated from the laboratories. Collected wastes were then brought to the designated WACS working area for sorting, weighing, and recording the following day. Figure 1 shows the vicinity map of the DOST-ITDI, laying out the location of the divisions and other waste sources, as well as the solid waste management facilities in the institution.

2.4 Waste sorting, weighing, and recording

Collected waste from different waste sources was pre-weighed and manually sorted the day after collection following the waste component categories shown in Table 2 as prescribed in the new WACS guidelines (JICA, 2020). The recyclable wastes were then sorted further into subcategories, plastics, paper, metals, and glass. During the conduct of wet season WACS, the recyclables and residuals with potential for recycling were further sorted into second level subcategories after the personnel were familiarized with the primary categories during the dry season WACS (Table 2).

Sorted waste was then stored in separate garbage bags and was weighed using a 40-kg capacity digital weighing scale (Dahongying) with 5 g increments. Measurements were then recorded in prepared raw data forms per waste source.

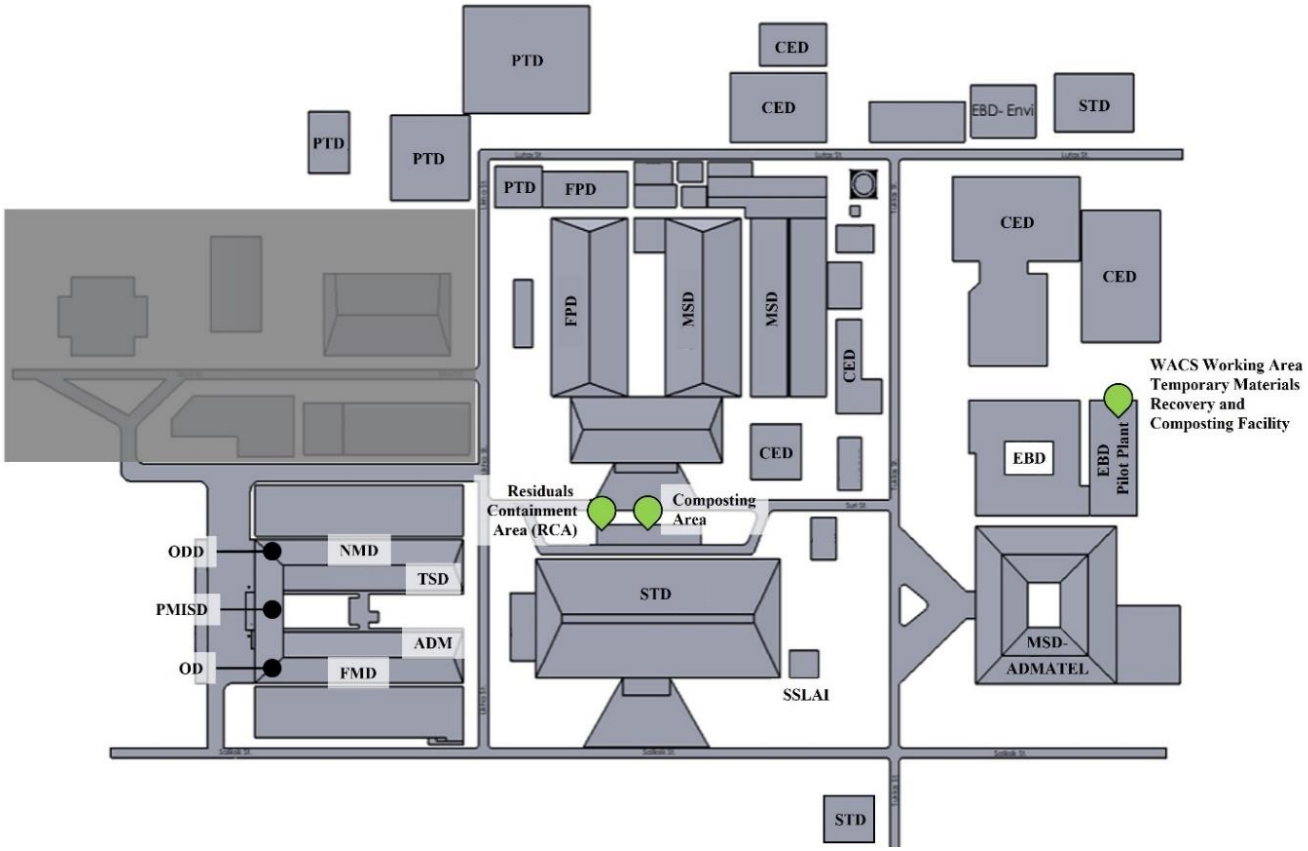

Figure 1. Vicinity map of DOST-ITDI showing the identified waste sampling sources in Table 1 and existing solid waste management facilities indicated by the green markers.

Table 2. Waste component categories, subcategories, and sample waste items (JICA, 2020)

Waste category	Subcategory and sample items
Biodegradables	Food/kitchen waste
	Garden/park waste
	Agricultural/farm waste
	Livestock wastes
Recyclables	Paper (white paper, cardboards, cartons, newspaper, textbooks, magazine, pamphlets, mixed paper, etc.)
	Plastics (PET bottles, beverage jugs, PVC pipes, squeezable bottles/tubes, microwavable containers, pails/chairs, Styrofoam, plastic trays and cutlery, others) Glass (bottles, flat glass, cullet)
	Metals (tin cans, aluminum cans and trays, copper tubes and wires, steel)
Residuals with potential for recycling	Flexible plastics(pouches, sachets, wrappers, tarpaulins, drinking straw, grocery/food bags) Leather Rubber (slippers, mats) Textile (rags)
Residuals for disposal	Soiled paper (coated paper, food contaminated paper)
	Soiled plastics (labo, etc.)
	Others (cigarette butts, etc.)
Special wastes	Hazardous wastes (WEEE, pesticide and cleaning containers, paint and chemical containers, etc.)
	Household Healthcare Wastes (Sanitary composites)
	Healthcare waste from hospitals (gloves, masks, syringes, expired medicines, etc.)
	Bulky wastes (bulky yard waste, rubber tires, construction/demolition/disaster debris

2.5 Bulk density determination

Bulk density of waste was determined following ASTM E1109-19 or the "Standard Test Method for Determining the Bulk Density of Solid Waste Fractions". A 0.6×0.6×0.6 m internal dimension bulk density box was used for the procedure in which sorted waste fractions were loaded, tamped three times, and weighed (ASTM, 2019). Weights were also determined using a 40-kg capacity digital weighing scale (Dahongying) with 5 g increments and a 60 kg capacity mechanical weighing scale (General Master) with 200 g increments for weight measurements exceeding the capacity of the digital scale, while a standard steel tape meter was used to measure the internal dimensions of the bulk density box. For waste fractions with smaller volumes, cardboard boxes and other smaller rectangular containers were used as makeshift bulk density boxes, taking note of their respective tare weights and dimensions. Bulk density (kg/m^3) was calculated using Equation (1) (JICA, 2020):

$$\text{Bulk density} = \frac{(W_G - W_T)}{V} \quad (1)$$

Where; W_G is the gross weight of the box and the waste (kg), W_T is the tare weight of the box (kg), and V is the volume of the box (m^3) based on the internal dimensions measured.

Figure 2 shows the waste handling flow for the waste samples, as well as the destination of the segregated wastes after the conduct of WACS.

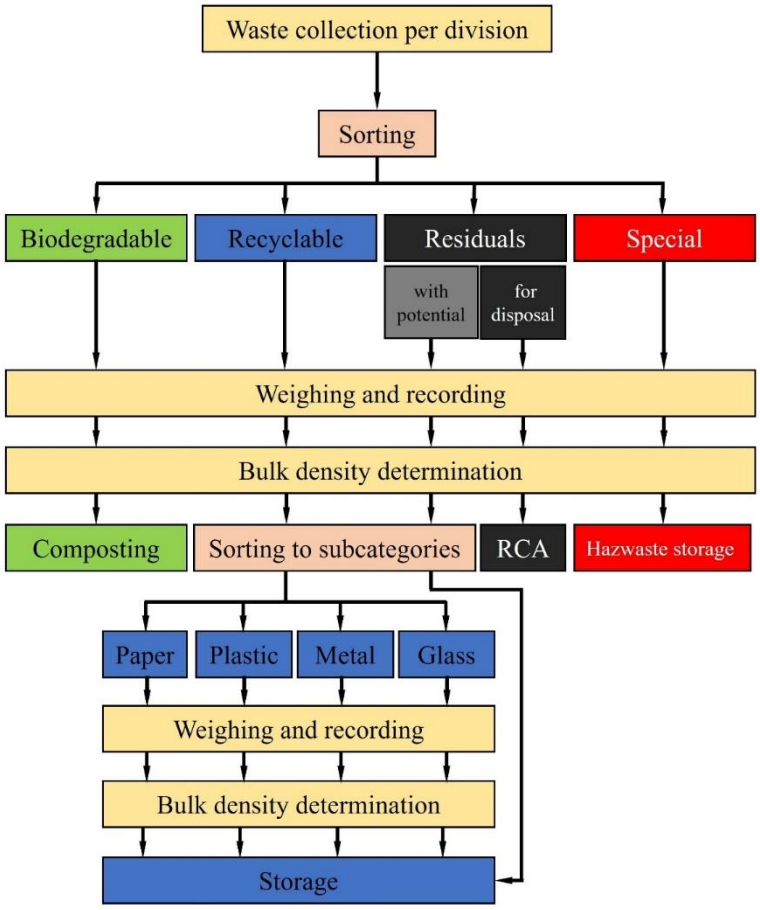

Figure 2. Waste handling flow for WACS

2.6 Data processing

Equation (2) was used in calculating average daily waste generation (kg/day) for each waste source and for the whole DOST-ITDI:

$$WG_{ave} = \frac{D_1 + D_2 + \cdots + D_n}{N} \quad (2)$$

Where; WG_{ave} is the average daily waste generation (kg/day), D_n is the weight of waste generated for the day (kg), and N is the number of WACS days.

On the other hand, per capita waste generation (PCG) or the amount of waste generated by an individual per day is calculated using Equation (3):

$$PCG = \frac{WG_{ave}}{P} \quad (3)$$

Where; PCG is the per capita generation (kg/capita/day), WG_{ave} is the average daily waste generation (kg/day), and P is the staff population.

Further, Equation (4) is used to determine the percent waste composition:

$$\%_{composition} = \frac{WG_{component}}{WG_{total}} \times 100\% \quad (4)$$

Where; $WG_{component}$ is the waste generation of a specific waste component and WG_{total} is the total waste generation.

Finally, potential waste diversion percentage is computed using Equation (5)

$$\%_{potential\ waste\ diversion} = \frac{WG_{biodegradables} + WG_{recyclables} + WG_{residuals\ with\ potential}}{WG_{total}} \times 100\% \quad (5)$$

Where; $WG_{biodegradables}$, $WG_{recyclables}$, and $WG_{residuals\ with\ potential}$ are the waste generation of biodegradables, recyclables, and residuals with potential for recycling, respectively, and WG_{total} is the total waste generation.

2.7 Statistical analysis

Statistical analysis, specifically one-way analysis of variance (ANOVA) and comparison of means, were applied to the processed data. Specifically, t-tests were applied to compare waste generation data between seasons, while Fisher Pairwise comparisons were applied to compare waste generation between waste sources and determine significant changes in waste generation for each working day. Minitab® statistical software was used for the one-way ANOVA analysis, while Microsoft Excel was used for the t-tests, as well as in preparing the bar and pie graphs presented.

2.8 Implementation of initial waste management programs

Initial solid waste management programs such as seminar-orientations on proper segregation to the DOST-ITDI staff and the utility personnel, implementation of a waste monitoring scheme, the establishment of a temporary materials recovery and composting facility, and partnerships with local recyclers were implemented after the conduct of the wet season WACS. These programs were primarily identified through information gathered from the WACS data, as well as in assessments and meetings with DOST-ITDI staff. The effects of these programs to the solid waste management practice, as well as the resulting waste diversion rate in the established temporary facility were determined through the data collected from the waste monitoring scheme implemented and is then processed and compared with the WACS results.

2.9 Waste generation projection

Considering the influence of population growth to waste generation (US EPA, 2023), the 5-year waste generation of DOST-ITDI was projected using the baseline PCG multiplied to the projected population which was calculated using Equation (6):

$$P_{current\ year} = P_{previous\ year} \times (1 + GR) \quad (6)$$

Where; $P_{current\ year}$ and $P_{previous\ year}$ are the projected population for the current year and the base year populations, respectively, and GR is the growth rate calculated using the population data from previous years. A linear population growth was assumed for DOST-ITDI as a more realistic projection considering the limitation set for the number of regular staff that can be employed by the institution in the Staffing Summary for 2024 of the Department of Budget and Management (DBM, 2024).

3. RESULTS AND DISCUSSION

3.1 Waste composition

3.1.1 Waste composition by major categories

Residuals for disposal constitutes the largest portion of waste generated at DOST-ITDI in both seasons, accounting for 35.93% during the dry season and 37.75% during the wet season. Figure 3(a) and 3(b) graphically compare the waste composition for the dry and wet season.

From a total of 91.56 and 77.54 kg/day dry and wet season waste generation, 32.9 and 29.27 kg/day are residuals for disposal (Figure 3(c)).

The residuals for disposal are mostly composed not only of used paper towels, bathroom tissue, and

soiled plastic bags, but of soiled paper food and beverage packaging as well. Although paper food packaging is currently being touted as a sustainable alternative to plastic packaging (Junior et al., 2022), contamination complicates and reduces its potential to be recovered and recycled, ending up as residuals for disposal as observed during the study.

Although there were changes in the waste generation per component, the overall percentage of waste generated during the dry and wet season are closely identical. The variation in biodegradable waste between seasons is attributed to changes in the research and development activities of the Food Processing Division, which is a major source of organic waste. Meanwhile, the increase in recyclables during the wet season may be due to the higher use of rigid plastic packaging to protect products from rain.

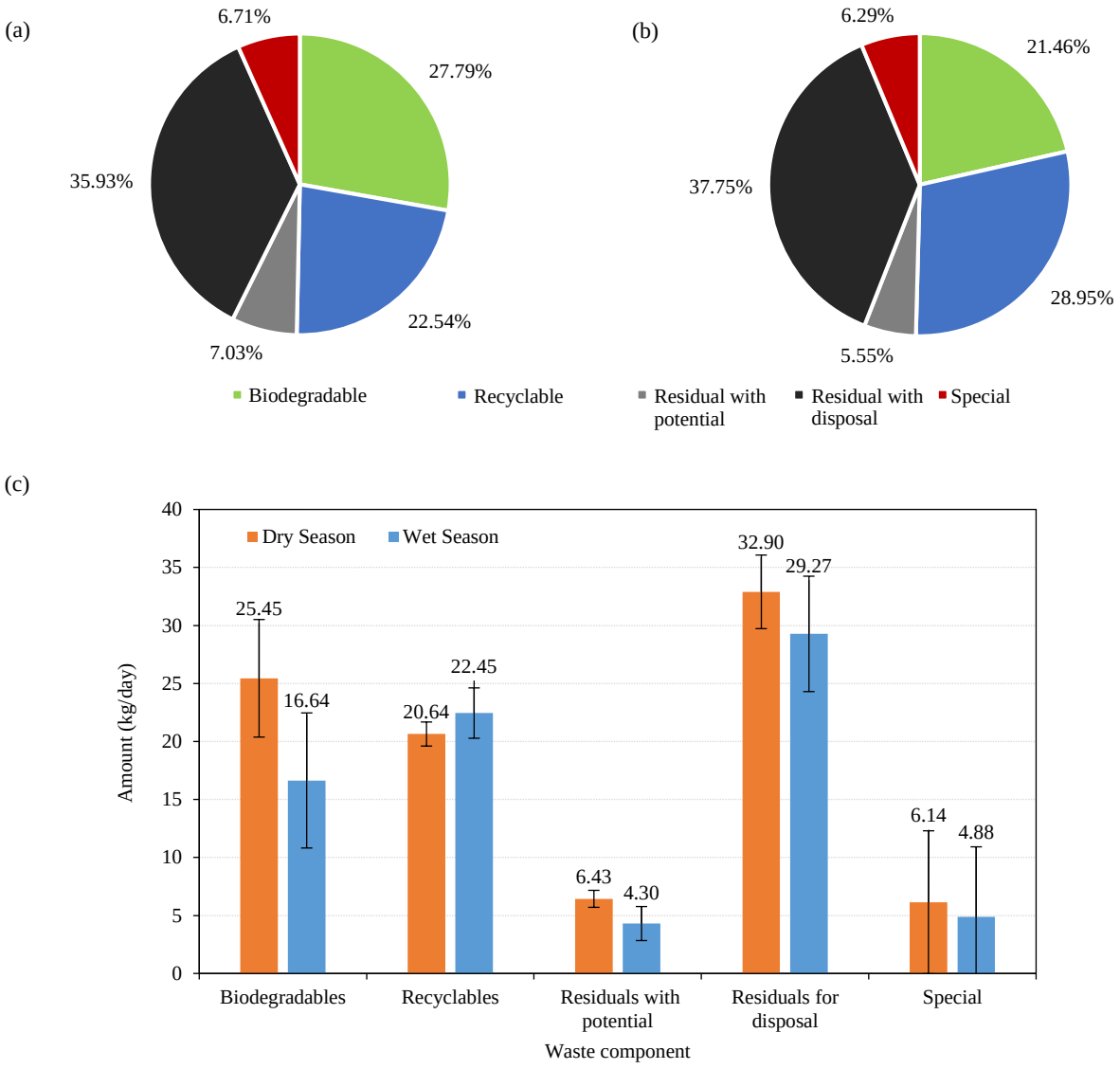

Figure 3. (a) Dry, (b) wet season waste composition, and (c) waste generation per composition

3.1.2 Waste composition by subcategories

Recyclable wastes were further sorted into subcategories namely, paper, plastics, metals, and glass. Figure 4 compares the percentage composition of the recyclable wastes per season and shows paper wastes as a steady major component of recyclable wastes which can be attributed to the heavy use of paper in DOST-ITDI for documentary requirements and reports which was also observed in other institutional sources (Palomar et al., 2019; Ciudad et al., 2022). An increase in the recyclable plastics being used and therefore disposed of was also further shown and supports the previous assumption of the increase in the use of rigid plastic packaging due to the wet weather.

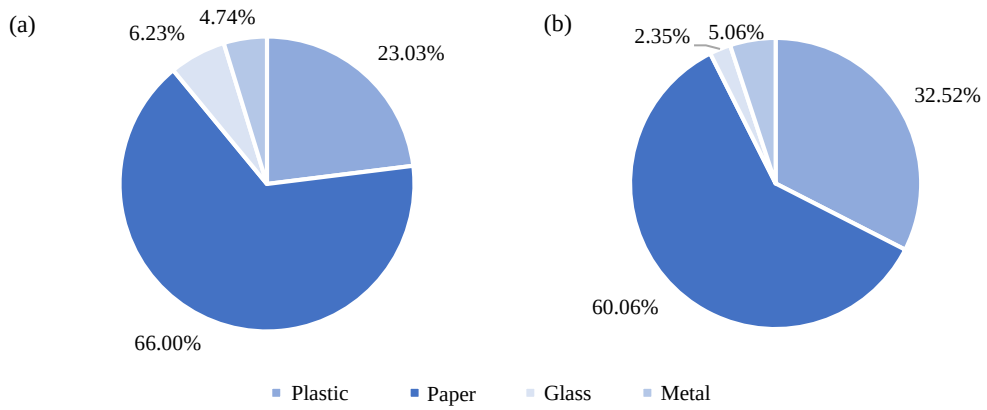

Figure 4. (a) Dry and (b) wet season percentage recyclable waste composition

Sorting into second-level recyclable subcategories shown the effect of the frequent equipment and supplies delivery (cartons and cardboard), documentation requirements (used white paper), and food and beverage consumption (PP and PET packaging) to the characteristics of recyclable wastes generated in DOST-ITDI (Figure 5(a)). On the other hand, the determined composition of residuals with potential for recycling (Figure 5(b)) exhibited the consumption habit of the DOST-ITDI staff, specifically in ordering food and beverages typically contained in paper clam shells or in paper cups (laminated paper), the continuous use of plastic bags in buying food and/or supplies (LDPE plastic bags), and the consumption of products in sachets (foil packs, sachets, wrappers). These findings reveal that the typical Filipino consumer habits, influenced by the prevalent sachet economy (Gozum, 2024) and reliance on single-use plastics (Schachter and Karasik, 2022), are also reflected in government offices.

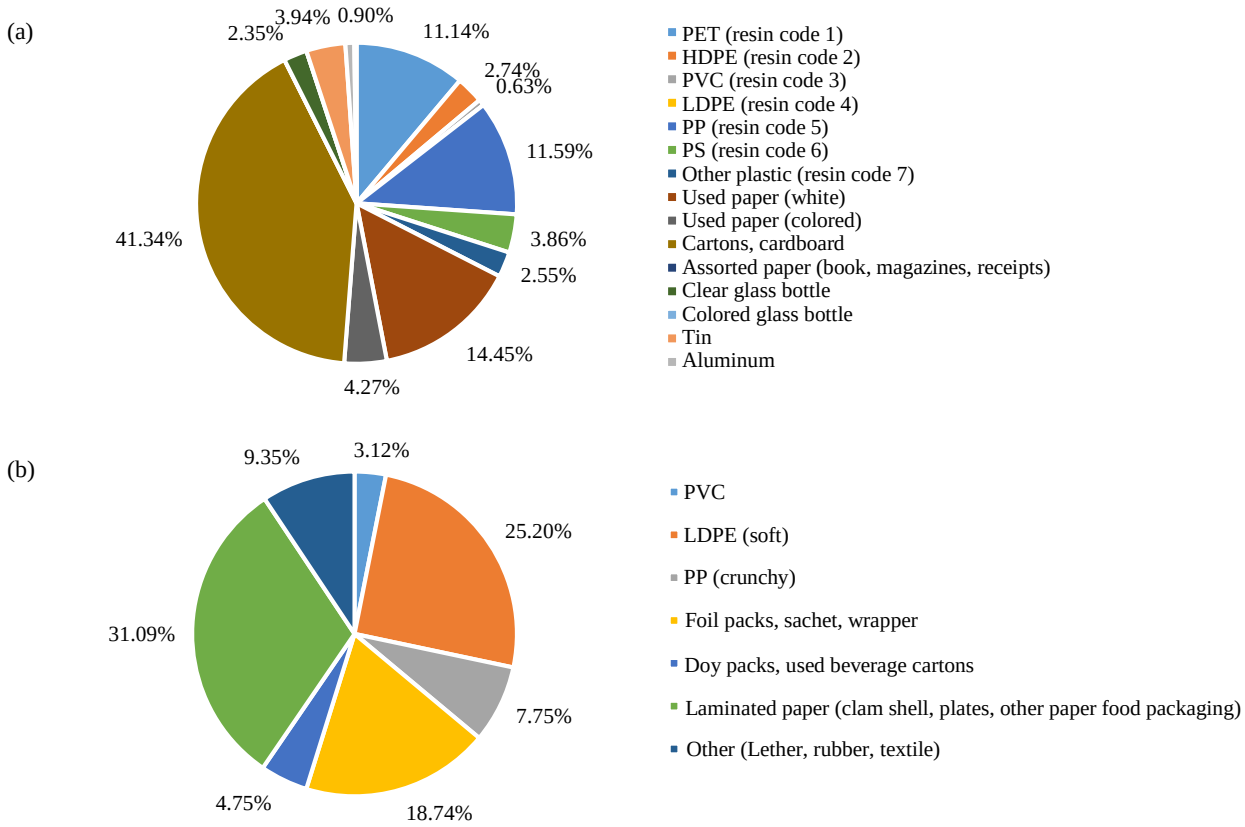

Figure 5. Percentage composition of (a) recyclables at second-level category and (b) residuals with potential for recycling determined during the wet season WACS

3.2 Waste generation

3.2.1 Per capita waste generation by major waste categories

Per capita generation for the total and per component waste generation were calculated and statistically compared using t-tests to determine significant changes between seasons (Table 3).

The comparisons show that although the per capita generation of residuals with potential for recycling has significantly changed between seasons (p-value=0.036, p-value<0.05 is significant), there is no significant change in the total per capita generation in DOST-ITDI between seasons (p-value=0.0502) implying consistent individual waste generation.

3.2.2 Waste generation per source

The waste contribution of each major waste source (research and development, technical services, support services, other sources), were also determined from the dry and wet season WACS data. Figure 6 shows the waste generation per major waste source for both seasons.

Table 3. Comparison overall per capita waste generation and per component PCG for dry and wet seasons

Component	Mean PCG (kg/capita/day)		p-value
	Dry season	Wet season	
Biodegradable	0.06±0.010	0.04±0.010	0.0570
Recyclable	0.05±0.002	0.05±0.005	0.2400
Residual with potential for recycling	0.01±0.002	0.01±0.003	0.0360
Residual for disposal	0.08±0.010	0.07±0.010	0.2250
Special waste	0.01±0.010	0.01±0.010	0.7690
Overall PCG	0.21±0.010	0.18±0.030	0.0502

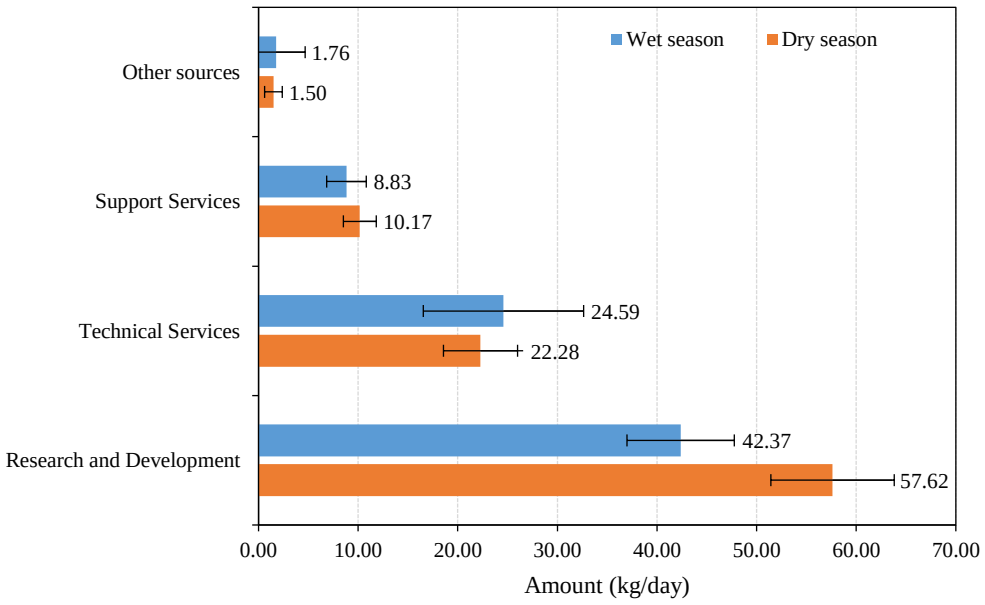

Figure 6. Waste generation per major waste source

The research and development divisions, with the largest population in DOST-ITDI, contribute the most to waste generation, accounting for 63% during the dry season and 55% during the wet season.

Subjecting the calculated PCG of each waste sources to t-test (Table 4) determined that R&D divisions experienced significantly different PCGs between dry and wet seasons (p-value=0.010) which may be due to changes in activities within the cluster between these periods affecting waste generation. However, as with the findings on waste components, the difference in PCG for R&D divisions between seasons did not affect the overall consistency of waste generation in DOST-ITDI.

Table 4. Comparison of dry and wet season PCG per major waste sources

Source	Mean PCG (kg/capita/day)		p-value
	Dry season	Wet season	
Research and development	0.25±0.03	0.19±0.02	0.0100
Technical services	0.17±0.03	0.18±0.06	0.7590
Support services	0.13±0.02	0.11±0.02	0.3390
Other sources	0.25±0.15	0.29±0.49	0.8680
Overall PCG	0.21±0.01	0.18±0.03	0.0502

Finally, Fisher Pairwise comparisons were applied to evaluate whether PCG values differ between major waste sources each season, identifying if staff from specific sources generate significantly more waste compared to others.

The confidence interval plot (Figure 8(a)) indicates that there is no significant overall difference in PCGs across waste sources at DOST-ITDI for both the dry (p=0.119) and wet seasons (p=0.784). However, a significant difference is observed between the PCGs of the R&D and support services divisions during the dry season. This indicates that individual waste generation rates across major sources are not significantly different, allowing a PCG of 0.18 to 0.21 kg/capita/day to be reliably used for estimating and projecting waste generation for the entire institution.

3.2.3 Weekly waste generation trend

Referring to both the plotted per capita waste generation data collected per day for each season (Figure 7), for the dry season, there seems to be consistency in the PCG values collected per day. On the other hand, the wet season PCG trend shows increased generation rates as the work week ends.

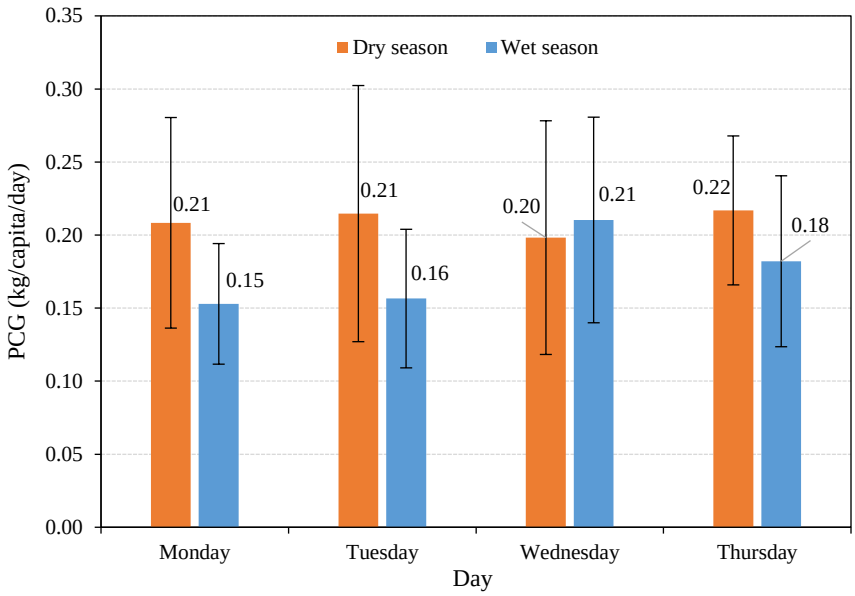

Figure 7. PCG trend for a whole week for both dry and wet seasons

Fisher Pairwise comparisons were then applied to compare PCGs per workday and determine if each day has significant differences in the per capita waste generation rate. Based on the group comparisons between PCGs collected from Monday to Thursday, there was no significant difference among the PCGs during the work week both for dry (p-value=0.613) and the wet season (p-value=0.528). These values then support the notion of a consistent weekly waste generation in the entire institution and further confirmation of the reliability of using the overall PCG values determined in the WACS. Figure 8(b) shows the generated interval plots for the group comparisons made between workdays.

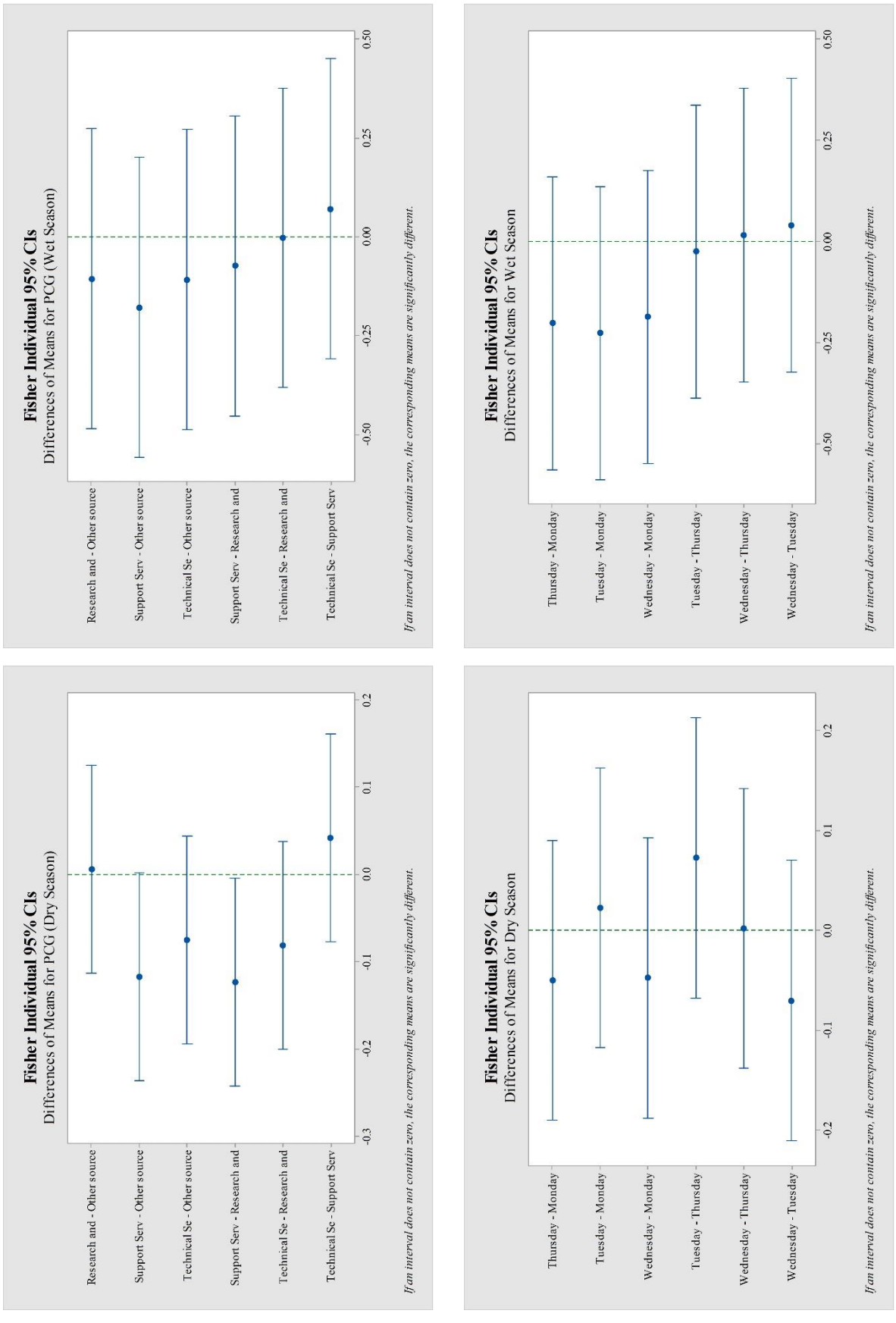

Figure 8. Fisher Individual 95% confidence interval plots comparing PCGs (a) per major waste source and (b) per workday for dry and wet seasons.

3.3 Bulk density

Table 5 shows the recorded loose bulk density values for major waste components and subcomponents for the dry and wet season, as well as bulk density values from other references. Note that no bulk density data for glass were determined due to low volume and generation during the conduct of WACS.

Table 5. Bulk density values for major waste components and subcomponents

Waste component	Bulk density (kg/m^3)			Reference
	Dry season	Wet season	Reference value	
Biodegradable	368.01±122.20	435.24±162.12	130-490	Worrell and Vesilind (2011)
Recyclable				
Plastic	33.43±2.59	28.08±5.18	42-130	Worrell and Vesilind (2011)
Paper	168.42±172.04	26.66±7.62	12-240	Worrell and Vesilind (2011)
Metal	94.48±37.12	58.92±8.59	30-44	Worrell and Vesilind (2011)
Residual with potential for recycling	20.80±7.78	16.95±3.96	-	-
Residual for disposal	39.17±5.89	36.69±2.87	-	-
Special	84.54±23.09	55.05±26.96	-	-

Individual bulk density values were also determined per second-level subcomponent of all recyclables and residuals with potential for recycling after enough amount was accumulated in the established temporary materials recovery facility (Table 6).

The measured bulk density values from waste samples collected in DOST-ITDI are comparable to the values presented in references (Worrell and Vesilind, 2011). Moreover, the bulk density measurements of plastic packaging wastes (including PVC, PP sheets, films, labels, bags, and multilayered packaging) serve as valuable reference values, addressing the current lack of data on their specific bulk densities. The measured bulk densities can be used as a reference to the preparation of storage spaces for the waste components in the planned permanent materials recovery facility or MRF.

Table 6. Bulk density values for recyclables and residuals with potential for recycling subcomponents

Component			Bulk density (kg/m^3)		Reference
			Measured	Reference values	
Recyclables	Plastics	PET (resin code 1)	22.88±1.09	18-24	Worrell and Vesilind (2011)
		HDPE (resin code 2) Containers	24.45±2.21	14	Worrell and Vesilind (2011)
		HDPE (resin code 2) Caps	136.79±2.46	-	Worrell and Vesilind (2011)
		PVC (resin code 3) rigid	-	-	-
		LDPE (resin code 4) rigid	-	-	-
		PP (resin code 5) rigid	19.59±1.32	-	-
		PS (resin code 6) expanded	5.40±0.17	5.4-5.7	Worrell and Vesilind (2011)
		Other Plastics (resin code 7)	-	-	-
	Paper	Used Paper (White)	168.42±2.09	240	Worrell and Vesilind (2011)
		Used Paper (Colored)	13.69±0.56	12-33	Worrell and Vesilind (2011)
		Cartons, Cardboard	34.61±2.43	9.9-237.3(old corrugated carton, OCC)	Worrell and Vesilind (2011)
	Glass	Clear	259.96±12.22	300-420	Worrell and Vesilind (2011)
		Colored	-	-	-
	Metals	Tin	76.63±1.88	504	Worrell and Vesilind (2011)
		Aluminum	22.40±0.60	30-44	Worrell and Vesilind (2011)
		Others (Copper, Steel)	-	-	-

Table 6. Bulk density values for recyclables and residuals with potential for recycling subcomponents (cont.)

Component			Bulk density (kg/m^3)		Reference
			Measured	Reference values	
Residuals with potential for recycling	Plastic sheets, labels, and films	PVC	6.38±0.13	-	-
		LDPE (Soft)	8.16±1.00	10.9$^{(loose\ plastic)}$ 13.4$^{(bubble\ wrap)}$	Worrell and Vesilind (2011)
		PP (Crunchy)	5.75±0.63	-	-
	Multilayered packaging	Foil packs, sachet, wrapper	18.85±0.74	-	-
		Doy packs, used beverage cartons	21.34±1.49	-	
		Laminated paper (clam shell, cups, plates, other paper food packaging)	14.87±1.61	-	

3.4 Implementation of initial waste management programs

3.4.1 Conduct of seminar-orientation on proper workplace waste management

A series of seminars on proper workplace waste management were conducted after WACS. These seminar-orientations discussed topics on national solid waste management policies, waste classifications, workplace waste management, as well as the summary of results of the conduct of WACS. Initial orientations were attended by the divisional representatives and committee members on safety, health, and environment, the clean and green committee, and the utility personnel. Further seminars were then conducted to individual divisions. In total, 11 seminars were conducted and attended by a total of 233 participants.

3.4.2 Establishment of temporary materials recovery and composting facility

A temporary materials recovery and composting facility was established at the EBD pilot plant to support the growing practice of waste segregation in DOST-ITDI. The temporary materials recovery facility (Figure 9(a)) consisted of segregated containers such as one-tonner bins and boxes which would contain the segregated recyclables and residuals with potential for recycling. The accumulated recyclables were then collected monthly by DOST-ITDI's partner recycler and local waste management service company that collects, sorts and processes various waste categories. In exchange for the collected recyclable waste items, DOST-ITDI receives reams of recycled A4 paper.

(a) (b)

Figure 9. (a) Temporary materials recovery facility for collected segregated recyclables; (b) Plastic drum used for pile composting of biodegradables

On the other hand, the composting facility established is composed of composting bins made of large plastic drums and containers (Figure 9(b)).

3.4.3 Waste generation monitoring

Waste generation monitoring involved the recording of weights of collected biodegradables prior

to composting, and residuals for disposal prior to transfer to the residuals containment area. In addition, the weights of accumulated recyclables and residuals with potential for recycling were recorded weekly before transferring to the temporary materials recovery facility.

Figure 10 shows the average daily waste generation and PCG from the monitoring data from August 2023 to March 2024 as compared to the July 2023 wet season WACS data. Note that special wastes are not included in the monitoring as it is currently being monitored as a component of hazardous wastes.

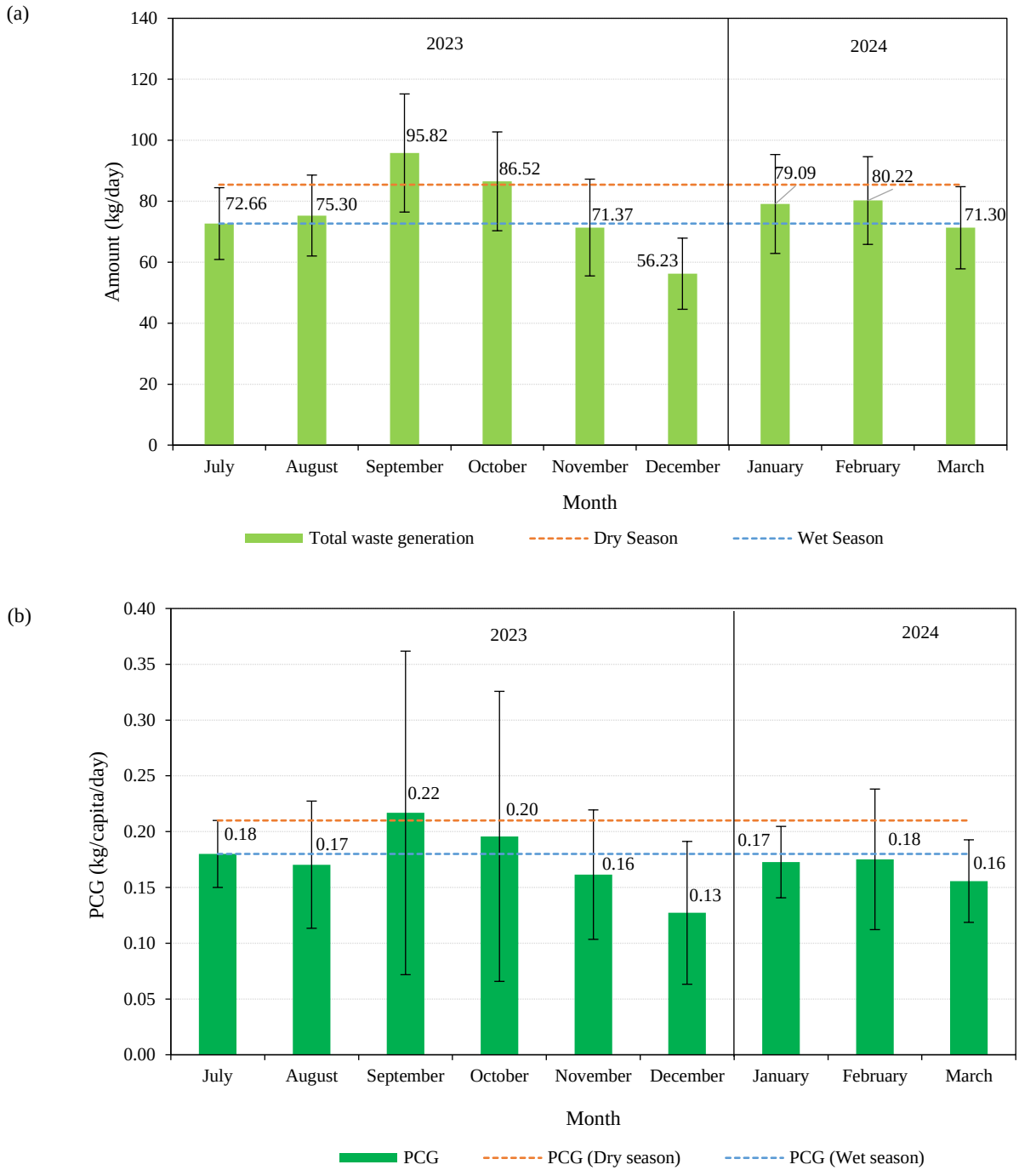

Figure 10. (a) Daily waste and (b) per capita generation from July 2023 to March 2024

The data trend in Figure 10(a) exhibited a decrease in waste generation in September 2023 and a decrease in December 2023, which is due to the decline of the number of staff reporting in office due to the holidays. However, with the continuation of regular operations at the beginning of 2024, the waste generation increased to normal levels. In addition, the recorded PCG values recorded (Figure 10(b)) are still

near or within the per capita range calculated during the dry (0.21 kg/capita/day) and wet (0.18 kg/capita/day) season WACS which indicates consistency in waste generation even at the individual level. This further supports the findings of waste generation consistency in DOST-ITDI while also suggesting that waste reduction practice is still lacking individually as the PCG rates are still comparable pre- and post-implementation of the initial solid waste management programs.

Finally, the monthly waste composition trend was also captured during the monitoring (Figure 11). A decrease in the percentage of residuals for disposal can be noted starting September 2023 which coincides with the implementation of the initial programs, indicating improving segregation in DOST-ITDI as other waste components are being properly sorted and recovered instead of being disposed. However, further waste recovery and implementation of other methods such as waste reduction or use of more reusable and recyclable products instead of disposables are necessary to further reduce residuals for disposal generation.

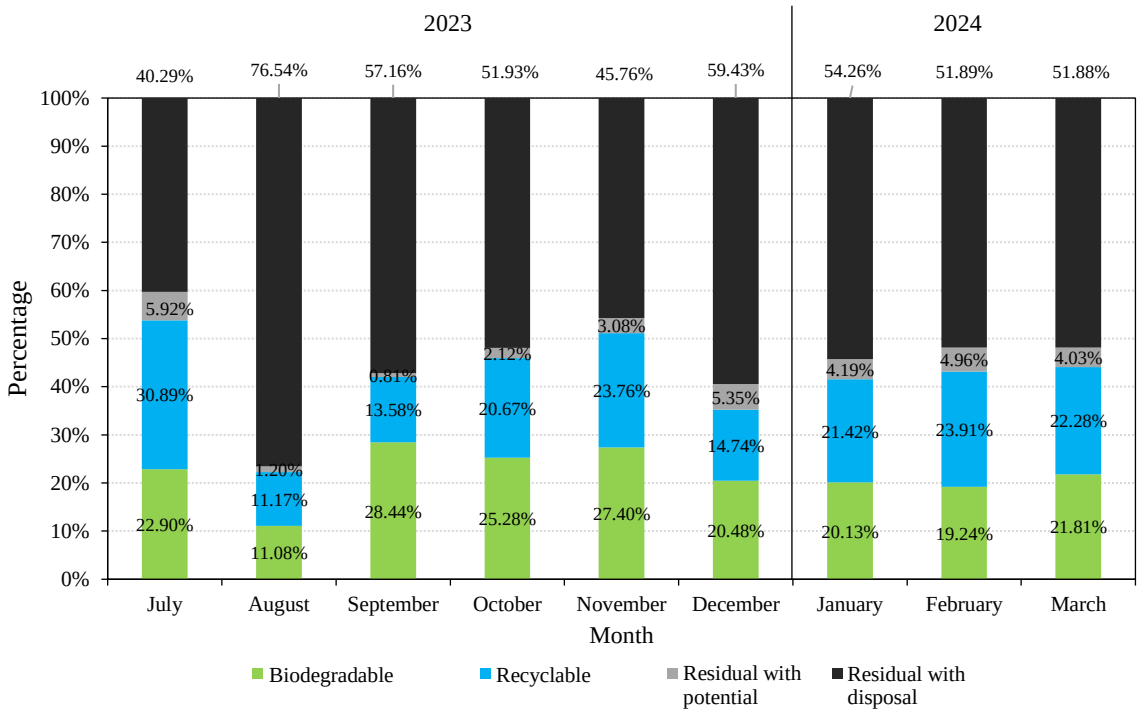

Figure 11. Percent waste composition trend from July 2023 to March 2024

3.4.4 Waste diversion

Although no waste diversion targets are imposed on specific waste sources such as institutions, the ultimate basis and baseline shall be on the results of waste characterization (DENR, 2001). As such, the potential waste diversion rate for DOST-ITDI is at 57.36% (dry season) as determined during WACS, or at 59.71% considering the exclusion of special wastes.

Figure 12 shows the percent waste diversion trend calculated from the monitoring data from the implementation of initial programs in August 2023 to March 2024.

The current waste diversion trend shows potential in achieving the adjusted potential waste diversion rate with the sustained operation of the temporary facilities established and segregation practice. However, as implied by the monitored waste composition and PCG rates, increased waste recovery and reducing residuals for disposal waste generation are necessary to achieve the current potential waste diversion target. Once achieved, the waste diversion target can then be increased to 80% following targets set for solid waste diversion in the Philippine Development Plan for 2017-2022 (NEDA, 2021).

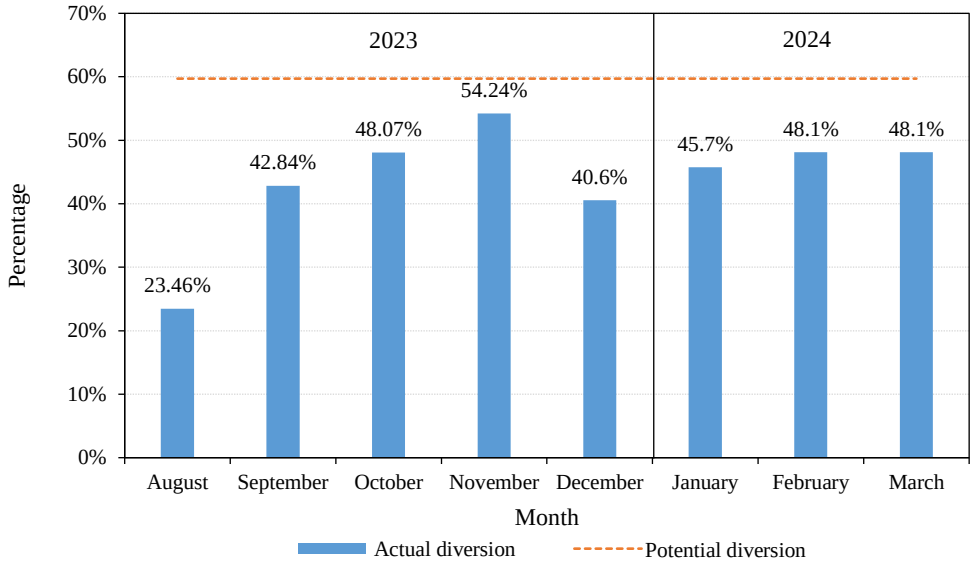

Figure 12. Waste diversion trend from August 2023 to March 2024

3.5 Waste generation projection

Using Equation (6) and using a growth rate, GR, of 4.57% based on the 2023 and 2024 staff population of 438 and 458, respectively, Figure 13a shows the 5-year population projection for DOST-ITDI, with 2024 as the base year.

The estimated ratio of non-regular staff (COS/JO/Casual) to the total population was set at an average of 30.65% and was also based on the 2023 (29.00%) and 2024 (32.31%) data. Note that the regular staff population was capped at 370 for the 2027 population projection and beyond due to the staffing limit stated earlier, and as such, latter population growth only relies on the increase in population of non-regular staff.

From the population projection, a 5-year waste generation for DOST-ITDI from 2025 to 2029 with 2024 as the base year was projected (Figure 13(b)). Note that for the waste generation projection, the dry season per capita generation (PCG) of 0.21 kg/capita/day was used, then multiplied to the projected population and the total number of working days per year. In the case of DOST-ITDI as a national government agency, one year is equivalent only to 264 days, or 22 working days multiplied to 12 months.

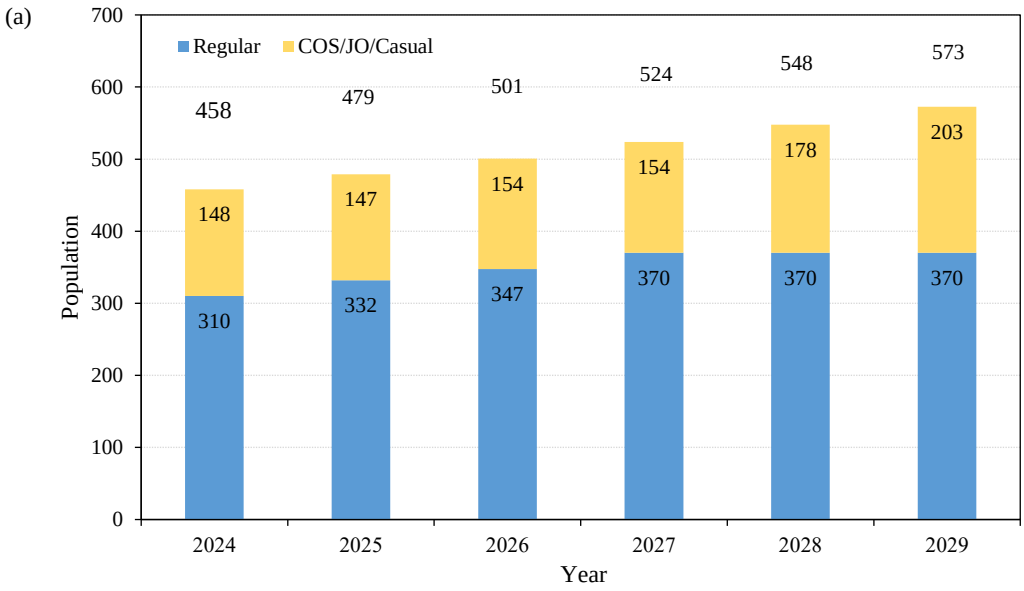

Figure 13. Five-year (a) population and (b) waste generation projection for DOST-ITDI

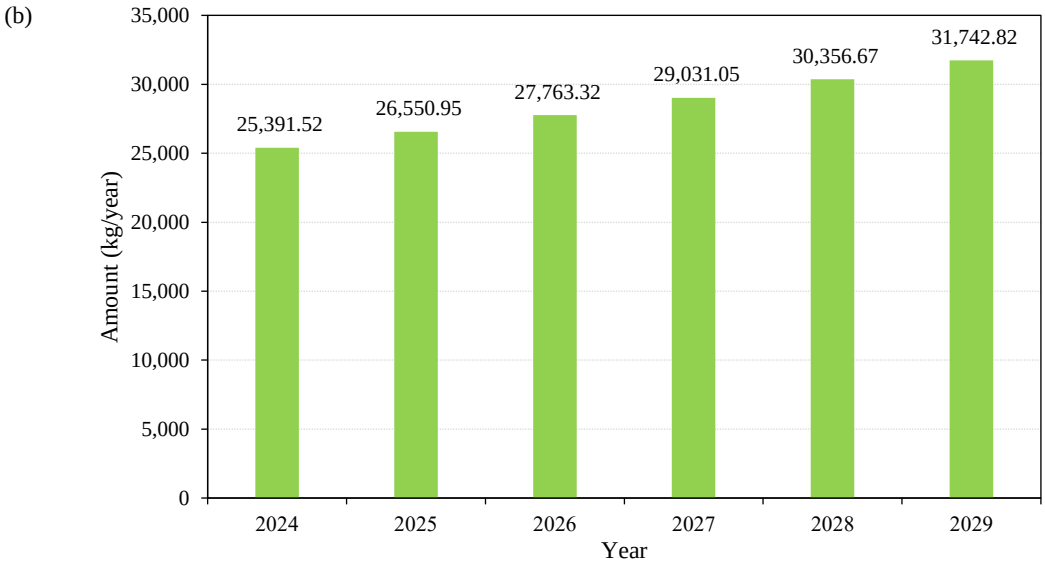

Figure 13. Five-year (a) population and (b) waste generation projection for DOST-ITDI (cont.)

With the projected increase from 25,391.52 kg/year (96.18 kg/day) in 2024 to 31,839.20 kg/year (120.60 kg/day), the need for an increased waste recovery and reduction strategies is emphasized to mitigate or at least slow the growth in waste generation. Finally, the establishment of a permanent materials recovery and composting facility is also paramount in ensuring the sustainability of the current waste diversion programs considering the projected increase in waste generation with the increase of staff population in DOST-ITDI.

4. CONCLUSION

The conduct of WACS highlighted the characteristics, generation rate of the identified waste sources, as well as the consistency of waste generation in DOST-ITDI between dry and wet seasons. The generated waste is composed of residuals for disposal (35.93% and 37.75%, dry and wet season), with the research and development divisions as the major source of waste due to its large population, contributing up to 63% of the waste generated by the institution. Further, per capita generation rates between seasons and between major sources were found to be consistent, indicating that the PCG of 0.18 and 0.21 kg/capita/day can be reliably used to estimate and project waste generation in DOST-ITDI. Finally, the implemented initial solid waste management programs based on the data gathered from the conduct of WACS showed potential in promoting waste segregation practice, ensuring waste diversion, and overall improving the waste management in the institution. However, additional strategies for waste recovery and reduction are still necessary to further reduce residuals for disposal and increase waste diversion rates, as well as the establishment of a permanent materials recovery and composting facility to sustainably support the management of the current and projected increase in solid waste generation in DOST-ITDI.

ACKNOWLEDGEMENTS

The success of the conduct of waste analysis and characterization study (WACS) was made possible through the collaboration of the proponents with the DOST-ITDI committees on Safety, Health, Security, and Environment, and on Clean and Green, as well as the cooperation of all utility personnel for aiding and their effort for the completion of the study.

REFERENCES

American Society for Testing and Materials (ASTM). ASTM E1109-19: Test Method for Determining the Bulk Density of Solid Waste Fractions. Pennsylvania, USA: ASTM International; 2019.

Asian Development Bank (ADB). Waste Analysis and Characterization Study (WACS). Report No: 3. ADB TA 3848-PHI: Metro Manila Solid Waste Management Project. Quezon City, Philippines: Department of Environment and Natural Resources; 2003.

Ciudad KL, Lucero CVE, Calonia VNE. Pre-COVID 19 Pandemic solid waste management and characterization in Caraga State University, Ampayon, Butuan City, Philippines. Journal of Ecosystem Science and Eco-Governance 2022;4(1):43-53.

Department of Budget and Management (DBM). Department of Science and Technology-Industrial Technology Development

Institute. Manila, Philippines: Department of Budget and Management; 2024. p. 223.

Department of Environment and Natural Resources (DENR). Department Administrative Order No. 34 s. 2001: Implementing Rules and Regulations of Republic Act 9003. Quezon City, Philippines: Department of Environment and Natural Resources; 2001.

Elayan JM, Cabiguin RZB, Tamang RT, Lacang GC. Solid wastes characterization in University of Science and Technology of Southern Philippines, Cagayan de Oro Campus. Journal of Biodiversity and Environmental Sciences 2019;15(4):52-28.

Environmental Management Bureau (EMB). National solid waste management status report: 2008-2018 [Internet]. 2018 [cited 31 Mar 2024]. Available from: https://emb.gov.ph/wp-content/uploads/2019/08/National-Solid-Waste-Management-Status-Report-2008-2018.pdf.

Gozum I. "Philippines 'sinking in sachets'-brand audit" [Internet]. 2024 [cited Apr 20, 2024]. Available from: https://www.rappler.com/environment/findings-philippines-plastic-brand-audit-2023/.

Industrial Technology Development Institute (DOST-ITDI). Industrial technology development institute: Who we are [Internet]. 2023 [cited Mar 31, 2024]. Available from: https://itdi.dost.gov.ph/index.php/who-we-are.

Japan International Cooperation Agency (JICA). Waste Analysis and Characterization Study (WACS): A standardized and mandatory guide for Philippine Local Government Units and Solid Waste Management Practitioners. Quezon City, Philippines: Department of Environment and Natural Resources; 2020.

Junior LM, Coltro L, Dantas FBH, Vieira RP. Research on food packaging and storage. Coatings 2022;12(11):Article No. 1714.

National Economic and Development Authority (NEDA). Ensuring ecological integrity, clean and healthy environment. In: Updated Philippine Development Plan: 2017-2022. Pasig City, Philippines: National Economic and Development Authority; 2021. p. 20-4.

National Solid Waste Management Commission (NSWMCa). DENR-EMB solid waste management division-national solid waste management commission secretariat: Solid waste generation [Internet]. 2023 [cited 31 Mar 2024]. Available from: https://nswmc.emb.gov.ph/.

National Solid Waste Management Commission (NSWMCb). NSWMC Resolution No. 1380 s. 2020: Adopting the Guidelines on the Waste Analysis and Characterization Study and its Related Manual. Quezon City, Philippines: Department of Environment and Natural Resources; 2020.

Palomar AAU, Sundo MB, Velasco P, Camus DRD. End-of-pipe waste analysis and integrated solid waste management plan. Civil Engineering Journal 2019;5(9):1970-82.

Philippine Atmospheric, Geophysical, and Astronomical Services Administration (DOST-PAGASA). Press release: Preparation for warm and dry season [Internet]. 2023a [cited 7 Apr 2024]. Available from: https://www.pagasa.dost.gov.ph/press-release/128.

Philippine Atmospheric, Geophysical, and Astronomical Services Administration (DOST-PAGASA). Press release: Onset of the rainy season [Internet]. 2023b [cited 7 Apr 2024]. Available from: https://www.pagasa.dost.gov.ph/press-release/138.

Schachter J, Karasik R. Plastic Pollution Policy Country Profile: Philippines-NI PB 22-10. North Carolina, USA: Duke University; 2022.

Tansengco ML, Herrera DL, Tejano JC, Esguerra RL. Development of a small-scale composter and its application in composting of biodegradable waste generated from a government institution. Asian Journal of Biological and Life Science 2016; 5(1):21-7.

United States Environmental Protection Agency (US EPA). Report on the environment-wastes [Internet]. 2023 [cited April 7, 2024]. Available from: https://www.epa.gov/report-environment/wastes.

Worrell WA, Vesilind PA. Appendix B: Bulk densities of refuse components. In: Worrell WA, Vesilind PA, editors. Solid Waste Engineering. 2nd ed. USA: Cengage Learning; 2011.

Environment and Natural Resources Journal

Volume 22
Issue 6
2024

Efficient Recycling of Domestic Cooked Food Waste into Hermicompost Using Black Soldier Fly Larvae

Hema B.P.*, Sanjay K.B., Arpitha Uday Nayak, Ghufran MD Maaz, and Rifa Taskeen

Department of Biotechnology, Sri Jayachamarajendra College of Engineering (SJCE), JSS Science and Technology University, JSS TI Campus, Mysuru, Karnataka, India

ARTICLE INFO

Received: 5 Feb 2024
Received in revised: 20 Sep 2024
Accepted: 3 Oct 2024
Published online: 31 Oct 2024
DOI: 10.32526/ennrj/22/20240032

Keywords:
Black Soldier Fly Larva (BSFL)/ *Hermetia illucens*/ Hermicompost/ Organic waste management/ Food waste recycling/ Bioconversion

*** Corresponding author:**
E-mail: hemabp@sjce.ac.in

ABSTRACT

Economic progress, urban expansion, and enhanced quality of life in India have led to the formation of densely populated megacities and a significant increase in municipal solid waste generation. Such waste consists of a substantial volume of residues from food waste, kitchen waste originating from residential complexes, restaurants, and remnants of agricultural activities. Consequently, handling municipal solid waste has become a critical issue. Though composting is being practiced as an eco-friendly means of recycling organic waste, it is laborious and time-consuming. In the recent past, researchers have suggested the use of black soldier fly larvae (BSFL) as an effective solution for solid waste management. This study aims to assess the degradation potential of BSFL, which is gaining attention in recycling technology due to its composting capabilities, and its ability to produce soil amendments suitable for agricultural purposes. To evaluate the ability of BSFL to degrade different types of organic wastes, with a focus on cooked food waste, the compost formed after 14 days of degradation was analyzed based on elemental composition and other parameters. Comparative examinations were made with different vermicompost samples and hermicompost produced using BSFL to check the effect on plant growth. The analysis showed a higher percentage of nitrogen (4.21%), and phosphorus (0.5%) in hermicompost. The C:N ratio was 12:1 which is suitable for agronomical purposes. This study concludes that, BSFL are useful as versatile bioconversion agents of cooked food waste and provide a promising organic recycling strategy for sustainable waste management.

1. INTRODUCTION

Food wastage is a significant global issue, generating approximately 1.3 billion tonnes annually. This statistic was highlighted by the Food and Agriculture Organization (FAO), which reported that a staggering one-third of the world's food production for human consumption is wasted annually (FAO, 2019). However, the consequences of improper food waste disposal are not just alarming in terms of large quantity; they also extend to environmental and health concerns. The inadequate management of solid waste, leads to the occupation of valuable landfill space, resulting in the proliferation of diseases and the emission of unpleasant odours, as noted by Hoornweg and Bhada-Tata (2012). It's important to recognize that landfills contribute significantly to the production of methane gas through anaerobic decomposition. Methane is a potent greenhouse gas, estimated to be 25 times more impactful than carbon dioxide when released directly into the atmosphere (Abdelfattah et al., 2021).

These environmental challenges associated with food waste and its disposal have led to concerns about the eco-friendliness of current waste management practices. This prompts a re-evaluation of waste minimization strategies, where composting has been the traditional approach and has its own merits and demerits. Composting, a long-practised

Citation: B.P. H, K.B. S, Nayak AU, Maaz GM, Taskeen R. Efficient recycling of domestic cooked food waste into hermicompost using black soldier fly larvae. Environ. Nat. Resour. J. 2024;22(6):565-573. (https://doi.org/10.32526/ennrj/22/20240032)

process, results in humus that enhances plant growth and reduces organic waste.

This is like vermicomposting, which also occurs through the interaction of microorganisms and earthworms in an aerobic setting, as described by Domínguez et al. (2000). Both methods contribute to sustainable waste management and soil enrichment. However, both composting and vermicomposting demands considerable space, high temperatures, and time. It may also face challenges such as vermin and odours. Vermicomposting introduces additional challenges, including the need to keep worms alive and separating worms from compost before use, adding to its complexity (Mahmood et al., 2021; Amuah et al., 2022). Sharma et al. (2024) have reviewed the potential of composting technology in recycling and reuse of organic matter for increasing the soil fertility perhaps they expressed the concern towards maturity, stability and quality of compost as there is no uniformity and global guidelines for compost.

Enebe and Erasmus (2023) have enumerated the merits of vermicomposting technology and some of the limitations such as labour intensive operation, require large area of land, waste processing is slow, vermicompost harvesting is difficult as it requires separating of earthworms from compost, cold environmental conditions will slow down the treatment process and accelerate the time. In light of inherent limitations of conventional composting and vermicomposting, an innovative solution emerges: Hermicomposting, by utilizing the larvae of black soldier fly (BSF). The black soldier fly, scientifically known as *Hermetia illucens* (Diptera: Stratiomyidae), is a slender fly measuring about 20 mm in length. Native to the southeastern United States, it's also found in tropical, subtropical regions and southern Europe (Müller et al., 2017). Belonging to the Hermetiinae subfamily within the Diptera order, this widely distributed species is of note for its exceptional ability to convert organic waste, including food waste, into valuable resources. For many years, researchers worldwide have suggested utilizing the larvae of the black soldier fly (*Hermetia illucens*) as a method to break down organic materials like food waste, thereby avoiding their fraction getting into landfills (Diener et al., 2011; Gabler, 2014).

Research shows that BSFL can reduce biowaste by up to 96.1% in weight and 89.0% in volume, as observed in a study by Mahmood et al. (2021).This remarkable capability primarily originates from the robust mouthparts of the BSFL and their higher enzymatic activity in the gut compared to other fly species. As a result, BSFL excels in decomposing food waste with remarkable efficiency (Cho et al., 2020). BSF is also a valuable resource insect known for its exceptional ability to efficiently convert various types of organic waste materials, including livestock manure like poultry or dairy waste. The impressive versatility in the food sources that *Hermetia illucens* can consume results in a diverse composition of its frass (the excrement of larvae), which holds noteworthy implications for soil enrichment. This frass contributes essential nutrients and organic matter to the soil, leading to shifts in the microflora within the soil and influencing plant behaviour, as elucidated by Schmitt and de Vries (2020). Extensive studies have depicted that the compost obtained from the BSFL can significantly enhance the growth, yield, and nutritional quality of vegetable crops, particularly in conjunction with mineral fertilizers, as reported by Anyega et al. (2021).

Notably, research findings indicate that the BSF's life cycle and larvae can effectively reduce heavy metal content in the feed through degradation. Even at significantly high concentrations, the impact of heavy metal elements on the growth of the BSF remains minimal (Diener et al., 2015). This further underscores the unique and valuable role that the BSF plays in waste management and environmental sustainability.

The BSF can efficiently convert organic waste materials like livestock manure (poultry or dairy waste). This conversion process yields larval biomass that boasts a substantial content of protein and fat, as highlighted in research by Rehman et al. (2023). This is particularly significant for poultry, as their dietary requirement of 18-20% crude protein, with specific composition challenges that grain feed alone cannot meet. Furthermore, the insect gut microbiota plays a pivotal role in various aspects, such as providing nutrients, stimulating the immune system, eliminating harmful microorganisms, influencing sex determination and hormonal signalling, and even affecting behaviours. The gut also proves crucial in breaking down challenging substances like lignin, polysaccharides, and resistance genes. This gut microbiota can be likened to a distinct "organ" with its metabolic capabilities, contributing to waste decomposition and producing beneficial substances for the host (Jiang et al., 2019). A notable ecological benefit lies in the potential reduction of harmful bacteria, such as *Escherichia coli* or *Salmonella*,

through the utilisation of BSF larvae in processing livestock manure, as highlighted by Rehman et al. (2023).

According to Müller et al. (2017), the larvae of *Hermetia illucens*, with their protein content of 42%, can serve as suitable feed for poultry and pig breeding, The chitin-rich outer covering derived from various stages of the BSF's life cycle, including larval moulting, adult emergence, and the adult flies adds considerable nutritional value to hermicompost, notably enhancing its nitrogen content, as noted by Terrell (2022). This underscores the far-reaching positive effects that the BSF and its byproducts can have on sustainable agriculture and waste management practices.

By connecting the dots between global food waste issues, environmental implications, and evolving waste management methods, it's evident that exploring advanced techniques like hermicomposting holds promise for a more sustainable and efficient approach to tackling food waste. This approach serves the purpose of redirecting these materials away from overburdened landfills, as highlighted by previous studies of Diener et al. (2011) and Gabler (2014). Considering the above facts and as per the suggestions of researchers worldwide, this study was intended to utilise BSFL as a viable method to break down organic waste materials, including domestic food waste as well as garden waste.

2. METHODOLOGY

2.1 Area of study

The research was conducted on the campus of the JSS Science and Technology University, Mysore, India. The BSF eggs were allowed to hatch out in a constructed room with a temperature of 30°C and relative humidity of 60-65% and trays were enclosed by mosquito nets to protect waste and larvae from predators and unfavourable weather conditions.

2.2 Black soldier fly

BSF eggs were procured from a black soldier fly insect farming training facility. On 1st day around 2gms of eggs were placed over a mesh as shown in Figure 1(a) and Figure 1(b). This mesh was kept over a tray containing poultry feed and wheat bran. After 2 days, the eggs hatched out and baby larvae, as shown in Figure 1(c) had fallen to the pre-feed. The hatched BSFL were kept in the pre-feed for 2 more days and then transferred to boxes containing different solid waste samples.

2.3 Treatment of waste samples

Initially, three different types of wastes *viz.* garden waste, kitchen raw waste, and cooked food waste were observed for the degradation rate. Garden waste consists of dry leaves and small pieces of plants and trees on the campus. Kitchen raw waste and cooked food waste were collected from the college campus hostel. The kitchen raw waste consisted of vegetables and fruits peel whereas kitchen cooked food waste comprised of leftover wheat breads, dosas, rice, sambar with lentils and pulses, and other foods.

Along with the three sample boxes, a control box without larvae was kept for each sample to compare the degradation rate. Initially, larvae to feed ratio was 1:10 which means for 15 g of worms, 150 g of feed was supplied in the form of organic waste. Since a faster rate of degradation was observed in cooked waste after 14 days, further studies were conducted with cooked food waste.

The hatched larvae were transferred to a container, with cooked food waste as feedstock as shown in Figure 1(d). The larvae to feed ratio was 1:2 which means for 1.5 kg of larvae, 3 kg of feed was supplied. After complete degradation, nutritional value of the compost was analysed.

2.4 Comparative study of vermicompost and hermicompost samples

The comparative studies were carried out and different samples of vermicompost were procured from different suppliers for the study. The details of the vermicompost bought from different places are as follows:

1. Leafy Tales Organic Vermicompost Fertilizer Manure (VC-1): Manufactured at Gurgaon
2. IFFCO Urban Gardens Nutri-Rich Vermicompost Manure (VC-2): Manufactured and Marketed by Aquagri Processing Pvt Ltd., New Delhi
3. Local Zoo Vermicompost (VC-3): Manufactured at Zoological Garden, Mysuru
4. Anitha Nursery Vermicompost (VC-4): Manufactured at Mysuru
5. Bhudevi Farm Vermicompost (VC-5): Manufactured at Mysuru
6. Hermicompost: Compost formed by degradation of cooked food waste by BSFL

(a) Eggs placed over a mesh

(b) BSFL eggs

(c) BSFL under microscope

(d) Hatched larvae feeding on cooked food waste

(e) Adult BSFL feeding on cooked food waste

(f) Hermicompost formed after 14 days of degradation

Figure 1. Treatment of cooked food waste using BSFL.

2.5 Analysis of compost

The elemental analysis was done for both hermicompost and vermicompost samples. For the analysis, above mentioned five compost samples collected from various vendors and hermicompost produced from this study were analysed for the parameters of pH, nitrogen (N), phosphorous (P), potassium (K), sodium (Na), and organic carbon(C).

The pH test was done using a digital pH meter. The dry sample was used for nitrogen and carbon analysis. Nitrogen analysis was done using the Energy Dispersive X-Ray Spectroscopy (EDAX) method as per standard guidelines. Organic carbon analysis was done by following the dry combustion method of Nelson and Sommers (Bhat et al., 2017).

For the other parameters, aqueous form of sample was required, hence, the sample preparation was done by dissolving 5 g of sample in 50 mL of water and Whatman filter paper was used for sample filtration. The dilution factor of 0.1 is considered for the calculation. Phosphorous analysis was done by following the standard procedure using Spectrophotometer (Stănescu et al., 2021). Potassium and Sodium analysis were carried out using a flame photometer (Banerjee and Prasad, 2020).

2.6 Plant growth studies using vermicompost and hermicompost samples

The two hundred saplings of tomato were procured from the local nursery. The saplings were transferred to the grow bags containing red soil and coco peat. They were kept in cooler area with a temperature of 30°C, humidity between 65-70% and bright light conditions. Different vermicompost and hermicompost samples were added to the respective pots later. Control plants without compost were also maintained in the study. The length of the plants grown in different varieties of compost and control plants was measured regularly to check the effect of compost on plant growth.

3. RESULTS AND DISCUSSION

3.1 Analysis of elemental composition of vermicompost and hermicompost samples

3.1.1 Total organic carbon concentration

The primary physio-chemical attributes of well-aged compost revolve around its organic matter and organic carbon content, as they serve as the foundation for all other vital macro and micronutrients. Furthermore, these attributes enhance various aspects of soil quality, including cation exchange capacity, biodiversity, and soil aggregation, thus impacting its chemical, biological, and physical characteristics positively (Muhamed and Umer, 2023). The composition of organic carbon in the composts was analysed by dry combustion method of Nelson and Sommers (Bhat et al., 2017). The organic carbon content was found to be 48.83%, the highest among all the composts as shown in Figure 2. A similar study shows the composition percentage of organic carbon to be 38.61% in composted BSF frass fertilizer (Anyega et al., 2021). Using poultry feed and wheat bran as pre feed and cooked food waste such as rice, which is rich in carbohydrates as feed for BSFL for composting might be the reason for increased carbon concentration in the compost. Lalander et al. (2019) are also of the opinion that poultry feed had the highest C/N ratio in their study with different feedstock for BSFL.

3.1.2 Total nitrogen concentration

The composition of nitrogen (N) in the compost produced by BSFL was studied using the EDAX method. The N content in the hermicompost was found to be 4.21% which was the highest among all the compost samples. Sarpong et al. (2019) have opined that the rise in nitrogen concentrations over time might be attributed to the reduction in the dry weight of organic matter (re-concentration) in the substrate due to larvae decomposition. Another possible explanation for this increase is the biochemical activities of the larvae and the secretion of nitrifying bacteria from their gut (Bernal et al., 2009). This observation aligns with findings from a study by Kim et al. (2011). The rest of the vermicompost samples was found to be in the range of 1 to 3.3%. Based on a database of samples from the U.S. Composting Council's Compost Analysis Proficiency Program (Sullivan et al., 2018), it is reported that to produce a good crop, the range of N in compost is 1 to 2%. If the total N content of compost is less than 1 percent, then N fertilization must be considered as a supplement after compost application. Whereas, if total N exceeds 2 percent, the compost can replace a portion of typical N fertilizer input for crop production. Nitrogen fertilizers lead to nitrate water pollution and greenhouse effect with nitrous oxide, nitrogen oxides, and ammonia, contributing to global warming and ozone layer depletion (Byrnes, 1990). Hermicompost which is rich in N composition due to the variety of the feed given to BSFL can be used not only as a compost but as a portion of N fertilizer thus, reducing negative impact on the environment by reducing the use of chemical fertilizers.

3.1.3 Total phosphorus concentration

The composition of phosphorous (P) in the compost produced by BSFL was studied using Spectrophotometry. Based on the reports of samples from the U.S. Composting Council's Compost Analysis Proficiency Program, to produce a good crop, the range of P should be 0.3 to 0.9% (Sullivan et al., 2018). The highest P percentage was observed in hermicompost sample of 0.5% which is in the optimal range for any compost. Since the hermicompost quality falls within the standard quality in agriculture, it is suitable for plant growth. The optimal percentage of potassium in the compost reported in this current study was analogous to the results (0.5%) found in composted BSF frass fertilizer (Anyega et al., 2021). Also, P availability from compost compares favourably with that of conventional phosphorus fertilizers (Crohn et al., 2013). To conserve the environment and cut costs on fertilizers, growers can decrease their phosphorus fertilizer usage in correlation with the P contribution provided by compost (Crohn, 2016).

3.1.4 Total potassium concentration

The composition of potassium (K) in the compost produced by BSFL was studied using flame photometry. According to the report of Sullivan et al. (2018), to produce a good crop, the range of K is 0.5 to 1.5%. If K exceeds 1.5 percent, the compost feedstocks can include manure, food waste, or grass clippings. This compost K is considered equivalent to fertilizer K as a source of K for plants. The K content in hermicompost was found to be 1.84% and the highest content was seen in VC-1. Since the quality of compost almost fell within the standard quality in agriculture, it is acceptable for plant growth.

3.1.5 Total sodium concentration

The composition of sodium (Na) in the compost produced by BSFL was studied using flame photometry. The Na content in all the samples was found to be within the optimum range. Na hermicompost was found to be 0.14% and the highest was observed in the VC-1 sample (Table 1). Compost containing more than 1 percent Na is considered to be quite high in concentration, and excess levels of Na can lead to sodicity and phytotoxicity problems (Crohn, 2016). Also based on a database of samples from the U.S. Composting Council's Compost Analysis Proficiency Program (Sullivan et al., 2018), to produce a good crop, the range of Na should be below 0.6%.

Table 1. Elemental composition and pH of vermicompost and hermicompost samples

Sample	OC (%)	N (%)	P (%)	K (%)	Na (%)	pH
VC-1	35.0	3.27	0.05	6.60	0.17	7.75
VC-2	21.6	1.38	0.02	1.90	0.10	7.20
VC-3	47.6	1.41	0.03	0.10	0.10	7.86
VC-4	31.7	1.80	0.03	0.13	0.03	7.98
VC-5	24.6	2.36	0.01	0.52	0.03	7.25
HC	48.83	4.21	0.50	1.84	0.14	7.03

VC-1: Leafy Tales Leafy Organic Vermicompost Fertilizer Manure, VC-2: IFFCO Urban Gardens Nutri-Rich Vermicompost Manure, VC-3: Local Zoo Vermicompost, VC-4: Anitha Nursery Vermicompost, VC-5: Bhudevi Farm Vermicompost, HC: Hermicompost

3.2 Analysis of pH for vermicompost and hermicompost samples

To ensure the high performance of a composting process, optimum level of pH 5.5-8.0 is required. The increase in pH level at the early stages of the composting process is because of an increase in the volume of ammonia released due to protein degradation. Decrease in pH level at the later stage of composting was caused by the volatilization of ammoniacal nitrogen and H^+ released due to microbial nitrification process by nitrifying bacteria (Eklind and Kirchmann, 2000). Among all the five vermicompost and hermicompost samples, a pH range of 7.03-7.98 was observed which was indeed in optimum level as shown in Figure 2(f).

3.3 C:N ratio of all the samples

The carbon-to-nitrogen ratio is crucial in composting process because microorganisms need a good balance of carbon and nitrogen to be active. The ratio directly affects the speed and efficiency of the process and determines the quality of the resulting compost. High C:N ratios can lead to prolonged composting duration and low C:N ratios can enhance nitrogen loss.

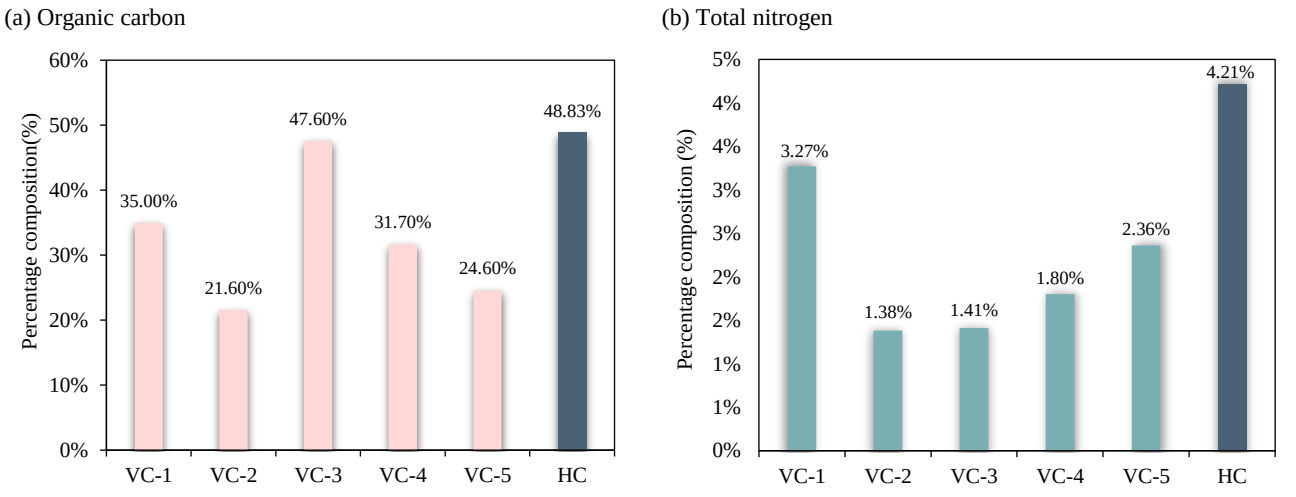

Figure 2. Graphs representing Elemental composition and pH of all composts. Graph (a), (b), (c), (d) and (e) represents the percentage composition of total organic carbon, total nitrogen, total phosphorus, total potassium, and total sodium respectively. Graph (f) represents the pH of different compost samples.

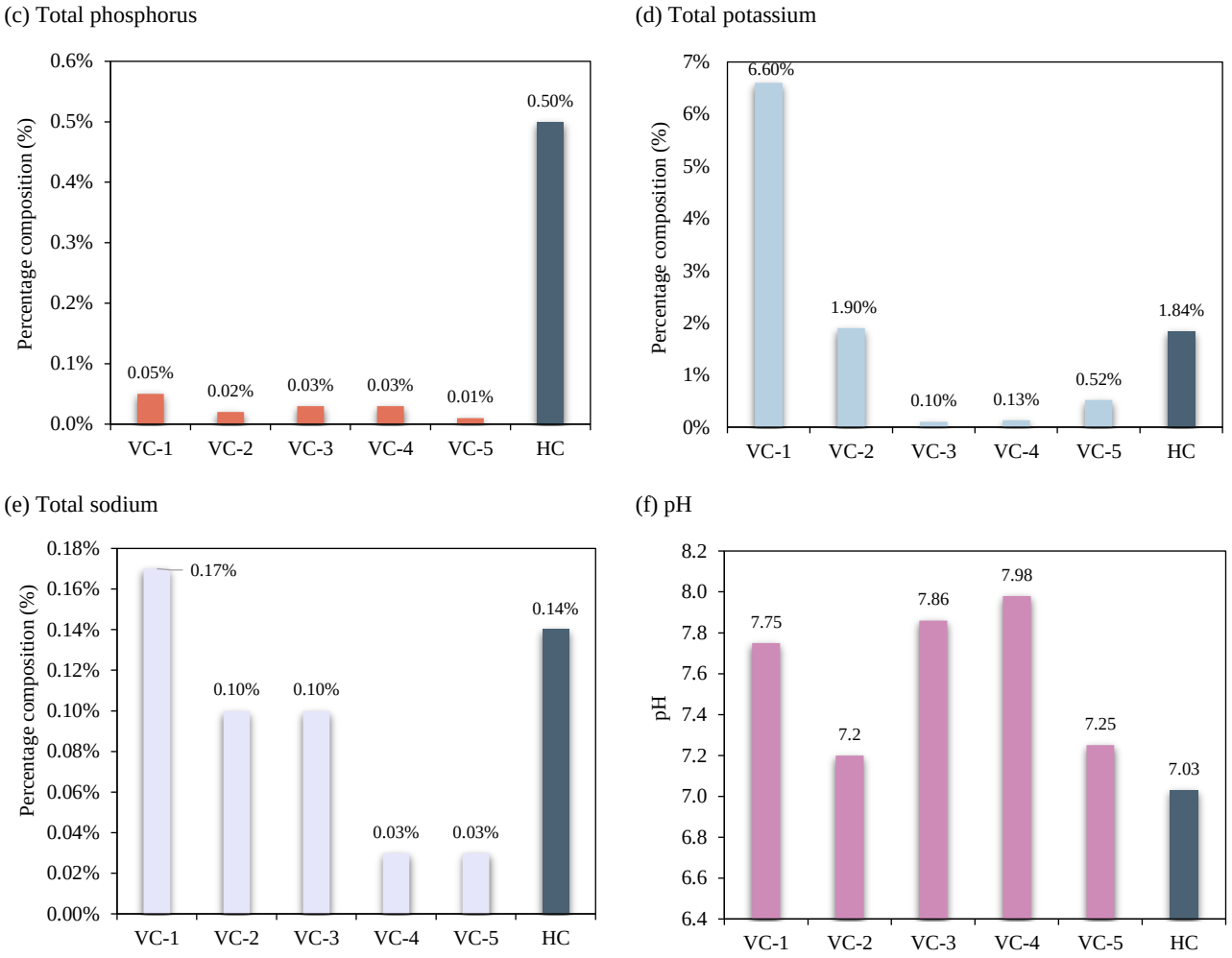

Figure 2. Graphs representing Elemental composition and pH of all composts. Graph (a), (b), (c), (d) and (e) represents the percentage composition of total organic carbon, total nitrogen, total phosphorus, total potassium, and total sodium respectively. Graph (f) represents the pH of different compost samples (cont.).

Table 2. C:N ratio of the samples

Sample	C:N Ratio
VC-1	10:1
VC-2	15:1
VC-3	34:1
VC-4	18:1
VC-5	10:1
HC	12:1

VC-1: Leafy Tales Leafy Organic Vermicompost Fertilizer Manure, VC-2: IFFCO Urban Gardens Nutri-Rich Vermicompost Manure, VC-3: Local Zoo Vermicompost, VC-4: Anitha Nursery Vermicompost, VC-5: Bhudevi Farm Vermicompost, HC: Hermicompost

It has been reported that a carbon-to-nitrogen (C:N ratio) value of 15 or below is highly preferable for agronomic purposes (Jereb, 2004; Pan et al., 2012). They have also suggested there where C:N ratio is less than 20, it is likely to cause the mineralization of organic nitrogen to inorganic which is suitable for plants. Therefore, the C:N ratio of hermicompost is within the limit as shown in Table 2 which strongly suggests that the larvae compost obtained is satisfactory for agricultural purposes. Any compost with a C:N ratio greater than 30 is likely to immobilize nitrogen if applied to soil (Bernal et al., 2009). Only one sample VC-3 had high carbon content, the rest are within the desirable range.

The plant growth studies with different compost samples exhibited significant differences in the plant height and number of leaves. The initial plant height was almost same within the range of 15-20 cm. Weekly observations were made for 5 weeks for all the compost samples with control. During this observation, it was noticeable that plants applied with hermicompost had grown significantly more when compared to all other vermicompost and control. The plant height in the 5th week of hermicompost plants as shown in Table 3 was in the range of 43-46 cm and with approximately 28 leaves, whereas other

vermicompost samples had an average height of 40 cm with an average number of 25 leaves. And control exhibited a slower growth of 32 cm plant height and 20 leaves. This indicates that the nutritional composition of hermicompost and the uptake of those nutrients by the tomato plants were superior when compared to that of vermicompost.

Table 3. Effect of hermicompost and selected vermicompost samples on the growth of tomato plants

Parameter	Compost	Time				
		1st week	2nd week	3rd week	4th week	5th week
Plant height	VC-1	26.67±1.58^{e}	30.66±1.70^{d}	35.46±2.19^{d}	39.06±1.98^{d}	42.16±1.92^{d}
	VC-2	21.63±3.92^{b}	26.00±4.01^{b}	30.70±3.72^{b}	34.50±3.83^{b}	38.23±3.48^{b}
	VC-3	24.13±3.49^{c}	27.63±3.98^{c}	32.80±3.46^{c}	37.03±3.41^{c}	40.80±3.37^{b}
	VC-4	24.00±3.60^{c}	28.90±4.44^{a}	34.00±4.15^{a}	38.23±3.49^{c}	41.73±3.34^{b}
	VC-5	22.23±4.62^{a}	27.43±4.06^{b}	31.96±4.24^{a}	36.70±4.31^{a}	39.90±4.37^{a}
	HA	24.83±1.95^{e}	31.20±1.60^{d}	37.63±1.85^{e}	42.63±1.92^{d}	46.53±1.20^{e}
	HB	19.87±2.48^{d}	26.96±1.73^{d}	33.20±1.05^{g}	38.16±1.06^{e}	43.06±1.19^{e}
	Control	21.06±0.90^{f}	24.13±1.02^{e}	26.66±1.55^{f}	28.76±1.97^{d}	31.70±2.61^{c}
Number of leaves	VC-1	11.67±1.52^{e}	21.33±1.52^{e}	21.33±1.52^{d}	24.00±1.00^{c}	26.00±1.00^{c}
	VC-2	10.67±1.15^{f}	19.66±2.30^{c}	20.00±2.64^{b}	21.00±1.00^{c}	25.00±2.00^{a}
	VC-3	12.00±2.00^{d}	19.00±2.64^{b}	20.33±1.15^{e}	22.66±1.52^{b}	24.33±2.08^{a}
	VC-4	12.00±2.64^{c}	20.66±1.52^{e}	21.33±2.08^{c}	23.00±1.00^{c}	26.00±1.00^{c}
	VC-5	10.00±3.60^{b}	16.66±3.51^{a}	21.66±1.52^{d}	22.66±1.52^{b}	25.33±1.52^{b}
	HA	11.33±1.52^{e}	18.33±2.08^{d}	21.00±1.00^{e}	23.00±1.00^{c}	28.00±1.00^{c}
	HB	13.67±4.50^{a}	20.33±1.52^{e}	23.66±1.52^{d}	23.66±1.52^{b}	28.33±0.57^{d}
	Control	9.33±0.57^{g}	17.00±1.00^{f}	16.00±3.46^{a}	18.66±2.08^{a}	20.00±1.00^{c}

VC-1: Leafy Tales Leafy Organic Vermicompost Fertilizer Manure, VC-2: IFFCO Urban Gardens Nutri-Rich Vermicompost Manure, VC-3: Local Zoo Vermicompost, VC-4: Anitha Nursery Vermicompost, VC-5: Bhudevi Farm Vermicompost, HA and HB are two samples of hermicompost.

4. CONCLUSION

The study initially aimed to transform various types of waste, including cooked waste, kitchen waste and garden waste. A rapid degradation rate was observed in samples with BSF larvae compared to control boxes without larvae. The highest degradation occurred after 14 days in cooked waste, surpassing the degradation of kitchen waste and dry waste. The BSFL demonstrated a greater waste degradation capacity during their 2 to 3 weeks larvae stage. This highlights the potential of BSF larvae to degrade cooked food waste within two weeks, in contrast to the longer time taken by other biological degradation.

Comparative examinations were made between hermicompost and vermicompost samples. The pH levels fell within the optimal range of 5.5-8.0, with hermicompost having the lowest pH at 7.03. Hermicompost also exhibited the highest carbon percentage (48.83%) compared to other vermicompost samples. Similarly, hermicompost showed superior nitrogen (4.21%), and phosphorus (0.5%) whereas vermicompost samples showed lesser quantity. Subsequent plant growth studies also showed that the plants had significantly better growth when provided with hermicompost than with vermicompost.

The objectives of this study were to assess the BSFL composting potential and to analyse the quality of hermicompost produced for agricultural purposes. The analysis indicated that hermicompost had a better C:N ratio compared to vermicompost samples. The parameters confirmed rapid decomposition and mineralization by BSFL, with the compost meeting standard quality for agricultural uses. Further studies are to be conducted to analyze physiochemical characteristics of the substrate and hermicompost, effect of climatic conditions and hermicompost on growth of different vegetable crops in varied seasons. Also, continued research to implement hermicomposting at domestic level and municipal level to bring in positive impacts of BSFL potential in food waste recycling for a cleaner and greener society.

REFERENCES

Abdelfattah EA, Abd El-Monem DH, Mahmoud AH, Aboelhassan AM, Ibrahim NY, Abdallah DB, et al. The various vulnerable products and services from organic waste management using black soldier fly, *Hermetia illucens*. Zoological and Entomological Letters 2021;1(1):44-56.

Anyega AO, Korir NK, Beesigamukama D, Changeh GJ, Nkoba K, Subramanian S, et al. Black soldier fly-composted organic fertilizer enhances growth, yield, and nutrient quality of three key vegetable crops in Sub-Saharan Africa. Frontiers in Plant Science 2021;12:Article No. 680312.

Amuah EEY, Fei-Baffoe B, Sackey LNA, Douti NB, Kazapoe RW. A review of the principles of composting: Understanding the processes, methods, merits, and demerits. Organic Agriculture 2022;12(4):547-62.

Banerjee P, Prasad B. Determination of concentration of total sodium and potassium in surface and ground water using a flame photometer. Applied Water Science 2020;10(5):Article No. 113.

Bernal MP, Alburquerque JA, Moral R. Composting of animal manures and chemical criteria for compost maturity assessment: A review. Bioresource Technology 2009;100(22): 5444-53.

Bhat SA, Singh J, Vig AP. Instrumental characterization of organic wastes for evaluation of vermicompost maturity. Journal of Analytical Science and Technology 2017;8:1-12.

Byrnes BH. Environmental effects of N fertilizer use: An overview. Fertilizer Research 1990;26:209-15.

Cho S, Kim CH, Kim MJ, Chung H. Effects of microplastics and salinity on food waste processing by black soldier fly (*Hermetia illucens*) larvae. Journal of Ecology and Environment 2020;44(1):Article No. 7.

Crohn DM, Chaganti VN, Reddy N. Composts as post-fire erosion control treatments and their effect on runoff water quality. Transactions of the ASABE 2013;56(2):423-35.

Crohn DM. Assessing compost quality for agriculture. University of California [Internet]. 2016 [cited 2023 Oct 20]. Available from: https://anrcatalog.ucanr.edu/pdf/8514.pdf.

Diener S, Studt Solano NM, Roa Gutiérrez F, Zurbrügg C, Tockner K. Biological treatment of municipal organic waste using black soldier fly larvae. Waste and Biomass Valorization 2011;2:357-63.

Diener S, Zurbrügg C, Tockner K. Bioaccumulation of heavy metals in the black soldier fly, *Hermetia illucens* and effects on its life cycle. Journal of Insects as Food and Feed 2015;1(4):261-70.

Domínguez J, Edwards CA, Webster M. Vermicomposting of sewage sludge: Effect of bulking materials on the growth and reproduction of the earthworm *Eisenia andrei*. Pedobiologia 2000;44(1):24-32.

Food and Agriculture Organization of the United Nations (FAO). The State of Food and Agriculture: Moving Forward on Food Loss and Waste Reduction. Rome, Italy: FAO; 2019.

Eklind Y, Kirchmann H. Composting and storage of organic household waste with different litter amendments. II: nitrogen turnover and losses. Bioresource Technology 2000;74(2): 125-33.

Enebe MC, Erasmus M. Vermicomposting technology: A perspective on vermicompost production technologies, limitations and prospects. Journal of Environmental Management 2023;345:Article No. 118585.

Gabler F. Using Black Soldier Fly for Waste Recycling and Effective *Salmonella* spp. Reduction [dissertation]. Swedish: Swedish University of Agricultural Sciences; 2014.

Hoornweg D, Bhada-Tata P. What a waste: A global review of solid waste management. Urban Development Series Knowledge Papers 2012;15:87-8.

Jiang CL, Jin WZ, Tao XH, Zhang Q, Zhu J, Feng SY, et al. Black soldier fly larvae (*Hermetia illucens*) strengthen the metabolic function of food waste biodegradation by gut microbiome. Microbial Biotechnology 2019;12(3):528-43.

Jereb G. Biodegradable Municipal Solid Waste Management [dissertation]. Polytechnic Nova Gorica, School of Environmental Sciences; 2004.

Kim W, Bae S, Park K, Lee S, Choi Y, Han S, et al. Biochemical characterization of digestive enzymes in the black soldier fly, *Hermetia illucens* (Diptera: Stratiomyidae). Journal of Asia-Pacific Entomology 2011;14(1):11-4.

Lalander CD, Diener S, Zurbrügg C, Vinnerås B. Effects of feedstock on larval development and process efficiency in waste treatment with black soldier fly (*Hermetia illucens*). Journal of Cleaner Production 2019;208:211-9.

Mahmood S, Zurbrügg C, Tabinda AB, Ali A, Ashraf A. Sustainable waste management at household level with black soldier fly larvae (*Hermetia illucens*). Sustainability 2021;13(17):Article No. 9722.

Muhamed JN, Umer MI. Nutrients contents and physical properties of hot composting of local organic waste in Duhok City, Iraq Kurdistan Region. The Seybold Report 2023;18(3):486-98.

Müller A, Wolf D, Gutzeit HO. The black soldier fly, *Hermetia illucens*: A promising source for sustainable production of proteins, lipids and bioactive substances. Journal of Biosciences 2017;72(9-10):351-63.

Pan I, Dam B, Sen SK. Composting of common organic wastes using microbial inoculants. 3 Biotech. 2012;2:127-34.

Rehman KU, Hollah C, Wiesotzki K, Rehman RU, Rehman AU, Zhang J, et al. Black soldier fly, *Hermetia illucens* as a potential innovative and environmentally friendly tool for organic waste management: A mini review. Waste Management and Research 2023;41(1):81-97.

Sarpong DE, Oduro-Kwarteng S, Gyasi SF, Buamah R, Donkor E, Awuah E, et al. Biodegradation by composting of municipal organic solid waste into organic fertilizer using the black soldier fly (*Hermetia illucens*) (Diptera: Stratiomyidae) larvae. International Journal of Recycling of Organic Waste in Agriculture 2019;8:45-54.

Schmitt E, de Vries W. Potential benefits of using *Hermetia illucens* frass as a soil amendment on food production and for environmental impact reduction. Current Opinion in Green and Sustainable Chemistry 2020;25:Article No. 100335.

Sharma A, Soni R, Soni SK. From waste to wealth: Exploring modern composting innovations and compost valorization. Journal of Material Cycles and Waste Management 2024;26(1):20-48.

Stănescu AM, Grigore A, Sîrbu C, Mihalache D, Rujoi B, Marin N. Estimation of measurement uncertainty for phosphorus spectrophotometric determination in organo-mineral fertilizers. Scientific Papers. Series A. Agronomy 2021;64(2):145-51.

Sullivan DM, Bary AI, Miller RO, Brewer LJ. Interpreting Compost Analyses. Oregon State University Extension Catalog [Internet]. 2018 [Cited 2023 Oct 25]. Available from: https://catalog.extension.oregonstate.edu/em9217.

Terrell C. Examining Black Soldier Fly (*Hermetia illucens*) Composting for Urban Ag Specialty Crop Production [dissertation]. Purdue University; 2022.

Environment and Natural Resources Journal

Volume 22
Issue 6
2024

Carbon Sequestration Assessment Using Satellite Data and GIS at Chiang Mai Rajabhat University

Ratchaphon Samphutthanont[1,2*], Worawit Suppawimut[1,2], Phathranit Kitthitinan[1,3], and Kitisak Promsopha[2]

[1]Department of Geography and Geoinformatics, Faculty of Humanities and Social Sciences, Chiang Mai Rajabhat University, Thailand
[2]Asian Air Quality Operations Center by Space Technology, Geoinformatics and Environmental Engineering (AiroTEC), Chiang Mai Rajabhat University, Thailand
[3]Department of Business Administration, Faculty of Management Sciences, Chiang Mai Rajabhat University, Thailand

ARTICLE INFO

Received: 27 Jun 2024
Received in revised: 25 Sep 2024
Accepted: 4 Oct 2024
Published online: 6 Nov 2024
DOI: 10.32526/ennrj/22/20240183

Keywords:
Carbon sequestration/ NDVI vegetation index/ Sentinel-2/ Geographic Information Systems (GIS)

*** Corresponding author:**
E-mail:
ratchaphon_sam@cmru.ac.th

ABSTRACT

This study conducted a project to assess carbon sequestration in the forest area of Chiang Mai Rajabhat University, Mae Rim Campus, covering a total area of approximately 5,600 rai, with about 75% consisting of dry dipterocarp forest. The Sentinel-2 satellite data from 2019 to 2023 were used to analyze and classify forest density using the Normalized Difference Vegetation Index (NDVI). It was classified into four NDVI levels: highest, high, moderate, and low. Then, eight sample plots were distributed across all density levels to collect field data on tree species, number of trees, height, and diameter. The biomass and carbon sequestration in the sample plots showed a strong correlation with vegetation density, with the highest average correlation in February, particularly on February 13, 2023, showing the highest correlation coefficient of 0.817. This relationship is described by the equation y=78.601x–25.726, indicating that this model is effective for estimating carbon sequestration. The analysis revealed that the area with the highest NDVI level of dry dipterocarp forest had the highest above-ground carbon sequestration rate of 16.25 tons per rai, whereas the forest with the lowest NDVI level had an above-ground carbon sequestration rate of 0.21 tons per rai. In total, the above-ground carbon sequestration for the trees amounted to 50,907.35 tons. This preliminary assessment serves as a promising foundation for future efforts the conservation and restoration of the university's forest area, contributing to sustainable strategies for mitigating global warming.

1. INTRODUCTION

Currently, we are facing the problem of global warming, scientifically believed to be caused by greenhouse gases released from human activities. In general, greenhouse gases are essential for maintaining the Earth's temperature by enveloping the atmosphere (TMD, 2024). However, excessive amounts of these gases can increase global temperatures, affecting ecosystems and living organisms. Carbon dioxide (CO_2), in particular, is the most abundant greenhouse gas in the atmosphere, primarily resulting from human activities (ISDNRE, 2020). Major sources of emissions are from electricity production, industrial operations, transportation, and agricultural activities, which are challenging to control (Manee-in, 2022). Nevertheless, the increase in CO_2 can be managed by expanding green areas with trees which use CO_2 to produce biomass for the stems, branches, leaves, and roots (Forest Learning, 2020), thereby sequestering carbon in various parts of the tree (Tripattanasuwan et al., 2010). As is obvious that forests can, thus, act as significant carbon sinks, storing CO_2 in above-ground biomass (IPCC, 2003; Brown, 1996; Mousiew et al., 2019). Restoring the remaining natural forest areas can provide a means of carbon sequestration to mitigate greenhouse gas issues

Citation: Samphutthanont R, Suppawimut W, Kitthitinan P, Promsopha K. Carbon sequestration assessment using satellite data and GIS at Chiang Mai Rajabhat University. Environ. Nat. Resour. J. 2024;22(6):574-584. (https://doi.org/10.32526/ennrj/22/20240183)

and reduce global warming (Mousiew et al., 2019). Therefore, assessing the carbon sequestration capacity of forest areas is beneficial for understanding the current status to strategically plan for effective forest restoration, conservation, and reforestation.

According to the guidelines issued by the Thailand Greenhouse Gas Management Organization (Public Organization) or TGO, remote sensing technology has been proposed as an option for assessing carbon sequestration of trees (TGO, 2023) since it provides rapid, reliable data and is economical. Currently, satellite imagery is widely applied in forest carbon sequestration assessments, using various satellites such as Landsat 5 (Boonsang and Arunpraparat, 2011), Landsat 7 (Chai-udom et al., 2016), Landsat 8 (Pannual et al., 2015; Lolupiman et al., 2016; Uttaruk et al., 2018; Sukarna et al., 2021), Landsat 9 (Khunrattanasiri et al., 2024), and the high-resolution Sentinel-2 (Kesornbua et al., 2022; Khunrattanasiri et al., 2023). These assessments involve classifying forest areas and using the Normalized Difference Vegetation Index (NDVI) alongside field survey data and allometric equations (Thongmee et al., 2019). The timing of satellite data collection can impact the accuracy of biomass assessment models due to forest phenology and leaf shedding (Theerakultomorn et al., 2022), whereas the biomass of natural forests varies based on forest type, tree species composition, forest density, terrain, and environmental factors (Faculty of Forestry Kasetsart University, 2011; Kavinpholasa, 2023). Accurate forest classification combined with field surveys can thus enhance the precision of tree biomass carbon sequestration assessments.

Chiang Mai Rajabhat University has a plan to achieve carbon neutrality as part of its social responsibility. Therefore, it has supported preliminary surveys and assessments to determine the spatial capability of trees for carbon sequestration, as no such project has previously been conducted. The objective of this study is to survey the area and apply satellite and geographic information systems (GIS) data to assess carbon sequestration in the natural forest area within Chiang Mai Rajabhat University, Mae Rim Campus. The study aims to estimate the amount of carbon stored as biomass in trees using an above-ground biomass assessment model and multiple linear regression analysis from Sentinel-2A satellite data, selecting the most reliable time frames. The findings will provide crucial information for conserving and restoring forest areas to enhance the capacity for CO_2 absorption, raise awareness of the loss of forest areas and support organizational projects to reduce, absorb, or offset CO_2, thereby contributing to ongoing global warming mitigation efforts.

2. METHODOLOGY

2.1 Study area

The study area is Chiang Mai Rajabhat University, Mae Rim Campus, located in Mae Rim District, Chiang Mai Province. It covers an area of 5,625.90 rai (Engineering and Architecture Division, Building and Grounds Department, Chiang Mai Rajabhat University, 2023) with geographical coordinates ranging from 19.009° N to 19.045° N latitude and 98.902° E to 98.945° E longitude. The forest type found in this area is the Dry Dipterocarp Forest, including tree species such as *Shorea obtusa* Wall. ex Blume, *Shorea siamensis* Miq, *Dipterocarpus obtusifolius* Teijsm ex Miq, *Dipterocarpus tuberculatus* Roxb, *Canarium subulatum* Guillaumin and *Memecylon edule* Roxb (Rattanachuchok, 2017). The predominant soil type in the Dry Dipterocarp Forest is sandy loam or lateritic soil, which retains little water (Woodland Campus Park, 2021). The terrain is characterized as flatlands and hills, with elevations ranging from 300 to 410 meters above sea level (m.a.s.l.). The average maximum and minimum temperatures occur in April and January, 36.5 and 14.9 degrees Celsius, respectively. The highest and lowest average rainfall amounts are recorded in August and January, totaling 216.9 and 4.2 millimeters, respectively (based on a 30-year standard from the Meteorological Department, 2010). Average annual rainfall in this area is 1,130.6 millimeters per year (RID, 2024).

2.2 Data and methods

2.2.1 Classification of land use within Chiang Mai Rajabhat University, Mae Rim Campus

Land use classification was conducted using visual interpretation methods with aerial photographs from the U.S. public domain and satellite images from Keyhole, Inc., available in Google Earth software (Intapiw, 2017). This was performed on April 19, 2023, categorizing into five types; forest, water bodies, open land, built-up areas, and agricultural areas.

2.2.2 Forest type classification

2.2.2.1 Normalized Difference Vegetation Index (NDVI)

The Normalized Difference Vegetation Index (NDVI) is calculated to assess vegetation health using near-infrared and red wavelength reflections. NDVI values range from -1 to 1 (Jensen, 2015; Theerakultomorn et al., 2022). Negative NDVI values indicate water bodies. Values approaching 0 indicate sparse vegetation, and values approaching +1 indicate dense green vegetation (Mongkonsawat et al., 2009; Theerapon, 2018). Equation (1) is used for general NDVI calculations, while Equation (2) adapts NDVI for Sentinel-2 satellite data:

$$\text{NDVI} = \frac{\text{NIR} - \text{RED}}{\text{NIR} + \text{RED}} \quad (1)$$

$$\text{NDVI}_{\text{Sentinel}-2} = \frac{\text{B8}-\text{B4}}{\text{B8}+\text{B4}} \quad (2)$$

Regarding Sentinel-2 satellite data from the HARMONIZED collection, the European Space Agency (ESA) adjusted the processing baseline on January 26, 2022, which resulted in negative digital number (DN) values. This differs from the previous data. To ensure a smooth analysis of these changes, the Sentinel-2 HARMONIZED collection dataset was used (Sentinelhub, 2021; Samphutthanont, 2024).

2.2.2.2 Forest NDVI classification

To assess aboveground carbon sequestration in trees, forest conditions are classified based on completeness of vegetation using satellite imagery (Pannual et al., 2015). The ISO Cluster Unsupervised Classification method is employed using the ISO Cluster and Maximum Likelihood Classification tools, classifying 2 lowest data clusters. Each cluster should have an adequate signature file. For example, to classify forest areas within a specific boundary, the forest area should constitute a substantial percentage (ArcGIS Pro 3.1, 2023). The classification divides the forest into four density levels: Low NDVI levels, Moderate NDVI levels, High NDVI levels, and Highest NDVI levels. In this context, the average NDVI data over 5 years from Sentinel-2 satellite imagery for the period 2019-2023 is used to represent the study area.

2.2.3 Survey of biodiversityd in forest areas

Field surveys were conducted from April to May 2024, collecting data by placing 2 sampling plots size 20 × 20 meters, 2 plots per forest density, totaling 8 plots to study all types of perennial tree species. The sampling method was purposive, ensuring spatial distribution across all areas with varying NDVI density. The trees, distributed throughout the study area, were selected for the DBH of 4.5 cm or more and the height greater than 1.3 m.

2.2.4 Calculation of biomass and carbon sequestration of sample plots

Field data were used to calculate the biomass of trees, separated into the components of stems, branches, and leaves, based on the allometric equations for dry dipterocarp forest by Ogawa et al. (1965), who studied the biomass of dry dipterocarp forest in Ping Khong District, Chiang Mai Province, Thailand as presented in Equations (3)-(5).

$$\text{Stem } (W_S) = 0.0396(D^2H)^{0.9326} \quad (3)$$

$$\text{Branch } (W_B) = 0.003487(D^2H)^{1.027} \quad (4)$$

$$\text{Leaf } (W_L) = \frac{22.5}{W_S+0.025} \quad (5)$$

Where; W_S=Biomass of stem (kg); W_B=Biomass of branches (kg); W_L=Biomass of leaves (kg); D=diameter at breast height (cm); H=Height of tree (m).

It is calculated from the average carbon content in plant tissues, including stems, branches, and leaves, with carbon fractions (CF) specified as 49.9%, 48.7%, and 48.3% respectively (Tsutsumi et al., 1983; Mousiew et al., 2019). Meanwhile, roots have a carbon fraction of 47.0% (IPCC, 2006; Mousiew et al., 2019).

2.2.5 Analysis of relationship between carbon sequestration and NDVI

The study analyzed the correlation between carbon sequestration and NDVI across 52 data sets, using a 1-square-meter grid on each 400-square-meter sample plot in order to obtain an average that is most appropriate for the area in which the sample plot boundaries overlap the Sentinel-2 data points, and to analyze the average NDVI index values and the time period that has the greatest carbon sequestration. Regression Analysis, the relationship between the dependent variable (Y) or carbon sequestration and the primary variable (X) or the NDVI index value in the sample plot area, shows the regression equation y=a+bx to explain the relationship between two variables from the R-Squared (R^2) value (Charoenhirunyingyos, 2018).

2.2.6 Carbon sequestration calculation by forest density

Carbon sequestration was estimated based on NDVI values during the peak correlation period, evaluating carbon stored within trees-stem, branch, and leaf and above-ground biomass.

3. RESULTS AND DISCUSSION

3.1 Land use

At Chiang Mai Rajabhat University, Mae Rim Campus, the predominant land use type was found to be Forest, occupying the largest area at 4,273.60 rai, accounting for 75.96%. This was followed by Building and Road, Miscellaneous, Bare soil, road, Agricultural, and Water, covering areas of 305.5 rai, 304.2 rai, 243.6 rai, 209.7 rai, 171.1 rai, and 118.2 rai, respectively, representing percentages of 5.43%, 5.41%, 4.33%, 3.73%, 3.04%, and 2.10%. This information is summarized in Table 1 and illustrated in Figure 1, indicating that the majority of the area is covered by forests.

Table 1. Current land use within Chiang Mai Rajabhat University, Mae Rim Campus

Landuse types	Area (rai)	Percentage (%)
Forest	4,273.60	75.96
Building and road	305.50	5.43
Miscellaneous	304.20	5.41
Bare soil	243.60	4.33
road	209.70	3.73
Agricultural	171.10	3.04
Water	118.20	2.10
Total	5,625.90	100.00

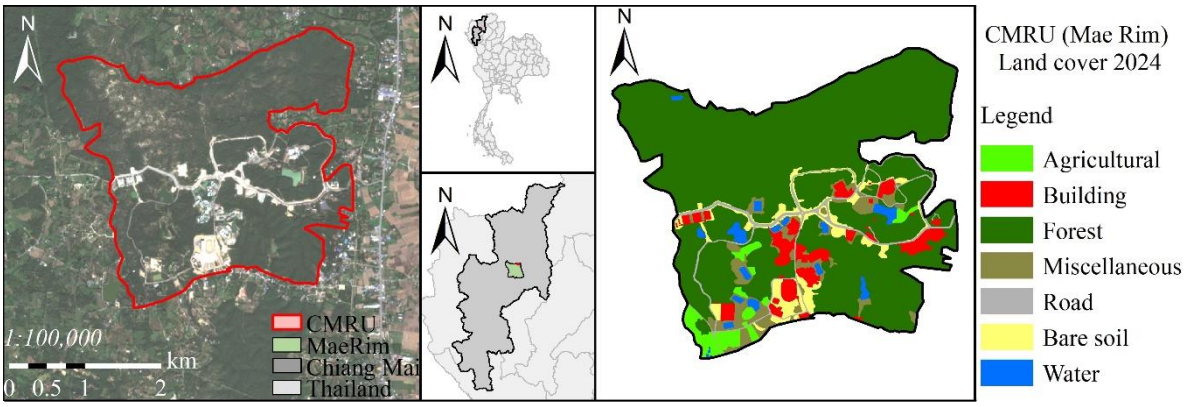

Figure 1. Map of Chiang Mai Rajabhat University, Mae Rim Campus (left) and Land Use (right)

3.2 Forest NDVI classification

3.2.1 Monthly NDVI values from 2019 to 2023

Within the study area, the highest average monthly NDVI value was observed in September, with a value of 0.688, due to high Vegetation Density in rainy season. Following this, October and November had NDVI values of 0.687 and 0.667, respectively. March was recorded the lowest average monthly NDVI value at 0.367, as it is the hottest month of the year, leading to dry conditions and dipterocarp forests. April and February had NDVI values of 0.430 and 0.449, respectively. The average NDVI value over the 5-year period was 0.579, as shown in Figure 2 and Table 2.

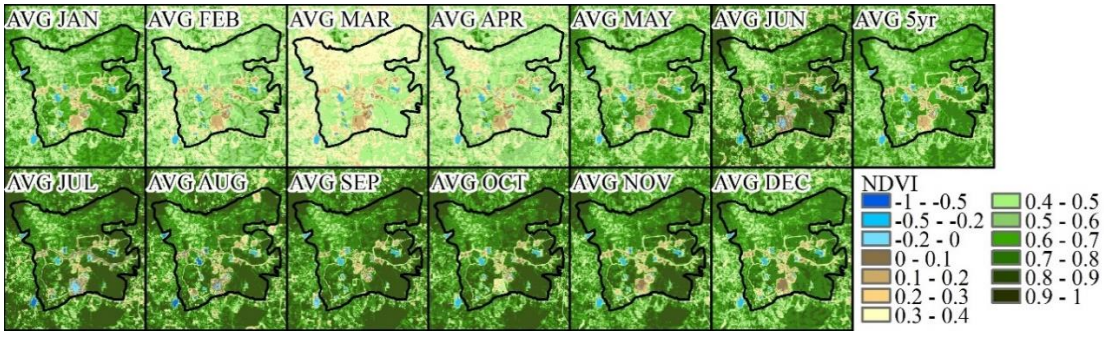

Figure 2. Monthly average NDVI from 2019-2023 and 5-year average NDVI

3.2.2 Classification of forest types based on NDVI density

Within the study area, forested areas were categorized into 4 types based on the 5-year average NDVI values using Unsupervised Classification. The largest area was classified as Highest NDVI levels, covering 2,107.30 rai, accounting for 49.75%. This was followed by areas classified as High NDVI levels, Moderate NDVI levels, and Low NDVI levels, which covered 1,536.30 rai, 550.2 rai, and 41.8 rai, respectively, accounting for 36.27%, 12.99%, and 0.99%, respectively. Therefore, the majority of the area is considered to have high forest density.

Regarding the monthly average NDVI values of forested areas, the values were arranged from lowest to highest for each month. The month with the lowest average NDVI was March, while the highest average NDVI was observed in September, as presented in Table 2 and Figure 3 and Figure 4.

Table 2. Average monthly NDVI of each forest type's density

AVG NDVI/level	Low NDVI levels	Moderate NDVI levels	High NDVI levels	Highest NDVI levels	AVG
January	0.288	0.457	0.592	0.688	0.556
February	0.251	0.372	0.468	0.554	0.449
March	0.239	0.324	0.381	0.434	0.367
April	0.237	0.353	0.453	0.522	0.430
May	0.248	0.414	0.576	0.688	0.546
June	0.288	0.471	0.651	0.789	0.607
July	0.369	0.575	0.731	0.830	0.666
August	0.330	0.546	0.704	0.806	0.653
September	0.343	0.571	0.729	0.818	0.688
October	0.363	0.588	0.741	0.818	0.687
November	0.365	0.578	0.731	0.811	0.667
December	0.337	0.538	0.691	0.775	0.630
AVG NDVI 5 year	0.339	0.490	0.618	0.708	0.579

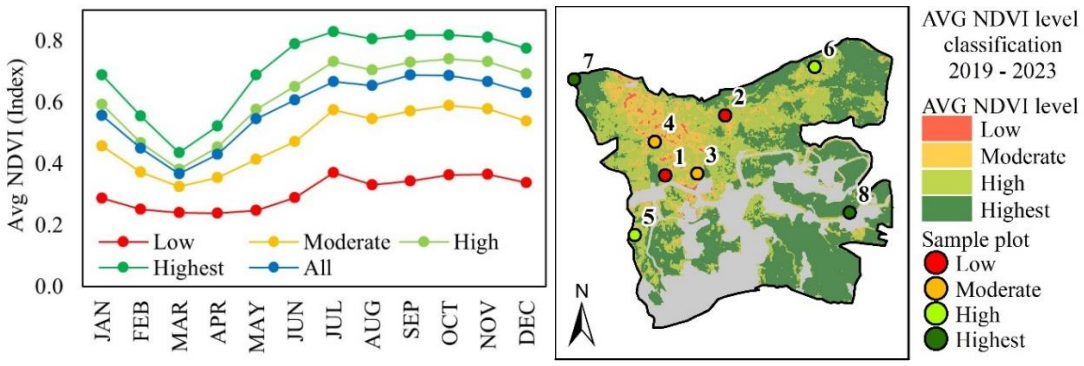

Figure 3. Average monthly NDVI (left) and plot locations (right)

3.3 Tree height and circumference within sample plots

The survey results of the sample plots revealed that the deciduous forest is dominated by species such as *Dipterocarpus obtusifolius* Teijsm. ex Miq, *Shorea obtusa* Wall. ex Blume, *Shorea siamensis* Miq, *Dipterocarpus tuberculatus* Roxb, *Canarium subulatum* Guillaumin, and *Memecylon edule* Roxb. In the areas with the highest NDVI levels, the highest average tree height was found to be 23.22 m in Plot 8, and 14.27 m in Plot 7. In contrast, in Low NDVI level areas, the lowest average tree height was 4.35 m in Plot 1 and 4.96 m in Plot 2. Regarding tree count, the highest number of trees was recorded in Plot 8 with 74 trees. Plot 7 had 33 trees, and the average diameter at breast height (DBH) was the highest at 15.55 cm. Forest areas classified under High, Moderate, and Low NDVI levels showed a decreasing trend in both tree count and DBH, corresponding to the NDVI values, as shown in Table 3.

3.4 Biomass and carbon sequestration of trees within sample plots

The Highest NDVI level areas exhibited the highest biomass quantity, with a value of 50.79 tons/rai, as well as carbon sequestration of 25.08 tons/rai. In contrast, the Low NDVI level areas had the lowest biomass quantity, at 1.04 tons/rai, and carbon sequestration of 0.51 tons/rai (Table 3). Thus, it can be concluded that the total biomass and carbon sequestration are significantly correlated, and when NDVI, indicating vegetation density and health, increases, both biomass and carbon sequestration also increase.

Table 3. Tree count, average DBH, height, biomass, and carbon sequestration of trees within sample plots

Plot	NDVI level	Number of trees	Trees/rai	Avg. DBH (cm)	Avg. H (m)	Biomass (tons/rai)	Carbon sequestration (tons/rai)	Survey date
1	Low	17	68	7.66	4.35	1.04	0.51	24 Apr 24
2	Low	19	76	6.63	4.96	1.14	0.56	1 May 24
3	Moderate	34	136	10.27	7.56	6.04	2.97	24 Apr 24
4	Moderate	36	144	10.90	8.21	6.96	3.43	1 May 24
5	High	50	200	10.70	7.15	8.33	4.11	23 Apr 24
6	High	63	252	10.71	7.39	9.90	4.88	24 Apr 24
7	Highest	33	132	15.55	14.27	22.53	11.13	23 Apr 24
8	Highest	74	296	12.76	23.22	50.79	25.08	25 Apr 24

Figure 4. Sample plots with low vegetation density in plot 1 (left) and highest vegetation density in plot 8 (right)

3.5 Relationship between carbon sequestration and NDVI index

The analysis of the correlation between carbon sequestration within sample plots and the NDVI index across 40 datasets revealed that the highest correlation coefficient (R^2) occurred in February, with a value of 0.717. January and December also showed notable correlation coefficients. Specifically, on February 13, 2023, the correlation coefficient peaked at 0.817. This relationship is expressed by the equation y=78.601x-25.726, indicating a suitable model for estimating carbon sequestration. This model suggests that during February, which typically experiences dry conditions and leaf shedding due to high temperatures and low rainfall, carbon sequestration processes are significantly affected as depicted in Table 4 and Figure 5.

3.6 Carbon sequestration

Analysis reveals that in the deciduous forest areas categorized as Highest NDVI level, the carbon sequestration rate above ground is highest, at 16.25 tons/rai. This is followed by High NDVI level, Moderate NDVI level, and Low NDVI level with rates of 9.38, 3.49, and 0.21 tons/rai, respectively. Within the study area, the average rate of above-ground carbon sequestration is 11.91 tons/rai. The total amount of above-ground carbon sequestration by all trees is calculated to be 50,907.35 tons, as shown in Table 5 and Figure 6.

Table 4. Correlation between carbon sequestration and monthly NDVI index

No.	NDVI	R Square	No.	NDVI	R Square	No.	NDVI	R Square
1	20 Jan 19	0.648	15	25 Mar 23	0.601	29	23 Oct 19	0.553
2	15 Jan 20	0.564	16	20 Apr 19	0.213	30	27 Oct 20	0.409
3	19 Jan 21	0.614	17	19 Apr 20	0.331	31	26 Nov 19	0.490
4	24 Jan 22	0.581	18	19 Apr 21	0.644	32	30 Nov 20	0.486
5	14 Jan 23	0.607	19	14-Apr-22	0.490	33	30 Nov 21	0.487
6	14 Feb 19	0.534	20	19-Apr-23	0.162	34	30 Nov 22	0.585
7	14 Feb 20	0.710	21	21 May 19	0.390	35	25 Nov 23	0.197
8	13 Feb 21	0.749	22	15 May 20	0.512	36	21 Dec 19	0.400
9	13 Feb 22	0.574	23	15 May 21	0.580	37	15 Dec 20	0.490
10	**13 Feb 23***	**0.817**	24	25 May 23	0.505	38	20 Dec 21	0.491
11	26 Mar 19	0.123	25	4 Jun 23	0.598	39	20 Dec 22	0.571
12	30 Mar 20	0.301	26	24 Jul 23	0.561	40	20 Dec 23	0.523
13	25 Mar 21	0.431	27	23 Aug 21	0.524			
14	25 Mar 22	0.279	28	18 Sep 19	0.573			

*On February 13, 2023, the highest correlation value was 0.817.

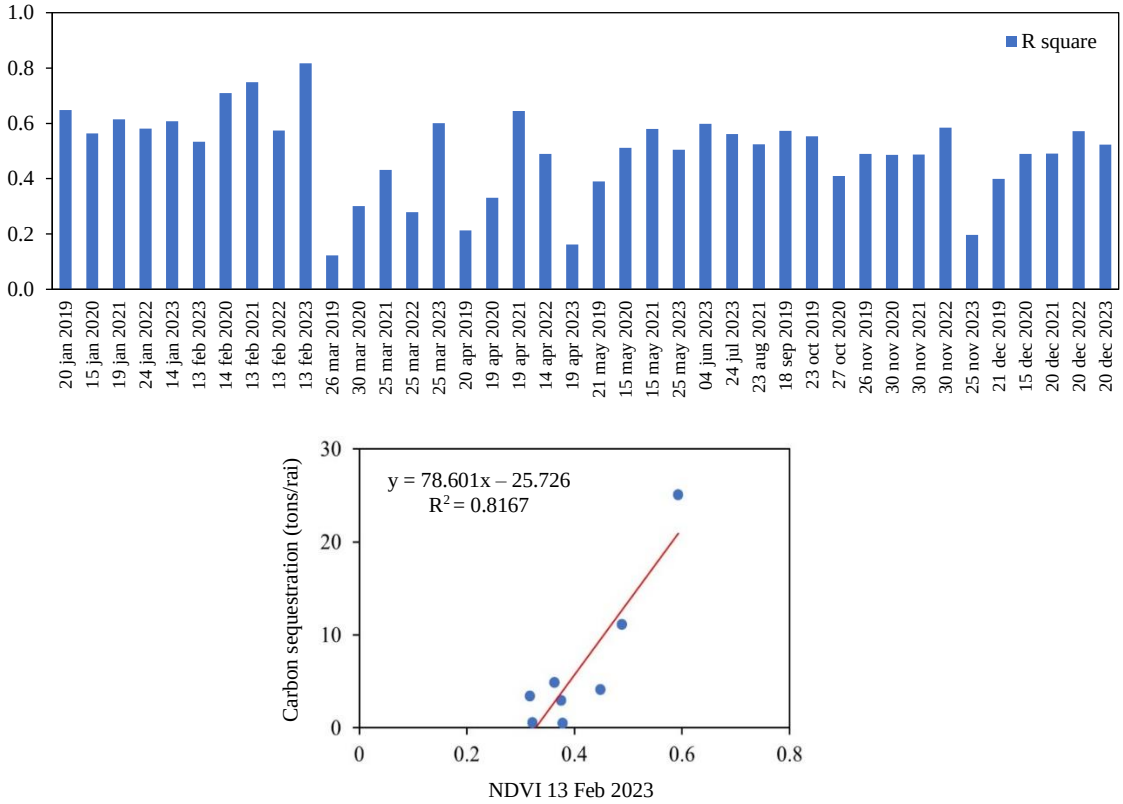

Figure 5. Relationship between carbon sequestration and the monthly NDVI index (top) and the correlation line graph for February 13, 2023 (bottom).

Table 5. Above ground carbon sequestration of trees classified by NDVI level

NDVI level	Area (rai)	Avg. carbon sequestration (tons/rai)	Sum carbon sequestration (tons)
Low	43.50	0.21	9.29
Moderate	562.62	3.49	1,963.24
High	1,551.60	9.38	14,551.39
Highest	2,115.88	16.25	34,383.44
All	4,273.60	11.91	50,907.35

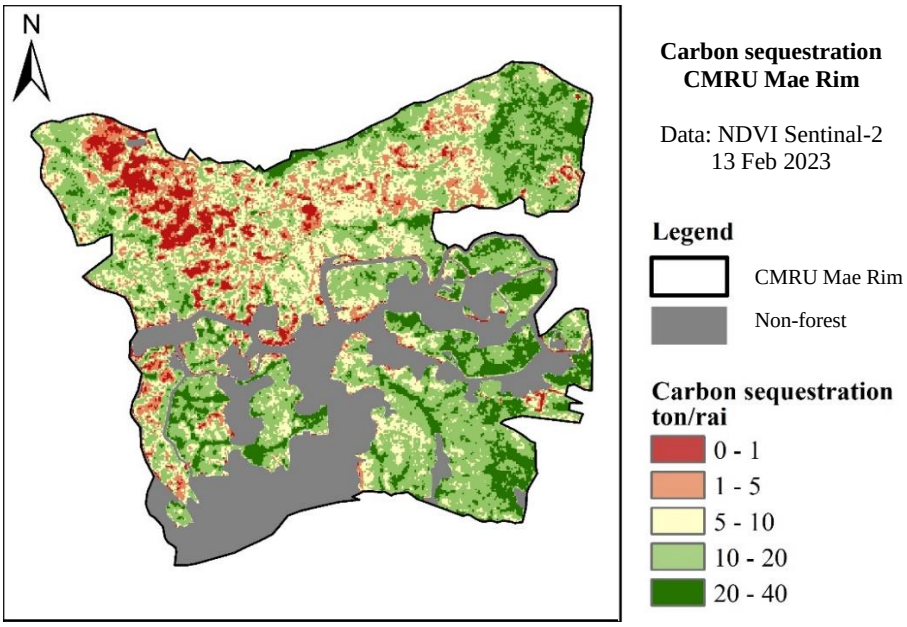

Figure 6. Map showing carbon sequestration in the study area

The study found that the average rate of above-ground carbon sequestration from the model in the dense forest areas categorized as Highest NDVI level is 16.25 tons/rai. Comparatively, a previous study (Theerakultomorn et al., 2022) estimated above-ground carbon sequestration in the deciduous forest area of Nong Rawiang, Rajamangala University of Technology Isan, Mueang Nakhon Ratchasima District, Nakhon Ratchasima Province, using Sentinel-2A satellite imagery captured on April 21, 2020, and carbon sequestration data from 10 sample plots each measuring 100 m^2. It found that the average above-ground carbon sequestration of the forest was 18.38 tons/rai, which is close to the average rate from this model.

Regarding the evaluation of above-ground carbon sequestration in the forest of the conservation area Mae Tuen Wildlife Sanctuary, Tak Province, it was found to be 8.74 tons/rai due to low fertility, low moisture, and frequent wildfires (Boonsang and Arunpraparat, 2011). This finding aligns with a study conducted in the Dipterocarpus forests of Manipur, Northeast India, where the carbon stock values ranged between 9.13 and 10.96 tons C/ha, highlighting the significant impact of environmental factors such as moisture availability and soil fertility on carbon sequestration rates (Debajit et al., 2014). In this study, the density of the mixed deciduous forest in plot 8, classified under the Highest NDVI levels group, is 296 trees/rai, which closely resembles the density of the mixed deciduous forest in the conservation forest area of Nikhom Fak Tha Cooperative, Uttaradit Province, which has 210 trees/rai (Phongthornphruek, 2015). These findings are further supported by research in Southeast Asian tropical forests, where carbon sequestration rates varied significantly depending on disturbance regimes like wildfires and local environmental conditions (Lasco et al., 2006). Comparing with Thammanu et al. (2021), which surveyed the mixed deciduous forest in the community forest of Mae Chieng Rai Lum, Lampang Province, calculated carbon sequestration and average tree density were 4.78 tons/rai and 142.48 trees/rai, respectively. These values are similar to the findings of this study in plot 4, which has a Moderate NDVI level with a tree density of 3.43 tons/rai and 144 trees/rai. Additionally, comparing carbon sequestration studies of three other mixed deciduous forests reveals varying results: Jundang et al. (2010) found an average carbon sequestration of 3.20 tons/rai and an average tree density of 125.28 trees/rai in the mixed deciduous forest of the Manjakiri Forest Garden in Khon Kaen Province, while Duangthip et al. (2022) reported an average carbon sequestration of 5.98 tons/rai and an average tree density of 302 trees/rai in the mixed deciduous forest of community forest in Tha Sala, Chiang Mai Province. Meanwhile, Kamjai et al. (2017) found higher values in the mixed deciduous forest in the community forest area of Ban Nong Yai, Kanchanaburi Province, with an average carbon sequestration of 6.19 tons/rai and an average tree density of 259.36 trees/rai. Therefore, it is evident

that carbon sequestration and tree density values vary significantly among different mixed deciduous forest areas studied. These findings are supported by multiple studies across different forest types, indicating that local conditions, forest management practices, and specific environmental factors play crucial roles in determining carbon sequestration potential.

This study's model for assessment carbon sequestration in trees using the NDVI index achieved the highest correlation (R^2) in February, with a value of 0.82. This is comparable to the model study in the Mae Moh Mine Area, Lampang Province, which used satellite data from February and reported a correlation value of 0.70 (Khunrattanasiri et al., 2023). It is also consistent with Boonsang and Arunpraparat (2011) model for estimating carbon sequestration in the mixed deciduous forest in the Mae Tuen Wildlife Sanctuary, Tak Province, which used February satellite data and had a correlation value of 0.75. However, Theerakultomorn et al. (2022) study used NDVI satellite data from April to model carbon sequestration in trees in the mixed deciduous forest area of Nong Rawiang Educational Center, Rajamangala University of Technology Isan, Nakhon Ratchasima Province, and found a correlation of 0.76. Additionally, Malik et al. (2023) studied the carbon sequestration model for trees in agroforestry areas in Rancakalong, Sumedang, Indonesia, using June NDVI data, achieving a correlation (R^2) of 0.80. For the model study on estimating carbon sequestration in a plantation forest using teak as the primary species in Tak Province (Thiteja et al., 2020), December NDVI data was used for the evaluation, resulting in a correlation (R^2) of 0.96. Therefore, it is evident that the correlation between the amount of carbon sequestration in sample plots and the NDVI values varies across different regions. The choice of timing is crucial, as selecting the appropriate period for the study area enhances the accuracy of the tree carbon sequestration assessment.

From the calculation of carbon sequestration, the CO_2 absorption, derived from the amount of above-ground carbon sequestration (TC) multiplied by the proportion between carbon dioxide and carbon (CO_2CF), where carbon dioxide (CO_2) has a molecular mass of 44 and carbon (C) and a molecular mass of 12, the proportion as 44/12, or 3.66, as in Equation (6) (Suthampaeng and Boonyanuphap, 2020). It was found that the forested areas within Chiang Mai Rajabhat University, Mae Rim Campus absorbed 186,320.90 tons of carbon dioxide (tCO_2).

$$CO_2 \text{ absorption} = TC \times CO_2CF \quad (6)$$

4. CONCLUSION

In this study, Dry Dipterocarp Forest within the boundaries of Chiang Mai Rajabhat University, Mae Rim campus, were classified visually, identifying a total area of 4,273.60 rai. Using ISO Cluster Unsupervised Classification with average NDVI data from 2019 to 2023, the Dry Dipterocarp Forest were categorized into four levels: Low NDVI levels, Moderate NDVI levels, High NDVI levels, and Highest NDVI levels, covering 0.99%, 12.99%, 36.27%, and 49.75% of the forest area, respectively.

Field surveys conducted during April to May 2024 gathered data and calculated the biomass and above-ground carbon sequestration of standing trees with a diameter equal to or greater than 4.5 cm and tree height greater than 1.3 m, using the allometric equation of dipterocarp forest, applied to sample plots measuring 20 × 20 m and totaling 8 plots. The plot categorized under Highest NDVI levels exhibited the highest biomass and above-ground carbon sequestration, decreasing with lower NDVI levels.

Analysis of the relationship between carbon sequestration quantity and monthly NDVI indices, averaging 52 data points, revealed that average NDVI decreased with lower NDVI levels, similar to biomass and above-ground carbon sequestration. The highest average NDVI value was observed in February, with the highest correlation coefficient (R^2), likely due to the leaf shedding period, enabling the estimation of above-ground carbon sequestration, averaging 11.91 tons/rai, totaling 50,907.35 tons of carbon sequestration.

ACKNOWLEDGEMENTS

This project has received funding from the Genetic Conservation Project of the Plant Genetic Conservation Project under the Royal Initiative of Her Royal Highness Princess Maha Chakri Sirindhorn (RSPG). We extend our gratitude for this support. Additionally, we would like to thank the Institute of Research and Development for facilitating the project, also AiroTEC, CMRU, for providing equipment, personnel, and various data. And finally, the project team would like to thank the administrators of Chiang Mai Rajabhat University for recognizing the importance of the project. This assessment of carbon

sequestration in forest areas of Chiang Mai Rajabhat University, Mae Rim Campus, is hoped to be valuable and a good starting point for future projects aimed at conserving and restoring university forest areas for sustainable global warming mitigation.

REFERENCES

ArcGIS Pro 3.1. Iso Cluster Unsupervised Classification (Spatial Analyst) [Internet]. 2023 [cited 2024 Apr 4]. Available from: https://pro.arcgis.com/en/pro-app/3.1/tool-reference/spatial-analyst/iso-cluster-unsupervised-classification.htm.

Boonsang S, Arunpraparat W. Estimation of above-ground carbon sequestration of forest using remote sensing techniques in Mae Tuen Wildlife Sanctuary, Tak Province. Thai Journal of Forestry 2011;30(3):14-23.

Brown S. Mitigation potential of carbon dioxide emission by management of forests in Asia. Ambio 1996;25(4):272-8.

Chai-Udom K, Karnchanasutham S, Nualchawee K, Sri-ngernyuang K, Sungpalee W. A causal relationship model among above-ground biomass and vegetation index in Lower Montane Forest, Doi Inthanon National Park Chiang Mai, Thailand. Phranakhon Rajabhat Research Journal (Science and Technology) 2016;11(1):27-35 (in Thai).

Charoenhirunyingyos S. Best correlation between vegetation indices and fresh fruit bunch of oil palm yield derived from LANDSAT 8. Srinakharinwirot University Journal of Social Sciences 2018;21(1):235-47 (in Thai).

Debajit R, Nepolion B, Ashesh KD. Assessment of aboveground and soil organic carbon stocks in Dipterocarpus forests of Barak Valley, Assam, Northeast India. International Journal of Ecology and Environmental Sciences 2014;40(1):15-28.

Duangthip N, Anongrak N, Kachina P, Khamyong S. Plant community structure and carbon storage in a dry dipterocarp community forest with using *Dipterocarpus tuberculatus* Roxb. Journal of Thai Forest Ecology 2022;6(1):13-30.

Engineering and Architecture Division, Building and Grounds Department, Chiang Mai Rajabhat University. Survey Report on the Boundaries of Chiang Mai Rajabhat University, Mae Rim Campus. Chiang Mai, Thailand: Chiang Mai Rajabhat University; 2023 (in Thai).

Faculty of Forestry Kasetsart University. Handbook on the Potential of Tree Species for Promotion under the Clean Development Mechanism Project in Forestry. Bangkok: Aksorn Siam Publishing; 2011 (in Thai).

Forest Learning. How is carbon stored in trees and wood products [Internet]. 2020 [cited 2024 Sep 3]. Available from: https://forestlearning.edu.au/images/resources/How%20carbon%20is%20stored%20in%20trees%20and%20wood%20products.pdf.

Intapiw S. Remote Sensing Application for Bypass Street: A Case Study of Nakhon Ratchasima Ringroad South Site Sec 4 [dissertation]. Thammasat University; 2017 (in Thai).

Intergovernment Panel on Climate Change (IPCC). Good Practice Guidance for Land Use, Land-Use Change and Forestry. The Institute for Global Environmental Strategies (IGES) [Internet]. 2003 [cited 2024 Sep 3]. Available from: https://www.ipcc-nggip.iges.or.jp/public/gpglulucf/ gpglulucf_ files /GPG_LULUCF_FULL.pdf.

The Institute for Sustainable Development of Natural Resources and Environment (ISDNRE). 7 Types of Greenhouse Gases: The Main Causes of Global Warming [Internet]. 2020 [cited 2024 Sep 5]. Available from: https://hub.mnre.go.th/th/knowledge/detail/65375.

Jensen JR. Introductory Digital Image Processing: A Remote Sensing Perspective. 4th ed. Glenview, US: Pearson Prentice Hall; 2015.

Jundang W, Puangchit L, Diloksumpun S. Carbon storage of dry dipterocarp forest and eucalypt plantation at Mancha Khiri Plantation, Khon Kaen Province. Kasetsart University Journal of Forestry 2010;29(3):36-44 (in Thai).

Kamjai K, Meunpong P, Diloksumpun S. Dynamics of dry dipterocarp forest and carbon sequestration at Nongyai Community Forest, Kanchanaburi Province. Kasetsart University Journal of Forestry 2017;36(2):55-66 (in Thai).

Kavinpholasa K. Carbon Sequestration in Biomass of Trees in Huay Satang Watershed Management Unit, Nan Province [dissertation]. Maejo University; 2023 (in Thai).

Kesornbua P, Hongkaew A, Salukkham E. Modelling of the predictive carbon storage in Para Rubber Plantation by using Sentinel-2A data. Advanced Science Journal 2022;22(1):61-77.

Khunrattanasiri W, Amarakul A, Rianthakool L, Hutayanon T. Above-ground carbon storage estimation of a reforestation site at Mae Moh Mine, Lampang Province, using Sentinel-2 Satellite data. Thai Journal of Forestry 2023;42(2):113-22.

Khunrattanasiri W, Amarakul A, Rianthakool L, Hutayanon T. Comparative study of Landsat 9 and Sentinel-2 satellite data for above-ground carbon sequestration estimation at Mae Moh mine reforestation site, Lampang Province, Thailand. Agriculture and Natural Resources 2024;58(2):175-82.

Lasco RD, MacDicken KG, Pulhin FB, Guillermo IQ, Sales RF, Cruz RVO. Carbon stock assessment of selectively logged Dipterocarpus forest and wood processing mills in the Philippines. Journal of Tropical Forest Science 2006; 18(4):166-72.

Lolupiman T, Nakhapakorn K, Ussawarujikulchai A. Estimation of above ground carbon stock in Para Rubber Plantation by application of remote sensing, Rayong Province. Journal of Science and Technology 2016;24(6):914-26.

Malik DA, Nasrudin A, Withaningsih S, Parikesit. Vegetation stands biomass and carbon stock estimation using NDVI - Landsat 8 imagery in mixed garden of Rancakalong, Sumedang, Indonesia. In IOP Conference Series: Earth and Environmental Science 2023;1211:Article No. 012015.

Manee-in K. Chapter 4 Global Carbon Dioxide Sources in the United States and Thailand [Internet]. 2022 [cited 2024 Sep 5]. Available from: https://tiche.org/.

Meteorological Department. 30-year Standard Values (1981-2010) [Internet]. 2010 [cited 2024 Jun 15]. Available from: https://www.tmd.go.th/weather/province/last30years-1981-2010/ chiang-mai/2/327501.

Mongkonsawat C, Wattanakit N, Kachai T, Mongkonsawat K, Chuayakhai D. Guidelines for analyzing drought in Northeastern Thailand using Satellite data indices. Proceedings of the Theos Satellite Technology for the Development of Thai Geoinformatics; 2009 September 8-9; Nusa Playa Hotel and Spa, Banglamung District, Chonburi; 2009.

Mousiew K, Thanacharoenchonpas K, Boonyanupap C. Valuation of carbon stock in undisturbed natural forest and mixed fruit tree-based agroforestry system by landslide and under natural succession. Thai Journal of Forestry 2019;38(1):81-95.

Ogawa H, Yoda K, Ogino K, Kira T. Comparative ecological studies on three main types of forest vegetation in Thailand, II. Plant Biomass. Nature and Life in Southeast Asia 1965;4:49-80.

Pannual W, Chuchip K, Jintana V. Above-ground carbon stock assessment of Khuan Khaeng Swamp Forest after severe Burning in 2012 using Satellite imagery. Thai Journal of Forestry 2015;34(1):16-28.

Phongthornphruek S. The biodiversity and plant association structure of dry Dipterocarp Forest in conservative forest of Fak Tha Land Settlement Cooperative, Fak Tha District, Uttaradit Province. Proceedings in the 4th National Forest Ecology Network Conference; 2015 January 22-23; Faculty of Agriculture, Naresuan University, Phitsanulok; 2015 (in Thai).

Rattanachuchok P. Survey and Collection for the Development of the Database System for the Biodiversity of Dry Dipterocarp Forest Plants in the Mae Rim Center, Chiang Mai Rajabhat University, Saluang-Keelek Campus: Research Report. Chiang Mai, Thailand: Chiang Mai Rajabhat University; 2017 (in Thai).

Royal Irrigation Department (RID). Average rainfall over a period of 30 years, Chiang Mai [Internet]. 2024 [cited 2024 Sep 3]. Available from: https://water.rid.go.th/hwm/wmoc/planing /wet/ management2567.pdf.

Samphutthanont R. Assessing agricultural burned areas using dNBR index from Sentinel-2 Satellite data in Chiang Mai, Thailand, from 2019 to 2023. Geographia Technica 2024; 19(2)46-56.

Sentinelhub. Sentinel-2 processing baseline changes and harmonize Values [Internet]. 2021 [cited 2024 Sep 5]. Available from: https://forum.sentinel-hub.com/t/sentinel-2-processing-baseline-changes-and-harmonizevalues/4635.

Sukarna RM, Birawa C, Junaedi A. Mapping above-ground carbon stock of secondary peat swamp forest using forest canopy density model Landsat 8 OLI-TIRS: A case study in Central Kalimantan Indonesia. Environment and Natural Resources Journal 2021;19(2):165-75.

Suthampaeng T, Boonyanuphap J. Assessment of carbon stock in green area of Naresuan University and carbon-credit trading guidelines. Agricultural Science Journal 2020;51(1):80-5 (in Thai).

Thailand Greenhouse Gas Management Organization (TGO). T-VER-TOOL-FOR/AGR-01 (Calculation for Carbon Sequestration) [Internet]. 2023 [cited 2024 Apr 12]. Available from: https://ghgreduction.tgo.or.th/th/tver-method/tver-tool/for-agr/download/4490/245/27.html.

Thammanu S, Han H, Marod D, Srichaichana J, Chung J. Above-ground carbon stock and REDD+ opportunities of community-managed forests in northern Thailand. PLoS ONE 2021; 16(8):e0256005.

Theerakultomorn T, Kamphala A, Prasomsub W, Tiyawongsuwan S, Khamwilai T. Above ground biomass assessment from Sentinel-2A data using multiple linear regression analysis. Proceedings of the 27th National Convention on Civil Engineering; 2022 August 24-26; Chiang Rai, Thailand; 2022.

Theerapon T. Calculation of Drought and Vegetation Indices from Surface Temperature of Landsat 8 Satellite Data and Comparison with Rice Yield in Ubon Ratchathani Province [dissertation]. Chulalongkorn University; 2018 (in Thai).

Thiteja S, Khamyong S, Boontun A, Charoenpanyanet A, Huttagosol P. Using normalized difference vegetation index (NDVI) to assess carbon storage of plantation forests in zinc-mined Mae Tao Watershed, Mae Sod District, Tak Province. Journal of Burapha Science 2020;25(1):51-63 (in Thai).

Thongmee T, Somart C, Chitsukha W. Evaluation of above-ground carbon sequestration of forest in Mahasarakham University using remote Sensing data. Journal of Science and Technology MSU 2019;38(6):586-97.

Thai Meteorological Department (TMD). Greenhouse effect [Internet]. 2024 [cited 2024 Sep 5]. Available from: http://climate.tmd.go.th/content/article/10.

Tripattanasuwan P, Diloksumpun S, Sataporn D, Rattanakaew J. Carbon Sequestration in the Biomass of Certain Plant Species Planted at the Phu Phan Royal Development Study Center, Sakon Nakhon Province. Thailand: Forest and Plant Conservation Research Office, Department of National Parks, Wildlife and Plant Conservation; 2010.

Tsutsumi T, Yoda K, Sahunalu P, Dhanmanonda P, Prachaiyo B. Forest: Felling, Burning and Regeneration, Shifting cultivation. Tokyo University: Japan; 1983.

Uttaruk Y, Rotjanakusol T, Laosuwan, T. Above ground carbon biomass assessment using satellite remote sensing reflection values. Food Agricultural Sciences and Technology 2018; 4(1):41-6.

Woodland Campus Park. Dry Dipterocarp Forest [Internet]. 2021 [cited 2024 Apr 4]. Available from: https://woodland.csc.ku.ac.th/?p=7084.

INSTRUCTION FOR AUTHORS

Publication and Peer-reviewing processes of Environment and Natural Resources Journal

Environment and Natural Resources Journal is a peer reviewed and open access journal that is published in six issues per year. Manuscripts should be submitted online at https://ph02.tci-thaijo.org/index.php/ennrj/about/submissions by registering and logging into this website. Submitted manuscripts should not have been published previously, nor be under consideration for publication elsewhere (except conference proceedings papers). A guide for authors and relevant information for the submission of manuscripts are provided in this section and also online at: https://ph02.tci-thaijo.org/index.php/ennrj/author. All manuscripts are refereed through a **single-blind peer-review** process.

Submitted manuscripts are reviewed by outside experts or editorial board members of **Environment and Natural Resources Journal**. This journal uses double-blind review, which means that both the reviewer and author identities are concealed from the reviewers, and vice versa, throughout the review process. Steps in the process are as follows:

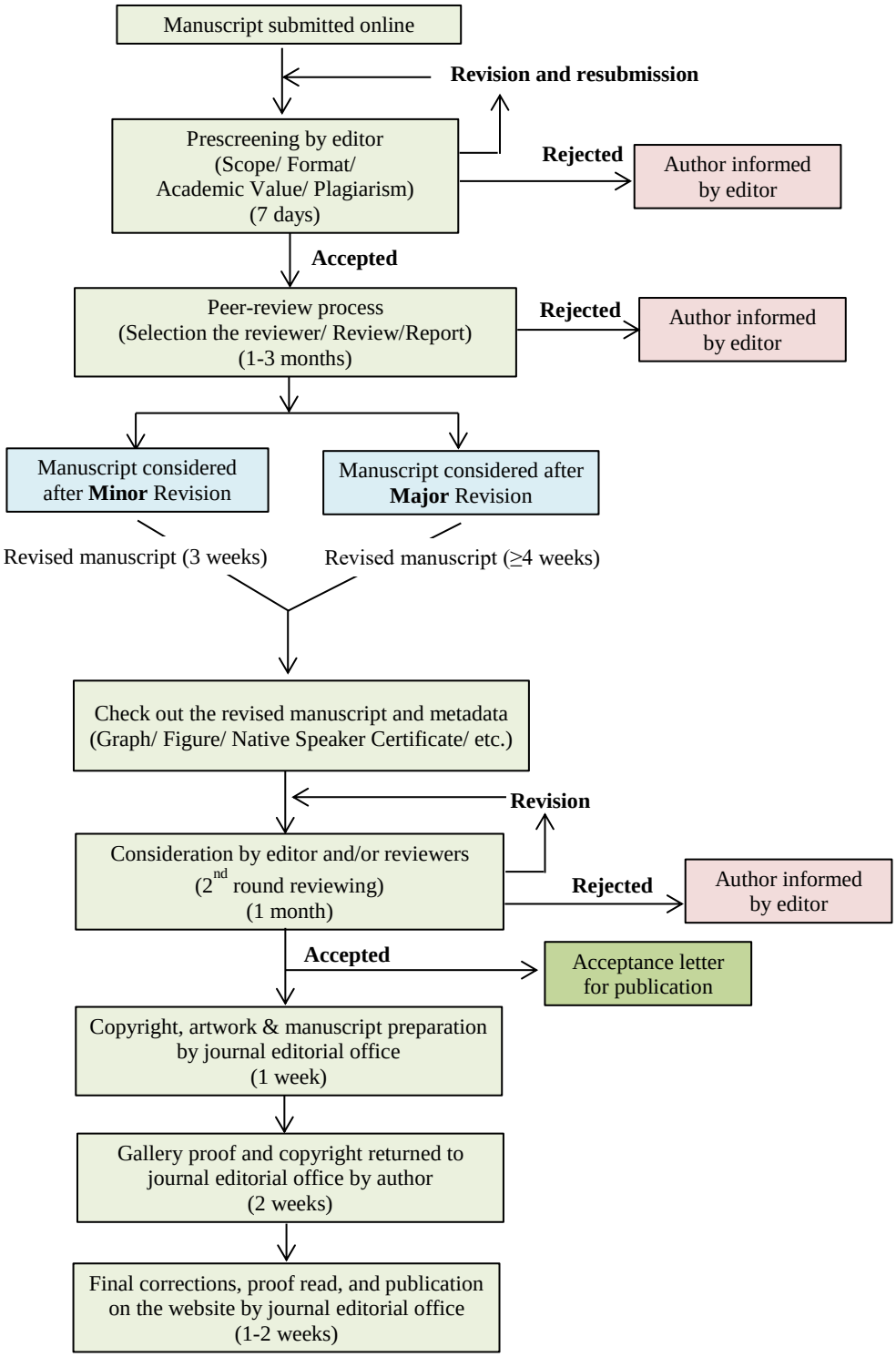

The Environment and Natural Resources Journal (EnNRJ) considers and accepts two types of articles for publication as follows:

- *Original Research Article*: This is the most common type of article. It showcases new, innovative or unique findings surrounding a focused research question. Manuscripts should not exceed 4,000 words (excluding references) - see more details in the Preparation of Manuscript section below.
- *Review Article (by invitation)*: This type of article focuses on the in-depth critical review of a special aspect of an environmental-related research question, issue, or topic. It provides a synthesis and critical evaluation of the state of the knowledge of the subject. Manuscripts should not exceed 6,000 words (excluding references).

Submission of Manuscript

The items that the author needs to upload for the submission are as follows:

Manuscript: The manuscript must be submitted as a Microsoft Word file (.doc or .docx). Refer to the **Preparation of Manuscript** section below for detailed formatting instructions.

Cover Letter: The letter should address the Editor and include the following: a statement declaring that the author's paper has not been previously published and is not currently under consideration by another journal.

- a brief description of the research the author reports in the paper, including why the findings are important and why the journal readers should be interested
- contact information of the author and any co-authors
- a confirmation that the author has no competing interests to disclose

Graphical Abstract (Optional): The author is encouraged to submit a graphical abstract with the manuscript. The graphical abstract depicts the research and findings with visuals. It attracts more potential readers as it lets them understand the overall picture of the article within a few glances. Note that the graphical abstract must be original and unpublished artwork. It should be a high-quality illustration or diagram in any of the following formats: TIFF, PDF, JPEG, or PNG. The minimum required size is 750 × 750 pixels (height × width). The size should be of high quality (600 dpi or larger) in order to reproduce well.

Reviewers Suggestion (mandatory): Please provide the names of three potential reviewers, with information about their affiliations as well as their email addresses. The recommended reviewers should not have any conflict of interest with the authors. Each reviewer must represent a different affiliation and not have the same nationality as the author. Please note that the editorial board retains the sole right to decide whether or not the recommended reviewers will be selected.

Declaration of Competing Interest: The author must include a declaration of competing interest form during submission. If there is no conflict of interest, please state, "The authors declare no conflict of interest." Otherwise, authors should declare all interests to avoid inappropriate influence or bias in their published work. Examples of potential conflicts of interest in research projects include but are not limited to financial interests (such as employment, consultancies, grants, and other funding) and non-financial interests (such as personal or professional relationships, affiliations, and personal beliefs).

CrediT (Contributor Roles Taxonomy) Author Statement or Author Contributions: For research articles with several authors, we require corresponding authors to provide co-author contributions to the manuscript using the relevant CRediT roles. CRediT is a taxonomy that shows the contributions of the author and co-author(s), reduces possible authorship disputes, and facilitates collaboration among research team members. The CRediT taxonomy includes 14 different roles describing each contributor's specific contribution to the scholarly output.

The roles are: Conceptualization; Data curation; Formal analysis; Funding acquisition; Investigation; Methodology; Project administration; Resources; Software; Supervision; Validation; Visualization; Roles/Writing – original draft; and Writing – review & editing.

Note that authors may have contributed through multiple roles, and those who contributed to the research work but do not qualify for authorship should be listed in the acknowledgments.

An example of a CRediT author statement is given below:
"Conceptualization, X.X. and Y.Y.; Methodology, X.X.; Software, X.X.; Validation, X.X., Y.Y. and Z.Z.; Formal Analysis, X.X.; Investigation, X.X.; Resources, X.X.; Data Curation, X.X.; Writing – Original Draft Preparation, X.X.; Writing – Review & Editing, X.X.; Visualization, X.X.; Supervision, X.X.; Project Administration, X.X.; Funding Acquisition, Y.Y."

Artwork for the Journal Cover: The author may provide and propose a piece of artwork (with a description) for the journal issue cover. This is an excellent opportunity for the author to promote their article, if accepted, on the cover of a published issue. Alternatively, the editorial team may invite the author to submit a piece of artwork for the cover after their manuscript has been accepted for publication. The final cover artwork selection will be made by the editorial team.

Final Author Checks: In addition to the basic requirements, the author should review this checklist before submitting their manuscript. Following it ensures the manuscript is complete and in accordance with all standards.

Preparation of Manuscript

Format and Style

The manuscript should be prepared strictly as per the guidelines given below. Any manuscript with an incorrect format will be returned, and the corresponding author may have to resubmit a new manuscript with the correct format.

Overall Format

The manuscript must be submitted as a Microsoft Word file (.doc or .docx). The formatting should be as follows:

- File format - .doc or .docx
- Page size - A4
- Page orientation - portrait (some landscape pages are accepted if necessary)
- Page margin - 2.54 cm (left and the right margin) and 1.9 cm (bottom and the top margin)
- Page number (bottom of the page)
- Line number
- Line spacing - 1.5
- Font - 12 point, Times New Roman (unless stated otherwise)

Unit - The use of abbreviation must follow the International System of Units (SI Unit) format.

- The unit separator is a virgule (/) and not a negative coefficient: 10 mg/L not 10 mgL^{-1}
- Liter always has a capital letter: mg/L

Equations

- Insert equations using the dedicated tool in Microsoft Word. Do not use pictures or text boxes.
- Equations that are referenced in the text should be identified by parenthetical numbers, such as (1), and should be referred to in the manuscript as “Equation 1”.

Inclusive Language: The language used in the manuscript acknowledges diversity, promotes equal opportunity, respects all people, and is sensitive to all aspects of differences. The manuscript content should not make assumptions about the beliefs or commitments of any individual. It should not imply superiority regarding age, race, ethnicity, culture, gender, sexual orientation, disability, or health conditions. Moreover, the manuscript must be free from bias, stereotypes, slang, and derogatory terms.

Reference Style: Vancouver style should be used for the reference list and in-text citations throughout the manuscript. Please follow the format of the sample references and citations, as shown in the Body Text Sections portion below.

Front Page

Title: The title of the manuscript should be concise and not longer than necessary. The title should be bold, 12-point size, and Times New Roman. The first letter of major words should be capitalized (as in standard title case).

Author(s) Name: The first and last names of all authors must be given, in bold, Times New Roman, and 12-point font.

Affiliation of All Author(s): Affiliation(s) must be in italics, Times New Roman, and 11-point font. Specify the Department/School/Faculty, University, City/Province/or State, and Country of each affiliation. Do not include positions or fellowships, or postal zip codes.
Each affiliation should be indicated with superscript Arabic numerals. The Arabic numeral(s) should appear immediately after the author’s name, and represent the respective affiliation(s).

Corresponding Author: One author should be responsible for correspondence, and their name must be identified in the author list using an asterisk (*).

- All correspondence with the journal, including article submission and status updates, must be handled by the corresponding author.

- The online submission and all associated processes should be operated by the corresponding author.

*Corresponding author: followed by the corresponding author's email address.

Example:

Papitchaya Chookaew[1], Apiradee Sukmilin[2], and Chalor Jarusutthirak[1*]
[1]Department of Environmental Technology and Management, Faculty of Environment, Kasetsart University, Bangkok, Thailand
[2]Environmental Science and Technology Program, Faculty of Science and Technology, Phranakhon Rajabhat University, Bangkok, Thailand
**Corresponding author: abcxx@xx.ac.th*

Abstract Page

Abstract: The abstract should include the significant findings paired with relevant data. A good abstract is presented in one paragraph and is limited to 250 words. Do not include a table, figure, or references.
Keywords - Up to six keywords are allowed, and they should adequately index the subject matter.

Highlights: Please include 3-5 concise sentences describing innovative methods and the findings of the study. Each sentence should contain at most 85 characters (not words).

Body Text Sections
The main body text of the manuscript normally includes the following sections: 1. Introduction 2. Methodology 3. Results and Discussion 4. Conclusions 5. Acknowledgments 6. Author Contributions 7. Declaration of Competing Interests 8. References

Introduction should include the aims of the study. It should be as concise as possible, with no subheadings. The significance of the problem and the essential background should also be given.

Methodology is sufficiently detailed so that the experiments can be reproduced. The techniques and methods adopted should be supported with standard references.
There should be no more than three levels of headings in the **Methodology and Results and Discussion** sections. Main headings are in bold letters, second-level headings are in bold and italic letters, and third-level headings are in normal letters.

Here is an example:

2. Methodology
2.1 Sub-heading
2.1.1 Sub-sub-heading

Results presents the key findings in figures and tables with descriptive explanations in the text.

Tables
- Tables - look best if all the cells are not bordered; place horizontal borders only under the legend, the column headings, and the bottom.

Figures
- Figures - should be submitted in color. The author must ensure that the figures are clear and understandable. Regardless of the application used to create them, when electronic artworks are finalized, please 'save as' or convert the images to TIFF or JPG and send them separately to EnNRJ. Images require a resolution of at least 600 dpi (dots per inch) for publication. The labels of the figures and tables must be Times New Roman, and their size should be adjusted to fit the figures without borderlines.
- Graph - The font style in all graphs must be Times New Roman, 9-10 size, and black color. Please avoid bold formatting, and set the border width of the graphs to 0.75 pt.

- Graph from MS Excel: Please attach an editable graph from MS Excel within your manuscript. Then please also submit the full MS Excel file used to prepare the graph as a separate document. This helps us customize our layout for aesthetic beauty.
- Graph from another program: Feel free to use whichever program best suits your needs. But as noted above, when your artwork is finalized, please convert the image to TIFF or JPG and send them separately Again, images should be at least 600 dpi. Do not directly cut and paste.

***All figures and tables should be embedded in the text, and also mentioned in the text.**

Discussion shows the interpretation of findings with supporting theory and comparisons to other studies. The Results and Discussion sections can be either separated, or combined. If combined, the section should be named Results and Discussion. **Conclusions** should include a summary of the key findings and take-home messages. This should not be too long, or repetitive but this section is absolutely necessary so that the argument of the manuscript is not uncertain or left unfinished.

Acknowledgments should include the names of those who contributed substantially to the work, but do not fulfill the requirements for authorship. It should also include any sponsor or funding agency that supported the work.

Author Contributions: For research articles with several authors, we require corresponding author contributions listed using the relevant CRediT roles. This should be done by the author responsible for correspondence.

Declaration of Competing Interest: The author must include a declaration of competing interest form during submission. If there is no conflict of interest, please state, "The authors declare no conflict of interest." Otherwise, authors should declare all interests to avoid inappropriate influence or bias in their published work.

References should be cited in the text by the surname of the author(s) and the year. This journal uses the author-date method of citation. The author's last name and date of publication are inserted in the text in the appropriate place. If there are more than two authors, “et al.” must be added after the first author’s name. Examples: (Frits, 1976; Pandey and Shukla, 2003; Kungsuwas et al., 1996). If the author’s name is part of the sentence, only the date is placed in parentheses: “Frits (1976) argued that . . .”

Please ensure that every reference cited in the text is also in the reference list (and vice versa).

In the list at the end of the manuscript, complete references must be arranged alphabetically by the surnames of the first author in each citation. Examples are given below.

Book

Tyree MT, Zimmermann MH. Xylem Structure and the Ascent of Sap. Heidelberg, Germany: Springer; 2002.

Chapter in a book

Kungsuwan A, Ittipong B, Chandrkrachang S. Preservative effect of chitosan on fish products. In: Steven WF, Rao MS, Chandrkachang S, editors. Chitin and Chitosan: Environmental and Friendly and Versatile Biomaterials. Bangkok: Asian Institute of Technology; 1996. p. 193-9.

Journal article

Muenmee S, Chiemchaisri W, Chiemchaisri C. Microbial consortium involving biological methane oxidation in relation to the biodegradation of waste plastics in a solid waste disposal open dump site. International Biodeterioration and Biodegradation 2015;102(3):172-81.

Journal article with Article Number

Sah D. Concentration, source apportionment and human health risk assessment of elements in $PM_{2.5}$ at Agra, India. Urban Climate 2023;49:Article No. 101477.

Non-English articles

Suebsuk P, Pongnumkul A, Leartsudkanung D, Sareewiwatthana P. Predicting factors of lung function among motorcycle taxi drivers in the Bangkok metropolitan area. Journal of Public Health 2014;44(1):79-92 (in Thai).

Article in press

Dhiman V, Kumar A. Biomass and carbon stock estimation through remote sensing and field methods of subtropical Himalayan Forest under threat due to developmental activities. Environment and Natural Resources Journal 2024. DOI: 10.32526/ennrj/22/20240018.

Published in conference proceedings

Wiwattanakantang P, To-im J. Tourist satisfaction on sustainable tourism development, Amphawa floating market Samut Songkhram, Thailand. Proceedings of the 1st Environment and Natural Resources International Conference; 2014 Nov 6-7; The Sukosol hotel, Bangkok: Thailand; 2014.

Ph.D./Master thesis

Shrestha MK. Relative Ungulate Abundance in a Fragmented Landscape: Implications for Tiger Conservation [dissertation]. Saint Paul, University of Minnesota; 2004.

Website

Orzel C. Wind and temperature: why doesn't windy equal hot? [Internet]. 2010 [cited 2016 Jun 20]. Available from: http://scienceblogs.com/principles/2010/08/17/wind-and-temperature-why-doesn/.

Report organization

Intergovernmental Panel on Climate Change (IPCC). IPCC Guidelines for National Greenhouse Gas Inventories: Volume 1-5. Hayama, Japan: Institute for Global Environmental Strategies; 2006.

Royal Gazette

Royal Gazette. Promotion of Marine and Coastal Resources Management Act 2059. Volume 132, Part 21, Dated 26 Mar B.E. 2558. Bangkok, Thailand: Office of the Council of State; 2015a. (in Thai).

Remark

** Please be note that manuscripts should usually contain at least 15 references and some of them must be up-to-date research articles.*

** Please strictly check all references cited in text, they should be added in the list of references. Our Journal does not publish papers with incomplete citations.*

Changes to Authorship

This policy of journal concerns the addition, removal, or rearrangement of author names in the authorship of accepted manuscripts:

Before the accepted manuscript

For all submissions, that request of authorship change during review process should be made to the form below and sent to the Editorial Office of EnNRJ. Approval of the change during revision is at the discretion of the Editor-in-Chief. The form that the corresponding author must fill out includes: (a) the reason for the change in author list and (b) written confirmation from all authors who have been added, removed, or reordered need to confirm that they agree to the change by signing the form. Requests form submitted must be consented by corresponding author only.

After the accepted manuscript

The journal does not accept the change request in all of the addition, removal, or rearrangement of author names in the authorship. Only in exceptional circumstances will the Editor consider the addition, deletion or rearrangement of authors after the manuscript has been accepted.

Copyright transfer

The copyright to the published article is transferred to Environment and Natural Resources Journal (EnNRJ) which is organized by Faculty of Environment and Resource Studies, Mahidol University. The accepted article cannot be published until the Journal Editorial Officer has received the appropriate signed copyright transfer.

Online First Articles

The article will be published online after receipt of the corrected proofs. This is the official first publication citable with the Digital Object Identifier (DOI). After release of the printed version, the paper can also be cited by issue and page numbers. DOI may be used to cite and link to electronic documents. The DOI consists of a unique alpha-numeric character string which is assigned to a document by the publisher upon the initial electronic publication. The assigned DOI never changes.

Mahidol University

Wisdom of the Land

Faculty of Environment and Resource Studies, Mahidol University, Thailand
999 Phutthamonthon Sai 4 Rd, Salaya, Phutthamonthon District, Nakhon Pathom 73170
E-mail: ennrjournal@gmail.com